NON-INVASIVE MULTIPLE-METHOD APPROACHES TO CHARACTERIZE LANDFORMS IN THE ANTHROPOCENE: A STUDY OF THE PERIGLACIAL CRITICAL ZONE

A Dissertation

by

RAQUEL GRANADOS AGUILAR

Submitted to the Office of Graduate and Professional Studies of
Texas A&M University
in partial fulfillment of the requirements for the degree of

DOCTOR OF PHILOSOPHY

Chair of Committee,	John R. Giardino
Committee Members,	Mark E. Everett
	John D. Vitek
	Kevin R. Gamache
Head of Department,	Julie Newman

May 2021

Major Subject: Geology

ABSTRACT

Prevalence of anthropogenic landforms and human impacts on geomorphic processes led to the development of Anthropogeomorphology and a proposed new geological epoch: the Anthropocene. Natural processes and environments are inherently complex, and anthropogenic influences increases the complexity of geomorphological problems. New approaches are required to study natural and anthropogenic processes. The intricate ways in which terrestrial systems are interconnected can be approached from a Critical Zone perspective, comprising interdisciplinarity, as well as multitemporal studies across spatial scales. A comprehensive understanding of form-process dynamics can only be reached by jointly interpreting subsurface and surface information. Multi-method approaches, strongly driven by technological advancements, are key to obtain data in modern geomorphology. Previously inaccessible areas are within reach, and scale issues are addressed using technology at varying resolutions. With growing interest in the built environment and in using cost-efficient and non-destructive techniques, non-invasive methods are increasingly preferred. Characterization of the subsurface has progressed from being accomplished by ground-truthing data from non-invasive methods, to solely depending on increasingly reliable non-destructive techniques, such as near-surface geophysics. A case study exemplifies the use of non-invasive methods in characterizing a rock glacier, a significant water source in the periglacial Critical Zone, where water resources are limited and severely impacted by climate change. The Upper Camp Bird rock glacier, located on level 3 of Camp Bird Mine in Ouray, Colorado, is

the rock glacier of interest. This research integrated meteorological, geomorphological, geological, and geophysical information to characterize the internal structure and hydrology of the selected rock glacier, while evaluating the suitability of two controlled-source electromagnetic induction systems. Near-surface geophysical surveys conducted employing time-domain and frequency-domain electromagnetic induction systems were interpreted to determine the internal structure of the rock glacier. The frequency-domain system was highly susceptible to local environmental conditions and was inapplicable to resolve the internal makeup of the rock glacier. The time-domain system allowed for deep subsurface penetration and realistic modeling of the internal structure of the rock glacier, which consists of an outer debris shell (<3 m thick), a frozen component (50m-80m thick), and a meltwater component or varying thickness found at different depths.

DEDICATION

To my mom.

ACKNOWLEDGEMENTS

My greatest appreciation goes to my committee chair, Dr. John R. Giardino, and my committee members, Dr. Mark E. Everett, Dr. John D. Vitek, and Dr. Kevin R. Gamache, for their continuous guidance, advice, and support throughout the course of my doctoral studies. Thanks to my professors at the University of Costa Rica, Rolando Mora Chinchilla, MSc and Elena Badilla Coto, MSc, as well as to Dr. René Castro for recommending me for this PhD opportunity. Thank you to the P.E.O. Sisterhood for awarding me with the International Peace Scholarship (IPS) in 2016-2017, your support was instrumental in the completion of my studies.

Thanks to my project backers at experiment.com for partially funding the field work for Article 3 (section 4) of this dissertation; to Mr. Gillman -Trustee of Camp Bird Colorado, Inc.– for permission to access and camp on Camp Bird property; to Anastasia Hedrick and Dr. David Gonzales for sharing information about Camp Bird mine; to Kevin O'Hara from GSSI for EMP-400 Profiler help; to PhD candidate Michael Martin and Mr. Charles Stoyer for IXG-TEM help; and many thanks to Dr. Taylor Rowley for GIS help.

My appreciation goes to Cameron Ramsey, MSc, Dennis Mmasa, MSc, and Maximilian Witek for their invaluable assistance in planning and conducting field work for this research, as well as with preliminary data analyses. Thank you to Dr. Potpreecha Pondthai for training and clarification on the use of the G-TEM system, as well as for his help conducting field work.

Thanks to CH2M for the Curricular Practical Training/internship experience, especially Dr. Nason McCullough, Diana Worthen, MSc, and Todd Cotten; as well as to Michael Lilly, MSc., from Geo-Watersheds Scientific for the opportunity to participate in the Geology & Geosciences Virtual Internship Program. Thank you to Mr. Phil Rumford and Ms. Brittany Martinez for your guidance and support during my time as a Graduate Assistant at the Gulf Coast Repository at IODP.

Thank you to the Coordinators at Project Literacy-Infused Science Using Technology Opportunities (LISTO), Dr. Cindy Guerrero, Dr. Kenneth Fleming, Allison Esparza, M.Ed., as well as the Principal Investigators at the Center for Research & Development in Dual Language & Literacy Acquisition, Dr. Rafael Lara-Alecio, Dr. Beverly Irby, and Dr. Fuhui Tong, for the learning, mentoring, and professional opportunities provided during my time as a Research Assistant at LISTO. Thanks to Dr. Sharmila Pathikonda for introducing me to team LISTO.

My gratitude to Dr. Tim Beach, and an anonymous reviewer for their valuable suggestions, which improved the quality of Article 1, as well as Dr. Rebecca Owens co-author of Article 1. Thank you to RECORDER for allowing reuse of figures from one of their articles.

Thanks also go to my mentors, professors, and colleagues, at the University of Costa Rica and at Texas A&M, for the many ways in which you have influenced my journey.

Finally, thanks to my family and friends for their constant encouragement, patience, and love.

CONTRIBUTORS AND FUNDING SOURCES

Contributors

This work was supervised by a dissertation committee consisting of Professors Dr. John R. Giardino, Dr. Mark E. Everett, and Dr. John D. Vitek of the Department of Geology and Geophysics and Professor Dr. Kevin R. Gamache of the Water Management and Hydrological Science Program.

The research for Article 1 (section 2) was conducted by the student, Dr. Rebecca Owens, and Dr. John R. Giardino. Article 2 (section 3) was a result of a collaboration between the student, Dr. John R. Giardino, and Cameron Ramsey, MSc.

Funding Sources

Field work was partially funded with contributions made by project backers on the crowdfunding platform for research experiment.com.

Funding to cover tuition was provided by the Department of Geology and Geophysics (Fall 2014 – Spring 2016), CH2M Internship (Summer 2015), the International Ocean Discovery Program (tuition & fees: Summer 2016 – Fall 2018), and Project Literacy-Infused Science Using Technology Opportunities (tuition: Spring 2019–Summer 2020, tuition & fees: Fall 2020-Spring 2021).

TABLE OF CONTENTS

Page

Page

Page

LIST OF FIGURES

Page

Page

Page

Page

Page

LIST OF TABLES

Page

1. INTRODUCTION

This dissertation explores the conceptual and practical approaches prevalent in modern geomorphological research. It has been argued that geomorphological processes are increasingly affected by anthropogenic actions (Suess, 1862; Haughton, 1866; Arrhenius, 1896; Woeikof, 1901; Shaler, 1905; Gilbert, 1917; Sherlock, 1922; Jacks and Whyte, 1939; Brown, 1970; Trimble, 1974; Trimble, 1975; Nir, 1983; Turner et al., 1990; Revkin, 1992; Gutiérrez and Naredo Pérez, 2005; Davis, 2011; Goudie and Viles, 2016), and geomorphologists can no longer study natural processes and environments without taking human activity into consideration. The prevalence of anthropogenic landforms (i.e., landfills, infrastructure, artificial islands, archaeological deposits) as well as the impacts of human activities in geomorphic processes (i.e., erosion/sedimentation rates) have led to the development of Anthropogeomorphology (Golomb and Eder, 1964) as a subdiscipline.

The second section of this dissertation considers the relevance of Anthropogeomorphology in Critical Zone studies, in what has been proposed by many scholars as a new geological epoch: the Anthropocene (Crutzen, 2006; Steffen et al., 2011; Lewis and Maslin, 2015a, 2015b).

Subsurface information is fundamental for a comprehensive understanding of the complex processes that create and modify surface features (Van Dam, 2012). Non-invasive and/or remote methods are preferred (Schrott et al., 2013; Van Dam, 2012; Viles, 2016; Aguilar et al., 2020) in studies in which accessibility to the site is restricted (i.e., remote or protected areas), the scale of the study requires this approach (i.e.,

watershed scale or larger), and/or the budget does not permit invasive methods (i.e., boreholes).

In section 3, the use of geophysical methods to study geomorphic processes and environments is discussed, with an emphasis on non-invasive methods as part of multiple method approaches.

A non-invasive methodology used to characterize the hydrological importance of a rock glacier in an alpine area is presented in section 4.

The periglacial Critical Zone is especially vulnerable to the impacts of climate change, threatening the availability of water resources. Rock glaciers are characteristic landforms in alpine environments that function as aquifers (Giardino et al., 1987; Giardino et al., 1992). The composition and internal structure of rock glaciers remains understudied (Duguay et al., 2015), thus, a clear understanding of the processes and fluid-mass pathways on and within a rock glacier has yet to be achieved. The research presented in in section 4 integrates geomorphological mapping, geological information, and geophysical investigations, to interpret the internal structure and hydrological flow connections of the Upper Camp Bird rock glacier.

The fifth section summarizes the concluding thoughts of the research presented throughout this dissertation.

1.1. References

Aguilar, R.G., Owens, R., Giardino, J.R., 2020. The expanding role of anthropogeomorphology in critical zone studies in the Anthropocene. Geomorphology 366, 107165. https://doi.org/10.1016/j.geomorph.2020.107165

Arrhenius, S., 1896. XXXI. On the influence of carbonic acid in the air upon the temperature of the ground. Philos. Mag, 41(251), 237-276.

Brown, E. H., 1970. Man shapes the earth. The Geographical Journal, 136(1), 74-85.

Crutzen, P. J., 2006. The "Anthropocene". In Earth system science in the Anthropocene (pp. 13-18). Springer, Berlin, Heidelberg.

Davis, R., 2011. Inventing the present: historical roots of the Anthropocene. Earth Sciences History, 30(1), 63-84.

Duguay, M. A., Edmunds, A., Arenson, L. U., Wainstein, P. A., 2015. Quantifying the significance of the hydrological contribution of a rock glacier–A review. In GEOQuébec 2015: Challenges from North to South, Québec, Canada.

Giardino, J. R., Shroder, J. F., Vitek, J. D., 1987. Rock Glaciers. London: Allen & Unwin, 416 pp.

Giardino, J. R., Vitek, J. D., Demorett, J. L., 1992. A model of water movement in rock glaciers and associated water characteristics. In: Dixon, J. C., Abrahams, A. D. (Eds.), Periglacial Geomorphology. Wiley, Chichester, West Sussex, pp. 159-184.

Golomb, B., Eder, H. M., 1964. Landforms made by man. Landscape, 14(1), 4-7.

Goudie, A. S., Viles, H. A., 2016. Geomorphology in the Anthropocene. Cambridge University Press.

Gutiérrez, A., Naredo Pérez, J. M., 2005. La incidencia de la especie humana sobre la faz de la Tierra (1955-2005). Universidad de Granada.

Haughton, S., 1866. Manual of geology. Longmans, Green, Reader, and Dyer.

Jacks, G. V., Whyte, R. O., 1939. The rape of the earth: a world survey of soil erosion. The rape of the earth: a world survey of soil erosion.

Lewis, S. L., Maslin, M. A., 2015a. A transparent framework for defining the Anthropocene Epoch. The Anthropocene Review, 2(2), pp.128-146.

Lewis, S. L., Maslin, M. A., 2015b. Defining the Anthropocene. Nature, 519(7542), 171.

Revkin, A., 1992. Global Warming: Understanding the Forecast. Abbeville Press, New York.

Schrott, L., Otto, J.C., Götz, J., Geilhausen, M., Otto, J.C., 2013. Fundamental classic and modern field techniques in Geomorphology–an overview. In Treatise on Geomorphology. Elsevier. pp. 6–21. doi: 10.1016/B978-0-12-374739-6.00369-9.

Shaler, N. S., 1905. Man and the Earth. Fox, Duffield.

Sherlock, R. L., 1922. Man as a geological agent: an account of his action on inanimate nature. HF & G. Witherby.

Steffen, W., Grinevald, J., Crutzen, P., McNeill, J., 2011. The Anthropocene: conceptual and historical perspectives. Philosophical Transactions of the Royal Society A: Mathematical, Physical and Engineering Sciences, 369(1938), 842-867.

Suess, E., 1862. Der Boden der Stadt Wien. Vienna: W. Braumüller.

Trimble, S. W., 1974. Man-induced soil erosion on the southern Piedmont. Soil Conservation Society of America.

Trimble, S. W., 1975. A volumetric estimate of man-induced soil erosion on the Southern Piedmont Plateau. Present and prospective technology for predicting sediment yields and sources. Publication ARS_S_40. US Department of Agriculture.

Turner, B. L., Clark, W. C., Kates, R. W., Richards, J. F., Mathews, J. T., 1990. The earth as transformed by human action: global and regional changes in the biosphere over the past 300 years. Cambridge Univ. Press.

Van Dam, R.L., 2012. Landform characterization using geophysics—Recent advances, applications, and emerging tools. Geomorphology, 137(1), pp.57-73. doi:10.1016/j.geomorph.2010.09.005.

Woeikof, A., 1901. De l'influence de l'homme sur la terre. In Annales de Géographie (Vol. 10, No. 50, pp. 97-114). Armand Colin.

2. THE EXPANDING ROLE OF ANTHROPOGEOMORPHOLOGY IN CRITICAL ZONE STUDIES IN THE ANTHROPOCENE*

2.1. Synopsis

Just as geomorphology evolved from a predominantly descriptive science to largely quantitative, a new framework for geomorphology is again required as rapidly increasing human population pushes anthropic-geomorphic processes to a dominant role in the Anthropocene. Understanding these processes requires new conceptual frameworks, interdisciplinarity, and a strong technology-assisted approach. We propose a focus on the Critical Zone as a useful conceptual framework in studies of Anthropocene geomorphology. Prior studies have assessed the Anthropocene with a focus on soils, which are generally considered the unifying thread of the Critical Zone. The Critical Zone in its entirety, however, extends from the top of the canopy to the base of the groundwater system. This concept thus permits a systems approach to geomorphology across scales, addressing the extensive role of human impact on Earth surface processes. Changing climatic conditions impact the delivery of water to the Critical Zone, causing an expansion of arid lands. Land-cover alteration is decreasing infiltration, armoring surfaces, increasing surface runoff, enhancing erosion rates, and is expected to expand in the future. Thus, the benefit of using the Critical Zone as a lens to study geomorphology will result in a broad, unified interdisciplinary study of the Anthropocene. These studies can be aided by modern technology, including drones and machine-learning applications. The trend toward technology-driven studies will continue throughout the geosciences, and geomorphology will be well-aided by its use. We

present a comprehensive review of the concept of the Anthropocene and the Critical Zone making a case for the necessity of a Critical Zone-approach to anthropogeomorphology.

2.2. Introduction

Human activities have had a growing and persistent impact on Earth for millennia (Ruddiman and Thomson, 2001; Ruddiman, 2003; Ehlers and Kraft, 2006; Szabó et al., 2010; Doughty et al., 2010; Price et al., 2011; Zalasiewicz et al., 2011; Ellis et al., 2013; Rick et al., 2013; Smith and Zeder, 2013; Glikson, 2013; Savenije et al., 2014; Arnáez et al., 2015; Fox et al., 2017; Ruddiman, 2017; Tarolli et al., 2014, 2019; Beach et al., 2015). The increasing impact has resulted in the recognition of human-driven activities that alter the surface of Earth as a geomorphic process and referred to as anthropogeomorphology. The term anthropogeomorphology was introduced by Golomb and Eder (1964). In our paper, we place anthropogeomorphology in the context of the Anthropocene and link human impact on Earth within the context of the newer title of the Critical Zone (Giardino and Houser, 2015). We conclude by presenting our view of where the discipline of geomorphology is being driven.

2.2.1. Recognition of humans' role as geomorphic agents

Marsh (1898) warned of future challenges resulting from anthropogenic environmental changes long before their formal consideration: “It is still too early to attempt scientific method in discussing this problem … human action has been or may be the most injurious or most beneficial in its influence upon the physical conditions of

the earth we inhabit" (Marsh, 1898, p. 6). Though discussed in an observational, qualitative manner, the warnings are clear:

> But man is everywhere a disturbing agent … Indigenous vegetable and animal species are extirpated, and supplanted by others of foreign origin, spontaneous production is forbidden or restricted, and the face of the Earth is either laid bare or covered with a new and reluctant growth of vegetable forms, and with alien tribes of animal life … [these changes are] insignificant in comparison with the contingent and unsought results which have flowed from them (Marsh, 1898, p. 17).

Today, these challenges are widespread and the subject of much quantitative, scientific literature. Landscape modification through excavation, production, and storage of waste materials in landfills, resource exploitation, and expansion of the built environment results in the deliberate transport of 57,000 million tonnes of sediment annually (Mt/yr), nearly three times the amount transported by fluvial processes (Price et al., 2011). Fig. 1 shows the volume of sediment transported by major rivers for the various continents. Land-cover alteration and mining operations have also resulted in modified fluvial systems and depressed groundwater supplies (Mayer, 1972; Bull, 1973; Bull and Scott, 1974; Lagasse et al., 1980; Morgan-Jones et al., 1984; Schlesinger et al., 1990; Lee et al., 1993; Klondof, 1994; Mossa, 1995; Mossa and McLean, 1997; Zhang and Schilling, 2006; Nie et al., 2011; Suriya and Mudgal, 2012; Wijesekara et al., 2012; Nugroho et al., 2013; Ahiablame et al., 2017), and altered albedo, contributing to anthropogenic climate change (Claussen et al., 2001; Matthews et al., 2003; Myhre and Myhre, 2003; Findell et al., 2007; Li et al., 2013; Abera et al., 2019; Hu et al., 2019; Münch et al., 2019). Replacement of native vegetation with agricultural fields is a leading cause of such alterations, coupled with expanding urbanization worldwide.

Introduction of domestic, synanthropic and invasive species have compacted soil, decreasing infiltration and altered vegetative cover. Estimates of the amount of ice-free land affected by human action varies from 20% to 100% (Hooke, 2012; Wohl, 2013). Even land left untouched is not immune to the effects of regional land-cover change; patches of undeveloped land have been fragmented to 990,000 bodies of land roughly a square kilometer in area, causing habitat to disconnect and fragmentation of natural geomorphic processes (Duncombe, 2019).

The realization that the collective actions of humans had significant effects on Earth inspired many observers, like Marsh, to study and discuss the role of human beings as a new geologic force (i.e. Suess, 1862; Haughton, 1866; Arrhenius, 1896; Woeikof, 1901; Shaler, 1905; Gilbert, 1917; Sherlock, 1922; Jacks and Whyte, 1939Brown, 1970; Trimble, 1974; Trimble, 1975; Nir, 1983; Turner et al., 1990; Revkin, 1992; Gutiérrez and Naredo Pérez, 2005; Davis, 2011) and distinguished the need to identify and name the timeframe of these occurrences accordingly (Fig. 2). The Anthropocene, proposed as a new epoch, indicates the time during which human influence became a dominant force on Earth (Crutzen, 2006; Steffen et al., 2011; Lewis and Maslin, 2015a, 2015b).

Figure 1 Volume of sediment transported by major rivers for various continents. Compiled from Chen et al. (2008) and Mouyen et al. (2018). Anthropogenic processes move 57,000 Mt/yr of sediment, an amount significantly higher than the combined effects of major rivers around the world. Reprinted with permission from Aguilar et al., 2020.

Ancient and modern anthropogenic modifications of the environment have inspired the creation of terms such as Noösphere (i.e., the sphere of human thought), Anthroposphere (i.e., the sphere of human environment), Technosphere (i.e., the sphere of technological advancements) and Archaeosphere (i.e., used interchangeably with Anthroposphere and Technosphere), to refer to a human-dominated environment. These terms encompass human modification of the natural environment through milestones related to human evolution, such as the discovery of fire, the use of tools, engineering of the built environment, anthropogenically driven faunal extinctions, land-use change and global environmental change (Doughty et al., 2010; Smith and Zeder, 2013; Glikson, 2013).

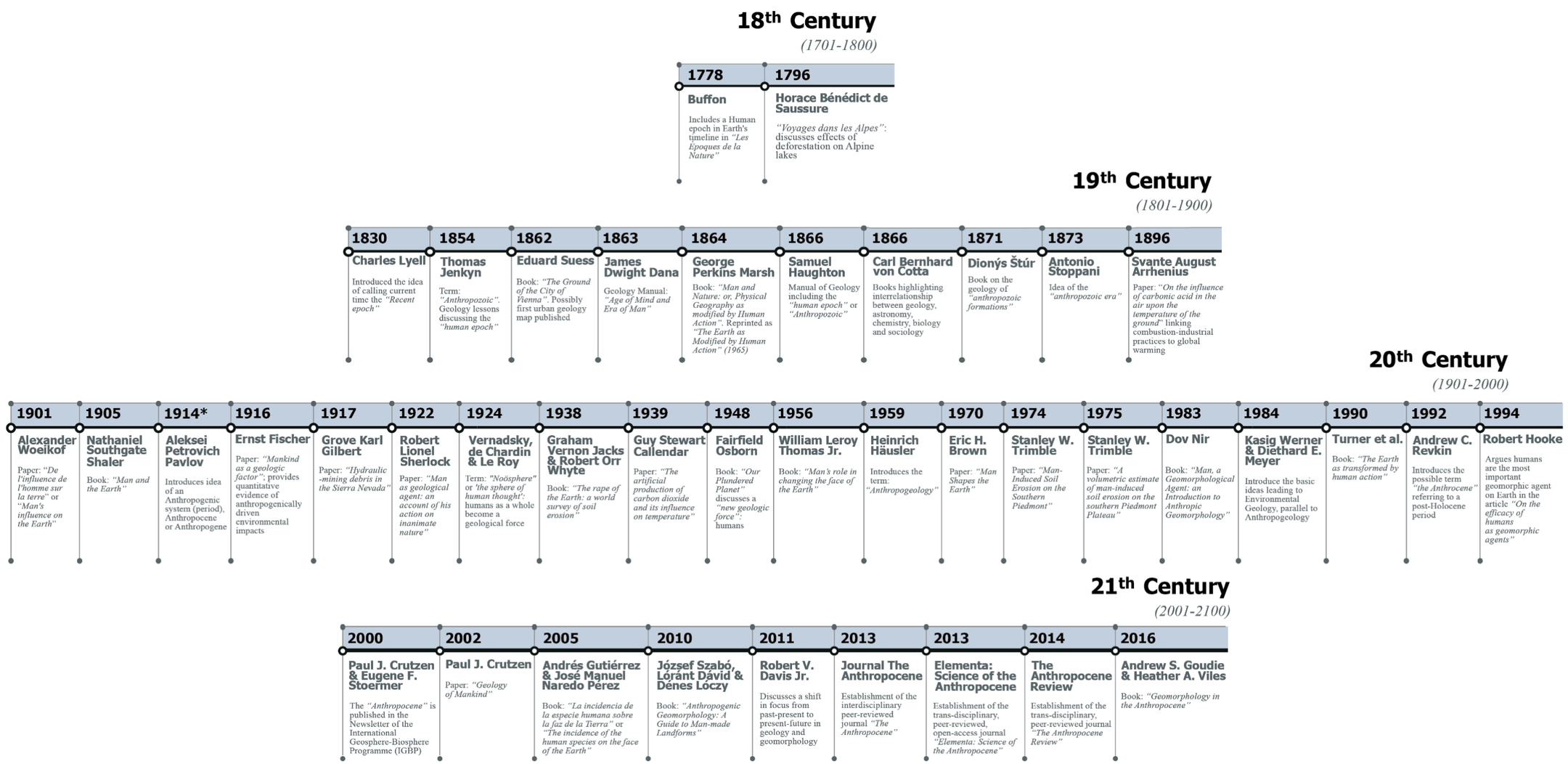

Figure 2 Timelines highlighting relevant publications related to anthropogeomorphology since the eighteenth century. *Häusler (2017) mentions 1914; Rull (2017a, 2017b) places it in 1922. Reprinted with permission from Aguilar et al., 2020.

The starting point for humans'' role as a primary force, however, is debatable. As Fox et al. (2017, p. 206) argue, "The anthroposphere … has evolutionary roots going back to the origins of our species, even if its effects on the Earth System may have only become glaringly obvious within the last 10,000 years or later." The time of initiation of the Anthropocene could be based on criteria from the climatic, geomorphological, sedimentological, or ecological record (Schlütz and Lehmkuhl, 2009; Price et al., 2011; Brown et al., 2013a, 2013b; Lewin and Macklin, 2014).

Goudie and Viles (2016) traced studies related to the effects of anthropogenic interventions in the environment back to 1796, citing a study by de Saussure (1796) in the Alps. Other studies and mention of the "human epoch" or "Anthropozoic" (i.e., Buffon, 1778) predate the introduction of terms like anthropogeology (Häusler, 1959), anthropogeomorphology (Golomb and Eder, 1964), and the Anthropocene (Crutzen, 2002), showing that the underlying concepts have been discussed repeatedly in the past two centuries and even farther back into Classical Antiquity (Beach et al., 2019a) but with different terms for different human impacts and time frames.

Controversy surrounds the acceptance of the role of humans as geologic agents; although wide acknowledgment of the impact of human activities on the environment is recognized, no consensus on the magnitude of such impacts is accepted by all. For example, Visconti (2014) restricts the effects of anthropological interventions to the near-surface, implying a small-scale significance and also a short-term manifestation of human-induced impacts on the landscape, in accordance with Moore's (2013) views.

This view is challenged, however, by Häusler (2017) who provides a compilation of quantitative evidence of humans as geologic and geomorphologic agents citing significant changes in rates of erosion and deposition, anthropogenic seismic activity, comparisons of human energy production/release to natural processes, and prevalence of anthropogenic "fossils" such as concrete structures and plastics. In addition, Hooke (1994, 2000) provides a qualitative and quantitative analysis of humans acting as geomorphic agents, focusing in Earth-moving activity. Examining the combined effect of intentional and unintentional Earth-moving, Hooke concludes that humans are responsible for contributing more to this measure than any other geomorphic agent.

Price et al. (2011) bring attention to impacts on the surface and subsurface including habitation and infrastructure, extraction, processing and wasting of natural resources, artificial ground, excavations, and ground shifting. They suggest identifying a "shallow zone of human interaction" in which all these processes occur. Here, the spheres of Earth interact with each other (Fig. 3), and resources essential for human existence are found.

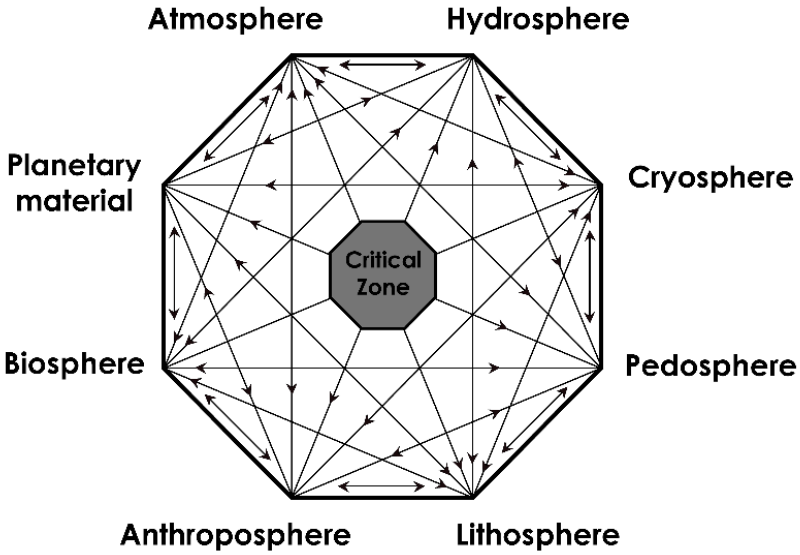

Figure 3 The spheres of Earth interact in an area called the Critical Zone. Modified from Giardino and Houser (2015). Reprinted with permission from Aguilar et al., 2020.

2.2.2. The Anthropocene proper

Throughout history, times of dramatic change, noted by appearance or disappearance of species, have been used to demark the beginning or end of specific time periods. We stand at the brink of such dramatic change today; climate change and land-cover alteration, both propelled by humans, are altering the system of Earth yet again by changing weather patterns, intensifying storm events, and threatening biota (Díaz et al., 2020). As human population continues to increase, the rate of geomorphic activity increases and creates significant challenges (Segura and Booth, 2010). Understanding the full scope of human impact on the surface of Earth requires consideration of the direct alterations to the natural environment, effects of prior human impact, attenuation of subsequent human impact through various feedback mechanisms,

and modification of connectivity of geomorphic systems (Vanacker et al., 2005; Chin et al., 2013; Jefferson et al., 2013; Wohl, 2013; Poeppl et al., 2017).

Discussion regarding the beginning of the Anthropocene and the formal acknowledgement as a geologic epoch draws a variety of views. Some scholars oppose the creation of a new geologic epoch focusing on human impacts, arguing the impacts of human actions will leave minimal evidence in the sedimentary record (Ruddiman, 2003; Autin and Holbrook, 2012; Gibbard and Walker, 2014; Visconti, 2014; Finney, 2014; Walker et al., 2015; Baskin, 2015; Head and Gibbard, 2015; Edwards, 2015; Gibbard and Lewin, 2016; Finney and Edwards, 2016; Ruddiman, 2017; Ruddiman, 2018). Lewin and Macklin (2014) suggest that the formalization of the Anthropocene epoch is subjective, of no practical value, and possibly irrelevant for geoscientists. Proponents of this view argue that the term is useful for environmental awareness and political action but not for the geosciences (Autin and Holbrook, 2012; Visconti, 2014; Edgeworth et al., 2015; Finney and Edwards, 2016; Rull, 2017a, 2017b). Still others argue the Anthropocene should be used as a general and flexible term (Edgeworth et al., 2015; Rull, 2017a, 2017b; Ruddiman, 2018).

Among those who support defining the Anthropocene, how to define the beginning of this human-dominated time remains undecided (Zalasiewicz et al., 2010; Doughty et al., 2010; Steffen et al., 2011; Glikson, 2013; Lewin and Macklin, 2014). Some scholars suggest the boundary should be placed as early as late Pleistocene, citing the role of humans in the extinction of large mammals (Doughty et al., 2010). Other scholars, however, suggest placing the boundary a few thousand years later coinciding

with significant human migrations at the beginning of the Holocene (Smith and Zeder, 2013). And, still other scholars suggest pushing the starting date forward to somewhere between 8000- and 2000 yr ago concurring with technological advances in agricultural practices (Ruddiman and Thomson, 2001; Ruddiman, 2003; Fuller et al., 2011; Certini and Scalenghe, 2011; Beach et al., 2015, 2019a, 2019b). Several other researchers suggest even more recent dates, including a potential marker coinciding with the Industrial Era in the eighteenth and nineteenth century (Crutzen and Stoermer, 2000), to a boundary coinciding with the detonation of nuclear weapons in the mid-twentieth century and consequent radionuclide fallout. Table 1 provides a summary of some of the events that have been proposed as markers of the beginning of the Anthropocene.

Table 1 Summary of some of the events proposed as markers of the Anthropocene. Reprinted with permission from Aguilar et al., 2020.

Beginning of the Anthropocene	**Event**	**Authors**
Late Pleistocene ~13,800 BP	Megafaunal extinctions Human-driven climate change	Doughty et al., 2010
Pleistocene–Holocene boundary 11,700 BP ~11000-9000 BP	Domestication of flora & fauna Human migrations Significant human niche construction	Smith and Zeder, 2013
8000-5000 BP	Agriculture/technological innovations in farming Global atmospheric change	Ruddiman and Thomson, 2001 Ruddiman, 2003
2000 BP	Anthropogenic land surface alteration; anthropogenic soils	Certini and Scalenghe, 2011 Beach et al., 2015, 2019a, 2019b

Table 1 Continued. Reprinted with permission from Aguilar et al., 2020.

Beginning of the Anthropocene	Event	Authors
1610 CE	New–Old World collision event Low point of CO_2 in glacier ice	Lewis and Maslin, 2015a, 2015b
1750-1800 CE Industrial Era	Atmospheric CO_2 and CH_4 concentrations above previous longer-term values	Crutzen and Stoermer, 2000
1950s AD Or post-1950s	Artificial radionuclides	Zalasiewicz et al., 2010 Steffen et al., 2011 Rose, 2015 Lewis and Maslin, 2015a, 2015b

Several scholars propose the creation of subdivisions of the Anthropocene to represent different milestones in the history of anthropogenic disturbances on natural processes. For example, Glikson (2013) divides the Anthropocene into four stages: Stage A: Early Anthropocene about two million years ago, coinciding with the discovery of fire; Stage B: Middle Anthropocene ~10,000 yr BP, a time in which agriculture became significant; and Stage C: Late Anthropocene ~1750 ADCE, corresponding with the Industrial Era. Building on Glikson's (2013) sub-divided Anthropocene, Kunnas (2017) proposed his four stages: The Early Anthropocene: 5000–14,000 yr BP, to highlight the impact of the domestication of animals and large-scale agriculture; the first acceleration phase of the Anthropocene: ~1750 ADCE, marking the beginning of fossil fuel combustion practices (i.e., the Industrial Revolution); the post-1950 Great Acceleration: a time recorded in the global record as nuclear bomb testing, which has resulted in the

accumulation of radioactive materials in sediments; and the potential labels “good Anthropocene” or the “bad Anthropocene”, which according to Kunnas (2017) would be selected in accordance with the outcomes of current times.

Goudie and Viles (2016, p. 13), in their extensive review of the Anthropocene, show the timelines of the Anthropocene in four sub-sections: Palaeoanthropocene: from 7000 BP to c. 1750; The Industrial Era: from c. 1750 to c. 1945; The Great Acceleration: from c. 1945 to c. 2000; and Earth System Stewardship from c. 2000–present. Brown et al. (2017) provide a different perspective, arguing that anthropogenic activities impact different environments at varying scales.

The Anthropocene Working Group (AWG) is tasked with developing a formal proposal for the definition of the Anthropocene as a chronostratigraphic unit, which they plan to finalize by 2021 (Subramanian, 2019). The AWG is composed of 34 members and is part of the Subcommission on Quaternary Stratigraphy (SQS), a constituent body of the International Commission on Stratigraphy (ICS). For example, the ICS has been deliberating on the Anthropocene Epoch and has designated three Holocene Stages: the Greenlandian, the Northgrippian, and the Meghalayan. The Meghalayan, which starts with cultural shifts coinciding with large scale drought, is also referred to as the 4.2 ka event (Walker et al., 2018).

Initially, the AWG focused on compiling evidence supporting the thesis that anthropogenic interventions could produce distinctive and long-lasting impacts in the stratigraphic record. In spite of opposition to formally defining the Anthropocene, in May of 2019 the AWG published the official stance and indicated the Anthropocene

should be defined by a Global-boundary Stratotype Section and Point (GSSP or 'golden spike'), placing the lower boundary in the 1950s, a date supported by Zalasiewicz et al. (2015, 2017). This stance has been strongly contested by those who insist that impacts prior to the 1950s cannot be considered under the framework used by the AWG (Ruddiman, 2018). At the writing of this paper, widespread agreement among scientists regarding the date and formalization of the Anthropocene remains unattained.

2.2.3. The Critical Zone

As stated by Price et al. (2011), understanding the full scope of human influence on Earth necessitates identification of a "shallow zone of human interaction". To this end, the Critical Zone as a conceptual framework for studying Anthropocene geomorphology is ideal. Soil is generally considered the unifying thread of the Critical Zone, but our proposal of the Critical Zone as a conceptual framework is not a proposal of a soil framework. Prior studies have taken such an approach to the Anthropocene (Richter, 2007; Certini and Scalenghe, 2011; Edgeworth et al., 2015; Richter et al., 2015; Lane et al., 2019), and such a recommendation would hardly be novel. The Critical Zone in its entirety extends from the top of the canopy to the base of the groundwater system (NRC, 2001; Giardino and Houser, 2015). This framework thus permits a systems approach to Anthropocene geomorphology, addressing the extensive role of human impact on interrelated surface and near-surface processes.

The concept of the Critical Zone, as proposed by the US National Research Council (2001), is not a new idea. Since the 1950s numerous geomorphologists (Strahler, 1950, 1952a, 1952b; Culling, 1957; Hack, 1960; Hack and Goodlett, 1960;

Chorley, 1962; and Chorley and Kennedy, 1971) explored the benefits of conducting geomorphologic studies from a general-systems-theory perspective. Encouraging a departure from Davis'' ideas, Chorley (1962, p. B1) proposed an open-system framework "… focusing of attention on the possible relationships between form and process", recognizing "… the multivariate character of most geomorphic phenomena", and directing "… attention to the heterogeneity of spatial organization". Systems thinking gained traction in geosciences because it leads to a better representation and consequent understanding of complex processes, while facilitating better interconnectivity with other scientific fields, in theoretical and applied approaches. Thus, the conceptual framework of geomorphic systems has significant overlap with Critical Zone Science (CZS).

The Critical Zone Observatory (CZO) program was created in 2005 with financial support from the US National Science Foundation (NSF), following a suggestion by the US National Research Council (NRC, 2001) to promote the study of processes, pathways, and feedbacks on the surface of Earth (Ashley, 1998). The definition of the Critical Zone has varied since the creation of the CZO program, in part because of the broadness of the original definition, the multidisciplinary nature of the Critical Zone research, and the need to incorporate environments that were not clearly initially included (Giardino and Houser, 2015). The Critical Zone is described as a thin, heterogeneous, changing, complex, and porous layer of Earth, comprising surface and subsurface environments, and which hosts essential resources to sustain life on our planet (NRC, 2001; The Critical Zone). Furthermore, this area hosts economically

important resources such as metallic and nonmetallic minerals, and what some call the "energy of the future" (renewable resources) that can be tightly linked to the Critical Zone, as solar panel farms and wind turbines for example, are spread throughout the surface of Earth.

Critical zone research is interdisciplinary and transdisciplinary (Sullivan et al., 2017; Giardino and Houser, 2015). Fig. 4 shows the interconnectivity between some of the disciplines involved in the study of the Critical Zone. According to Sullivan et al. (2017), contributions from disciplines, such as ecology and biology, must also be included in Critical Zone research, as life-sustaining resources as well as many nutrient-producing and microbe-driven weathering occur within this near-surface area. Anderson et al. (2007) and Brantley et al. (2007) refer to the Critical Zone as a "weathering engine" or "weathering reactor" in which chemical, physical, biological, and geological processes act together through time, at millimetric to global scales, producing outputs that influence responses from the atmosphere, the hydrosphere, and the pedosphere. Earth systems interact with each other through diverse pathways in the Critical Zone in a complex, dynamic way in which inputs of energy and mass are transformed, leading to the production of sediment, and life-sustaining nutrients that move with water and other agents of transport (Banwart et al., 2013; Anderson et al., 2004; Brantley et al., 2006; Giardino and Houser, 2015). In general, Critical-Zone Science focuses on coupled processes, energy fluxes, and connectivity between systems, occurring in what Brantley et al. (2017) call the dynamic "living skin" of Earth.

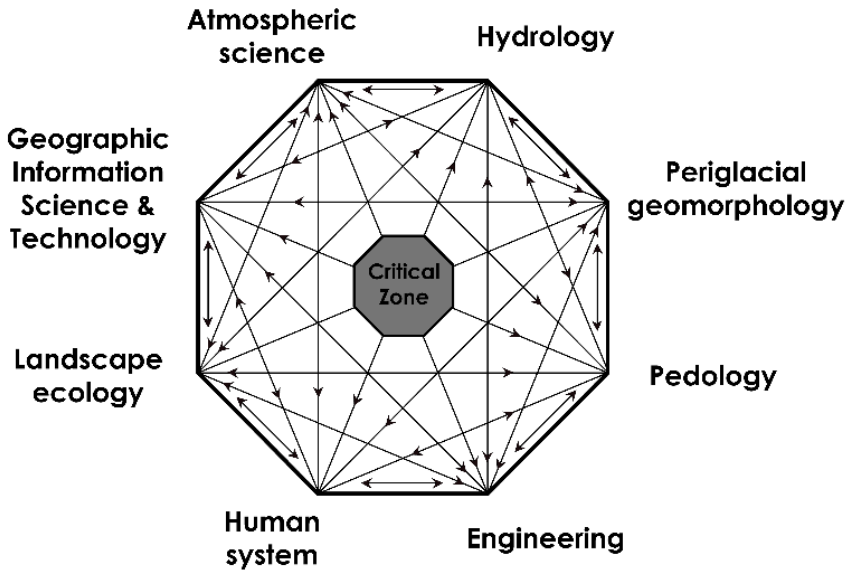

Figure 4 Interactions between some of the relevant disciplines and fields concerned with the Critical Zone. Modified from Giardino and Houser (2015). Reprinted with permission from Aguilar et al., 2020.

Minor et al. (2019) highlight the benefits of using a Critical Zone conceptual approach to biogeographical and ecological studies, while also presenting an integrated model of transfer of matter and energy via diverse pathways across subsystems of Earth. The approach presented by Minor et al. (2019) validates how Critical Zone Science can benefit from borrowed methodologies and tools traditionally used in biogeography and ecology. This combined approach could foster understanding and prediction of the effects of global warming and change in land cover, particularly on the hydrosphere and the biosphere.

By 2015, 64 Critical Zone observatories had been established around the world (Fig. 5) (Giardino and Houser, 2015). Critical Zone Observatories (CZOs) are chosen to study a particular environment by an interdisciplinary team of researchers. The goal is a compilation of an extensive record of processes and interactions generated by multiple sampling techniques over varying temporal and spatial scales. These records are analyzed using multidisciplinary approaches, allowing the generation of integrated models to understand the complex processes occurring in the Critical Zone of Earth (Banwart, 2013).

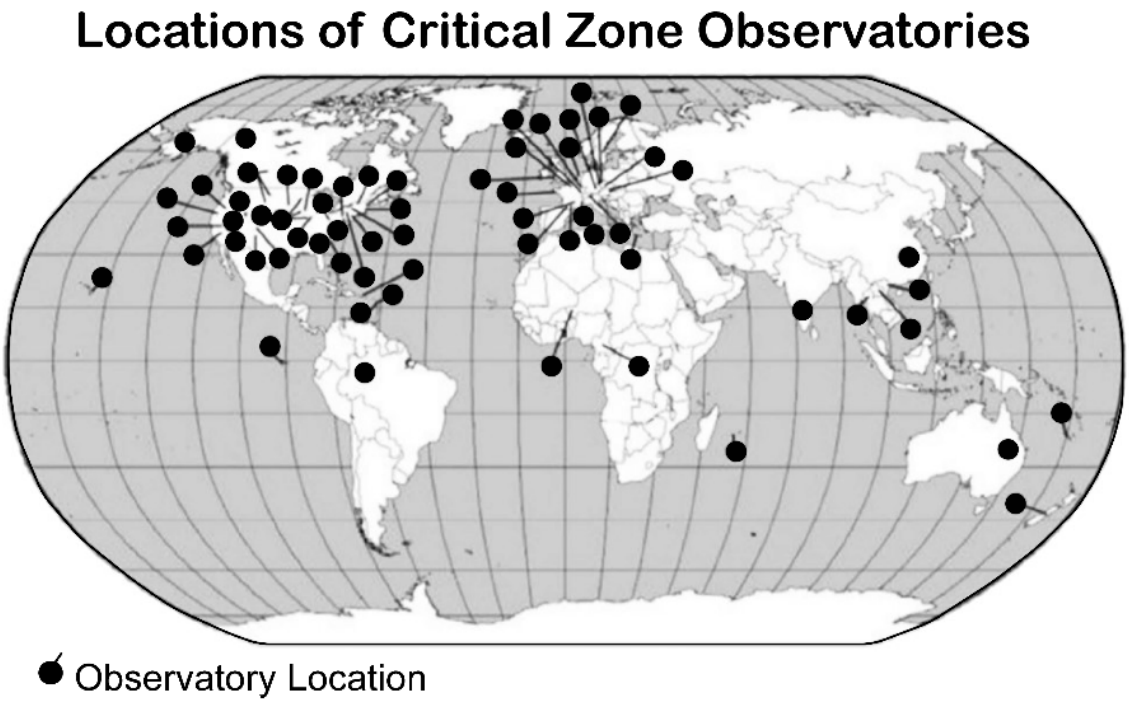

Figure 5 Distribution of the 64 CZOs around the world. Modified from Giardino and Houser (2015). Reprinted with permission from Aguilar et al., 2020.

Critical Zone Observatories are located in different environments to facilitate the study of processes controlled by location-dependent factors (i.e., climate, slope, geology). Examples of these observatories in karst environments include those in France (Jourde et al., 2018) and in Southwest China (Zhang et al., 2019). Hillslope processes are studied at the CZOs in Luquillo, Puerto Rico (Dialynas et al., 2015), the Adirondack Mountains of New York, Boulder Creek, Colorado, Susquehanna Shale Hills, Pennsylvania, and the southern Sierra Nevada, California. The CZOs at Damma Glacier, Switzerland, and Bonanza Creek, Alaska, focus on glacial and periglacial environments. Coastal environments are one of the foci of the Eel River Critical Zone Observatory (ERCZO), California (criticalzone.org) and the Christina River Basin CZO, Delaware/Pennsylvania (Aufdenkampe et al., 2012). Intensively Managed Landscapes (IML-CZO) are studied in the midwestern United States at the Minnesota River, Clear Creek, and Sangamon River watersheds, which enables researchers to study fluvial processes in this area (Lewis et al., 2014).

One must go beyond interdisciplinarity when studying Critical-Zone processes to truly understand the CZ structure and evolution. One must approach a CZO as an entity, instead of focusing on its individual components, to move toward a sustainable future (Brantley et al., 2017). It is interesting to note that these ideas are similar to those proposed by many geomorphologists for more than a century such as Chorley (1960, p. B1) who argued that geomorphologists should “direct attention to the whole landscape assemblage”. Because the Critical Zone approach has provided a coherent framework for studying the interactions between processes from an interdisciplinary perspective, we

propose a Critical Zone approach be used to study Anthropocene geomorphology for its role as an interface between several Earth spheres and its inherent perspective on the system.

2.2.3.1. Anthropocene-epoch impacts on Critical Zone

As an interface between Earth spheres, the Critical Zone is particularly susceptible to a cascade of changes induced by anthropogenic influence in any one component. In addition to a changing climate, the Anthropocene has introduced new forcings on these sensitive environments through arrival of domestic and invasive animal populations, alteration of land cover, and soil degradation.

2.2.3.1.1. Domestic and invasive populations

Animals are known to influence geomorphic processes through actions, such as burrowing, digging, trampling, damming, and hillslope loading (Butler, 2018), and cause direct alteration to the Critical Zone. Human influence on and management of animal populations has modified the rate and intensity of these processes. Grazing and trampling by domesticated hoofed animals induces increased sediment flux in fluvial systems and accelerated erosion of fine sediment, while also impacting water infiltration and gully erosion (Neff et al., 2005; Butler, 2013; Waters et al., 2016).

Human exploration introduces exotic species to new geographic regions and with them, new geomorphic impacts (Butler, 2006). Introduction of burrowing rodents to sub-Antarctic islands free of natural predators led to removal of sediment from solifluction lobes and conduits for warm water and air, inducing accelerated soil erosion (Eriksson and Eldridge, 2014). Likewise, removal or reduction of populations alters geomorphic

processes by reducing the role of one population and increasing the role of its competitors. Reduction in predators, for example, has led to an increase of deer populations in North America and their impact on riparian vegetation (Seagle and Liang, 2001). Trapping of the North American beaver altered fluvial systems by dramatically reducing sediment storage in beaver ponds and changing flow regimes (Marston, 1994; Butler, 1995; Butler and Malanson, 2005; Pollock et al., 2007; Green and Westbrook, 2009).

2.2.3.1.2. Alteration of the land cover

As early as the mid-Holocene, expansion of farmland led to alluvial adjustment of proximal rivers (Brown et al., 2013a, 2013b). With the expansion of agriculture came changes to hydrology and rates of sedimentation, including an increase in fine-grained anthropogenic alluvium and lacustrine sedimentation (Macklin et al., 2014; Beach et al., 2015). Early alterations to landscapes by deforestation and agricultural practices are thought to have modified ancient soil horizons so that the start of the Anthropocene can be distinguished by changes in paleosols (Certini and Scalenghe, 2011; Stephens et al., 2019). Modern urbanization alters the rates of geomorphic processes (Simon and Rinaldi, 2006), introduces hybrid urban landforms (Dixon et al., 2017) and reduces the extent of the natural environment (El Banna and Frihy, 2009). Fluvial systems adjust to direct effects of channelization, dam construction, and channel diversion as well as changes in watershed levels, such as land-cover change, riparian habitat destruction, and mining (Marsh, 1864; Thomas, 1956; Williams and Wolman, 1984; Butler, 2006; Gregory, 2006; Wohl, 2006, Brown et al., 2013a, 2013b; Skalak et al., 2013).

2.2.3.1.3. Soil degradation

The abundance of human-derived material during the Anthropocene has produced new forms of sediment. Often called legacy sediment, it drives lateral, longitudinal, vertical, and temporal connectivity in fluvial systems and impacts water quality (James, 2013; Wohl, 2015). The Anthropocene will undoubtedly be marked by sedimentological markers made of materials like plastic, concrete, aluminum, and other substances unknown prior to human influence. Research into geomorphological impact of specific sediments, such as microplastics, is growing rapidly. Microplastics, defined as plastic remnants under 5 mm in diameter, are washed into the marine environment with other sediments. High levels of microplastics have been detected in major inland lakes, which should logically lead to investigation of rivers, because rivers are a main source of lake and marine plastics (McCormick et al., 2014).

Microplastics have been found in sediments of the St. Lawrence River (Castaneda et al., 2014) at an average density of 13,759 per m^2, with a maximum density of 136,926 per m^2. Fish in these localities have been shown to have microplastics in their bellies, implying a health threat to the fish and to those who would eat them. The prevalence of microplastics is likely to increase with proximity to urbanization. McCormick et al. (2014) tested for microplastics in an urban river upstream and downstream of Chicago and found that microplastic concentrations increased from 1.94 per m^3 upstream of Chicago to 17.93 per m^3 downstream. They found that the microplastics also created new biota assemblages for bacteria, influencing ecological nuances of the river. Additionally, wastewater treatment sites are known sources of

microplastics in the form of microbeads, because they remove microbeads during treatment, returning them to the environment (Castaneda et al., 2014; Rezania et al., 2018).

Current research in microplastics focuses on water quality and ecological disturbance, but the geomorphological implications have not been considered. Other assessments of anthropogenic sediment acknowledge their influence on the geomorphic system (Gill, 1996; Maholland, 2002; Kaufmann and Hughes, 2006; Ramos-Scharrón and MacDonald, 2007; James, 2013; Jordan et al., 2016). Vörösmarty et al. (2003) examined the prevalence of anthropogenically-derived sediment in large-river impoundments. Langedal (1997) found that rates of floodplain sedimentation along the Knabeåna-Kvina rivers in Norway increased from 0.5 mm to 4.3 mm annually because of deposition of molybdenum mine tailings. Research of the role of human activity on overall sedimentation processes remains a relevant undertaking in geomorphology. Additionally, much research remains to be done investigating the role and pathways of specific anthropogenically-sourced sediment in geomorphic systems.

2.3. Anthropogeomorphic landforms and processes in the Critical Zone

We have highlighted the importance of the Critical Zone in consideration of Anthropocene geomorphology because the Critical Zone is the interface between various Earth subsystems. We now turn our attention to landscapes altered by humans to the point that they may be considered anthropomorphic landscapes. Anthropogeomorphology as a process presents a direct long-term or permanent

anthropogenic alteration of the Critical Zone, altering the geosphere, hydrosphere, and biosphere at or near the various interfaces.

Hooke et al. (2012) estimates that humans have modified over 50% of the land surface of Earth, reducing ecosystem services that are provided, seemingly for free, from the plants, animals, insects, and microbes all sharing with humans. In the last century, powerful technologies have enabled people to accelerate this process. Hooke (1994, p. 845) remarked that, "One might ask how long such rates of increase can be sustained and whether it will be rational behavior or catastrophe that brings them to an end."

Estimates of the amount of ice-free land affected by human action vary from 20% to 100% (Hooke et al., 2012; Wohl, 2013). These changes stem from human action involving moving sediment or changing sediment fluxes, and many have indirect consequences that extend beyond the immediate spatial and temporal effects (Hooke et al., 2012). The role humans play as the dominant geomorphic agent on Earth (Hooke, 1994; Szabó, 2010) stems from a demand for resources to satisfy a skyrocketing population — a demand beyond what can be sustained long-term. Over the past century, world population has increased 6-fold, croplands of the world have almost doubled, the area of pasture has increased by ~75%, and tropical forests acreage has decreased by ~25%. Similarly, almost all of the major reservoirs of the world were constructed during the past sixty years (Walling, 2008). Regions of undeveloped land have been fragmented to 990,000 bodies of land roughly a square kilometer in area, causing habitat disconnect and fragmentation of natural geomorphic processes (Duncombe, 2019).

It is difficult to accurately determine how much of landscape alterations are the result of human activity alone, natural processes alone, or a combination of natural processes that have been modified by humans (Hooke, 1994, 2000). Hooke (1994) estimates that on a worldwide-basis, humans move more of the planet around (about 45 gigatons annually) than do rivers, glaciers, oceans, or wind. As a comparison, he estimated that meandering rivers may move about 39 gigatons of sediment a year. Other researchers (Hooke, 1994, 2000) have estimated that rivers deliver about 24 gigatons of sediment to the oceans each year. This enormous volume is aided by human activity. Soil erosion from agricultural fields, built environment construction sites, and other sources contributes significantly to sediment loads in rivers (Hooke, 1994; Montgomery, 2007). Changes in sediment load have many important implications. For example, changes in sediment flux to oceans will result in alterations to global biogeochemical cycles (Walling, 2008). Knowing the role and volume of human-derived sediment relative to the global sediment transport flux is useful when planning future land development. In addition to impacts on geomorphological processes, ecosystem service loss through anthropogenic biogeochemical cycles might be predicted and thus mitigated in advance.

On one hand, it is well-established that human activities have increased the volume of sediment by soil erosion (Rosewell, 1996; Syvitski et al., 2005; Kao and Milliman, 2008; Mouyen et al., 2018), and on the other hand, sediment transport by rivers has often decreased because of human activity (Syvitski et al., 2005; Walling, 2006; Naik and Jay, 2011; Wang et al., 2016). Determining whether humans move more

sediment than a combination of other geomorphic processes is difficult because the indirect effects of human activities are far-reaching. The global sediment discharge to the ocean remains unknown, and its measurement remains a challenge, because it requires continuous monitoring of suspended and bedload sediment transport at the mouth of every river, which is difficult and expensive (Syvitski, 2008; Mouyen et al., 2018).

The impact of anthropogenic influence on landscapes is not merely comparable to other geomorphic processes, but surpasses their effectiveness (Hooke, 1994; Szabó et al., 2010). In the Anthropocene, humans are a dominant part of the natural world (Church, 2010; Thornbush and Krakauer, 2017), and their influence should be considered as geomorphic agents, not as external forcing factors. Thus, in the following sections, we discuss anthropogenic landforms in the context of various environments, which become long-term or permanent features of the geomorphic landscape.

2.3.1. Anthropogeomorphic landscapes in the coastal environment

Coastal systems are naturally dynamic in that changes that take place in one element of this system bring about change in others (Davis and Barnard, 2000). In the Anthropocene, however, the adjustments of coasts to anthropogenic climate change are more intense and frequent than before. Global warming is playing a major role in this change as evidenced by the United Nations' Intergovernmental Panel on Climate Change (IPCC) when they stated in 2019:

> Global warming has already reached 1°C above the pre-industrial level, as a result of past and current greenhouse gas emissions. Overwhelming evidence suggests that this is resulting in profound consequences for ecosystems and humans. The ocean is warmer, more acidic, less productive, and more energetic

> as tropical storms get more destructive. Melting glaciers and ice sheets are causing sea level rise, and coastal extreme events are becoming more severe (IPCC, 2019, p. 1).

In addition to indirect alterations to coastlines resulting from climate change, humans directly alter the coastal landscape by efforts to stabilize the natural environment and by constructing new built environments. In both situations, new geomorphic landforms are created as part of the natural environment, and these human-created landforms remain as permanent fixtures.

Anthropogeomorphic features intended to stabilize coastal environments change pre-existing geomorphic processes, often leading to degradation (Davis and Barnard, 2000; Feagin et al., 2010; Bernatchez et al., 2011). As Feagin et al. (2010) explain, the human idea to stabilize a natural environment is to erect hard, impervious structures intended to hold the line against environmental adjustment rather than managing the extent and succession of native vegetation. In the United States, the former approach on barrier island systems leads to patchy vegetative stabilization and heightened erosion. For example, the construction of the seawall along the Gulf Coast side of Galveston Island has resulted in the disappearance of beaches in front of the seawall (Fig. 6) and accelerated erosion where the sea wall does not exist (Giardino et al., 1987).

Figure 6 The seawall along Galveston Island, Texas. Note the lack of a sand beach in front of the seawall. (Photo by J. Giardino, 1988). Reprinted with permission from Aguilar et al., 2020.

Coastlines take on a distinctly anthropogenic nature with the addition of structures intended to improve the coastal environment. Many of these structures are intended to disrupt the longshore current or wave energy. Jetties and groins protrude perpendicular from coastlines and modify coastlines. They increase the accumulation of sediment in the updrift direction and deplete it in the downdrift direction.

Seawalls and breakwaters are built parallel to shorelines, with seawalls against the land and breakwaters in open water. Both introduce new long-term positive relief structures to coasts. Breakwaters further modify the coastal environment by disrupting incoming wave patterns, thus, altering longshore drift and wave erosion processes. Seawalls also protect against wave erosion by armoring the shoreline and subsequently stabilizing the shoreline with a hard structure. Unfortunately, in some instances, such as a storm-surge, the seawall can act as a dam and may prolong flooding if the structure is breached.

Efforts to reduce reliance on fossil fuels have led to efforts to harness tidal energy, making tidal barrages a feature of many coastal inlets. Effects of these and other coastal engineering features are summarized in Fig. 7.

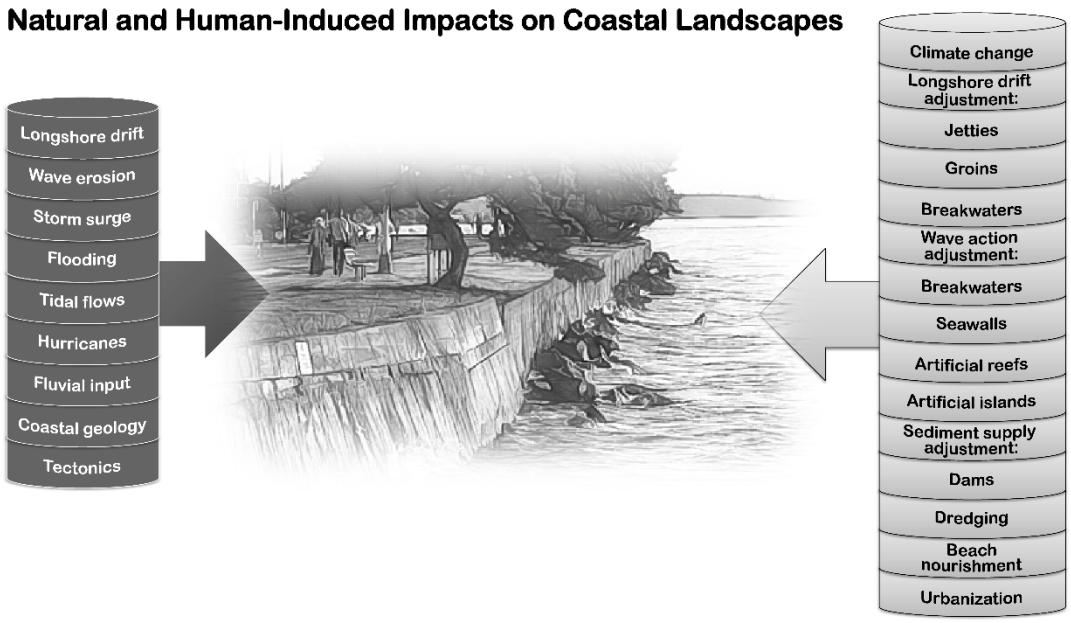

Figure 7 Natural induced impacts (left) and anthropogenic impacts (right) on coastal landscapes. Reprinted with permission from Aguilar et al., 2020.

Adjustments to the submarine coastal environment are equally prominent. Offshore dredging has created bathymetry alterations visible even decades after the operation (Li et al., 2019), and beach renourishment or artificial island construction that often follows creates entirely new coastal environments (Giardino et al., 1987). Artificial reefs are constructed as habitat restoration or for surf production and in turn modify wave patterns.

On the Atlantic and Gulf Coast regions of the United States, barrier islands are a prominent feature of the coastal system. Barrier-inlet systems are ever changing and important elements of the coastal zone and particularly vulnerable to anthropogenic change. As people began to live and recreate on the coast, pressure to provide an efficient means for transporting them to the barriers intensified. This was often done by dredging material from the estuaries and bays landward of the barrier and using that material for constructing roads from the mainland to the barrier islands (Davis and Barnard, 2000). Increasing rates of development required further dredge and fill construction for adding waterfront houses in some locations and many coastal features were stabilized by hard construction (Davis and Barnard, 2000). Barrier islands are naturally unstable, migrating, and changing in response to factors such as sea level rise and extreme episodic storm events, and attempts to halt such adjustment modify the entire system.

In Florida, enhanced dredge-and-fill operations during the 1950s created series of upland areas separated by finger canals, produced from what was originally mangrove communities and seagrass beds (Davis and Barnard, 2000). In Longkou Bay, China, Li et al. (2019) detected modified bathymetry decades after dredge-and-fill was used to maintain and enhance port and coastline developments. The volume of sediment transported by dredge-and-fill is immense; recent airport expansions have used hundreds of millions of cubic meters of dredged sediment in Asia and the United States (Douglas and Lawson, 2003). This technique is also used in the construction of artificial islands.

Artificial islands are constructed to create prestige housing and to meet recreation, military strategy, and transportation needs. All of these human-built landforms modify coastal geomorphology through disruption of wave patterns and ecological health by disturbance of the water column and bottom sediment (De Groot, 1979; Goudie and Viles, 2016; Chee et al., 2017).

Notable examples of artificial island construction are The Pearl in Doha, Qatar, and The Palm, The World, and The Universe in Dubai, United Arab Emirates (Fig. 8). The Pearl-Qatar is a human-made island, spanning approximately 1.5 km^2, that was constructed for recreation, luxury residences, and shopping. In a push to encourage tourism, The Pearl-Qatar is among the first properties in Qatar available for ownership by non-Qataris (NASA, 2018). This echoes a common justification for construction of new land: economic benefits to the country are expected to outweigh the economic, ecological, or historical costs of construction. The Pearl-Qatar, for example, sits on a historically important pearl-diving location in Qatar. Construction of artificial islands off the coast of Dubai have buried coral reefs and oyster beds under millions of tons of sand and rock and contributed to the decline of fish stocks and turtles. The islands are also altering currents, exacerbating erosion on the natural beaches of Dubai (Krane, 2005). Yet they are also proving immensely lucrative for the economy of Dubai: thousands of residential and vacation homes have sold for $780,000–$1.4 million, and entire islands are sold for $7 million–$35 million (Krane, 2005). Indeed, search for wealth, leisure, and accommodation is driving anthropogeomorphic changes in the Persian Gulf, as they do around the world.

Figure 8 The image is a view of The Pearl near Doha, Qatar. The Pearl is an artificial island that was created to resemble a string of pearls. The image was captured by one of the astronauts of expedition 53 from the International Space Station (ISS) on 10/23/2017. Reprinted with permission from Aguilar et al., 2020.

2.3.2. Anthropogeomorphic landscapes in the fluvial environment

The fluvial environment is highly vulnerable to change by anthropogenic processes because of its favorability as a settlement site and its multiplicity of resources. Anthropogenic-driven climate change results in changes to the amount and intensity of precipitation, and increased evapotranspiration in the fluvial environment (Goudie, 2006; Goudie and Viles, 2016). Rivers are more immediately affected by direct human alteration to the river channels (Fig. 9) and watersheds through channelization, dams and river restoration projects (Hootsmans et al., 2015). Fig. 10 presents a summary of natural and anthropogenic impacts on fluvial environments.

Fluvial landforms are determined by the nature of the fluvial processes at work. The presence of floodplains, oxbow lakes, meanders, yazoo tributaries and backswamps are typical in low-gradient stream channels with dominantly lateral channel erosion. Such channels often have high width-to-depth ratios and gentle channel slopes. Anthropogenic influence creates new fluvial landforms and modifies preexisting features. Dams and levees create new positive relief structures, which are long-term or become permanent parts of the fluvial landscape and modify the channel upstream and downstream.

Figure 9 San Antonio Riverwalk: an example of human modification of a river channel. San Antonio River, San Antonio, Texas. (Photo by J. Giardino, 2017). Reprinted with permission from Aguilar et al., 2020.

Upstream of a dam, sediment accumulates and lowers channel slope (Owens, 2019). The increase in local base level increases lateral channel erosion upstream of the

dam and augments floodplain landforms. Downstream of the dam, landform development varies based upon management. The decrease in sediment flux and regular flow downstream of a dam often leads to narrower channels and, as flooding is typically reduced by dams, floodplain features are less pronounced (Owens, 2019). Types of dams and management should be considered in any assessment of a modified river channel.

Management of a dam that does not release water from its impoundment in anticipation of coming precipitation will increase flooding upstream of the dam and cause flashier flows downstream, leading to less stable channels with higher rates of migration. Rivers with numerous dams in sequence have further altered geomorphology, as the downstream effects of one dam are not dissipated before the upstream effects of the next dam occur. The morphology of a reach affected by multiple dams is distinct from the typical upstream or downstream effects of singular dams (Jefferson et al., 2013).

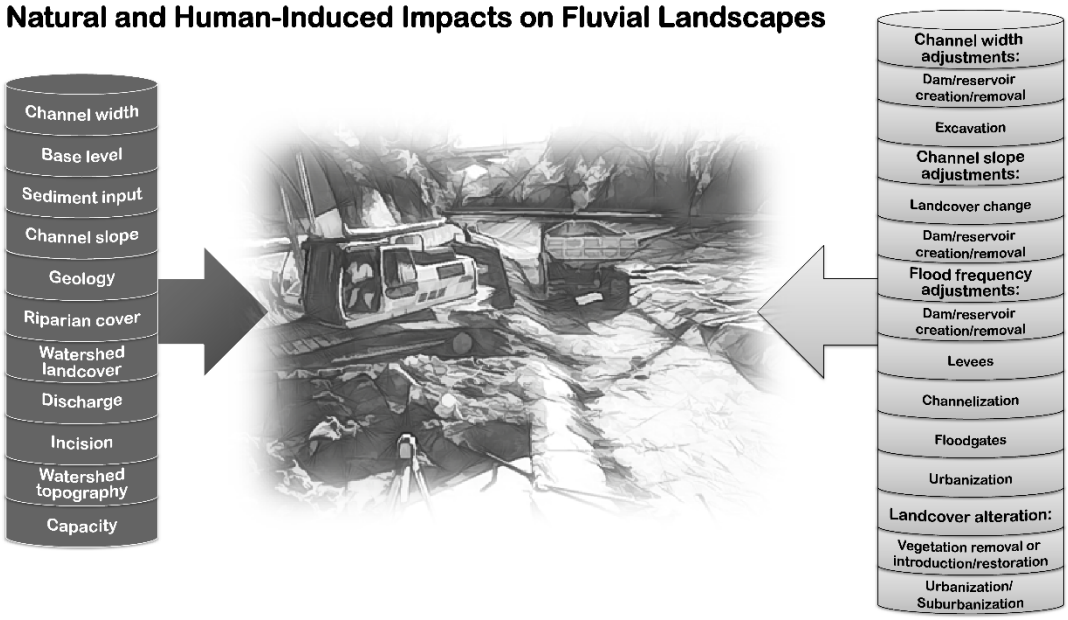

Figure 10 Natural induced impacts (left) and anthropogenic impacts (right) on fluvial landscapes. Reprinted with permission from Aguilar et al., 2020.

Levees are positive relief structures that trend parallel to river channels as flood control measures. Yazoo tributaries are commonly formed or more pronounced by the presence of artificial levees as the drainage pattern adjusts to augmented banks. Reduction of floods in the immediate vicinity of rivers means that excess energy is less frequently expended overbank to the adjacent floodplain, but is directed downstream. Higher rates of flow are, thus, experienced in the channel more frequently, and cause downstream regions to experience increased erosion leading to channel migration and cutoff loops. If a levee is breached by an unusually high flood, water is less apt to drain back into the channel once the flood has passed because of the presence of the levee. The presence of levees leads to more pronounced backswamps in the floodplains of such modified channels.

2.3.2.1. Effects of land-cover change in watershed

Of the various ways humans alter their environment, change in land-cover has the largest global impact (IPBES, 2019). The growth of the urban built environment coincides with the alteration of land cover as natural cover is segmented or replaced with impervious cover. Conventional wisdom predicts that change in land cover associated with urbanization or conversion to farmland leads to increased runoff, decreased evapotranspiration, and decreased infiltration (Schlesinger et al., 1990; Zhang and Schilling, 2006; Nugroho et al., 2013; Ahiablame et al., 2017). These effects directly alter processes in fluvial geomorphology and slope processes. Zhang and Schilling (2006) observed an increase in streamflow from 1940 to 2006 in the upper Mississippi River basin resulting from conversion of natural, perennial vegetation to cultivated soybean farms.

Hydrological recovery can be induced by returning a watershed to its original cover, but scales of recovery vary. Zhu and Li (2014) assessed a watershed in which residential and commercial lands increased from 5.2% and 1.0% to 8.3% and 2.8%, respectively, and agricultural land decreased from 28.3% to 18.9% during the years 1984–2010. Despite efforts by the United States National Park Service, which increased forested land from 65% to 69.5% during this same time period, SWAT (a hydrologic quality model developed by United States Department of Agricultural-Agricultural Research Service) simulation indicated a 3% increase in streamflow. Stream flows from forested sub-watersheds stabilized, but near urban centers streamflow increased by more than 10%. In a separate study from the Srepok watershed in Vietnam, reforestation

efforts increased forest cover by 41 ha during the years 2000–2010, correlating with decreased surface, lateral, and groundwater flow (Quyen et al., 2014).

Despite conventional wisdom that alteration of land cover associated with urbanization leads to increases in runoff and river discharge, interactions between site-specific factors (i.e., watershed slope, soil attributes, vegetation characteristics, climate, etc.) suggest that standardized watershed responses to the alteration of land cover are unlikely (Guzha et al., 2018). Guzha et al. (2018), for example, found no significant trends in streamflow resulting from removal of forested lands in East Africa. In a study in 2013, alteration of grassland to farmland, forest, and urban areas in the Upper Du watershed in China did not exert a significant influence on either streamflow or sediment yield (Yan et al., 2013).

With geomorphic processes now dominated by human influence, one cannot propose a general prediction for the response of watersheds to formulaic changes in land cover. A watershed response and the ensuing fluvial response to the alteration of land cover is dependent on traditional factors such as soil type, geology, topography, climate, and nature of the alteration of the land cover, and also on land management procedures and distribution of human population. Quantifying the effects of a nonstationary process, like land management, would be supremely difficult, thus, making a general prediction model for the effects of human alteration on the fluvial system highly unlikely.

2.3.3. Anthropogeomorphic landscapes in the glacial and mountain environments

Humans have modified the alpine landscape through activities such as mining, built landscapes, farming, grazing, lumbering, roads, train tracks, water impoundment,

ski trails, and river restoration (Gamache et al., 2018). Humans have also impacted landforms produced by natural geomorphic processes (Fig. 11). Moraines, for example, are often productive borrow sources for gravel, sand, and aggregate (Gamache et al., 2018).

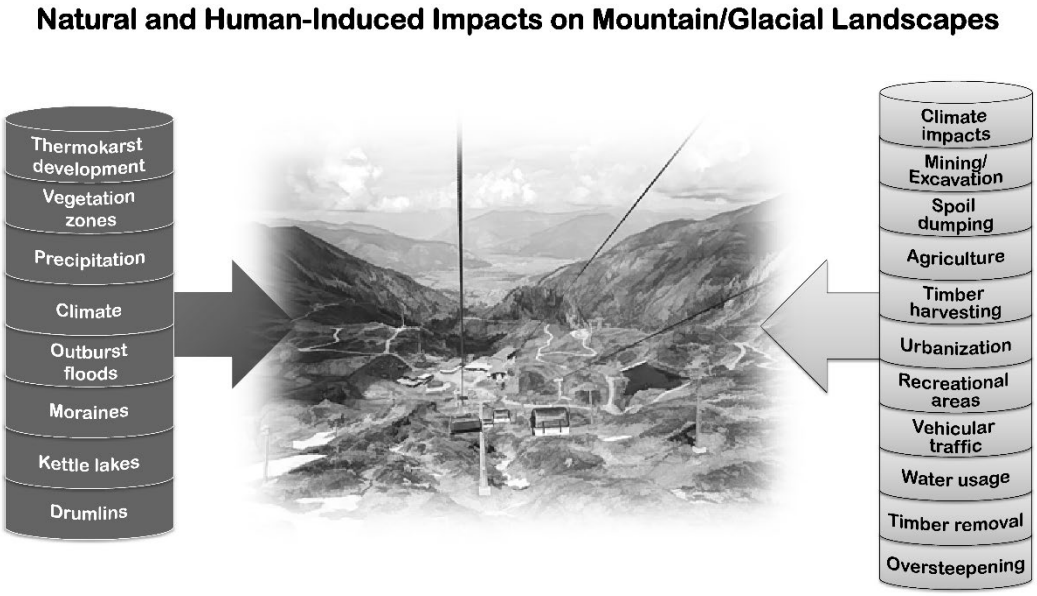

Figure 11 Impacts of natural and anthropogenic processes on mountain and glacial landscapes. Reprinted with permission from Aguilar et al., 2020.

Mining of natural resources to meet human demands is a direct disturbance of the natural workings of the Critical Zone (Fig. 12). Removal of mineral matter reduces the quantity of solid soil material available in the Critical Zone, and also removes potential storage sites for soil water and habitat for near-surface organisms. In some cases, excavation may lead to over-steepening of slopes and increased danger of mass movements (Gamache et al., 2018).

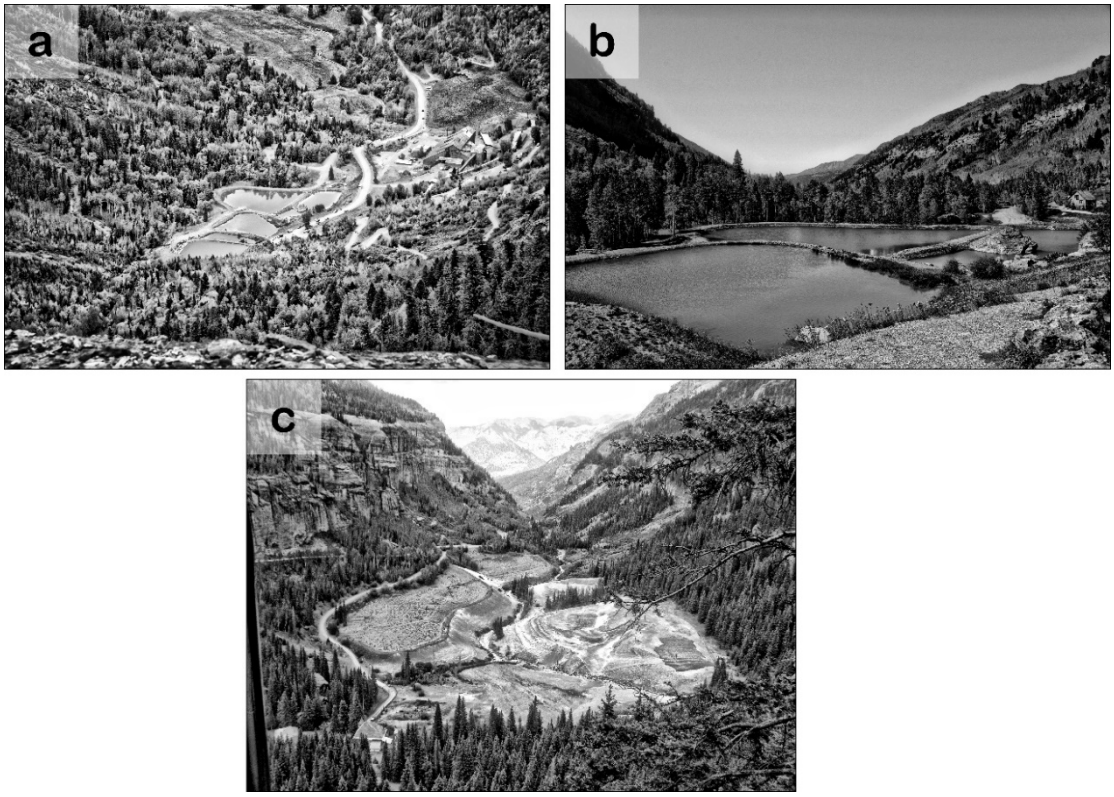

Figure 12 (a) Settling ponds of the Pandora Mill near Telluride, Colorado; (b) ground view of the settling ponds; (c) mine tailings from the Camp Bird Mine near Ouray, Colorado. (Photos by J. Giardino, 2016). Reprinted with permission from Aguilar et al., 2020.

Growth of mountain towns has modified drainage such that, when subdivisions are built, many minor geomorphic features are destroyed, increasing the likelihood of increased risk from geomorphic processes. Specifically, steeper slopes are produced to create flat surfaces for building. In addition, the covering of pervious surfaces with house footprints, concrete, roads, and parking-lot surfaces has greatly decreased infiltration and increased surface runoff (Gamache et al., 2018). Moreover, city infrastructure plays a role in altering the environment. Early mountain roads, where

present, provide narrow regions of slope modification and impervious surfaces. High traffic corridors contribute external heat and vibrations to the soil, compromising slope stability (Fig. 13). US-550 was originally constructed as a narrow unpaved route between Ouray and Silverton, Colorado, USA. As a result of increased tourism, protection from avalanches and other forms of mass movement has been attempted as seen in this avalanche protection (Fig. 14).

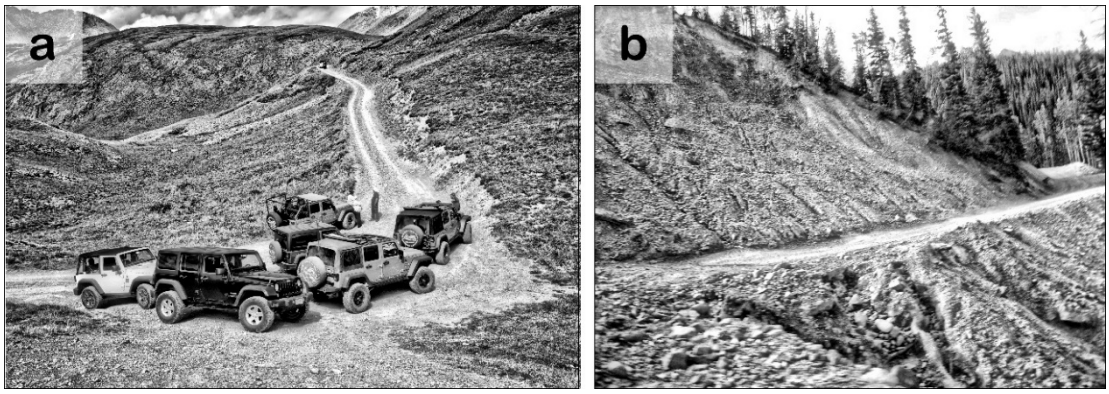

Figure 13 a) 4 × 4 vehicles cause considerable erosion to former mining trails along Black Bear Trail, San Juan Mountains, Colorado; (b) highly weathered volcanics on the Corkscrew Trail are susceptible to accelerated erosion resulting from heavy use by 4 × 4s. (Photos by J. Giardino, 2017). Reprinted with permission from Aguilar et al., 2020.

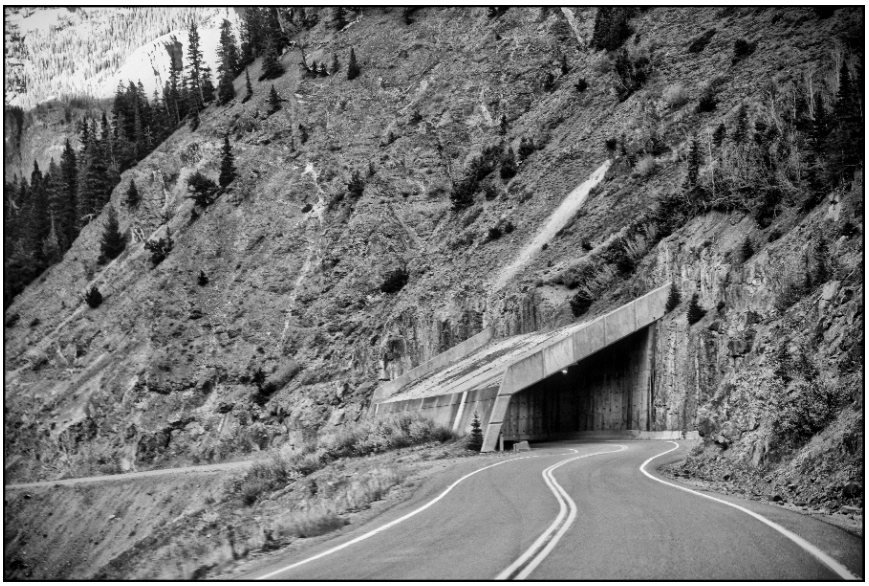

Figure 14 Avalanche snowshed on US-550 between Silverton and Ouray, Colorado. (Photo by J. Giardino, 2017). Reprinted with permission from Aguilar et al., 2020.

Ski runs, mountain roads, bike trails, and hiking paths cause impacts ranging from minor to significant, and mountain sports are growing dramatically, and the impact will be significant. The introduction of nontraditional mountain sports also alters the landscape. In Telluride, Colorado, for example, a vast area has been used for creation of a golf course and the landscape has been completely altered through the removal of vegetation and flattening of slopes (Gamache et al., 2018). Recreational trails also contribute to increased mass movement and increased channel-rut runoff. Off-road vehicles create channels and then compact the materials, allowing water to flow freely down newly created channels (Martin and Butler, 2017; Gamache et al., 2018).

Climate warming also results in permafrost melting with thaw lakes being created as well as beaded drainage. The island of Shishmaref, Alaska, has experienced accelerated erosion over the last decade. The village of Shishmaref, an Inupiat

community, which is located along the northern shore of the island, has experienced flooding and erosion driven by climate change. Because the Bering Strait is no longer frozen throughout the winter, the front of the island is being impacted by winter storm surges, which has caused more than 61 m of erosion. The erosion has impacted the community to such an extent that the community voted to relocate the whole village but have experienced numerous delays (Fig. 15).

Figure 15 House tipping in Shishmaref, Alaska. (Photo by J. Giardino, 2006). Reprinted with permission from Aguilar et al., 2020.

2.3.4. Anthropogeomorphic landscapes formed by energy resources

The infrastructure required to harvest renewable resources can have significant effects on the land surface at varying scales; however, such effects are understudied. Rising temperatures of up to 0.72 °C per decade in regions where land cover is modified

to build windmill farms, can be attributed to the turbulence generated by wind turbines, which in turn modify energy-mass exchanges between the atmosphere and the land surface (Wang and Wang, 2015; Zhou et al., 2012). Goudie (2020) reports surface destabilization in desert areas where wind farms have been established. Cook and McCuen (2011) studied the nexus between the change in land cover, hydrology, and soil erosion in areas with solar panel farms. Cook and McCuen (2011) indicate solar panels can increase the kinetic energy of rainfall by an order of magnitude, which impacts the potential for erosion of the soil according to the type land cover.

Landforms produced by future expansion of renewable energy will be unique to the Anthropocene. In an effort to combat the global reliance on fossil fuels, demands for solar, wind, and/or geothermal energy have risen in recent decades and are expected to increase. Less often discussed is the potential effects of large-scale renewable energy operations on geomorphology. Li et al. (2018) provide a comprehensive overview of studies of the effects of solar and wind farms on climate change. Hu et al. (2016) found that solar-panel electricity generation will redistribute the energy from the sun, thus, affecting regional and global climates. Without the solar panels, solar radiation reaching the surface is either absorbed or reflected, but with the solar panels, a portion of absorbed solar radiation is diverted to electricity generation.

According to Keith et al. (2004), large amounts of wind power can produce non-negligible climatic change at continental scales because of interactions of wind turbines with the atmospheric boundary layer. In the Li et al. (2018) study, combined effects of large-scale wind farms and solar farms in the Sahara are modeled. Wind farms caused

significant regional warming on near-surface air temperature (+2.16 K) and increased precipitation as much as +0.25 mm/day. Fig. 16 is an example of a wind farm in West Texas.

Figure 16 Wind farm in West Texas. (Photo by J. Giardino, 2019). Reprinted with permission from Aguilar et al., 2020.

Impacts of solar farms on temperature and precipitation are similar to those of wind farms. When wind and solar farms are deployed together in the Sahara, precipitation increases from 0.24 mm/day in the control run to 0.59 mm/day in the case of combined wind and solar farms, a ~150% increase, and the temperature increase is slightly larger than for the solar farm alone.

Changes to local climate patterns will undoubtedly have lasting effects on geomorphology, particularly in arid regions where even occasional rainfall is known to rapidly produce ephemeral streams and replenish playa lakes. This action is especially enhanced because the introduction of anthropogenic structures occurs more rapidly than

natural environmental changes and with greater effect. Thus, resultant climate change may occur more rapidly than natural environmental evolution would. A sudden increase in precipitation in arid environments, those most likely to capitalize on large-scale solar operations, will contribute to flash floods and rapidly widening stream channels, hence increased erosion.

Wind farms are also prevalent in coastal environments, having potential impacts on coastal geomorphology. Coastal wind turbines are becoming increasingly higher capacity and located in deeper water. Additionally, it is increasingly common for more than one wind farm to occur in a local area (Bailey et al., 2014). Little research has been conducted on the geomorphic effects of extensive offshore wind farms, but potential effects may be extrapolated from the expected effects on marine habitat. Turbines, for example, may act as artificial reef structures (Bailey et al., 2014). In addition to providing habitat for marine invertebrates, reefs will disrupt incoming wave patterns and alter subsequent shoreline erosion. Because safety buffers often prohibit boating and shipping operations in their vicinity, reduced choppiness from water vessels may decrease disruption of seafloor and shoreline sediment.

2.3.5. Anthropogenic hillslope landforms

Hillslope landscapes are impacted by much of the same anthropogenic forces already discussed (Fig. 17). Introduction of hoofed livestock is known to trample sediment and vegetation, causing soil compaction, decreased infiltration, and increased runoff (Butler, 1995). Replacement of natural vegetation with impermeable land cover or agricultural production often increases runoff as well, whereas re-introduction of native

vegetation to previously modified regions may decrease runoff and increase infiltration. Introduction of housing developments results in oversteepening of slopes to allow for housing-pad construction, as well as increased sediment yield because of vegetation removal. After the construction phase, natural land cover is generally replaced with low permeability, high albedo coverings that modify runoff, infiltration, and local weather temperatures. Mining and excavation processes likewise remove significant amount of sediment and overburden and introduce permanent changes to regional topography.

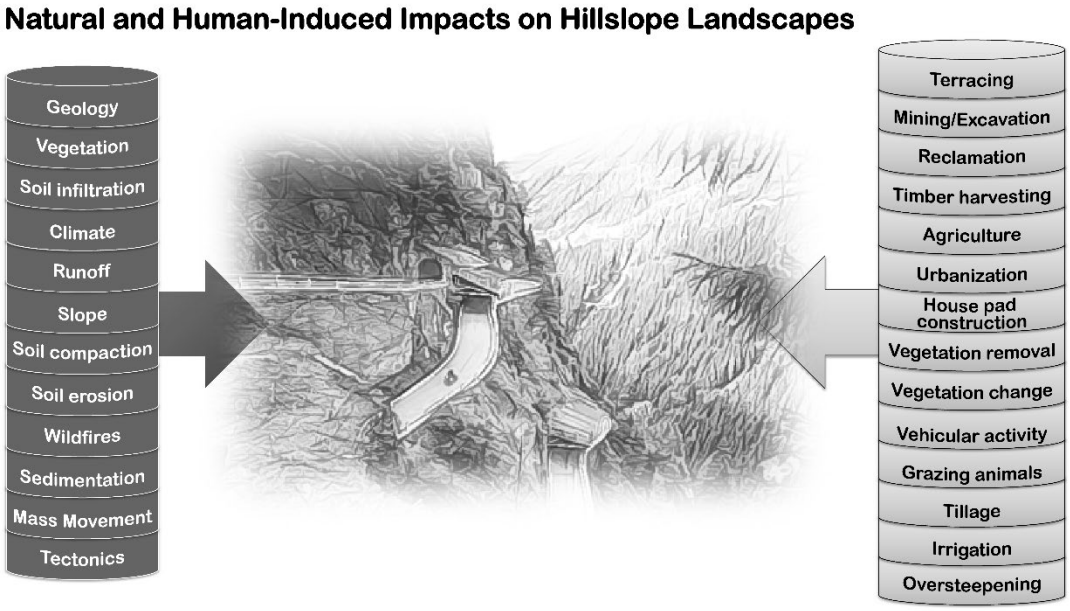

Figure 17 Environmental and anthropogenic factors influencing hillslope landscapes. Reprinted with permission from Aguilar et al., 2020.

Agriculture introduces many slope-related changes. In addition to the trampling effects of livestock, tillage and replacement of natural vegetation with crops compromises soil integrity, potentially increasing runoff and soil erosion. In some

regions, this is avoided by the introduction of agricultural terraces. Terraces are perhaps the starkest anthropogenic hillslope landforms. Agricultural terraces are often built in mountain regions to provide more surface area for farming on hillslopes and have significant geomorphic impact (Fig. 18). Collapsed stone walls, small mass movements, sheet-wash erosion, piping, rills, gullies and debris flows are all found in terraced landscapes (Arnáez et al., 2015). Terraces generally increase infiltration, which decreases runoff and soil erosion. Under certain circumstances, however, abandoned or cultivated terraces can accelerate soil erosion as a result of factors such as slope, lithology, soil surface cover, quality of construction, vegetative cover and land use, and the abandonment period of the terrace (Arnáez et al., 2015).

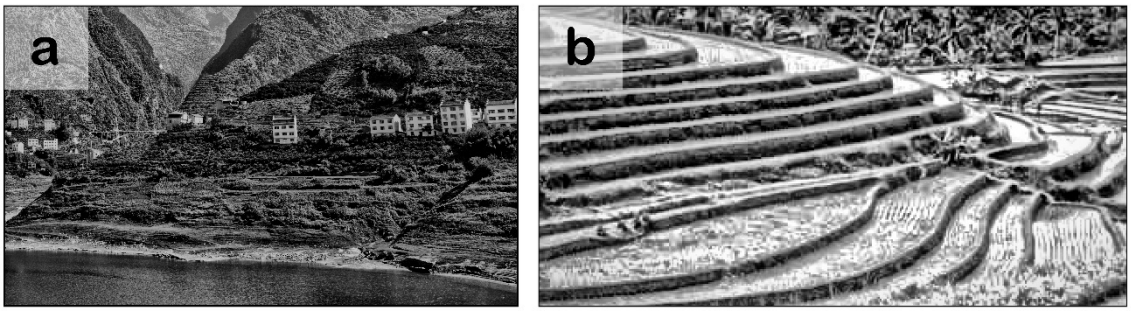

Figure 18 (a) Agricultural terraces on the Yangtze River, China (photo by J. Giardino, 2018). (b) Rice patty agriculture in Bali, Indonesia (photo by J. Giardino, 1986). Reprinted with permission from Aguilar et al., 2020.

Geomorphic effects can vary with location within each terrace. Soil saturation is reached faster in the inner parts of terraces with more shallow soil, causing increased runoff, and high infiltration rates in external sections often generate subsurface runoff. Farming terraces have a significant effect on hydrological processes because their

presence reduces overall slope, irrigation ditches reorganize the drainage network, and soil distribution and characteristics are reorganized. Terraces also alter hydromorphic processes by reducing hydrologic connectivity in the watershed and introducing piping (Arnáez et al., 2015). The aforementioned outcomes are dependent on the quality of construction of such terraces (Beach et al., 2015).

2.3.6. Anthropogenic landscapes produced by conflict

One of the impacts of humans on the surface of Earth that is sparsely mentioned in the geomorphology literature is the landscape that remains after a conflict. The impact of bombs has been recognized by Hupy and Koehler (2012), and they introduced the term bombturbation to describe the impact of the explosion from the detonation of an ordinance on the surface of Earth and soil structure. Examination of a Google Earth image (Fig. 19) of Pointe du Hoc in France today still shows a pocked surface that was created by the heavy bombing of this location in World War II. One can also examine a Google Earth image of the Vicksburg Battlefield in Mississippi and see the trenches that were dug during the long conflict during the Vicksburg Campaign during the US Civil War.

Figure 19 Example of bombturbation in Pointe du Hoc, France. Google Earth Engine, 2019. Reprinted with permission from Aguilar et al., 2020.

More recent conflicts such as the Vietnam War also show these bombturbation impact features caused by the extensive carpet bombing by B-52s. These features are conical-shaped impact craters. For example, even though it is in a tropical environment, the area around Khe Sanh, Vietnam, still shows these impact craters.

Today, conflicts in Iraq, Afghanistan, Yemen and Syria are creating human altered landscapes. In many of these areas, traditional bombs carried and released by aircraft are being replaced with drone bombing. This new approach is resulting in a more restrictive type of bombturbation impact.

2.4. Technology-assisted approach to geomorphology

Geomorphology has a long, rich history of field-based research. Over the years, geomorphology has evolved from meticulously drawn diagrams and detailed field notes in field books and field sketches from horseback, through recording observations with

analogue cameras, elaborately designed sampling protocols extending over temporal and spatial scales, mathematical modeling, remote sensing techniques, geochemical and geophysical methodologies, to big data sets and artificial intelligence. Incorporating new tools and techniques has expanded the geomorphologist's understanding of process and form. In this section we present an overview of advances in remote sensing techniques, geophysical methods, and big data, machine learning and artificial intelligence.

2.4.1. Remote sensing methods

Dafflon et al. (2017) point out that modern geomorphological studies include the use of traditional methods (observation and measurement) aided by highly advanced technology with remote sensing techniques, as the use of aerial photography, satellite images, and UAVs or drones facilitate landscape studies through time at varying spatial scales. According to Clapuyt et al. (2017), techniques used in geomorphological studies, particularly landslide monitoring, have progressed from interpretation of historical and current aerial images, often limited by the low frequency of data acquisition (cost of flight campaigns), to methods with high temporal and spatial resolution such as satellite imagery. Table 2 summarizes the methods detailed by Clapuyt et al. (2017). Accurate 3-D models, usually in the form of a Digital Elevation Model, of the surface can be constructed from high resolution data allowing for more thorough geomorphic studies. As Clapuyt et al. (2017) note, however, most methods are still economically costly, which makes them unsuitable for monitoring purposes.

Several models can be utilized to produce a 3-D representation of the terrain from a 2-D image by using mathematics to graphically represent natural geographical

features (Li et al., 2005). The most commonly used models correspond with the Digital Terrain Model (DTM) and the Digital Elevation Models (DEM). The distinction between a DTM and a DEM is that a DEM refers to an expression of the distance from a datum whereas the DTM encompasses other surface features, including elevation (Li et al., 2005). According to Li et al. (2005) the elements included in the construction of a DTM are dependent on the purpose of the study and the discipline of the researcher.

Other commonly used techniques in geomorphic investigations correspond with radar methods such as Synthetic Aperture Radar (SAR) and Light Detection and Ranging (LiDAR). These methods are widely used for a variety of applications, including detection of surface deformation (Clapuyt et al., 2017). LiDAR imagery can be acquired with an airborne LiDAR system (ALS) as well as with a ground-based or terrestrial system such as Terrestrial Laser Scanning (TLS) (Clapuyt et al., 2017). At the Calhoun Critical Zone Observatory (CCZO), DEMs generated from LiDAR data were used to determine the parameters needed as inputs for gully erosion development and remediation models (Bastola et al., 2018). The data allowed Bastola et al. (2018) to evaluate practices for erosion control and calculate their effectiveness. In the case of SAR, data collection platforms can be satellite-based or ground-based (GB-SAR). These techniques are effective in multi-temporal studies, but the acquisition of the aircraft and spacecraft data is still costly, and it can be challenging to use terrestrial platforms in complex topography.

Data acquisition challenges have driven geoscientists to look for cost-effective and adaptable technologies that can be employed in rough terrain, as well as for

landform change monitoring applications. The use of UAV as platforms for data collection is becoming common practice in many geomorphic studies. Geomorphological mapping of periglacial landforms using images from a long-range UAV is exemplified by Dąbski et al. (2017). The authors favor the use of UAVs in remote regions like Antarctica to obtain high resolution imagery and produce accurate landform change maps. UAV platforms are also useful in engineering geology settings. Congress et al. (2018) proved the effectiveness of using data collected with an UAV to monitor change in an anthropogenic feature, specifically pavement deformation and cracking.

Table 2 Comparison of methods used to generate DEMs in mass movement monitoring studies. After Clapuyt et al. (2017). Reprinted with permission from Aguilar et al., 2020.

Technique	Resolution	Advantages	Limitations
Aerial photographs	Regional (several meters)	Allows visual interpretation and construction of DEMs	Costly campaigns limit monitoring; not ideal for high-resolution studies
Satellite imagery	Decimeters	Allows visual interpretation and construction of high-resolution DEMs	Costly imagery; limiting for monitoring applications

Table 2 continued. Reprinted with permission from Aguilar et al., 2020.

Technique	Resolution	Advantages	Limitations
Radar methods: Synthetic Aperture Radar (SAR)Light Detection and Ranging (LiDAR)	Airborne: regional (several meters) Ground-based: high-resolution (centimeters)	Methods can be airborne or ground-based to develop DEMs. Great for monitoring applications	Ground-based LiDAR in complex terrain requires overlap to produce adequate results
UAV image-based structure-from-motion algorithm (UAV-SfM)	Decimeter to centimeter	Cost-effective and suitable for use in complex terrain and remote areas	Requires at least 70% overlap to produce adequate results and ground control points to georeference the images

A digital image processing technique called Structure from Motion (SfM) is used to produce 3-D topography from images captured using UAV-mounted cameras. This technique is also referred to as Aerial Structure from Motion (ASfM) digital photogrammetry image processing technique (Bonali et al., 2019). According to Fonstad et al. (2013), the UAV-SfM approach is user and budget friendly, while producing high resolution data comparable to that of aerial LiDAR. Kasprzak et al. (2018) report obtaining more detailed microtopography from their UAV-SfM DTM than with the aerial LiDAR imagery, highlighting that UAV-SfM does not always yield better resolution than aerial LiDAR. Authors such as Cook (2017) and Carey et al. (2019)

compared the resolution of LiDAR and UAV-SfM data, confirming the advantages of UAV-SfM over LiDAR in terms of time of deployment and interpretation, as well as cost effectiveness.

Some of the limitations of the UAV-SfM method include the presence of artifacts in the generated topographic models after the automated filtration process (Kasprzak et al., 2018), and the inability to mount both a GPS and a camera on small UAVs (Fonstad et al., 2013). The availability of larger platforms makes it possible to produce close range photogrammetry (CRP) using UAVs. A global navigation satellite system (GNSS) and a high definition camera were mounted on a UAV platform to perform a UAV-CRP study (Congress et al., 2018). The authors recommend combining the use of the GNSS with ground control points (GCPs) but highlight the need for less GCPs using this approach.

Monitoring geomorphic change is accomplished by collecting and analyzing high resolution multi-temporal data. Some authors refer to these types of data as 4-D. Cucchiaro et al. (2018) provide a methodology for the data collection and processing stages of a rapid geomorphic change investigation. The authors utilize complementary terrestrial SfM and UAV-SfM data to quantify erosion and sedimentation volumes, determine the magnitude and distribution of processes, and evaluate the validity of using check dams to mitigate erosion in debris flow catchments.

The UAV-SfM approach has been applied to study fluvial processes and environments (Fonstad et al., 2013; Izumida et al., 2017; Cook, 2017; Nesbit et al., 2018; Langhammer and Vacková, 2018; Strick et al., 2019), mass movement (Peppa et al.,

2017; Clapuyt et al., 2017; Yu et al., 2017; Valkaniotis et al., 2018; Eltner et al., 2018; Cucchiaro et al., 2019; Carey et al., 2019; Peppa et al., 2019), glacial landforms (Rossini et al., 2018; Midgley et al., 2018), coastal processes and landforms (Anzidei et al., 2017; Guisado-Pintado et al., 2019), and volcanic processes (Darmawan et al., 2018; Gomez and Kennedy, 2018; De Beni et al., 2019; Dering et al., 2019). Other applications include granite tor mapping (Kasprzak et al., 2018), lava flow mapping (Favalli et al., 2018), and tectonic feature mapping (Giletycz et al., 2017; Bonali et al., 2019).

2.4.2. Geophysical methods

Geophysical methods have been used to solve geomorphological problems since the twentieth century. Commonly used geophysical methods in geomorphology include Ground Penetrating Radar (GPR), Electromagnetic methods (EM), Electrical Resistivity Tomography (ERT), and seismic methods. Other applicable but less commonly used methods include the Induced Polarization (IP), Self-potential (SP), surface Nuclear Magnetic Resonance (sNMR), and gravity methods. A review of geophysical methods used in Critical Zone investigations is provided by Parsekian et al. (2015). Table 3 presents commonly used geophysical methods in the study of geomorphological processes and environments, as well as examples of applications.

Table 3 Commonly used geophysical methods in the study of geomorphological processes and environments and examples of applications. Reprinted with permission from Aguilar et al., 2020.

Application	Method
Tectonic processes	GPR (Kruse, 2013) EM (Pavan Kumar et al., 2019; Gürer et al., 2017) ERT (Kruse, 2013) Seismic (Kruse, 2013)
Periglacial processes, environments, and landforms	GPR (Degenhardt and Giardino, 2003; Schrott et al., 2013; Hauck and Kneisel, 2008; Colombo et al., 2018) ERT (Hauck and Kneisel, 2008; Stan et al., 2017; Colombo et al., 2018; Doetsch et al., 2015) IP (Doetsch et al., 2015) SP (Colombo et al., 2018) Seismic (Kruse, 2013)
Fluvial processes and environments	ERT (Robinson et al., 2008; Khalil et al., 2018) EM (Rapti-Caputo et al., 2009; Robinson et al., 2008) IP (Robinson et al., 2008; Ntarlagiannis et al., 2016) Seismic (Calvès et al., 2019; El-Mowafy and Marfurt, 2016)
Critical Zone studies	GPR (Yu et al., 2016; Guo et al., 2020) ERT (Leopold et al., 2013; Guo et al., 2020) Seismic (Befus et al., 2011; Flinchum et al., 2018; Novitsky et al., 2018; Wang et al., 2019) sNMR (Flinchum et al., 2019)

Table 3 Continued. Reprinted with permission from Aguilar et al., 2020.

Application	Method
Coastal processes and environments	GPR (Wegmann et al., 2012) EM (Paine et al., 2015; Weymer et al., 2015; Wernette et al., 2018; Raimbault et al., 2018) sNMR (Keating et al., 2018)
Karst environment	GPR (Carbonel et al., 2015; Artugyan et al., 2015; Bottari et al., 2017) ERT (Siart et al., 2013; Carbonel et al., 2015; Bottari et al., 2017; Lazzari et al., 2010) EM (Bottari et al., 2017) SP (Artugyan et al., 2015; Giampaolo et al., 2016) Seismic (Van Dam, 2012; Kruse, 2013) Gravity (Kaufmann and Romanov, 2016; Kaufmann and Romanov, 2017)
Mass movement	GPR (Brody et al., 2015; Bernatek-Jakiel and Kondracka, 2016) ERT (Naudet et al., 2008; Marescot et al., 2008; Perrone et al., 2014; Bottari et al., 2018; Kasprzak et al., 2019) EM (Solberg et al., 2016; Gallistl et al., 2018) IP (Gallistl et al., 2018) SP (Naudet et al., 2008; Wang et al., 2018; Santoso and Hasanah, 2019) Seismic (Brody et al., 2015; Chen et al., 2019; Huntley et al., 2019)

Landform characteristics such as geometry, internal structure, and makeup can be interpreted from geophysical surveys (Van Dam, 2012). Monitoring rapidly occurring geomorphic change in distinct environments can be accomplished by integrating surface

feature characterization with subsurface geophysical investigations (Kruse, 2013). Other applications of geophysical methods in geomorphology include multitemporal landform studies at varying spatial scales (Schrott et al., 2013; Schrott and Sass, 2008), determination of rates of erosion and sedimentation (Church, 2010), studying impact structures (Bobée et al., 2010) and geomorphological mapping of extraterrestrial bodies (Rodriguez et al., 2015). Anthropogenic structures are also studied using geophysical techniques. Pazzi et al. (2016) used ERT and EM in an urban environment to study subsurface anthropogenic features.

Non-invasive near-surface geophysics methods can be used in combination with invasive methods (i.e., drilling and trenching) to validate geologic interpretations, to assess the performance and applicability of the method to a geomorphic environment, and to determine its effectiveness in addressing a specific research question. The use of geophysical methods (non-invasive and borehole geophysics) in the study of geomorphic processes, particularly in deep Critical Zone studies (Robinson et al., 2008; Slim et al., 2015; St. Clair et al., 2015; Parsekian et al., 2015; Riebe et al., 2017) is becoming the norm because it allows for a better understanding of the subsurface-surface connectivity and for further understanding of geomorphic process dynamics (Kruse, 2013).

Ground Penetrating Radar (GPR), electrical conductivity, and magnetic susceptibility surveys were conducted at the Luquillo Critical Zone Observatory (Comas et al., 2019). The authors used the geophysical data to study the mechanisms driving the accelerated erosion and weathering rates at a landscape scale. Comas et al. (2019) complemented their geophysical interpretations with direct coring and stress modeling.

A multiple-method approach like the one used by Comas et al. (2019) can be time-consuming and the field expeditions costly. However, CZOs are inclined to using multiple methods because they investigate complex and interconnected processes, with a high level of detail, through time.

2.4.3. Big data, machine learning and artificial intelligence

Scientific research has been revolutionized by the advent of big data, artificial intelligence, and GPU computing. “Big data” refers to databases of zettabyte size (billions of terabytes) that can contain massive amounts of data in the form of text, numerical values, images, e-mail, GPS data, or even data acquired from social networks (Spina, 2019). Artificial intelligence (AI) aids in the processing of big data by simulating typical behaviors of the human brain through complex algorithms that mimic decision-making through machine learning (Spina, 2019). GPU Parallel Computing (GPGPU) involves the processing of data by the processors present in the graphics card (GPU) and has allowed the computation, in relatively short times, of huge amounts of data with an efficiency of at least two orders of magnitude greater compared to the past (Spina, 2019).

The evolution of big data introduces more data than can be effectively processed by traditional geomorphic research methods and necessitates new approaches to geomorphologic research (Tooth, 2007; Stepinski and Vilalta, 2010; Spina, 2019). Advances in geomorphic mapping, for example, have not adequately kept up with advances in data collection (Stepinski and Vilalta, 2010; Ebert-Uphoff et al., 2019). Geomorphologists, therefore, must utilize the opportunities provided by artificial

intelligence, GPU computing, and automated mapping processes (Stepinski and Vilalta, 2010; Spina, 2019). If geomorphology is to aid in mitigating and adapting to future environmental change, we need to systematically incorporate a stronger geomorphological perspective into the science of global change; the Anthropocene represents an appropriate platform from which to inject that perspective (Meadows, 2016).

Critical Zone studies deal with complex interconnected chemical, physical, biological and geological processes of multivariate nature, across temporal and spatial scales (Brantley et al., 2007). Today in the US, much NSF-sponsored research is focusing on the Critical Zone. To understand the transfer of mass and energy through the system, Critical Zone scientists utilize multiple methods and models, requiring powerful computational resources to interpret large such datasets.

Efforts to find ways to work with such complex and large models and data sets include the increasingly relevant attempts made to automate certain components of data processing, and to produce reliable methodologies for remote studies, particularly important in a time in which geomorphologists expand research interests to explore planetary bodies, which is driving interest in machine learning and artificial intelligence techniques.

An example of the application of technological advances in the study of anthropogenic landforms is the methodology developed by Sofia et al. (2014) for automatic detection of terraced slopes, which the authors think has potential to be used for the identification of other anthropogenic features, and to aid in the study of mass

movement resulting from agricultural practices. Their protocol, Slope Local Length of Auto-Correlation (SLLAC), uses an algorithm applied to LiDAR DTMs to produce maps used in detection and characterization of terraced landscapes. These techniques are often necessary in areas where vegetation does not allow for photo interpretation, as well as studying areas where it is difficult to obtain access. A similar approach was utilized by Beach et al. (2019b) to identify ancient canal systems under the tropical forest in Central America.

A technique that utilizes fuzzy logic (which looks for approximate patterns) in combination with neural networks to essentially replicate the way in which humans link processes and concepts in order to make decisions called Fuzzy Cognitive Map (FCM) was used by Houser et al. (2015) to quantify the effects of human interventions on an aeolian environment. Their study analyzed the reactivation of dunes within the South Texas Sand Sheet.

Tien Bui et al. (2019) developed a model that uses artificial intelligence and machine learning algorithms to generate predicted gully erosion maps in a watershed in Iran. The authors assessed the accuracy of the ensemble model and concluded it is a very useful approach to this problem. As long as site-specific conditioning factors are identified and ranked as needed, this model is applicable to areas in which conditions are similar to those described in the article and the distance to the river was the most important factor in the development of gully erosion.

Advances on machine learning methods by Wang and Wu (2019) make crater identification on the surface of extra-terrestrial bodies faster and more accurate. Their

approach uses overlapping 2-D (surface images) and 3-D DEMs information from the same area from which the training samples can be selected. It allows updates and retraining that, according to the authors, results in better training samples (automatically selected) that lead to a quicker learning process. This method was validated on data sets from Mars and the moon.

2.5. Concluding thoughts

2.5.1. The Anthropocene from the perspective of the Critical Zone

As geomorphology progresses, new research paradigms emerge. As Naylor et al. (2002) explain, biogeomorphological research tends to focus on aspects of the two-way linkages between ecological and geomorphological processes, but shortcomings exist with approaches to biogeomorphological research. Namely, biological impacts on geomorphology are often considered without reference to other influential factors or the reverse impacts of geomorphology on ecology. Additionally, existing research has primarily been focused on erosional landforms rather than measuring the construction or protection provided by organisms. Third, research has focused on process studies at individual study sites and has not attempted to link findings to other scales of geomorphological inquiry (Naylor et al., 2002).

Naylor et al. (2002) suggest opening the sphere of biogeomorphological research by encouraging extension of the network of bioprocess observations using standardized methods to other environments and longer timespans, focusing further on bioconstruction and bioprotection, and investigating the complexity of biogeomorphic interactions. Additionally, new theoretical and technological advances should be used to

advance the field of biogeomorphology (Naylor et al., 2002; Talalay, 2014). Slaymaker (2009) outlines four needs for the future of biogeomorphology: a stronger intellectual and philosophical rationale for geomorphology as a discipline, establishment of a basis of unity, reconciliation of interest in unique landform sequences with that of prediction, and adaptation to an increasingly anthropogenically modified world.

Church (2010) observes that geomorphology is diversifying: it is becoming a more rigorous geophysical science, while also becoming more concerned with human, social, and economic values, environmental change, conservation ethics, human impact on the environment, and with issues of social justice and equity. Its progression will require coordination of the scientific community to enhance synergies between modeling and observation of complex Earth-surface phenomena, and develop educational initiatives (Murray et al., 2009; Keylock, 2010). A focus on the Critical Zone in anthropogenic geomorphology allows a framework for interdisciplinary research that incorporates multiple Earth spheres susceptible to human influence. We propose this approach to Anthropocene geomorphology for its utility in incorporating effects of multiple Earth spheres and modification of systems and feedback mechanisms resulting from past and current human influence.

2.6. References

Abera, T. A., Heiskanen, J., Pellikka, P., Rautiainen, M., & Maeda, E., 2019. Non-radiative processes drive surface temperature dynamics during land cover changes in the Horn of Africa. In Geophysical Research Abstracts (Vol. 21).

Ahiablame, L., Sinha, T., Paul, M., Ji, J. H., Rajib, A., 2017. Streamflow response to potential land use and climate changes in the James River watershed, Upper Midwest United States. Journal of Hydrology: Regional Studies, 14, 150-166.

Anderson, S. P., Blum, J., Brantley, S. L., Chadwick, O., Chorover, J., Derry, L. A., Drever, J.I., Hering, J.G., Kirchner, J.W., Kump, L.R., Richter, D. White, A.F., 2004. Proposed initiative would study Earth's weathering engine. Eos, Transactions American Geophysical Union, 85(28), 265-269.

Anderson, S. P., von Blanckenburg, F., White, A. F., 2007. Physical and chemical controls on the critical zone. Elements, 3(5), 315-319.

Anzidei, M., Bosman, A., Carluccio, R, Casalbore D., D'Ajello Caracciolo, F., Esposito, A., Nicolosi, I., Pietrantonio, G., Vecchio, A., Carmisciano, C., Chiappini, M.., 2017. Flooding scenarios due to land subsidence and sea-level rise: a case study for Lipari Island (Italy), Terra Nova, 29(1), pp. 44–51. doi: 10.1111/ter.12246.

Arnáez, J., Lana-Renault, N., Lasanta, T., Ruiz-Flaño, P., Castroviejo, J., 2015. Effects of farming terraces on hydrological and geomorphological processes. A review. Catena, 128, 122-134.

Arrhenius, S., 1896. XXXI. On the influence of carbonic acid in the air upon the temperature of the ground. Philos. Mag, 41(251), 237-276.

Artugyan, L., Ardelean, A., Urdea, P., 2015. Characterization of Karst Terrain Using Geophysical Methods Based on Sinkhole Analysis: A Case Study of the Anina Karstic Region (Banat Mountains, Romania). Sinkholes and the Engineering and Environmental Impacts of Karst: Proceedings of the Fourteenth Multidisciplinary Conference. University of South Florida Tampa Library, pp. 387–398. doi: 10.5038/9780991000951.1044.

Ashley, G.M., 1998. Where are we headed? “Soft” rock research into the new millennium. Geological Society of America Abstract/Program, vol. 30. p. A-148.

Aufdenkampe, A. K., Karwan, D. L., Aalto, R. E., Marquard, J., Yoo, K., Wenell, B., Chen, C., 2012 (December). Whole watershed quantification of net carbon fluxes by erosion and deposition within the Christina River Basin Critical Zone Observatory. In AGU Fall Meeting Abstracts.

Autin, W. J., Holbrook, J. M., 2012. Is the Anthropocene an issue of stratigraphy or pop culture. GSA Today, 22(7), 60-61.

Bailey, H., Brookes, K. L., Thompson, P. M., 2014. Assessing environmental impacts of offshore wind farms: lessons learned and recommendations for the future. Aquatic biosystems, 10(1), 8.

Banwart, S. A., Chorover, J., Gaillardet, J., Sparks, D., White, T., Anderson, S., Aufdenkampe, A., Bernasconi, S., Brantley, S.L., Chadwick, O. Dietrich, W. E., 2013. Sustaining Earth's Critical Zone basic science and interdisciplinary solutions for global challenges. University of Sheffield, Sheffield, 48.

Baskin, J., 2015. Paradigm dressed as epoch: The ideology of the Anthropocene. Environmental Values, 24(1), 9-29.

Bastian, O., Schreiber, KF., 1994. Analysis and ecological assessment of the landscape (Jena / Stuttgart: Gustav Fischer).

Bastola, S., Dialynas, Y. G., Bras, R. L., Noto, L. V., Istanbulluoglu, E., 2018. The role of vegetation on gully erosion stabilization at a severely degraded landscape: A case study from Calhoun Experimental Critical Zone Observatory. Geomorphology. Elsevier B.V., 308, pp. 25–39. doi: 10.1016/j.geomorph.2017.12.032.

Beach, T., Luzzadder-Beach, S., Cook, D., Dunning, N., Kennett, D.J., Krause, S., Terry, R., Trein, D., Valdez, F., 2015. Ancient Maya impacts on the Earth's surface: An Early Anthropocene analog?. Quaternary Science Reviews, 124, pp.1-30.

Beach, T., Luzzadder-Beach, S., Dunning, N., 2019a. Out of the Soil: Soil (Dark Matter Biodiversity) and Societal 'Collapses' from Mesoamerica to the Mesopotamia and Beyond in Partha Dasgupta, Peter Raven, Anna McIvor (Eds.) Proceedings of the Vatican Workshop on Biological Extinction, Cambridge University Press, ISBN:9781108711814.

Beach, T., Luzzadder-Beach, S., Krause, S., Guderjan, T., Valdez, F., Fernandez-Diaz, J.C., Eshleman, S., Doyle, C., 2019b. Ancient Maya wetland fields revealed under tropical forest canopy from laser scanning and multiproxy evidence. Proceedings of the National Academy of Sciences, 116(43), pp.21469-21477.

Befus, K. M., Sheehan, A. F., Leopold, M., Anderson, S. P., Anderson, R. S., 2011. Seismic constraints on critical zone architecture, Boulder Creek Watershed, Front Range, Colorado, Vadose Zone Journal, 10(3), pp. 915–927. doi: 10.2136/vzj2010.0108.

Bernatchez, P., Fraser, C., Lefaivre, D., Dugas, S., 2011. Integrating anthropogenic factors, geomorphological indicators and local knowledge in the analysis of coastal flooding and erosion hazards. Ocean & coastal management, 54(8), 621-632.

Bernatek-Jakiel, A., Kondracka, M., 2016. Combining geomorphological mapping and near surface geophysics (GPR and ERT) to study piping systems. Geomorphology. Elsevier B.V., 274, pp. 193–209. doi: 10.1016/j.geomorph.2016.09.018.

Bonali, F. L., Tibaldi, A., Marchese, F., Fallati, L., Russo, E., Corselli, C., Savini, A., 2019. UAV-based surveying in volcano-tectonics: An example from the Iceland rift, Journal of Structural Geology. Elsevier, 121(February), pp. 46–64. doi: 10.1016/j.jsg.2019.02.004.

Bottari, C., Albano, M., Capizzi, P., D'Alessandro, A., Doumaz, F., Martorana, R., Moro, M. Saroli, M., 2018. Recognition of Earthquake-Induced Damage in the Abakainon Necropolis (NE Sicily): Results from Geomorphological, Geophysical and Numerical Analyses. Pure and Applied Geophysics, 175(1), pp. 133–148. doi: 10.1007/s00024-017-1653-4.

Bottari, C., Aringoli, D., Carluccio, R., Castellano, C., Caracciolo, F.A., Gasperini, M., Materazzi, M., Nicolosi, I., Pambianchi, G., Pieruccini, P., Sepe, V., 2017. Geomorphological and geophysical investigations for the characterization of the Roman Carsulae site (Tiber basin, Central Italy). Journal of Applied Geophysics. Elsevier B.V., 143, pp. 74–85. doi: 10.1016/j.jappgeo.2017.03.021.

Brantley, S. L., Goldhaber, M. B., Ragnarsdottir, K. V., 2007. Crossing disciplines and scales to understand the critical zone. Elements, 3(5), 307-314.

Brantley, S.L., White, T.S., White, A.F., Sparks, D., Richter, D., Pregitzer, K., Derry, L., Chorover, J., Chadwick, O., April, R., Anderson, S. Amundson, R., 2006. Frontiers in Exploration of the Critical Zone, An NSF-sponsored workshop, 30pp. National Science Foundation, Washington, D.C.

Brody, A. G. Pluhar, C.J., Stock, G.M., Greenwood, W.J., 2015. Near-Surface Geophysical Imaging of a Talus Deposit in Yosemite Valley, California, Environmental & Engineering Geoscience, 21(2), pp. 111–127. doi: 10.2113/gseegeosci.21.2.111.

Brown, A. G., Tooth, S., Bullard, J. E., Thomas, D. S., Chiverrell, R. C., Plater, A. J., Chiverrell, R.C., Plater, A.J., Murton, J., Thorndycraft, V.R., Tarolli, P., Rose, J., Wainwright, J., 2017. The geomorphology of the Anthropocene: emergence, status and implications. Earth Surf. Process. Landf. 42(1), 71-90.

Brown, A. G., Tooth, S., Chiverrell, R. C., Rose, J., Thomas, D. S., Wainwright, J., Bullard, J.E., Thorndycraft, V.R., Aalto, R., Downs, P., 2013a. The Anthropocene: is there a geomorphological case?. Earth Surf. Process. Landf. 38(4), 431-434.

Brown, A., Toms, P., Carey, C., Rhodes, E., 2013b. Geomorphology of the Anthropocene: time-transgressive discontinuities of human-induced alluviation. Anthropocene, 1, 3-13.

Brown, E. H., 1970. Man shapes the earth. The Geographical Journal, 136(1), 74-85.

Butler, D. R., 1995. Zoogeomorphology: animals as geomorphic agents. Cambridge University Press.

Butler, D. R., 2006. Human-induced changes in animal populations and distributions, and the subsequent effects on fluvial systems. Geomorphology, 79(3-4), 448-459.

Butler, D. R., 2018. Zoogeomorphology in the Anthropocene. Geomorphology, 303, 146-154.

Butler, D. R., Malanson, G. P., 2005. The geomorphic influences of beaver dams and failures of beaver dams. Geomorphology, 71(1-2), 48-60.

Butler, D.R., 2013. Grazing influences on geomorphic systems. J. Shroder, L.A. James, C.P. Harden, J.J. Clague (Eds.), Treatise on Geomorphology, Geomorphology of Human Disturbances, Climate Change, and Natural Hazards, vol. 13, Academic Press, San Diego, CA, pp. 68-73.

Calvès, G., Calderon, Y., Roso, V., Bonnel, C., Roddaz, M., Brusset, S., Baby, P., Clift, P.D., 2019. Past Amazon Basin fluvial systems, insight into the Cenozoic sequences using seismic geomorphology (Marañón Basin, Peru). Journal of South American Earth Sciences. Elsevier, 90 (November 2018), pp. 440–452. doi: 10.1016/j.jsames.2018.12.019.

Carbonel, D. Rodríguez-Tribaldos, V., Gutiérrez, F., Galve, J.P., Guerrero, J., Zarroca, M., Roqué, C., Linares, R., McCalpin, J.P., Acosta, E., 2015. Investigating a damaging buried sinkhole cluster in an urban area (Zaragoza city, NE Spain) integrating multiple techniques: Geomorphological surveys, DInSAR, DEMs, GPR, ERT, and trenching. Geomorphology. Elsevier B.V., 229, pp. 3–16. doi: 10.1016/j.geomorph.2014.02.007.

Carey, J. A., Pinter, N., Pickering, A.J., Prentice, C.S., Delong, S.B., 2019. Analysis of Landslide Kinematics Using Multi-temporal Unmanned Aerial Vehicle Imagery, La Honda, California. Environmental and Engineering Geoscience, XXV(4), pp. 1–17. doi: 10.2113/EEG-2228.

Castaneda, R.A., Avlijas, S., Simard, M., Ricciardi, A., 2014. Microplastic pollution in St. Lawrence River sediments. Canadian Journal of Fisheries and Aquatic Science.

Certini, G., Scalenghe, R., 2011. Anthropogenic soils are the golden spikes for the Anthropocene. The Holocene, 21(8), 1269-1274.

Chee, S. Y., Othman, A. G., Sim, Y. K., Adam, A. N. M., Firth, L. B., 2017. Land reclamation and artificial islands: Walking the tightrope between development and conservation. Global ecology and conservation, 12, 80-95.

Chen, Q., Zhang, S., Chang, S., Liu, B., Liu, J., Long, J., 2019. Geophysical Interpretation of a Subsurface Landslide in the Southern Qinshui Basin. Journal of Environmental and Engineering Geophysics, 24(3), pp. 433–449. doi: 10.2113/JEEG24.3.433.

Chen, X., Yan, Y., Fu, R., Dou, X., Zhang, E., 2008. Sediment transport from the Yangtze River, China, into the sea over the Post-Three Gorge Dam Period: A discussion. Quaternary International, 186(1), 55-64.

Chin, A., Florsheim, J.L., Collins, B.D., Wohl, E., 2013. Feedbacks in human-landscape systems. Environmental Management. doi: 10.1007/s00267-013-0031-y

Chorley, R. J., 1962. Geomorphology and general systems theory. US Geological Survey Professional Paper, 500-B, 1-10.

Chorley, R. J., Kennedy, B. A., 1971. Physical geography: a systems approach. Prentice Hall.

Church, M., 2010. The trajectory of geomorphology. Progress in Physical Geography: Earth and Environment, 34(3), pp. 265–286. doi: 10.1177/0309133310363992.

Clapuyt, F., Vanacker, V., Schlunegger, F., Van Oost, K., 2017. Unravelling earth flow dynamics with 3-D time series derived from UAV-SfM models. Earth Surface Dynamics, 5(4), pp. 791–806. doi: 10.5194/esurf-5-791-2017.

Claussen, M., Brovkin, V., Ganopolski, A., 2001. Biogeophysical versus biogeochemical feedbacks of large-scale land cover change. Geophysical research letters, 28(6), 1011-1014.

Colombo, N., Sambuelli, L., Comina, C., Colombero, C., Giardino, M., Gruber, S., Viviano, G., Vittori Antisari, L., Salerno, F., 2018. Mechanisms linking active rock glaciers and impounded surface water formation in high-mountain areas. Earth Surface Processes and Landforms, 43(2), pp. 417–431. doi: 10.1002/esp.4257.

Comas, X., Wright, W., Hynek, S.A., Fletcher, R.C., Brantley, S.L., 2019. Understanding fracture distribution and its relation to knickpoint evolution in the Rio Icacos watershed (Luquillo Critical Zone Observatory, Puerto Rico) using landscape-scale hydrogeophysics. Earth Surface Processes and Landforms, 44(4), pp. 877–885. doi: 10.1002/esp.4540.

comte de Buffon, G. L. L., 1778. Des époques de la Nature.

Congress, S. S. C., Puppala, A. J., Lundberg, C. L., 2018. Total system error analysis of UAV-CRP technology for monitoring transportation infrastructure asset.

Engineering Geology. Elsevier, 247(November), pp. 104–116. doi: 10.1016/j.enggeo.2018.11.002.

Cook, K. L. 2017. An evaluation of the effectiveness of low-cost UAVs and structure from motion for geomorphic change detection. Geomorphology. Elsevier B.V., 278, pp. 195–208. doi: 10.1016/j.geomorph.2016.11.009.

Cook, L. M., McCuen, R. H., 2011. Hydrologic response of solar farms. Journal of Hydrologic Engineering, 18(5), 536-541.

Crutzen, P. J., 2002. Geology of Mankind. Nature. 415, 23.

Crutzen, P. J., 2006. The “Anthropocene”. In Earth system science in the Anthropocene (pp. 13-18). Springer, Berlin, Heidelberg.

Crutzen, P. J., Stoermer, E. F., 2000. The "Anthropocene". IGBP Newsletter, 41, 17-18.

Cucchiaro, S., Cavalli, M., Vericat, D., Crema, S., Llena, M., Beinat, A., Marchi, L., Cazorzi, F., 2019. Geomorphic effectiveness of check dams in a debris-flow catchment using multi-temporal topographic surveys, Catena. Elsevier, 174(November 2018), pp. 73–83. doi: 10.1016/j.catena.2018.11.004.

Culling, W. E. H., 1957. Multicyclic streams and the equilibrium theory of grade: Jour. Geology, v. 65, p. 259-274.

Dąbski, M., Zmarz, A., Pabjanek, P., Korczak-Abshire, M., Karsznia, I., Chwedorzewska, K.J., 2017. UAV-based detection and spatial analyses of periglacial landforms on Demay Point (King George Island, South Shetland Islands, Antarctica). Geomorphology, 290(November 2016), pp. 29–38. doi: 10.1016/j.geomorph.2017.03.033.

Dafflon, B., Leger, E., Peterson, J., Falco, N., Wainwright, H. M., Wu, Y., Tran, A.P., Brodie, E., Williams, K.H., Versteeg, R., Hubbard, S. S., 2017 (December). Critical zone co-dynamics: Quantifying interactions between subsurface, land surface, and vegetation properties using UAV and geophysical approaches. In AGU Fall Meeting Abstracts.

Dana, J. D., 1895. Manual of Geology: Treating of the principles of the science with special reference to American geological history. American Book Company.

Darmawan, H., Walter, T.R., Brotopuspito, K.S., Nandaka, I.G.M.A., 2018. Morphological and structural changes at the Merapi lava dome monitored in 2012–15 using unmanned aerial vehicles (UAVs). Journal of Volcanology and Geothermal Research, 349, pp.256-267. doi: 10.1016/j.jvolgeores.2017.11.006.

Davis, R. A., Barnard, P. L., 2000. How anthropogenic factors in the back-barrier area influence tidal inlet stability: examples from the Gulf Coast of Florida, USA. Geological Society, London, Special Publications, 175(1), 293-303.

Davis, R., 2011. Inventing the present: historical roots of the Anthropocene. Earth Sciences History, 30(1), 63-84.

De Beni, E., Cantarero, M., Messina, A., 2019. UAVs for volcano monitoring: A new approach applied on an active lava flow on Mt. Etna (Italy), during the 27 February–02 March 2017 eruption. Journal of Volcanology and Geothermal Research, 369, pp.250-262.doi: 10.1016/j.jvolgeores.2018.12.001.

De Groot, S. J., 1979. An assessment of the potential environmental impact of large-scale sand-dredging for the building of artificial islands in the North Sea. Ocean Management, 5(3), 211-232.

de Saussure, H. B., 1796. Voyages dans les Alpes (Vol. 3).

Degenhardt, J. J., Giardino, J. R., 2003. Subsurface investigation of a rock glacier using ground-penetrating radar: Implications for locating stored water on Mars. Journal of Geophysical Research: Planets, 108(E4).

Dering, G.M., Micklethwaite, S., Thiele, S.T., Vollgger, S.A., Cruden, A.R., 2019. Review of drones, photogrammetry and emerging sensor technology for the study of dykes: Best practises and future potential. Journal of Volcanology and Geothermal Research. doi: 10.1016/j.jvolgeores.2019.01.018.

Dialynas, Y. G., Bastola, S., Bras, R. L., Marín-Spiotta, E., Silver, W. L., Arnone, E., Noto, L. V., 2015 (December). Influence of Soil Erosion and Landslide Occurrence on Soil Organic Carbon Storage and Loss in the Luquillo Critical Zone Observatory, Puerto Rico. In AGU Fall Meeting Abstracts.

Díaz, S., Settele, J., Brondízio, E., Ngo, H., Guèze, M., Agard, J., Arneth, A., Balvanera, P., Brauman, K., Butchart, S., Chan, K., 2020. Summary for policymakers of the global assessment report on biodiversity and ecosystem services of the Intergovernmental Science-Policy Platform on Biodiversity and Ecosystem Services. Presented at Plenary of the Intergovernmental Science-Policy Platform on Biodiversity and Ecosystem Services Seventh session. Paris, 29 April–4 May 2019.

Dixon, S. J., Viles, H. A., Garrett, B. L., 2017. Ozymandias in the Anthropocene: The city as an emerging landform. Area. (50) 117-125. doi 10.1111/area.12358.

Doetsch, J., Ingeman-Nielsen, T., Christiansen, A.V., Fiandaca, G., Auken, E., Elberling, B., 2015. Direct current (DC) resistivity and induced polarization (IP) monitoring

of active layer dynamics at high temporal resolution. Cold Regions Science and Technology, 119, pp.16-28. doi: 10.1016/j.coldregions.2015.07.002.

Doughty, C. E., Wolf, A., Field, C. B., 2010. Biophysical feedbacks between the Pleistocene megafauna extinction and climate: The first human-induced global warming?. Geophys. Res. Lett., 37(15). doi:10.1029/2010GL043985

Douglas, I., Lawson, N., 2003. Airport construction: materials use and geomorphic change. Journal of air transport management, 9(3), 177-185.

Duncombe, J., 2019. We have broken nature into more than 990,000 little pieces, Eos, 100, https://doi.org/10.1029/2019EO136354. Published on 05 November 2019.

Ebert-Uphoff, I., S. M. Samarasinghe, E. A. Barnes., 2019. Thoughtfully using artificial intelligence in Earth science, Eos, 100, https://doi.org/10.1029/2019EO135235. Published on 11October 2019.

Edgeworth, M., deB Richter, D., Waters, C., Haff, P., Neal, C., Price, S. J., 2015. Diachronous beginnings of the Anthropocene: The lower bounding surface of anthropogenic deposits. The Anthropocene Review, 2(1), 33-58.

Edwards, L. E., 2015. What is the Anthropocene?. Eos, Earth and Space Science News, 97(2), 6-7.

Ehlers, E., Kraft, T. (Eds.), 2006. Earth System Science in the Anthropocene. New York: Springer. http://dx.doi.org/10.1007/b137853

El Banna, M. M., Frihy, O. E., 2009. Human-induced changes in the geomorphology of the northeastern coast of the Nile delta, Egypt. Geomorphology, 107(1-2), 72-78.

Ellis, E. C., Fuller, D. Q., Kaplan, J. O., Lutters, W. G., 2013. Dating the Anthropocene: Towards an empirical global history of human transformation of the terrestrial biosphere. Elem. Sci. Anth., 1. p.000018. http://doi.org/10.12952/journal.elementa.000018

El-Mowafy, H.Z., Marfurt, K.J., 2016. Quantitative seismic geomorphology of the middle Frio fluvial systems, south Texas, United States. AAPG Bulletin, 100(4), pp.537-564. doi: 10.1306/02011615136.

Eltner, A., Maas, H.G., Faust, D., 2018. Soil micro-topography change detection at hillslopes in fragile Mediterranean landscapes. Geoderma, 313, pp.217-232. doi: 10.1016/j.geoderma.2017.10.034.

Eriksson, B., Eldridge, D. J., 2014. Surface destabilisation by the invasive burrowing engineer Mus musculus on a sub-Antarctic island. Geomorphology, 223, 61-66.

Favalli, M., Fornaciai, A., Nannipieri, L., Harris, A., Calvari, S., Lormand, C., 2018. UAV-based remote sensing surveys of lava flow fields: a case study from Etna's 1974 channel-fed lava flows. Bulletin of Volcanology, 80(3), p.29. doi: 10.1007/s00445-018-1192-6.

Feagin, R. A., Smith, W. K., Psuty, N. P., Young, D. R., Martínez, M. L., Carter, G. A., Lucas, K.L., Gibeaut, J.C., Gemma, J.N., Koske, R. E., 2010. Barrier islands: coupling anthropogenic stability with ecological sustainability. Journal of Coastal Research, 26(6), 987-992.

Findell, K.L., Shevliakova, E., Milly, P.C.D., Stouffer, R.J., 2007. Modeled impact of anthropogenic land cover change on climate. Journal of Climate, 20(14), pp.3621-3634.

Finney, S. C., 2014. The 'Anthropocene' as a ratified unit in the ICS International Chronostratigraphic Chart: fundamental issues that must be addressed by the Task Group. Geological Society, London, Special Publications, 395(1), 23-28.

Finney, S. C., Edwards, L. E., 2016. The "Anthropocene" epoch: Scientific decision or political statement. GSA Today, 26(3), 4-10.

Flinchum, B.A., Holbrook, W.S., Grana, D., Parsekian, A.D., Carr, B.J., Hayes, J.L., Jiao, J., 2018. Estimating the water holding capacity of the critical zone using near-surface geophysics. Hydrological Processes, 32(22), pp.3308-3326. doi: 10.1002/hyp.13260.

Flinchum, B.A., Holbrook, W.S., Parsekian, A.D., Carr, B.J., 2019. Characterizing the Critical Zone Using Borehole and Surface Nuclear Magnetic Resonance. Vadose Zone Journal, 18(1). doi: 10.2136/vzj2018.12.0209.

Fonstad, M.A., Dietrich, J.T., Courville, B.C., Jensen, J.L., Carbonneau, P.E., 2013. Topographic structure from motion: a new development in photogrammetric measurement. Earth surface processes and Landforms, 38(4), pp.421-430. doi: 10.1002/esp.3366.

Fox, T., Pope, M., Ellis, E. C., 2017. Engineering the Anthropocene: Scalable social networks and resilience building in human evolutionary timescales. The Anthropocene Review, 4(3), 199-215.

Fuller, D. Q., Van Etten, J., Manning, K., Castillo, C., Kingwell-Banham, E., Weisskopf, A., Qin, L., Sato, Y.I., Hijmans, R. J., 2011. The contribution of rice agriculture and livestock pastoralism to prehistoric methane levels: An archaeological assessment. The Holocene, 21(5), 743-759.

Gallistl, J., Weigand, M., Stumvoll, M., Ottowitz, D., Glade, T., Orozco, A.F., 2018. Delineation of subsurface variability in clay-rich landslides through spectral induced polarization imaging and electromagnetic methods. Engineering Geology, 245, pp.292-308. doi: 10.1016/j.enggeo.2018.09.001.

Gamache, K., Giardino, J. R., Zhao, P., Owens, R. H., 2018. Bivouacs of the Anthropocene: Urbanization, landforms, and hazards in mountainous regions. In Urban Geomorphology (pp. 205-230). Elsevier.

Giampaolo, V., Capozzoli, L., Grimaldi, S., Rizzo, E., 2016. Sinkhole risk assessment by ERT: The case study of Sirino Lake (Basilicata, Italy). Geomorphology, 253, pp.1-9. doi: 10.1016/j.geomorph.2015.09.028.

Giardino, J. R., Bednarz, R. S., Bryant, J. T., 1987. Nourishment of San Luis Beach, Galveston Island, Texas: an assessment of the impact. American Society of Civil Engineers.

Giardino, J. R., Houser, C. (Eds.), 2015. Principles and dynamics of the Critical Zone (Vol. 19). Elsevier.

Gibbard, P. L., Lewin, J., 2016. Partitioning the quaternary. Quaternary Science Reviews, 151, 127-139.

Gibbard, P. L., Walker, M. J. C., 2014. The term 'Anthropocene'in the context of formal geological classification. Geological Society, London, Special Publications, 395(1), 29-37.

Gilbert, G. K., 1917. Hydraulic-mining debris in the Sierra Nevada (No. 105). US Government Printing Office.

Giletycz, S.J., Chang, C.P., Lin, A.T.S., Ching, K.E., Shyu, J.B.H., 2017. Improved alignment of the Hengchun Fault (southern Taiwan) based on fieldwork, structure-from-motion, shallow drilling, and levelling data. Tectonophysics, 721, pp.435-447. doi: 10.1016/j.tecto.2017.10.018.

Gill, T.E., 1996. Eolian sediments generated by anthropogenic disturbance of playas: human impacts on the geomorphic system and geomorphic impacts on the human system. Geomorphology, 17(1-3), pp.207-228.

Glikson, A., 2013. Fire and human evolution: the deep-time blueprints of the Anthropocene. Anthropocene, 3, 89-92.

Golomb, B., Eder, H. M., 1964. Landforms made by man. Landscape, 14(1), 4-7.

Gomez, C., Kennedy, B., 2018. Capturing volcanic plumes in 3D with UAV-based photogrammetry at Yasur Volcano–Vanuatu. Journal of Volcanology and Geothermal Research, 350, pp.84-88. doi: 10.1016/j.jvolgeores.2017.12.007.

Goudie, A. S., 2006. Global warming and fluvial geomorphology. Geomorphology, 79(3-4), 384-394.

Goudie, A. S., Viles, H. A., 2016. Geomorphology in the Anthropocene. Cambridge University Press.

Goudie, A.S., this issue. The human impact in geomorphology – 50 years of change, Geomorphology, https://doi.org/10.1016/j.geomorph.2018.12.002.

Green, K. C., Westbrook, C. J., 2009. Changes in riparian area structure, channel hydraulics, and sediment yield following loss of beaver dams. Journal of Ecosystems and Management, 10(1).

Green, S. M., Dungait, J. A., Tu, C., Buss, H. L., Sanderson, N., Hawkes, S. J., Xing, K., Yue, F., Hussey, V.L., Peng, J., Johnes, P., 2019. Soil functions and ecosystem services research in the Chinese karst Critical Zone. Chemical Geology, 119107.

Gregory, K. J., 2006. The human role in changing river channels. Geomorphology, 79(3-4), 172-191.

Guisado-Pintado, E., Jackson, D.W., Rogers, D., 2019. 3D mapping efficacy of a drone and terrestrial laser scanner over a temperate beach-dune zone. Geomorphology, 328, pp.157-172. doi: 10.1016/j.geomorph.2018.12.013.

Guo, L., Mount, G.J., Hudson, S., Lin, H., Levia, D., 2020. Pairing geophysical techniques improves understanding of the near-surface Critical Zone: Visualization of preferential routing of stemflow along coarse roots. Geoderma, 357, p.113953. doi: 10.1016/j.geoderma.2019.113953.

Gürer, A., Bayrak, M., Gürer, Ö.F., 2009. A VLF survey using current gathering phenomena for tracing buried faults of Fethiye–Burdur Fault Zone, Turkey. Journal of applied geophysics, 68(3), pp.437-447. doi: 10.1016/j.jappgeo.2009.03.011.

Gutiérrez, A., Naredo Pérez, J. M., 2005. La incidencia de la especie humana sobre la faz de la Tierra (1955-2005). Universidad de Granada.

Guzha, A. C., Rufino, M. C., Okoth, S., Jacobs, S., Nóbrega, R. L. B., 2018. Impacts of land use and land cover change on surface runoff, discharge and low flows: Evidence from East Africa. Journal of Hydrology: Regional Studies, 15, 49-67.

Hack, J. T., 1960. Interpretation of erosional topography in humid temperate regions: Am. Jour. Sci., v. 258-A, p. 80-97.

Hack, J. T., Goodlett, J. C., 1960. Geomorphology and forest ecology of a mountain region in the central Appalachians: U.S. Geol. Survey Prof. Paper 347, 66 p.

Hauck, C., Kneisel, C., 2008. Applied geophysics in periglacial environments. Cambridge University Press. doi: 10.1017/CBO9780511535628.

Haughton, S., 1866. Manual of geology. Longmans, Green, Reader, and Dyer.

Häusler, H., 2017. Did anthropogeology anticipate the idea of the Anthropocene?. The Anthropocene Review, 5(1), 69-86.

Häusler, H.,1959. Das Wirken des Menschen im geologischen Geschehen. Eine Vorstudie zur Anthropogeologie als allgemeines Ergebnis geologisch-technischer Untersuchungen im Großraum von Linz. Naturkundliches Jahrbuch der Stadt Linz 1959: 163–319.

Head, M. J., Gibbard, P. L., 2015. Formal subdivision of the Quaternary System/Period: Past, present, and future. Quaternary International, 383, 4-35.

Hooke, R. L., 1994. On the efficacy of humans as geomorphic agents: GSA Today, v. 4, p. 217, 224–225.

Hooke, R. L., 2000. On the history of humans as geomorphic agents. Geology, 28(9), 843-846.

Hooke, R. L., Martín-Duque, J. F., Pedraza, J., 2012. Land transformation by humans: a review. GSA today, 22(12), 4-10.

Hootsmans, J., Rowley, T. Giardino, J. R., 2015. River Restoration and Long-Term Monitoring: San Miguel River, Telluride, Colorado. GSA meeting abstracts.

Houser, C., Bishop, M. P., Barrineau, P., 2015. Characterizing instability of aeolian environments using analytical reasoning. Earth Surface Processes and Landforms, 40(5), 696-705.

Hu, A., Levis, S., Meehl, G. A., Han, W., Washington, W. M., Oleson, K. W., van Ruijven, B.J., He, M., Strand, W. G., 2016. Impact of solar panels on global climate. Nature Climate Change, 6(3), 290.

Hu, Y., Hou, M., Zhao, C., Zhen, X., Yao, L., Xu, Y., 2019. Human-induced changes of surface albedo in Northern China from 1992-2012. International Journal of Applied Earth Observation and Geoinformation, 79, pp.184-191.

Huntley, D., Bobrowsky, P., Hendry, M., Macciotta, R., Best, M., 2019. Multi-technique geophysical investigation of a very slow-moving landslide near Ashcroft, British Columbia, Canada. Journal of Environmental and Engineering Geophysics, 24(1), pp.87-110. doi: 10.2113/JEEG24.1.87.

Hupy, J. P., Koehler, T., 2012. Modern warfare as a significant form of zoogeomorphic disturbance upon the landscape. Geomorphology, 157, 169-182.

James, L.A., 2013. Legacy sediment: definitions and processes of episodically produced anthropogenic sediment. Anthropocene, 2, pp.16-26.

IPBES, 2019. "Intergovernmental Science-Policy Platform on Biodiversity and Ecosystem Services (IPBES) Media Release." from https://www.ipbes.net/news/Media-Release-Global-Assessment.

IPCC Special Report on the Ocean and Cryosphere in a Changing Climate (SROCC). September 25, 2019. Retrieved November 1, 2019.

Izumida, A., Uchiyama, S., Sugai, T., 2017. Application of UAV-SfM photogrammetry and aerial lidar to a disastrous flood: repeated topographic measurement of a newly formed crevasse splay of the Kinu River, central Japan. Natural Hazards and Earth System Sciences, 17(9), p.1505. doi: 10.5194/nhess-17-1505-2017.

Jacks, G. V., Whyte, R. O., 1939. The rape of the earth: a world survey of soil erosion. The rape of the earth: a world survey of soil erosion.

James, L. A., 2013. Legacy sediment: definitions and processes of episodically produced anthropogenic sediment. Anthropocene, 2, 16-26.

Jefferson, A. J., Wegmann, K. W., Chin, A., 2013. Geomorphology of the Anthropocene: Understanding the surficial legacy of past and present human activities. Anthropocene, (2), 1-3.

Jordan, H., Hamilton, K., Lawley, R., Price, S.J., 2016. Anthropogenic contribution to the geological and geomorphological record: A case study from Great Yarmouth, Norfolk, UK. Geomorphology, 253, pp.534-546.

Jourde, H., Massei, N., Mazzilli, N., Binet, S., Batiot-Guilhe, C., Labat, D., Steinmann, M., Bailly-Comte, V., Seidel, J.L., Arfib, B., Charlier, J.B., 2018. SNO KARST: A French network of observatories for the multidisciplinary study of critical zone processes in karst watersheds and aquifers. Vadose Zone Journal, 17(1).

Kao, S. J., Milliman, J. D., 2008. Water and sediment discharge from small mountainous rivers, Taiwan: The roles of lithology, episodic events, and human activities. The Journal of Geology, 116(5), 431-448.

Kasprzak, M., Jancewicz, K., Michniewicz, A., 2018. UAV and SfM in detailed geomorphological mapping of granite tors: an example of Starościńskie Skały (Sudetes, SW Poland). Pure and Applied Geophysics, 175(9), pp.3193-3207. doi: 10.1007/s00024-017-1730-8.

Kasprzak, M., Jancewicz, K., Różycka, M., Kotwicka, W., Migoń, P., 2019. Geomorphology-and geophysics-based recognition of stages of deep-seated slope deformation (Sudetes, SW Poland). Engineering Geology, 260, p.105230. doi: 10.1016/j.enggeo.2019.105230.

Kaufmann, P.R., Hughes, R.M., 2006. Geomorphic and anthropogenic influences on fish and amphibians in Pacific Northwest coastal streams. In American Fisheries Society Symposium (Vol. 48, No. 429, p. 55).

Kaufmann, G., Romanov, D., 2016. Structure and evolution of collapse sinkholes: combined interpretation from physico-chemical modelling and geophysical field work. Journal of Hydrology, 540, pp.688-698. doi: 10.1016/j.jhydrol.2016.06.050.

Kaufmann, G., Romanov, D., 2017. The Jettencave, Southern Harz Mountains, Germany: Geophysical observations and a structural model of a shallow cave in gypsum/anhydrite-bearing rocks. Geomorphology, 298, pp.20-30. doi: 10.1016/j.geomorph.2017.09.027.

Keating, K., Binley, A., Bense, V., Van Dam, R.L., Christiansen, H.H., 2018. Combined geophysical measurements provide evidence for unfrozen water in permafrost in the adventdalen valley in Svalbard. Geophysical Research Letters, 45(15), pp.7606-7614. doi: 10.1029/2017GL076508.

Keith, D. W., DeCarolis, J. F., Denkenberger, D. C., Lenschow, D. H., Malyshev, S. L., Pacala, S., Rasch, P. J., 2004. The influence of large-scale wind power on global climate. Proceedings of the National Academy of Sciences, 101(46), 16115-16120.

Keylock, C. J., 2010. Introduction to special issue: The future of geomorphology. Progress in Physical Geography. 34(3) 261–264. doi: 10.1177/0309133310364932

Khalil, M.A., Bobst, A., Mosolf, J., 2018. Utilizing 2D electrical resistivity tomography and very low frequency electromagnetics to investigate the hydrogeology of natural cold springs near Virginia City, Southwest Montana. Pure and Applied Geophysics, 175(10), pp.3525-3538. doi: 10.1007/s00024-018-1865-2.

Krane, J., 2005 (March 8). Arab island resorts are reshaping geography. Retrieved from http://www.nbcnews.com/id/7051051/ns/world_news/t/arab-island-resorts-are-reshaping-geography/#.XcXL49VKi00

Kruse, S., 2013. 'Near-Surface Geophysics in Geomorphology', in Treatise on Geomorphology. Elsevier, pp. 103–129. doi: 10.1016/B978-0-12-374739-6.00047-6.

Kumar, G.P., Nagar, M., Choudhary, V., Prasad, A.D., 2019. Shallow subsurface imaging of the Wagad active fault system (Kachchh, northwestern India) by time domain electromagnetic studies. Journal of Earth System Science, 128(3), p.65. doi: 10.1007/s12040-019-1090-0.

Kunnas, J., 2017. Storytelling: From the early Anthropocene to the good or the bad Anthropocene. The Anthropocene Review, 4(2), 136-150.

Lane, S.N., Bakker, M., Costa, A., Girardclos, S., Loizeau, J.L., Molnar, P., Silva, T., Stutenbecker, L., Schlunegger, F., 2019. Making stratigraphy in the Anthropocene: climate change impacts and economic conditions controlling the supply of sediment to Lake Geneva. Scientific reports, 9(1), pp.1-11.

Langedal, M., 1997. The influence of a large anthropogenic sediment source on the fluvial geomorphology of the Knabeåna-Kvina rivers, Norway. Geomorphology, 19(1-2), 117-132.

Langhammer, J., Vacková, T., 2018. Detection and mapping of the geomorphic effects of flooding using UAV photogrammetry. Pure and Applied Geophysics, 175(9), pp.3223-3245. doi: 10.1007/s00024-018-1874-1.

Lazzari, M., Loperte, A., Perrone, A., 2010. Near surface geophysics techniques and geomorphological approach to reconstruct the hazard cave map in historical and urban areas. Advances in Geosciences, 24(January 1972), pp. 35–44. doi: 10.5194/adgeo-24-35-2010.

Leopold, M., Völkel, J., Huber, J., Dethier, D., 2013. Subsurface architecture of the Boulder Creek Critical Zone Observatory from electrical resistivity tomography. Earth Surface Processes and Landforms, 38(12), 1417-1431.

Lewin, J., Macklin, M. G., 2014. Marking time in geomorphology: should we try to formalise an Anthropocene definition?. Earth Surf. Process. Landf. 39(1), 133-137.

Lewis, Q. W., Rhoads, B. L., Andresen, W., 2014 (December). Stream Channel Change in an Intensively Managed Agricultural Landscape: Implications for Critical Zone Processes. In AGU Fall Meeting Abstracts.

Lewis, S. L., Maslin, M. A., 2015a. A transparent framework for defining the Anthropocene Epoch. The Anthropocene Review, 2(2), 128-146.

Lewis, S. L., Maslin, M. A., 2015b. Defining the Anthropocene. Nature, 519(7542), 171.

Li, D., Tang, C., Hou, X., Zhang, H., 2019. Rapid Morphological Changes Caused by Intensive Coastal Development in Longkou Bay, China. Journal of Coastal Research, 35(3), pp.615-624.

Li, H., Harvey, J., Kendall, A., 2013. Field measurement of albedo for different land cover materials and effects on thermal performance. Building and environment, 59, pp.536-546.

Li, Y., Kalnay, E., Motesharrei, S., Rivas, J., Kucharski, F., Kirk-Davidoff, D., Bach, E., Zeng, N., 2018. Climate model shows large-scale wind and solar farms in the Sahara increase rain and vegetation. Science, 361(6406), 1019-1022.

Li, Z., Zhu, Q., Gold, C., 2005. Digital Terrain Modeling: Principles and Methodology. CRC Press.

Macklin, M.G., Lewin, J., Jones, A.F., 2014. Anthropogenic alluvium: An evidence-based meta-analysis for the U.K. Holocene. Anthropocene, 6, 26-38.

Maholland, B.L., 2002. Geomorphic assessment of natural and anthropogenic sediment sources in an eastern Sierra Nevada watershed (Doctoral dissertation, University of Nevada, Reno).

Marescot, L., Monnet, R., Chapellier, D., 2008. Resistivity and induced polarization surveys for slope instability studies in the Swiss Alps. Engineering Geology, 98(1-2), pp.18-28. doi: 10.1016/j.enggeo.2008.01.010.

Marsh, G. P., 1898. The Earth as Modified by Human Action: A Last Revision of "Man and Nature". Charles Scribner’s Sons. New York.

Marston, R., 1994. River entrenchment in small Mountain Valleys of the Western USA: influence of beaver, grazing and clearcut logging/L'incision des cours d'eau dans les petites vallées montagnardes de l'ouest américain: l'influence des castors, du pâturage et des coupes forestières à blanc. Géocarrefour, 69(1), 11-15.

Martin, R., Butler, D. R., 2017. A Framework for Understanding Off-trail Trampling Impacts in Mountain Environments. In The George Wright Forum (Vol. 34, No. 3, pp. 354-367). George Wright Society.

Matthews, H.D., Weaver, A.J., Eby, M., Meissner, K.J., 2003. Radiative forcing of climate by historical land cover change. Geophysical Research Letters, 30(2).

McCormick, A., Hoellein, T.J., Mason, S.A., Schluep, J., Kelly, J.J., 2014. Microplastic is an abundant and distinct microbial habitat in an urban river. Environmental Science and Technology.

Meadows, M. E., 2016. Geomorphology in the Anthropocene: Perspectives from the Past, Pointers for the Future?. In Geomorphology and Society (pp. 7-22). Springer, Tokyo.

Midgley, N.G., Tonkin, T.N., Graham, D.J., Cook, S.J., 2018. Evolution of high-Arctic glacial landforms during deglaciation. Geomorphology, 311, pp.63-75. doi: 10.1016/j.geomorph.2018.03.027.

Minor, J., Pearl, J. K., Barnes, M. L., Colella, T. R., Murphy, P. C., Mann, S., Barron-Gafford, G. A., 2019. Critical Zone Science in the Anthropocene: Opportunities for biogeographic and ecological theory and praxis to drive earth science integration. Prog. Phys. Geogr.

Montgomery, D.R., 2007. Soil erosion and agricultural sustainability. Proceedings of the National Academy of Sciences, 104(33), pp.13268-13272.

Moore, K. D., 2013. Anthropocene is the wrong word. Earth Island Journal, 28(1), 19-20.

Mouyen, M., Longuevergne, L., Steer, P., Crave, A., Lemoine, J. M., Save, H., Robin, C., 2018. Assessing modern river sediment discharge to the ocean using satellite gravimetry. Nature communications, 9(1), 3384.

Münch, Z., Gibson, L., Palmer, A., 2019. Monitoring Effects of Land Cover Change on Biophysical Drivers in Rangelands Using Albedo. Land, 8(2), p.33.

Murray, A. B., Lazarus, E., Ashton, A., Baas, A., Coco, G., Coulthard, T., Fonstad, M., Haff, P., McNamara, D., Paola, C., Pelletier, J., 2009. Geomorphology, complexity, and the emerging science of the Earth's surface. Geomorphology, 103(3), 496-505.

Myhre, G., Myhre, A., 2003. Uncertainties in radiative forcing due to surface albedo changes caused by land-use changes. Journal of Climate, 16(10), 1511-1524.

Naik, P. K., Jay, D. A., 2011. Distinguishing human and climate influences on the Columbia River: changes in mean flow and sediment transport. Journal of hydrology, 404(3-4), 259-277.

NASA Earth Observatory. (2018, April 3) The Pearl-Qatar. Retrieved from https://earthobservatory.nasa.gov/images/91941/the-pearl-qatar

National Research Council (NRC), 2001. Basic research opportunities in earth science. National Academy Press, Washington DC, USA.

Naudet, V., Lazzari, M., Perrone, A., Loperte, A., Piscitelli, S., Lapenna, V., 2008. Integrated geophysical and geomorphological approach to investigate the snowmelt-triggered landslide of Bosco Piccolo village (Basilicata, southern Italy). Engineering Geology, 98(3-4), pp.156-167. doi: 10.1016/j.enggeo.2008.02.008.

Naylor, L. A., Viles, H. A., Carter, N. E. A., 2002. Biogeomorphology revisited: looking towards the future. Geomorphology, 47(1), 3-14.

Neff, J. C., Reynolds, R. L., Belnap, J., Lamothe, P., 2005. Multi-decadal impacts of grazing on soil physical and biogeochemical properties in southeast Utah. Ecological applications, 15(1), 87-95.

Nesbit, P.R., Durkin, P.R., Hugenholtz, C.H., Hubbard, S.M., Kucharczyk, M., 2018. 3-D stratigraphic mapping using a digital outcrop model derived from UAV images and structure-from-motion photogrammetry. Geosphere, 14(6), pp.2469-2486. doi: 10.1130/GES01688.1.

Nir, D., 1983. Man, a geomorphological agent: an introduction to anthropic geomorphology. Jerusalem: Keter.

Novitsky, C.G., Holbrook, W.S., Carr, B.J., Pasquet, S., Okaya, D., Flinchum, B.A., 2018. Mapping inherited fractures in the critical zone using seismic anisotropy from circular surveys. Geophysical Research Letters, 45(7), pp.3126-3135. doi: 10.1002/2017GL075976.

Ntarlagiannis, D., Robinson, J., Soupios, P., Slater, L., 2016. Field-scale electrical geophysics over an olive oil mill waste deposition site: Evaluating the information content of resistivity versus induced polarization (IP) images for delineating the spatial extent of organic contamination. Journal of Applied Geophysics, 135, pp.418-426. doi: 10.1016/j.jappgeo.2016.01.017.

Nugroho, P., Marsono, D., Sudira, P., Suryatmojo, H., 2013. Impact of land-use changes on water balance. Procedia Environmental Sciences, 17, 256-262.

Owens, R., 2019. Personal field observations on the Colorado River, Texas.

Paine, J.G., Collins, E.W., Costard, L., 2015. Discriminating Quaternary Depositional Units on the Texas Coastal Plain Using Airborne Lidar and Near-Surface Geophysics. Gulf Coast Association of Geological Societies Transactions. Society of Exploration Geophysicists and Environment and Engineering Geophysical Society, pp. 313–322. doi: 10.4133/SAGEEP.28-010.

Parsekian, A.D., Singha, K., Minsley, B.J., Holbrook, W.S., Slater, L., 2015. Multiscale geophysical imaging of the critical zone. Reviews of Geophysics, 53(1), pp.1-26. doi: 10.1002/2014RG000465.

Pavan Kumar, G.P., Nagar, M., Choudhary, V., Prasad, A.D., 2019. Shallow subsurface imaging of the Wagad active fault system (Kachchh, northwestern India) by time domain electromagnetic studies. Journal of Earth System Science. Springer India, 128(3), p. 65. doi: 10.1007/s12040-019-1090-0.

Peppa, M.V., Mills, J.P., Moore, P., Miller, P.E., Chambers, J.E., 2017. Brief communication: Landslide motion from cross correlation of UAV-derived morphological attributes. Natural Hazards and Earth System Sciences, 17(12), pp.2143-2150. doi: 10.5194/nhess-17-2143-2017.

Peppa, M.V., Mills, J.P., Moore, P., Miller, P.E., Chambers, J.E., 2019. Automated co-registration and calibration in SfM photogrammetry for landslide change detection. Earth Surface Processes and Landforms, 44(1), pp.287-303. doi: 10.1002/esp.4502.

Perrone, A., Lapenna, V., Piscitelli, S., 2014. Electrical resistivity tomography technique for landslide investigation: a review. Earth-Science Reviews, 135, pp.65-82. doi: 10.1016/j.earscirev.2014.04.002.

Poeppl, R. E., Keesstra, S. D., Maroulis, J., 2017. A conceptual connectivity framework for understanding geomorphic change in human-impacted fluvial systems. Geomorphology, 277, 237-250.

Pollock, M. M., Beechie, T. J., Jordan, C. E., 2007. Geomorphic changes upstream of beaver dams in Bridge Creek, an incised stream channel in the interior Columbia River basin, eastern Oregon. Earth Surface Processes and Landforms, 32(8), 1174-1185.

Price, S.J., Ford, J.R., Cooper, A.H., Neal, C., 2011. Humans as major geological and geomorphological agents in the Anthropocene: the significance of artificial ground in Great Britain. Phil. Trans. Roy. Soc. A 369, 1056–1084.

Quyen, N. T. N., Liem, N. D., Loi, N. K., 2014. Effect of land use change on water discharge in Srepok watershed, Central Highland, Viet Nam. International Soil and Water Conservation Research, 2(3), 74-86.

Raimbault, C., Duperret, A., Le Gall, B., Authemayou, C., 2018. Structural inheritance and coastal geomorphology in SW Brittany, France: An onshore/offshore integrated approach. Geomorphology, 306, pp.141-154. doi: 10.1016/j.geomorph.2018.01.018.

Ramos-Scharrón, C.E. and MacDonald, L.H., 2007. Measurement and prediction of natural and anthropogenic sediment sources, St. John, US Virgin Islands. Catena, 71(2), pp.250-266.

Rapti-Caputo, D., Bratus, A., Santarato, G., 2009. Strategic groundwater resources in the Tagliamento River basin (northern Italy): hydrogeological investigation integrated with geophysical exploration. Hydrogeology journal, 17(6), pp.1393-1409. doi: 10.1007/s10040-009-0459-6.

Revkin, A., 1992. Global Warming: Understanding the Forecast. Abbeville Press, New York.

Rezania, S., Park, J., Din, M., Taib, S., Talaikhozani, A., Yadav, K., Kamyab, H., 2018. Microplastics pollution in different aquatic environments and biota: A review of recent studies. Marine Pollution Bulletin. 133. 191-208.

Rick, T. C., Kirch, P. V., Erlandson, J. M., Fitzpatrick, S. M., 2013. Archeology, deep history, and the human transformation of island ecosystems. Anthropocene, 4, 33-45.

Riebe, C. S., Hahm, W. J., Brantley, S. L., 2017. Controls on deep Critical Zone architecture: A historical review and four testable hypotheses. Earth Surface Processes and Landforms, 42(1), 128-156.

Robinson, D.A., Binley, A., Crook, N., Day-Lewis, F.D., Ferré, T.P.A., Grauch, V.J.S., Knight, R., Knoll, M., Lakshmi, V., Miller, R., Nyquist, J., 2008. Advancing process-based watershed hydrological research using near-surface geophysics: A vision for, and review of, electrical and magnetic geophysical methods. Hydrological Processes: An International Journal, 22(18), pp.3604-3635.doi: 10.1002/hyp.6963.

Rodriguez, J.A.P., Platz, T., Gulick, V., Baker, V.R., Fairén, A.G., Kargel, J., Yan, J., Miyamoto, H., Glines, N., 2015. Did the martian outflow channels mostly form during the Amazonian Period?. Icarus, 257, pp.387-395. doi: 10.1016/j.icarus.2015.04.024.

Rose, N. L., 2015. Spheroidal carbonaceous fly ash particles provide a globally synchronous stratigraphic marker for the Anthropocene. Environmental Science & Technology, 49(7), 4155-4162.

Rosewell, C., 1996. Rates of erosion and sediment transport in Australia. In Erosion and Sediment Yield: Global and Regional Perspectives: Proceedings of an International Symposium Held at Exeter, UK, from 15 to 19 July 1996 (No. 236, p. 139). IAHS.

Rossini, M., Di Mauro, B., Garzonio, R., Baccolo, G., Cavallini, G., Mattavelli, M., De Amicis, M., Colombo, R., 2018. Rapid melting dynamics of an alpine glacier with repeated UAV photogrammetry. Geomorphology, 304, pp.159-172. doi: 10.1016/j.geomorph.2017.12.039.

Ruddiman, W. F., 2003. The anthropogenic greenhouse era began thousands of years ago. Clim. Change, 61 (3), 261-293.

Ruddiman, W. F., 2018. Three flaws in defining a formal 'Anthropocene'. Prog. Phys. Geogr., 42(4), 451-461.

Ruddiman, W. F., Thomson, J. S., 2001. The case for human causes of increased atmospheric CH4 over the last 5000 years. Quat. Sci. Rev. 20 (18), 1769-1777.

Ruddiman, W., 2017. Geographic evidence of the early anthropogenic hypothesis. Anthropocene, 20, 4-14.

Rull, V., 2017a. The "Anthropocene" uncovered. Collectanea Botanica, 36, e008.

Rull, V., 2017b. The "Anthropocene": neglects, misconceptions, and possible futures. EMBO reports, 18(7), 1056-1060.

Santoso, B., Hasanah, M.U., 2019, August. Landslide investigation using self potential method and electrical resistivity tomography (Pasanggrahan, South Sumedang, Indonesia). In IOP Conference Series: Earth and Environmental Science (Vol. 311, No. 1, p. 012068). IOP Publishing. doi: 10.1088/1755-1315/311/1/012068.

Savenije, H. H., Hoekstra, A. Y., van der Zaag, P., 2014. Evolving water science in the Anthropocene. Hydrology and Earth System Sciences, 18(1), 319-332.

Schlesinger, W. H., Reynolds, J. F., Cunningham, G. L., Huenneke, L. F., Jarrell, W. M., Virginia, R. A., Whitford, W. G., 1990. Biological feedbacks in global desertification. Science, 247(4946), 1043-1048.

Schlütz, F., Lehmkuhl, F., 2009. Holocene climatic change and the nomadic Anthropocene in Eastern Tibet: palynological and geomorphological results from the Nianbaoyeze Mountains. Quaternary Science Reviews, 28(15-16), 1449-1471.

Schrott, L., Sass, O., 2008. Application of field geophysics in geomorphology: advances and limitations exemplified by case studies. Geomorphology, 93(1-2), pp.55-73. doi: 10.1016/j.geomorph.2006.12.024.

Schrott, L., Otto, J.C., Götz, J., Geilhausen, M., Otto, J.C., 2013. Fundamental classic and modern field techniques in Geomorphology–an overview. In Treatise on Geomorphology. Elsevier. pp. 6–21. doi: 10.1016/B978-0-12-374739-6.00369-9.

Seagle, S. W., Liang, S. Y., 2001. Application of a forest gap model for prediction of browsing effects on riparian forest succession. Ecological Modelling, 144(2-3), 213-229.

Segura, C., Booth, D.B., 2010. Effects of Geomorphic Setting and Urbanization on Wood, Pools, Sediment Storage, and Bank Erosion in Puget Sound Streams. Journal of the American Water Resources Association (JAWRA) Vol. 46(5).

Shaler, N. S., 1905. Man and the Earth. Fox, Duffield.

Sherlock, R. L., 1922. Man as a geological agent: an account of his action on inanimate nature. HF & G. Witherby.

Siart, C., Forbriger, M., Nowaczinski, E., Hecht, S., Höfle, B., 2013. Fusion of multi-resolution surface (terrestrial laser scanning) and subsurface geodata (ERT, SRT) for karst landform investigation and geomorphometric quantification. Earth Surface Processes and Landforms, 38(10), pp.1135-1147. doi: 10.1002/esp.3394.

Simon, A., Rinaldi, M., 2006. Disturbance, stream incision, and channel evolution: The roles of excess transport capacity and boundary materials in controlling channel response. Geomorphology. Vol. 79.

Skalak, K.J., Benthem, A.J., Schenk, E.R., Hupp, C.R., Galloway, J.M., Nustad, R.A. Wiche, G.J., 2013. Large dams and alluvial rivers in the Anthropocene: The impacts of the Garrison and Oahe Dams on the Upper Missouri River. Anthropocene, 2, 51-64.

Slaymaker, O., 2009. The future of geomorphology. Geography Compass, 3(1), 329-349.

Slim, M., Perron, J. T., Martel, S. J., Singha, K., 2015. Topographic stress and rock fracture: a two-dimensional numerical model for arbitrary topography and preliminary comparison with borehole observations. Earth Surf. Process. Landf. 40(4), 512-529.

Smith, B. D., Zeder, M. A., 2013. The onset of the Anthropocene. Anthropocene, 4, 8-13.

Sofia, G., Marinello, F., Tarolli, P., 2014. A new landscape metric for the identification of terraced sites: the Slope Local Length of Auto-Correlation (SLLAC). ISPRS Journal of Photogrammetry and Remote Sensing, 96, 123-133.

Solberg, I.L., Long, M., Baranwal, V.C., Gylland, A.S., Rønning, J.S., 2016. Geophysical and geotechnical studies of geology and sediment properties at a quick-clay landslide site at Esp, Trondheim, Norway. Engineering Geology, 208, pp.214-230. doi: 10.1016/j.enggeo.2016.04.031.

Spina, R., 2019. Big Data and Artificial Intelligence Analytics in Geosciences: Promises and Potential. GSA Today, 29(1).

St. Clair, J., Moon, S., Holbrook, W. S., Perron, J. T., Riebe, C. S., Martel, S. J., Carr, B., Harman, C., Singha, K., Richter, D. D., 2015. Geophysical imaging reveals topographic stress control of bedrock weathering. Science 350: 534–538.

Stan, D., Stan-Kłeczek, I., Kania, M., 2017. Geophysical approach to the study of a periglacial blockfield in a mountain area (Ztracené kameny, Eastern Sudetes, Czech Republic). Geomorphology, 293, pp.380-390. doi: 10.1016/j.geomorph.2016.12.004.

Steffen, W., Grinevald, J., Crutzen, P., McNeill, J., 2011. The Anthropocene: conceptual and historical perspectives. Philosophical Transactions of the Royal Society A: Mathematical, Physical and Engineering Sciences, 369(1938), 842-867.

Stephens, L., Fuller, D., Boivin, N., Rick, T., Gauthier, N., Kay, A., Marwick, B., Geralda, C., Armstrong, D., Barton, C.M., Denham, T., 2019. Archaeological assessment reveals Earth's early transformation through land use. Science, 365(6456), pp.897-902.

Stepinski, T. F., Vilalta, R., 2010. Machine Learning Tools for Geomorphic Mapping of Planetary Surfaces. In Machine Learning. IntechOpen.

Strahler, A. N., 1950. Equilibrium theory of erosional slopes approached by frequency distribution analysis. Part I. American Journal of Science, 248, 673-696.

Strahler, A. N., 1952A. Dynamic basis of geomorphology: Geol. Soc. America Bull., v. 63, p. 923-938.

Strahler, A. N., 1952B. Hypsometric (area-altitude) analysis of erosional topography: Geol. Soc. America Bull., v. 63, p. 1117- 1142.

Strick, R.J.P, Ashworth, P.J., Sambrook Smith, G.H., Nicholas, A.P., Best, J.L., Lane, S.N., Parsons, D.R., Simpson, C.J., Unsworth, C.A., Dale, J., 2019. Quantification of bedform dynamics and bedload sediment flux in sandy braided rivers from airborne and satellite imagery. Earth Surface Processes and Landforms, 44(4), pp.953-972. doi: 10.1002/esp.4558.

Subramanian, M., 2019. Anthropocene now: influential panel votes to recognize Earth's new epoch. Nature, 21, 2019.

Suess, E., 1862. Der Boden der Stadt Wien. Vienna: W. Braumüller.

Sullivan, P. L., Wymore, A. S., McDowell, W. H., Aronson, E., Arvin, L., Bales, R., Berhe, A., 2017. New Opportunities for Critical Zone Science. 2017 CZO Arlington Meeting White Booklet.

Syvitski, J. P., Vörösmarty, C. J., Kettner, A. J., Green, P., 2005. Impact of humans on the flux of terrestrial sediment to the global coastal ocean. science, 308(5720), 376-380.

Szabó, J., Dávid, L., Lóczy, D. (Eds.), 2010. Anthropogenic geomorphology: a guide to man-made landforms. Springer Science & Business Media.

Talalay, P. G., 2014. Perspectives for development of ice-core drilling technology: a discussion. Annals of Glaciology, 55(68), 339-350.

Tarolli P, Preti F, Romano N., 2014. Terraced landscapes: from an old best practice to a potential hazard for soil degradation due to land abandonment. Anthropocene 6, 10–25.

Tarolli, P., Cao, W., Sofia, G., Evans, D., Ellis, E. C., 2019. From features to fingerprints: A general diagnostic framework for anthropogenic geomorphology. Prog. Phys. Geogr. 43(1), 95-128.

The Critical Zone. http://criticalzone.org/national/research/the-critical-zone-1national/ (accessed 15 November 2019).

Thomas, W. L., 1956. Man's Role in Changing the Face of the Earth. Chicago, London, 10-13.

Thornbush, M., Krakauer, N., 2017. Introduction to the Special Issue on Climate Change and Geosciences.

Tien Bui, D., Shirzadi, A., Shahabi, H., Chapi, K., Omidavr, E., Pham, B. T., Talebpour Asl, D., Khaledian, H., Pradhan, B., Panahi, M., Bin Ahmad, B., 2019. A Novel Ensemble Artificial Intelligence Approach for Gully Erosion Mapping in a Semi-Arid Watershed (Iran). Sensors, 19(11), 2444.

Tooth, S., 2007. Arid geomorphology: investigating past, present and future changes. Progress in Physical Geography, 31(3), 319-335.

Trimble, S. W., 1974. Man-induced soil erosion on the southern Piedmont. Soil Conservation Society of America.

Trimble, S. W., 1975. A volumetric estimate of man-induced soil erosion on the Southern Piedmont Plateau. Present and prospective technology for predicting sediment yields and sources. Publication ARS_S_40. US Department of Agriculture.

Turner, B. L., Clark, W. C., Kates, R. W., Richards, J. F., Mathews, J. T., 1990. The earth as transformed by human action: global and regional changes in the biosphere over the past 300 years. Cambridge Univ. Press.

Valkaniotis, S., Papathanassiou, G., Ganas, A., 2018. Mapping an earthquake-induced landslide based on UAV imagery; case study of the 2015 Okeanos landslide, Lefkada, Greece. Engineering Geology, 245, pp.141-152. doi: 10.1016/j.enggeo.2018.08.010.

Van Dam, R.L., 2012. Landform characterization using geophysics—Recent advances, applications, and emerging tools. Geomorphology, 137(1), pp.57-73. doi: 10.1016/j.geomorph.2010.09.005.

Vanacker, V., Molina, A., Govers, G., Poesen, J., Dercon, G., Deckers, S., 2005. River channel response to short-term human-induced change in landscape connectivity in Andean ecosystems. Geomorphology, 72(1-4), 340-353.

Visconti, G., 2014. Anthropocene: another academic invention? Rendiconti Lincei, 25, 281-92.

Vörösmarty, C. J., Meybeck, M., Fekete, B., Sharma, K., Green, P., Syvitski, J. P., 2003. Anthropogenic sediment retention: major global impact from registered river impoundments. Global and planetary change, 39(1-2), 169-190.

Walker, M., Gibbard, P., Lowe, J., 2015. Comment on "When did the Anthropocene begin? A mid-twentieth century boundary is stratigraphically optimal" by Jan Zalasiewicz et al.(2015), Quaternary International, 383, 196–203. Quaternary International, 383, 204-207.

Walker, M., Head, M.J., Berkelhammer, M., Björck, S., Cheng, H., Cwynar, L., Fisher, D., Gkinis, V., Long, A., Lowe, J., Newnham, R., 2018. Formal ratification of the subdivision of the Holocene Series/Epoch (Quaternary System/Period): two new Global Boundary Stratotype Sections and Points (GSSPs) and three new stages/subseries. Episodes, 41(4), pp.213-223.

Walling, D. E., 2006. Human impact on land–ocean sediment transfer by the world's rivers. Geomorphology, 79(3-4), 192-216.

Walling, D., 2008. The changing sediment loads of the world's rivers. Annals of Warsaw University of Life Sciences-SGGW. Land Reclamation, 39, 3-20.

Wang, F., Okeke, A.C.U., Kogure, T., Sakai, T., Hayashi, H., 2018. Assessing the internal structure of landslide dams subject to possible piping erosion by means of microtremor chain array and self-potential surveys. Engineering Geology, 234, pp.11-26. doi: 10.1016/j.enggeo.2017.12.023.

Wang, S., Fu, B., Piao, S., Lü, Y., Ciais, P., Feng, X., Wang, Y., 2016. Reduced sediment transport in the Yellow River due to anthropogenic changes. Nature Geoscience, 9(1), 38.

Wang, S., Wang, S., 2015. Impacts of wind energy on environment: A review. Renewable and Sustainable Energy Reviews, 49, 437-443.

Wang, W., Chen, P., Keifer, I., Dueker, K., Lee, E.J., Mu, D., Jiao, J., Zhang, Y., Carr, B., 2019. Weathering front under a granite ridge revealed through full-3D seismic ambient-noise tomography. Earth and Planetary Science Letters, 509, pp.66-77. doi: 10.1016/j.epsl.2018.12.038.

Wang, Y., Wu, B., 2019. Active machine learning approach for crater detection from planetary imagery and digital elevation models. IEEE Transactions on Geoscience and Remote Sensing.

Waters, C. N., Zalasiewicz, J., Summerhayes, C., Barnosky, A. D., Poirier, C., Gałuszka, A., Cearreta, A., Edgeworth, M., Ellis, E.C., Ellis, M., Jeandel, C., 2016. The Anthropocene is functionally and stratigraphically distinct from the Holocene. Science, 351(6269), aad2622.

Wegmann, K.W., Bohnenstiehl, D.R., Bowman, J.D., Homburg, J.A., Windingstad, J.D., Beery, D., 2012. Assessing coastal landscape change for archaeological purposes: integrating shallow geophysics, historical archives and geomorphology at Port Angeles, Washington, USA. Archaeological Prospection, 19(4), pp.229-252. doi: 10.1002/arp.

Wernette, P., Houser, C., Weymer, B. A., Everett, M. E., Bishop, M. P., Reece, B., 2018. Influence of a spatially complex framework geology on barrier island geomorphology. Marine geology, 398, 151-162.

Weymer, B.A., Everett, M.E., de Smet, T.S., Houser, C., 2015. Review of electromagnetic induction for mapping barrier island framework geology. Sedimentary Geology, 321, pp.11-24. doi: 10.1016/j.sedgeo.2015.03.005.

Williams, G. P., Wolman, M. G., 1984. Downstream effects of dams on alluvial rivers. United States Geological Survey Professional Paper 1286.

Woeikof, A., 1901. De l'influence de l'homme sur la terre. In Annales de Géographie (Vol. 10, No. 50, pp. 97-114). Armand Colin.

Wohl, E., 2006. Human impacts to mountain streams. Geomorphology, 79(3-4), 217-248.

Wohl, E., 2013. Wilderness is dead: Whither Critical Zone studies and geomorphology in the Anthropocene?. Anthropocene, 2, 4-15.

Wohl, E., 2015. Legacy effects on sediments in river corridors. Earth-Science Reviews, 147, 30-53.

Yan, B., Fang, N. F., Zhang, P. C., Shi, Z. H., 2013. Impacts of land use change on watershed streamflow and sediment yield: An assessment using hydrologic modelling and partial least squares regression. Journal of Hydrology, 484, 26-37.

Yu, M., Huang, Y., Zhou, J., Mao, L., 2017. Modeling of landslide topography based on micro-unmanned aerial vehicle photography and structure-from-motion. Environmental earth sciences, 76(15), p.520. doi: 10.1007/s12665-017-6860-x.

Yu, X., Duffy, C., Gil, Y., Leonard, L., Bhatt, G., Thomas, E., 2016. Cyber-innovated watershed research at the shale hills critical zone observatory. IEEE Systems Journal, 10(3), pp.1239-1250. doi: 10.1109/JSYST.2015.2484219.

Zalasiewicz, J., Waters, C. N., Summerhayes, C. P., Wolfe, A. P., Barnosky, A. D., Cearreta, A., Crutzen, P., Ellis, E., Fairchild, I.J., Gałuszka, A., Haff, P., 2017. The Working Group on the Anthropocene: Summary of evidence and interim recommendations. Anthropocene, 19, 55-60.

Zalasiewicz, J., Waters, C. N., Williams, M., Barnosky, A. D., Cearreta, A., Crutzen, P., Ellis, E., Ellis, M.A., Fairchild, I.J., Grinevald, J., Haff, P.K., 2015. When did the Anthropocene begin? A mid-twentieth century boundary level is stratigraphically optimal. Quaternary International, 383, 196-203.

Zalasiewicz, J., Williams, M., Haywood, A., Ellis, M., 2011. The Anthropocene: a new epoch of geological time? Phil. Trans. R. Soc. A 369A, 835–841.

Zalasiewicz, J., Williams, M., Steffen, W., Crutzen, P., 2010. The New World of the Anthropocene. Environ. Sci. Technol. 44(7), 2228-2231.

Zhang, Q., Han, G., Liu, M., Wang, L., 2019. Geochemical Characteristics of Rare Earth Elements in Soils from Puding Karst Critical Zone Observatory, Southwest China. Sustainability, 11(18), 4963.

Zhang, Y. K., Schilling, K. E., 2006. Increasing streamflow and baseflow in Mississippi River since the 1940 s: Effect of land use change. Journal of Hydrology, 324(1-4), 412-422.

Zhou, L., Tian, Y., Baidya, R.S., Thorncroft, C., Bosart, L.F., Hu, Y., 2012. Impacts of wind farms on land surface temperature. Nat. Clim. Change, 2, 539–543.

Zhu, C., Li, Y., 2014. Long-term hydrological impacts of land use/land cover change from 1984 to 2010 in the Little River Watershed, Tennessee. International Soil and Water Conservation Research, 2(2), 11-21.

3. USE OF GEOPHYSICAL METHODS IN GEOMORPHOLOGY: KEYS TO VIEWING THE UNSEEN

3.1. Synopsis

Furthering our understanding of complex landscapes, landforms, and processes requires investigations across scales, considering surface and subsurface structure and characteristics. Technological advances provide tools and methods that allow data collection at varying scales as well as non-destructive and/or remote access to valuable information. Non-invasive methods are ideal to conduct research in previously unreachable areas and areas where traditional methodologies are not feasible (i.e., urban areas, environmentally protected, archaeological sites). Geomorphologists are increasingly interested in using non-invasive methodologies as demonstrated by recent literature. Current methodologies applied to studies across geomorphic environments are adapted from other disciplines, thus, involving interdisciplinary collaborative research teams. Data collected at different scales (i.e., regional to point scale) require careful integration but using a multiple-method approach helps overcome limitations associated with individual instruments and methods. This section summarizes the methodologies employed in a variety of geomorphic environments to solve frequently encountered geomorphological problems, with a focus on non-invasive geophysical methods utilized as a part of multi-method approaches.

3.1.1. Introduction

Geomorphic features were traditionally characterized based on information extracted from topographic maps, aerial photos, and field research, including outcrops,

trenches, and boreholes. These methods are restricting as outcrops are spatially limited; and trenching and borehole drilling result in costly (time and resources) investigations (Van Dam, 2012). Traditional methods used in Geomorphology have benefited from technological advances (Vitek, 2013) such as newly developed and improved instrumentation, as well as advances in methods and equipment for data collection and processing, leading to what is referred to as modern geomorphology (Church, 2010; Schrott et al., 2013). Tools and techniques developed in other disciplines are adapted to the needs of modern geomorphologists (Viles, 2016) and used to produce more accurate maps and to obtain higher-resolution information, thus, improving understanding of surface and sub-surface processes. These advances can additionally be used to study landform development through time and space (Schrott et al., 2013; Schrott and Sass, 2008), as well as to determine the composition, internal structure, and subsurface extension (Van Dam, 2012).

Since the twentieth century, geomorphological studies have advanced with the use of geophysical methods (Schrott and Sass, 2008). Increased interest in incorporating geophysical methods in geomorphology is attributed to a combination of factors including the availability of user-friendly, lightweight, versatile, and non-invasive equipment (Schrott et al., 2013), as well as more powerful computers (i.e., personal and large-scale)(Church, 2010). These conditions facilitate the use of multiple method approaches in modern geomorphic studies which are typically comprised by a combination of two or more of the following methods: traditional field work, remote sensing data from aerial photographs, satellite images, airborne and terrestrial LIDAR,

and UAV surveys, age-dating methods, geophysical surveys, and high-resolution data from monitoring instrumentation (i.e., data loggers, force, displacement, and temperature sensors, etc.) (Van Dam, 2012; Viles, 2016; Aguilar et al., 2020). The scale and purpose of the study will determine the methods to employ. Geophysical surveys can be repeated over time to study rapidly changing geomorphic environments, and concurrent subsurface explorations and surface characterization are recommended to understand the dynamics of geomorphic processes. Remote sensing data are ideal in regional (i.e., large spatial scale) studies whereas ground-based (i.e., small spatial scale) techniques yield higher-resolution information. The acquisition of the differing types of data should be done with coinciding scales to ensure appropriate integration of remotely sensed and geophysical data (Kruse, 2013).

"A science such as geomorphology may, indeed, be shaped by technological change and development because new research questions may be able to be answered with the advent of new techniques" (Viles, 2016, p. 122). Geophysical applications have enhanced our understanding of geomorphological processes in a variety of fields. Remarkably, modeling rates of erosion and sedimentation at large scales (i.e., time and space) became possible through the interpretation of geophysical data and previously inaccessible information concerning the surface and near-surface of Earth is available as a result of airborne and seaborne geophysical explorations (Church, 2010). Geophysical explorations allow a glimpse into the unobserved and to enhance our understanding of the relationships between underground and above ground processes.

Schrott and Sass (2008) highlight the importance of interdisciplinary collaboration in geomorphological studies using geophysical techniques, to ensure adequate interpretation of geophysical data. A growing trend in geomorphology, particularly in Critical Zone (i.e., integrated system of interacting components and processes comprising the outermost layers of the continental crust) (National Research Council, 2001) studies, is to depart from researching under multidisciplinary approaches (involvement without interaction of several disciplines), and instead utilize interdisciplinary approaches (i.e., integration of several disciplines to solve a complex problem) (Chamorro et al., 2015). Critical Zone research is generally conducted through time at varying spatial scales within the boundaries of a watershed using multiple techniques, including geophysical surveys used in characterizing Critical Zone (Viles, 2016; Aguilar et al., 2020) geometry and processes (see Robinson et al., 2008; Leopold et al., 2013; Parsekian et al., 2015; St. Clair et al., 2015; Riebe et al., 2017) and in deep Critical Zone investigations (Slim et al., 2015).

In this section, geomorphological studies that employ geophysical techniques are discussed. Case studies are organized by the geomorphological process and presented with minimal location-dependent descriptions, highlighting the most relevant research questions addressed in the current literature, are presented in section 3.2. As the common practice is to employ a multiple method approach, the reader can expect to find the same methods applied in a variety of settings and in combination with different geophysical techniques. In section 3.3, two tables are presented, one table summarizes the applicability of some geophysical methods (table 4), and the other one directs the

reader to current literature exemplifying the application of geophysical methods in geomorphological studies (table 5). The tables complement the information presented in Section 3.2 and can provide insight into the process of selecting appropriate geophysical methods to solve geomorphological problems. Section 3.4 concludes this section with a discussion of the application of geophysical methods to address cutting-edge geomorphological questions.

The reader is encouraged to consult Reynolds (2011) and Everett (2013) for an extensive discussion of near-surface geophysical methods, as well as exemplary case studies, and Van Dam (2012) for an overview of the application of terrestrial geophysical methods to landform characterization. The Treatise on Geomorphology (1st Ed.), particularly Vol. 14 (Schrott et al., 2013) and Vol. 3 (Kruse, 2013) provide additional in-depth information about geophysical techniques used in geomorphology, and Vol. 14 (Bristow, 2013) examines the method of ground-penetrating radar. Hauck and Kneisel (2008) is of importance for those interested in geophysical applications in periglacial environments.

For a detailed discussion of the physics behind the methods covered in this section, the reader is directed to the Treatise on Geophysics (2nd Ed). Specifically, Vol. 11 (Phillips, 2015) discusses the gravitational method (Gravity), Binley (2015) focuses on electrical methods (Direct Current Resistivity (DC) and Induce Polarization (IP), Müller-Petke and Yaramanci (2015) explain the nuclear magnetic resonance method (NMR), van der Kruk (2015) reviews ground-penetrating radar (GPR), Jackson (2015) examines self-potential methods (SP), and Fitterman (2015) concentrates on active-

source electromagnetic methods (Frequency-Domain Electromagnetics (FDEM) and Time-Domain Electromagnetics (TDEM). Vol. 6 (Tucker, 2015) provides an overview of the state of knowledge in landscape evolution, as well as some geophysical applications used to advance the understanding of process mechanics.

Relevant resources to consult include Nazarian et al. (1983), Nazarian and Stokoe (1986), Park et al. (1999), Socco and Strobbia (2004), and Socco et al. (2010) for the seismic surface wave method, Knapp and Steeples (1986a), Knapp and Steeples (1986b) for seismic refraction and Steeples and Miller (1998) for seismic reflection techniques, Davis and Annan (1989) and Jol (2009) for GPR, Revil and Jardani (2013) for the SP method, Loke and Barker (1996) and Barker and Loke (1996) for electrical methods, specifically Electrical Resistivity Tomography (ERT). Lastly, we recommend reviewing Ward and Hohmann (1988) and Spies (1989) for Electromagnetic Methods (EM).

3.2. Geomorphological applications of geophysical methods

Geomorphological investigations are commonly carried out to determine the mechanisms that act together to create or modify landforms and landscapes. The driving agents of geomorphic change are dependent on factors such as climate, lithology, and tectonic setting, which are inherently linked to the geographic location. Research questions in geomorphology are broad, but it is common for geomorphologists to be interested in a process or geomorphic environment. For this reason, this section is organized per geomorphic process-environment.

Figure 20 corresponds with a conceptual model illustrating the use of several methods to study the geomorphic environments and processes discussed in this section. Selecting an appropriate method or a combination of different methods to conduct a geomorphological study is dependent on the research question or questions, the temporal and spatial scale, local conditions (i.e., accessibility), as well as available funding. The majority of the case studies presented in this section utilize multiple method approaches to conduct geomorphological research. Most of the geophysical methods employed in these investigations are non-invasive; however, the reader can expect to find mentions of combined approaches that include the use of destructive methods (i.e., borehole geophysics). Section 3.3 of this document provides additional references illustrating the use of geophysical methods in geomorphological studies.

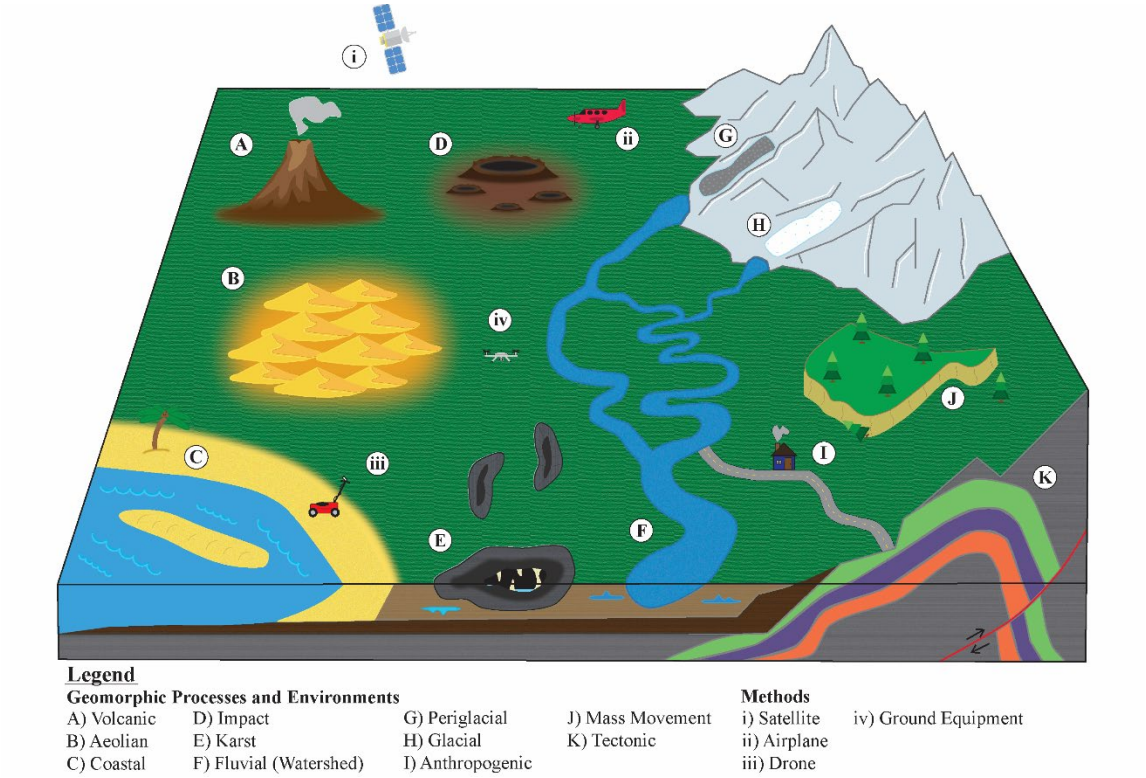

Figure 20 Conceptual model illustrating the geomorphic environments and processes, as well as some of the methods discussed in this section.

This section summarizes case studies chosen to exemplify the application of geophysical methods in geomorphological research; a brief description of the problem, the methodology, and the conclusions of each case study is included. The summaries are organized by geomorphic environment-process including coastal, eolian, watershed, glacial, periglacial, tectonic, karst, mass movement, and volcanic. Examples of characterization of impact features are also included.

A subsection is dedicated to the identification of anthropogenic features and processes; however, many of the cases discussed in other subsections are conducted in

urbanized areas (i.e., studies related to karst processes in the built environment are mentioned in the karst subsection). Examples of every possible application cannot be included in a single section. The reader is encouraged to think of their research topic of interest in a general way. For example, if the research focus is on the stability of anthropogenic landforms, such as mine spoils and landfills, the reader can consult the subsection on mass movement.

The goal of this section is to discuss the use of geophysical techniques in specific geomorphic processes and environments; however, the reader should bear in mind that the various geophysical techniques are not process-dependent and are used to study a variety of processes across geomorphic environments.

3.2.1. Fluvial (watershed) processes-environment

Robinson et al. (2008) discuss the rise of hydrogeophysics in process-oriented hydrological studies at a watershed level. Hydrogeological problems that can be addressed using geophysics include mapping contamination plumes, determining water pathways, and aquifer characterization (Robinson et al., 2008). The authors propose a multiple-method, cross-scale approach to study hydrological flow across the watershed, with an interdisciplinary scope that integrates hydrological information with geological, physical, chemical, and biological components. Although not stated by the authors, such a comprehensive approach is essentially a Critical-Zone approach, which can be applied across geomorphic environments.

The use of electrical and magnetic methods for hydrological applications, particularly airborne and ground-based systems, is extensively discussed by Robinson et

al. (2008). The authors present their assessment on the applicability of different geophysical methods to obtain data at the following scales: basin (2500–25000 km^2), sub-basin (250–2500 km^2), watershed (80–250 km^2), sub-watershed (1–80 km^2), catchment (0.1–1 km^2), and point scale. Airborne methods are recommended for studies at sub-watershed scale and greater, whereas ground methods such as magnetotelluric, seismic, and gravity methods, are deemed suitable across scales. Ground-based electromagnetic methods and ground penetrating radar (GPR) are useful at a point to sub-watershed scale (up to 80 km^2), whereas electrical resistivity, induced polarization (IP), and magnetic resonance are restricted to areas of up to 1 km^2 (Robinson et al., 2008).

Similarly, the authors present a summary of the hydrological variables that can be resolved with geophysical data. Lithological characteristics and pore fluid electrical conductivity can be determined using airborne or ground-based electromagnetic data, the latter can also provide information about stratification. Ground-based GPR is useful in determining moisture content, rock stratification, faulting and fracturing, whereas electrical resistivity adds pore fluid electrical conductivity and lithologic factors to the hydrological properties than can be determined using the method (Robinson et al., 2008).

Among the advantages of using geoelectrical methods for hydrological applications, Robinson et al. (2008) include the affordability, reliability, and ease of operation of the instrumentation, as well as the convenience of the availability of trusted imaging tools. Good targets for resistivity methods include clay layers, high salinity, and variable moisture content. Difficulties linked with resistivity imaging include slow data

collection and challenging data processing, setting up long arrays is labor-intensive, and the ground must be penetrable with electrodes (Robinson et al., 2008).

Electromagnetic methods are non-invasive, and useful for mapping the distribution of electrical resistivity in the subsurface. Advantages of electromagnetic techniques include considerable depth of penetration (i.e. hundreds of meters), the possibility to develop 2D or quasi-2D resistivity models from measurements along a profile, proven to help in the characterization of aquifers. Some disadvantages of using electromagnetic methods comprise the need to invert the data, and in the case of GPR higher frequencies yield higher resolution but decrease the depth of penetration (Robinson et al., 2008).

3.2.1.1. Fluvial (watershed) processes-environment

Koruk et al. (2020) used a multiple-method approach to study groundwater-surface interaction at varying temporal and spatial scales. The authors employed the different methodologies in a hierarchical manner, starting at a regional scale and going all the way down to point scale (i.e., piezometers, samples). Using geological, geomorphological, and water quality data (i.e. major ions) collected at a watershed scale, the authors selected the sections of the river where midscale studies, including geophysical surveys, were to be conducted. Instrumentation employed at the reach scale includes electromagnetic induction (EMI) equipment, fiber-optic distributed temperature sensors (FO-DTS), piezometers, and data loggers (i.e., temperature loggers, water level data logger) (Koruk et al., 2020).

A boat equipped with the EMI system, a GPS, a data logger (i.e., to measure water depth), and a conductivity probe, gathered data along a 2 km reach of the stream (Koruk et al., 2020). The effects of stream depth and electrical conductivity, once determined, can be removed from the apparent electrical conductivity. Thus, variations in streambed texture and/or pore-water electrical conductivity are interpreted from variations in the measured electrical conductivity (Binley et al., 2013). Accordingly, Koruk et al. (2020) interpret areas of high permeability/porosity or pore water electrical conductivity contrasts as potential sites of groundwater upwelling. These interpretations guided the data collection at a point scale. The authors highlight that data collected at varying scales on a highly heterogeneous medium are not always in agreement, but coupling diverse methods helps validate results and interpretations.

3.2.1.2. Fluvial geomorphology

Electrical Resistivity Tomography (ERT) was used by Scapozza and Laigre (2014) to identify paleochannels in a highly urbanized floodplain. The authors calculated the relationship between electrical resistivity and temperature for the lithologies of their study area (Fig. 21A). The surface arrangement of electrodes and subsurface distribution of electric current and equipotentials is shown in figure 21B. The most common electrode arrangements can be found in figure 21C, whereas figure 21D shows an example of a pseudo-section generated using a Wenner array.

Differences in the grain size of the sediments can be detected with ERT as ranges of resistivity values have been associated with deposits of varying grain sizes. A contrast in resistivity readings would indicate the location of paleochannels, which are composed

of coarser sediments than other facies in this fluvial environment (Scapozza and Laigre, 2014).

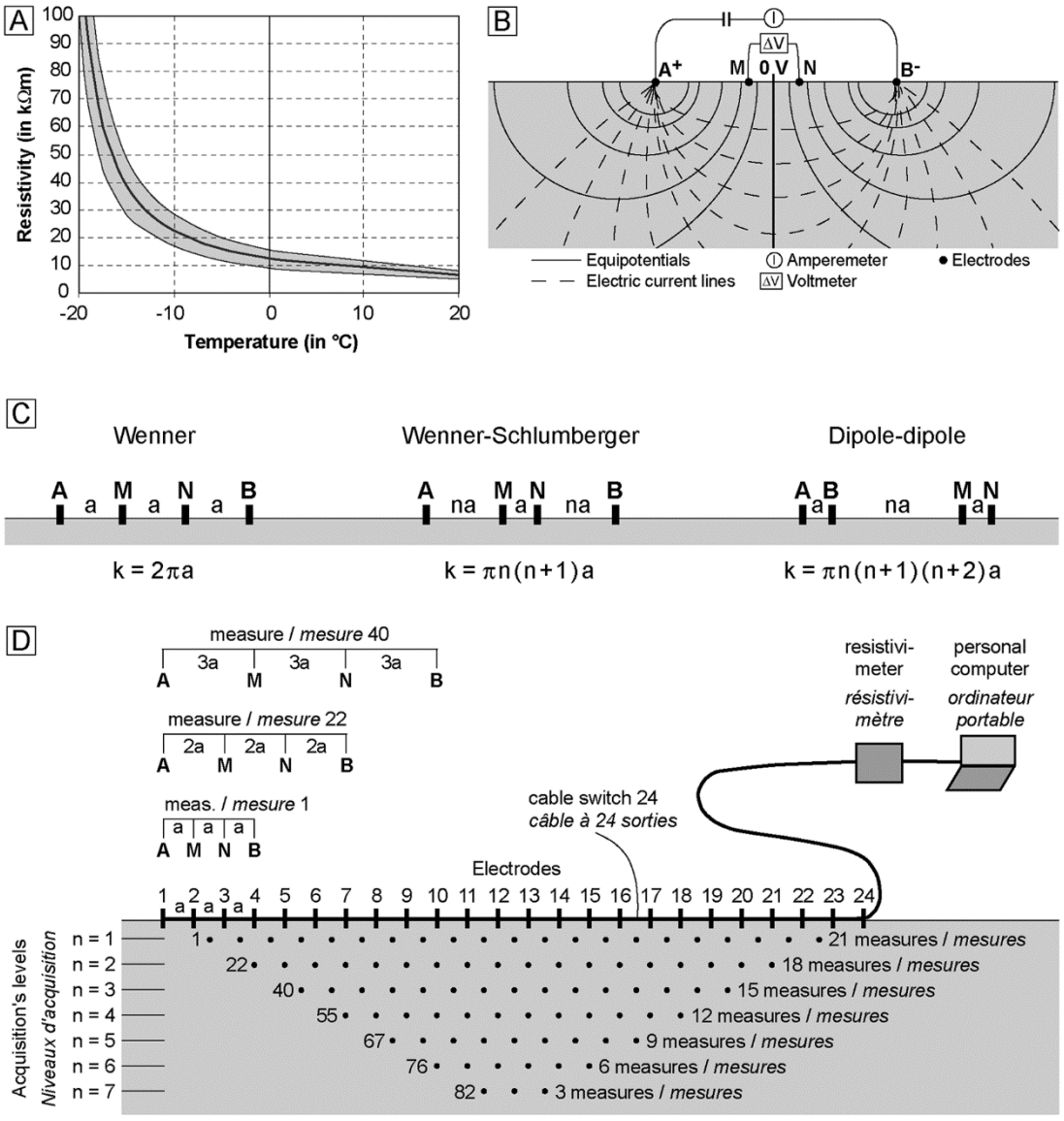

Figure 21 A) The ratio of electrical resistivity and temperature calculated for the lithologies in the area B) distribution of subsurface electric currents and equipotential C) commonly employed electrode arrays D) pseudo-section generated using a Wenner configuration. Reprinted with permission from Scapozza and Laigre, 2014.

The authors selected areas of interest from a DEM and conducted ERT measurements across the proximal floodplain and the distal floodplain of the river. Instead of a continuous ERT profile across the floodplain, Scapozza and Laigre (2014) produced two sections (fig. 22) to avoid anthropogenic features (i.e., railroads, structures). Data processing included the use of inversion software to determine the resistivity of the materials from the measured apparent-resistivities (Scapozza and Laigre, 2014). The authors conclude ERT is an appropriate method for the identification of paleo-landforms that have been buried by natural and anthropogenic processes in the fluvial environment.

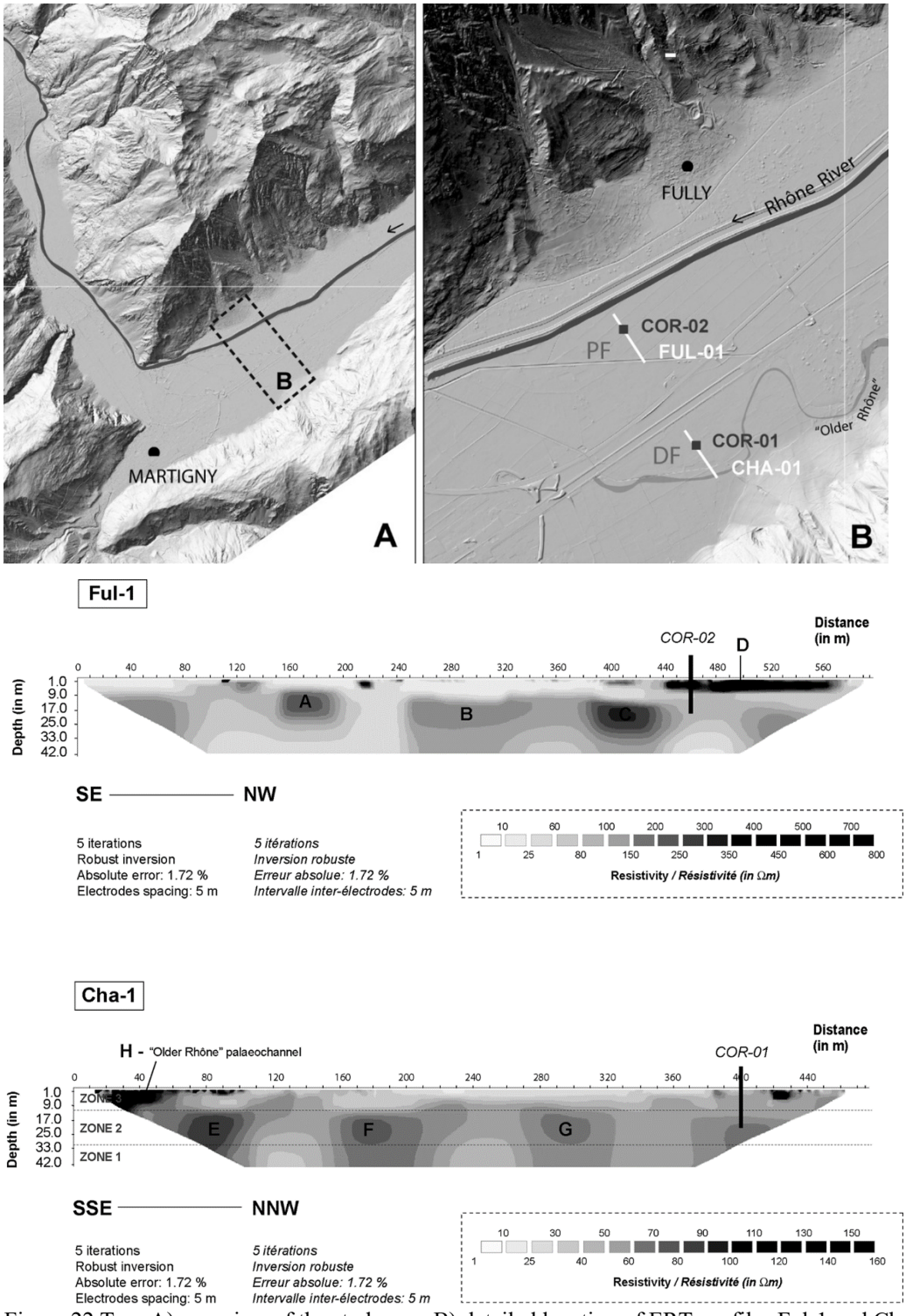

Figure 22 Top: A) overview of the study area B) detailed location of ERT-profiles Ful-1 and Cha-1 in the floodplain; PF = proximal floodplain; DF = distal floodplain; COR-01; COR-02 = boreholes. Bottom: ERT profiles Ful-1 and Cha-1; palaeochannels labeled with letters. Reprinted with permission from Scapozza and Laigre, 2014.

3.2.2. Coastal processes-environment

3.2.2.1. Geologic mapping of barrier islands

Determining the factors controlling the evolution of the barrier island system is essential in assessing the risk and informing coastal management in the context of changing climatic conditions. According to Weymer et al. (2015), limited understanding exists of the linkages between island geomorphology, antecedent geology, subsurface structure, groundwater dynamics and barrier island response to sea-level rise.

Traditionally, studies on evolution of barrier islands are conducted on sub-systems of the barrier island using mostly boreholes (i.e., invasive method) in combination with bathymetry, seismic and/or GPR surveys (Weymer et al., 2015). Some of the disadvantages associated with the use of traditional methods in this environment highlighted by Weymer et al. (2015) include cost-effectiveness (i.e. marine geophysics), limited (i.e., coring) to no (remote sensing) subsurface information, sensitive to saltwater (i.e., GPR).

Weymer et al. (2015) conducted a review of the methods employed in researching controls and evolution on barrier island systems. The authors recognized a lack of publications studying the interdependence between subsurface hydrology and surface geomorphology. This motivates Weymer et al. (2015) to propose the use of EMI methods, partly because of the portability and user-friendliness associated with EMI systems, and because these methods allow continuous subsurface mapping of the whole barrier island system. Furthermore, the authors highlight the appropriateness of

integrating high-resolution information obtained using EMI methods with hydrogeologic and geomorphic data in addressing the problem of studying complex and dynamic environments, such as the coastal environment.

Weymer et al. (2015) conducted EMI surveys in two areas along a barrier island. The first survey was conducted to verify the location of paleo-channels mapped by Fisk (1959) using invasive techniques (i.e., boreholes and trenches). The EMI survey extends approximately 10 km across three of the paleo-channels. Weymer et al. (2015) used a handheld frequency domain system in the in-line vertical dipole mode at 3 frequencies, yielding 3 different skin depths (i.e., skin depth is inversely proportional to the used frequency). The authors plotted the variations alongshore in maximum dune height (i.e., derived from LiDAR) and apparent-conductivity (i.e., obtained using EMI). The plot was finalized after using a smoothing filter so that the authors could combine the new information with the maps produced by Fisk (1959). Using this approach, Weymer et al. (2015) determined the level of agreement between the locations of the paleo-channels interpreted from geophysical data and the locations inferred by Fisk (1959).

To further demonstrate the applicability of EMI sensors in researching the relationship between lithology and island morphology, Weymer et al. (2015) produced a 2D EMI grid survey over a storm deposit in the backshore environment. The authors conducted the EMI survey on a washover channel which they identified as recovered based on satellite imagery. Changes in the apparent-conductivity values measured within the channel, correspond with variations in the grain size of the deposits (i.e., sand vs

clay). Detecting variations in subsurface geology complement surface data, which helps identify controls on morphology of coastal features (Weymer et al., 2015).

3.2.2.2. Coastal landscape change and geoarchaeology

Historically chosen for human settlement, the coastal environment is subjected to natural and anthropogenic geomorphic forces (Wegmann et al., 2012). Preservation of archaeological sites in the dynamic coastal environment is poor because of exposure to sea-level changes and erosion (Ranasinghe and Stive, 2009); however, anthropogenic deposits are unintentionally preserving archaeological sites (Wegmann et al., 2012). Informing urban and archaeological developmental planning efforts requires mapping natural and anthropogenic deposits, assessing the impact of anthropogenic and natural geomorphic agents on the coastal landscape, and identifying and quantifying buried landforms to determine potential archaeological sites (Wegmann et al., 2012).

Wegmann et al. (2012) combined direct observations (i.e., topographic analysis from outcrops, detailed stratigraphy from boreholes), dating techniques (i.e., radiocarbon geochronology) and historical information (i.e., topographic and bathymetric maps, photographs and remote sensing data (LiDAR) with near-surface geophysics (GPR surveys), in a coastal environment with a history of anthropogenic modification. Using a multiple method approach allowed Wegmann et al. (2012) to determine the thickness and distribution of natural and anthropogenic deposits in the subsurface, and to produce a reconstruction of the paleo-landscape in their study area.

After conducting a GPR surveying campaign on sites of archaeological interest with a system equipped with GPS and an odometer, the authors stacked the radar signals

received from each profile. Low-frequency-noise was removed using a high-pass filter, whereas attenuation and geometric spreading were addressed using a gain function (Wegmann et al., 2012; Conyers and Leckebusch, 2010; Annan, 2005). Point and line reflectors, found in anthropogenically-modified environments, include buried pipes and railroad materials. The authors fitted the shapes of the hyperbolas of the reflectors to determine the mean-radar velocity for the area and consequently the depth of the reflectors. Basement reflectors represent the interface between the paleo-topography and the mechanical fill (i.e., anthropogenic deposits). The authors used the strength and continuity of each reflector, the local dip angle and interface relief to identify the reflectors. Available well stratigraphy was used to verify reflector depth. Lastly, Wegmann et al. (2012) included the interpreted interface within the GPR software and determined the thickness of the anthropogenic fill using the difference between the LiDAR-derived modern topography and the elevation of the interface.

The authors propose their interdisciplinary approach is applicable in other coastal areas of historic and archaeological importance, particularly in the stages of permitting and planning development, as well as in any planned anthropogenic modification of the coastal environment.

3.2.3. Aeolian processes-environment

3.2.3.1. Dune structure and development in a polar desert

Slipfaceless dunes such as whaleback and zibar are predominant in arid environments (Goudie, 2013). Imaging the internal composition of dunes aids in understanding the factors governing dune migration (i.e., underlying geomorphological

features, climatic conditions) (Bristow et al., 2010). Insufficient studies exist on the internal structure of slipfaceless dunes; however, the study of dune development and evolution in polar deserts has implications for planetary geomorphology (Bristow et al., 2010). The prevalence of frozen slipfaceless dunes in Antarctica makes it a good location to evaluate methodologies for studying the analog Martian dunes in future explorations, motivating Bristow et al. (2010) to use remote sensing methods and GPR surveys as future Martian missions are equipped with GPR.

Bristow et al. (2010) used LiDAR imagery to obtain morphometric and topographic data of the dunes, whereas grain size distribution was derived from shallow samples taken along the axis of the dunes. The authors used those surficial data and a geodimeter to complement the GPR survey data. The subsurface investigation of frozen dunes consisted of over 3 km of GPR profiles conducted using antennas at two frequencies.

The authors used common midpoint (CMP) surveys to estimate the radar velocity through the subsurface, which is needed to determine the depth of the profiles (Bristow, 2013). The calculated velocities fall within velocities recorded by Reynolds (2011) for dry and ice. Using a mean velocity and the antenna frequency, Bristow et al. (2010) determined the radar signal. To calculate the theoretical depth resolution, the authors used ¼ of the wavelength of the radar signal. Data interpretation for this study included standard practices such as topographic correction of the profiles, and radar stratigraphy and facies analysis as described by Jol and Bristow (2003). Using a non-invasive methodology, Bristow et al. (2010) identify the sedimentary structures within the

selected dune field. The inclination and shape of the reflectors of the GPR profiles are used by Bristow et al. (2010) to determine the direction of the accretion and the migration of the dunes. Using this information, the authors can infer the relative age of the sediments. The authors can also identify variations in grain sizes (i.e., sand wedges) along the GPR profiles.

Interpretation of the subsurface data, lead the authors to conclude changes occurred in the wind regime in the area, leaving evidence of episodes of truncation and deposition in the stratigraphic record of the dunes. The truncation surfaces interpreted from GPR surfaces are, according to Bristow et al. (2010), associated with the reactivation of zibar surfaces. Lastly, Bristow et al. (2010) conclude the morphology of the dunes is governed by wind regime, rather than by the underlying moraine as proposed by Selby et al. (1974) and Calkin and Rutford (1974).

3.2.4. Glacial processes-environment

3.2.4.1. Determination of the thickness of glacial ice

Non-invasive airborne geophysics methods were employed by Paxman et al. (2019) to produce the first detailed subglacial sedimentary basin model for the Pensacola-Pole Basin (PBB), in East Antarctica. The authors produced an assemblage of measurements for ice thickness from several airborne geophysical campaigns including gravity, magnetics, and ice-penetrating radar (radioglaciology) data. A DEM of the bedrock was also derived from the airborne data (Paxman et al., 2019).

Corrections and filters were applied to the merged geophysical data in the processing stages, allowing the authors to create a multi-layered gravity model in which

surficial ice, subglacial surface, and mantle are depicted (Paxman et al., 2019). An additional layer was added to show low density sedimentary rocks. After some forward modeling, the authors produced a 2-D representation of the basin. A 3-D model of the sedimentary basin was produced using a tension spline interpolation of the modeled sediment thickness. The non-uniqueness of forward gravity models requires the determination of the uncertainty of the calculated sediment thickness (Kruse, 2013; Paxman et al., 2019).

Additional modeling methods applied in this study include gravity power spectra regression used to identify boundaries between materials (i.e., ice-sediments-basement), magnetic depth-to-source modeling (to estimate sediment thickness) used to validate the models derived from gravity data, and magnetic models (from magnetic anomalies) used to validate geologic interpretations. An example of the data analyzed by Paxman et al. (2019) is shown in figure 23.

Erosional and topographic features identified in this study, allow the authors to reconstruct the sedimentary history of the basin. The relative velocity of the ice sheet in the basin was interpreted from gravity and magnetic anomalies, leading the authors to conclude the ice is fast-flowing in the northern regions of the basin and slow-flowing in the south. Paxman et al. (2019) note that the onset of streaming nearly aligns with a subglacial lithological transition from the southern to the northern PPB. The authors hypothesize that fast-flowing ice increased erosion in the northern part of the basin resulting in the differences in geology, or the northern PPB represents a gap in the depositional record because of a lack of accommodation space. Additional geophysical

explorations are recommended by the authors to determine the most accurate interpretation of the depositional history of this basin.

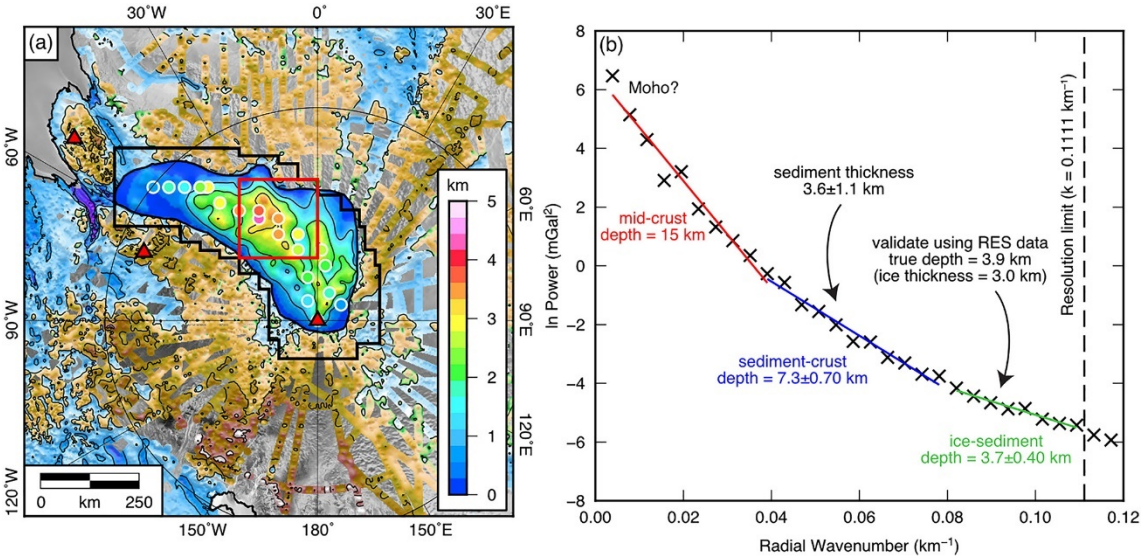

Figure 23 Thickness of the sedimentary rocks. (a) Isopach map. Contours every 1 km. Colored circles = sediment thickness. Red triangles = seismic stations. Present-day bedrock elevation in the background. (b) Power spectral method for sediment thickness determination. Reprinted from Paxman et al., 2019.

3.2.5. Periglacial processes-environment

3.2.5.1. Periglacial landforms and processes

Semiarid mountainous areas in the periglacial environment host solid water within landforms such as rock glaciers, debris-covered glaciers, and ice glaciers (Azócar and Brenning, 2010; Bodin et al., 2010). Global warming is diminishing water storage in glaciers, making it important to identify and quantify ice volumes stored within periglacial landform assemblages (Monnier et al., 2014). Subsurface investigations are necessary to differentiate the components of such complex depositional landform assemblages, to determine the spatial relationships between the features, and ultimately

to understand the origin, evolution and dynamics of the landforms (Monnier et al., 2014).

Mapping the geomorphological features of the glacier foreland was accomplished by combining geomorphological (i.e., characterization of surface features), sedimentological (i.e., petrological analysis, clast morphometry), remotely sensed (aerial imagery), and geophysical data (GPR) (Monnier et al., 2014). The internal make up of rock glaciers and debris-covered glaciers is complex. Using geophysical tools allows the detection of massive ice, cavities, and high-moisture materials. Identifying and locating the distribution of ice, water and voids, informs the interpretation of morphogenetics and dynamics of the landform assemblage (Monnier et al., 2014). Interpretation of GPR surveys (i.e., after migration, gain application, and topographic correction of the data) shows massive ice layers preserved in rock glaciers, evidencing the potential for and providing necessary information to estimate volumes of water storage within periglacial landforms in the area (Monnier et al., 2014).

3.2.5.2. Rock glaciers

Determining the internal structure of rock glaciers using non-invasive methods is a common objective in investigations of the periglacial environment. Degenhardt and Giardino (2003) selected GPR to study alpine rock glaciers as surrogates for landforms of similar characteristics identified on Mars. The authors mention the portability, user friendliness, and quality of data produced using GPR as some of the advantages of the method. A longitudinal GPR transect (parallel to the long axis) was conducted to map the distribution of internal ice, to determine the thickness of the rock glacier, and to

establish relationships between surface morphology (ridges and furrows) and internal structure of the landform (Degenhardt and Giardino, 2003). Seven horizons were identified in the longitudinal profile and interpreted as recognizable subhorizontal units. The internal makeup of this rock glacier corresponds with alternating layers of ice-rich and ice-poor debris and discontinuous ice lenses, representing depositional facies resulting from changes in snow and debris input (Degenhardt, 2009).

According to Degenhardt and Giardino (2003), the correspondence between the location of the surficial features (ridges and furrows) and the appearance of folds in the internal layers of the rock glacier, indicates the origin, direction and distribution of compressive stresses through the landform. Seasonal frost accumulation and/or groundwater input must have occurred for the development of ice in the rock glacier, and the thickness of the debris cover provides insulation to preserve the ice (Degenhardt and Giardino, 2003). Given the similarities found on surface characteristics between this alpine rock glacier and the Mars lobate landforms, the authors conclude that permafrost and ice lenses groundwater might also be preserved within the Martian rock glaciers.

3.2.6. Tectonic processes

3.2.6.1. Tracing buried faults

Cities located in tectonically active areas are subjected to the effects of seismic activity on infrastructure. In some cases, the surficial expressions of active faults are discontinuous, making it challenging to inform urban planning. Subsurface investigations are required in areas where tracing buried faults is needed. Gürer et al. (2009) conducted Very Low Frequency Electromagnetic (VLF) surveys to identify fault

lines suspected to be buried beneath alluvial quaternary deposits. According to the authors, remotely located VLF radio transmitters can be used as an electromagnetic source (15-30 kHz frequency bandwidth), and a magnetometer deployed over the area of interest can capture the electric (measured with grounded probes) and magnetic (picked up by coils mounted in a cylinder with a preamplifier) field components of the signal. Gürer et al. (2009) performed their measurements in the H-polarization mode because the direction of the wave propagation is perpendicular to the fault strike.

According to Gürer et al. (2009), magnetic anomalies are usually imperceptible in H-polarization mode, but site conditions can strengthen these magnetic variations producing strong and characteristic fault responses. In this case, the authors attributed the magnetic field variations to a strong conductivity contrast between the fault zone and the surrounding medium, and to the parallel orientation of two fault branches which act as parallel conductors, thus producing successive anomalies. The authors conclude that conducting and interpreting VLF surveys is convenient and straightforward, making it possible to locate and visualize buried fault branches.

3.2.6.2. Tectonic evolution and landform development

An interdisciplinary approach integrating paleoseismological, geomorphological, and near-surface geophysical data was used by Pavan Kumar et al. (2019) to study the tectonic evolution and consequent landform development of an active intraplate region. The authors selected a Time Domain Electromagnetic (TDEM) method to locate subsurficial shallow fault zones. Geologic contacts and structural features are evidenced by a contrast in the electric resistivity values (Pavan Kumar et al., 2019).

The soundings were conducted sending an alternating current through a transmitter loop (single turn) at varying frequencies, which produced a secondary magnetic field measured during the time-off period by a receiver in central loop configuration (Pavan Kumar et al., 2019). Signal-to-noise ratio was improved by stacking the measurements, and the apparent-resistivity was calculated using an equation that related the recorded voltage and the injected current. Inversion software was used to produce 1-D models resistivity models (i.e., assuming a horizontally layered earth model) which were combined to create a resistivity section (Pavan Kumar et al., 2019).

Using TDEM, Pavan Kumar et al. (2019) were able to image the subsurface of their study area to a depth of 200 m and obtain essential information about Holocene tectonic events. The interpretations of the geophysical data lead them to determine the basement is located at around 75-80 m depth. High resistivity values (100 Ωm) are interpreted as faulted blocks separated by infill material (<20 Ωm). The wedge morphology of the imaged infill indicates syntectonic sedimentation, whereas the distribution of the resistivity values along the section indicates differences in the level of activity.

3.2.7. Karst processes-environment

3.2.7.1. Geologic mapping of karst systems

Kaufmann and Romanov (2017) produced a three-dimensional model of a karst system using a combination of geophysical methods. Physical properties of materials (i.e. electrical resistivity, dielectric permeability, density) can be derived from geophysical surveys and the geometry of structures in the subsurface is evidenced by

variations detected by geophysical systems (Kaufmann and Romanov, 2017). The methods selected for this study include gravity to detect voids, electrical resistivity imaging to locate water and characterize sediments, self-potential to detect water flow, and ground penetrating radar to identify structural features.

The authors recorded location with GPS, elevation by leveling, and gravity data to input in the processing software to obtain subsurface density values. ERI profiles were obtained using a Wenner and Schlumberger array, and resistivity values were derived using inversion software. The electrical conductivity of the water was measured using a hand-held conductivity meter. Non-polarizable copper-copper sulfate electrodes and a multi meter were used to determine self-potential in the vadose zone. GPR data collected using a monostatic antenna was processed, filtered, and migrated before interpretation (Kaufmann and Romanov, 2017). It is important to note that the results of the GPR surveys are less conclusive than the other methods used by the authors. This observation was also made by Bottari et al. (2017).

Kaufmann and Romanov (2017) used hydrogeochemical properties derived from geophysical data which they input in a numerical modeling software to produce a three-dimensional structural model of their study area. Their model indicates areas susceptible to flooding in the cave system as well as the degree of karstification of the lithologies in the area.

3.2.7.2. Anthropogenic alteration of the karst environment

The karst environment provides necessary resources for human settlements including construction materials and water resources, evidenced by the prevalence of archaeological sites in karts areas (Bottari et al., 2017). Landform-human interactions at an ancient settlement (Roman) are the main focus of the study by Bottari et al. (2017) in an area where sinkholes, dolines and karst depressions are characteristic. The authors combined archeological (historical records, published results from site excavations), geomorphological, geological (shallow boreholes), and geophysical (ERT, FDEM, GPR) data, to characterize their study area.

Bottari et al. (2017) conducted several ERT soundings to achieve three main goals: 1) to identify deep structures at the basement, 2) to characterize the doline structure, and 3) to validate the results of the FDEM survey. The FDEM method was used to evaluate the level of alteration and determine the extension of the target layer (calcareous tufa), as well as to detect archaeological artifacts. The authors used GPR to further characterize the doline structure. Bottari et al. (2017) report good agreement between the results of the different geophysical surveys conducted in the doline area. Interpretation of the data allowed the authors to conclude that the ancient inhabitants of the area had mined the mineral resources available. Geophysical data shows evidence of continuous collapse and remediation attempts in the doline structure. Borehole data validates these interpretations, as anthropogenic fillings are found in the stratigraphic record.

3.2.8. Mass movement and erosion processes

3.2.8.1. Landslide characterization

A morpho-structural model of a coastal landslide was developed by Lissak et al. (2014). The authors integrated newly collected and historical surface (i.e., high-resolution and field topography) and subsurface (i.e., geotechnical and geophysical) data. The methodological model presented by Lissak et al. (2014) illustrates data sources, analysis, and expected results of the integration of geomorphological, geophysical, and geotechnical interpretations, in the context of landslide investigations. This study employs invasive and non-invasive methods that are commonly used in research related to slope stability.

Lissak et al. (2014) used electrical resistivity tomography (ERT) and seismic refraction tomography in their investigation. The authors used a Wenner–Schlumberger configuration for their ERT surveys. This array has been deemed adequate in mass-movement investigations as exemplified by Naudet et al. (2008) and Jongmans et al. (2009). Inversion software was used to obtain resistivity values from the 2D apparent-resistivity profiles (Lissak et al., 2014). The seismic-refraction profile allowed the authors to obtain subsurface information up to 10 m deeper than the ERT surveys. Structures of P-wave velocities (longitudinal and vertical) can be imaged using seismic tomography (Lissak et al., 2014). The authors calculated the velocity fields using the quasi-Newton P-wave tomography inversion algorithm formulated by Gance et al. (2012).

The internal structure of the landslide was determined from the interpretation of the geophysical data, and subsequent correlation with lithological information. The

authors used variations in electrical resistivity values and P-wave velocities to distinguish between subsurficial layers. In areas where borehole information is not available, interpretations can be validated using published values for similar lithologies.

3.2.8.2. Subsurface erosion by soil piping processes

Piping systems developing in the subsurface of a mountainous area were studied by Bernatek-Jakiel and Kondracka (2016) using geophysical methods. The authors mapped and determined the morphometric characteristics of surface features caused by subsurface erosion, used tracing dye to determine the connectivity between pipes in the system, conducted soil surveys (i.e., excavations and sample analyses) to obtain pedological properties, and carried out geophysical explorations to determine the extent and internal structure of piping systems located in the area of study. The most widely used geophysical method for subsurface erosion investigations is GPR, which the authors used along with ERT.

Bernatek-Jakiel and Kondracka (2016) determined the desired depth of penetration from previous research in the area and selected the frequency of the GPR antennas accordingly. Anomalies in the reflections and hyperbolas were interpreted as possible pipes on the GPR profiles, and the extent of the piping was estimated by combining various profiles (Bernatek-Jakiel and Kondracka, 2016). ERT surveys were conducted using the Wenner-Schlumberger electrode configuration, which was also selected based on target depth and the lithology of the area. The contrast between areas affected by piping and the surrounding clayey materials allowed the authors to identify the areas with high resistivity values as potential pipe locations on the ERT profiles.

An important conclusion from this investigation is that without subsurface information determined from the interpretation of geophysical surveys, the extent of the piping systems can be underestimated. According to Bernatek-Jakiel and Kondracka (2016), in areas in which subsurface erosion is in the early stages of development, up to 49% of piping activity was underestimated when only surface features were considered, whereas in highly developed piping systems the miscalculation was of around 10%.

3.2.8.3. Internal structure of landslide dams

Wang et al. (2018b) coupled two non-invasive geophysical methods to determine the potential for failure of landslide dams in a mountainous area. The authors highlight the importance of studying the internal structure of these dams, which are destabilized by piping and overtopping processes. The purpose of the geophysical investigations is to locate seepage zones and evidence of internal erosion within the landslide dams. According to Wang et al. (2018b) the self-potential (SP) method can detect anomalies caused by subsurficial flow along preferential pathways, hence allowing the delineation of areas where soil piping occurs. Microtremor chain array surveys (MTMs) provide information about the physical properties and internal geometry of the dams because phase velocity varies according to properties of the soil (i.e. density). For instance, areas characterized by low phase velocity can be interpreted as poor or moderately consolidated materials, whereas more consolidated sediments tend to yield higher phase velocity.

Characterizing the internal structure of these landslide dams is necessary to take preventive measures that can reduce the risk of damage to infrastructure and loss of lives

in areas where landslide dams occur frequently. The non-invasive nature of the methods selected, as well as their portability, budget, user and environmental friendliness, and conclusive results, proves them appropriate for landslide risk assessment purposes (Wang et al., 2018b).

3.2.9. Volcanic processes-environment

3.2.9.1. Internal structure and evolution of a volcanic system

Geophysical methods are useful to determine the internal structure while studying active volcanic systems dynamics. Brothelande et al. (2016) demonstrate the applicability of time-domain electromagnetics (TDEM), electrical resistivity tomography (ERT), self-potential (SP), magnetic surveys, in combination with ground temperature and CO_2 soil concentration measurements, to map structures (i.e., lava flows, hydrothermal systems) that provide insight on caldera resurgence processes. The authors conducted different geophysical surveys over several years and integrated the data with tectonic, geologic, and geomorphologic data.

Brothelande et al. (2016) report conclusive results from the geophysical investigations which allowed them to determine the extension (in 2-D) of lava fields within the caldera. Interpretation of the data sets allowed the detection of extensive hydrothermal activity which indicates a shallow magmatic body underneath. Hydrothermal alteration can decrease the structural stability of the landform. Assessment of landslide hazards becomes another topic of interest in this tectonically active scenario, as unconsolidated materials make up the volcanic edifices. Further geophysical

investigations are recommended to characterize the interpreted magmatic intrusion (Brothelande et al., 2016).

3.2.10. Characterization of impact features

Accurate maps representing the extent of impact features (i.e., astroblemes) can be produced using geophysical methods. Bobée et al. (2010) integrate near-surface and borehole geophysical and geological data to characterize an eroded impact structure. These structures are highly fractured and complex, making it relevant to study the connectivity with the basement and water storage potential. Coincident data sets from direct current (DC) resistivity and TDEM soundings were modeled using a mutually constrained inversion (MCI) algorithm. This data optimization process allowed the authors to introduce constraints and correlate the models (Bobée et al., 2010).

The authors used a deep borehole to conduct measurements of electrical resistivity, gamma ray, magnetic susceptibility downhole and obtained acoustic imagery and stratigraphic logs. A heterogeneous distribution of resistivity values was determined from the geophysical investigations of the impactites (i.e., fallout breccias, impact breccias) (Bobée et al., 2010). The information was integrated by Bobée et al. (2010) into a model containing resistivity profiles (validated by a gravity model), considering surface topography, using specialized software.

Obodovsky (2019) uses an interpolation software to process 2D seismic data and determine the characteristics of an astrobleme in the Western Canadian Sedimentary Basin. Analysis of the seismic data coupled with the geological history of the area led the author to conclude that the area where the impact occurred was rapidly eroded

following the impact, thus removing the characteristic bowl morphology of the structure. The central uplift remains and is clearly identifiable in figure 24.

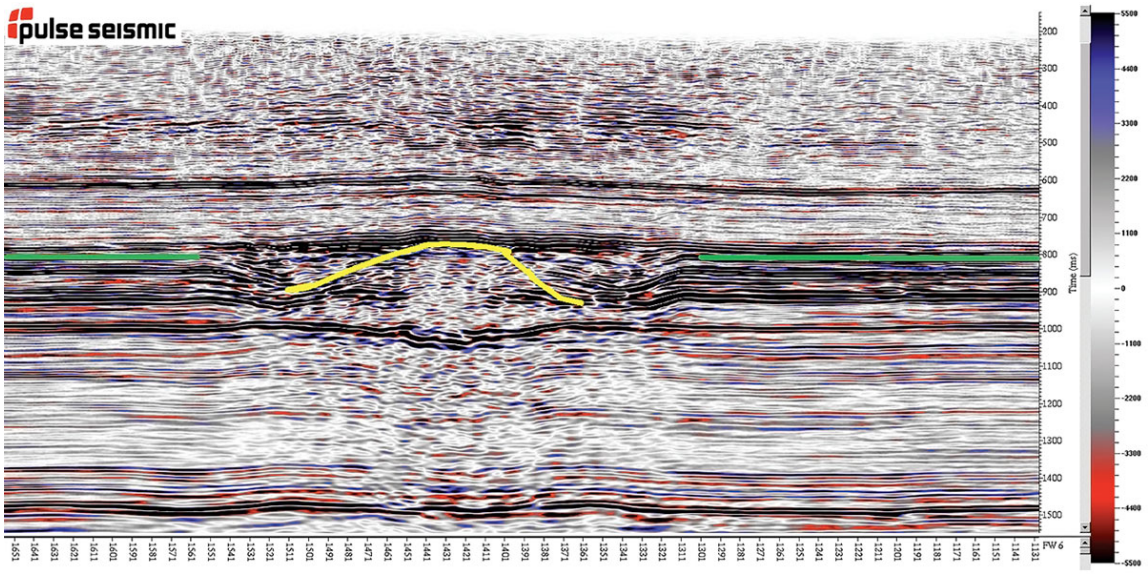

Figure 24 2D line cross section of the astrobleme. The yellow line is the approximate outline of the central peak, while the green lines show where the surface was eroded down to such that we no longer see the original crater rim. Seismic data owned by Pulse Seismic and processed by Divestco (Obodovsky, 2019). Reprinted with permission from Recorder, 2019.

3.2.11. Identification of anthropogenic features-processes

3.2.11.1. Anthropogenic mounds in an urban environment

Pazzi et al. (2016) discuss the challenges of studying landform morphogenetics in the built environment (i.e., urban geomorphology). These challenges included physical constraints in densely populated/built areas and environmental noise (i.e., traffic) that could interfere with geophysical surveys. Given these considerations, the

methods selected for their study are strictly non-invasive. The authors developed a multistep diagnostic flowchart to illustrate their proposed methodology as shown in figure 25.

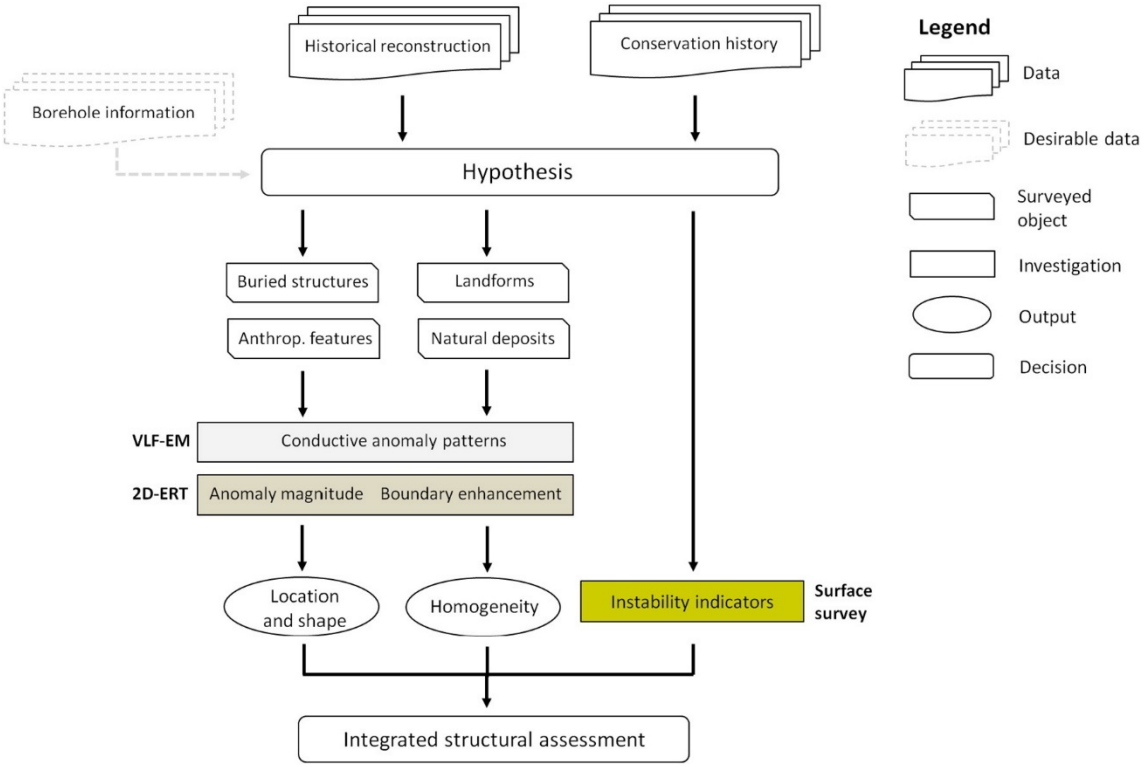

Figure 25 Flowchart of the electric and electromagnetic geophysical approach proposed and implemented by Pazzi et al. (2016). Reprinted from Pazzi et al. 2016.

The approach proposed by Pazzi et al. (2016) consists of a combination of historical data, surface surveying of the features of interest (i.e., natural, anthropogenic, and/or mixed origin), and geophysical surveying to characterize subsurface features.

Very low frequency electromagnetic (VLF-EM) and 2D electrical resistivity tomography (2D-ERT) were selected to test the applicability of the proposed framework. The authors highlight the advantageous characteristics of both methods. According to Pazzi et al. (2016), these methods are complementary, because they measure the same physical property (i.e., electrical resistivity), with differences in resolution (2D-ERT provides higher resolution), data collection speed (VLF-EM is faster), susceptibility to environmental obstacles (VLF-EM adapts well to microtopography), and the type of data generated (VLF-EM provides qualitative and VLF-EM quantitative information).

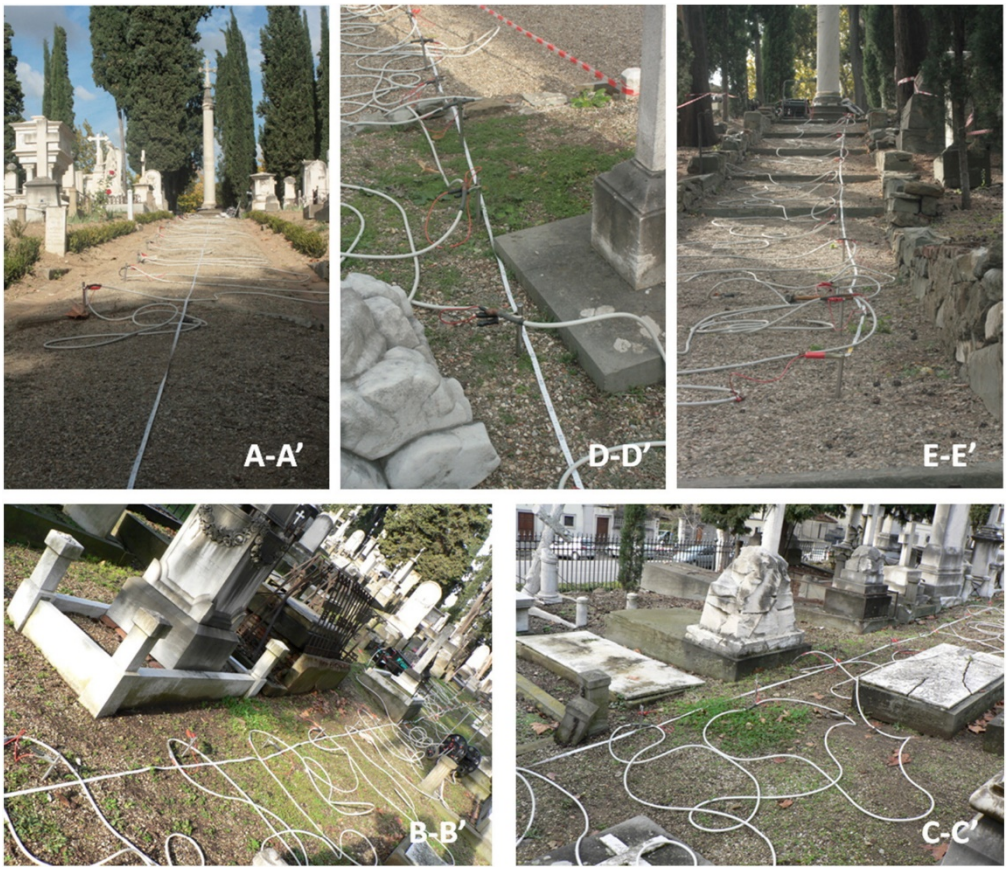

Figure 26 Arrangement of the 2D-ERT across the Cemetery (from A-A′ to E-E′). Reproduced with permission from Pazzi et al., 2016.

Pazzi et al. (2016), used a flexible arrangement of the 2D-ERT to create cross sections across a cemetery (fig. 26). Figure 27 shows the pseudo-sections of current density from VLF-EM profiles orthogonal to the AA′ ERT and filtered by the Karous-Hjelt and three parallel profiles to the ERT itself (T1–T3), which according to the authors were extracted and processed as a VLF line. Figure 28 corresponds with a tilt pattern map of the Cemetery onto the Karous-Hjelt filtered in-phase component of the VLF-EM survey. In situ inspections revealed (B–C) clusters of tilted tombs; (D–E)

gravestones displaced along the slope, and (F) severely damaged; (G) CC′ and EE′ ERTs (Pazzi et al., 2016).

The results of their investigation prove the efficacy of the methodology. The authors were able to identify the origin of subsurficial structures based on morphological (i.e., size and shape) and electrical (i.e., resistivity values of anthropogenic materials) characteristics derived from the geophysical soundings. Pazzi et al. (2016) expect their approach to be used to assess the condition of anthropogenic structures, locating areas in risk of failure (i.e., ground instability), and informing decision making processes related to the efforts of mitigation of structural damage.

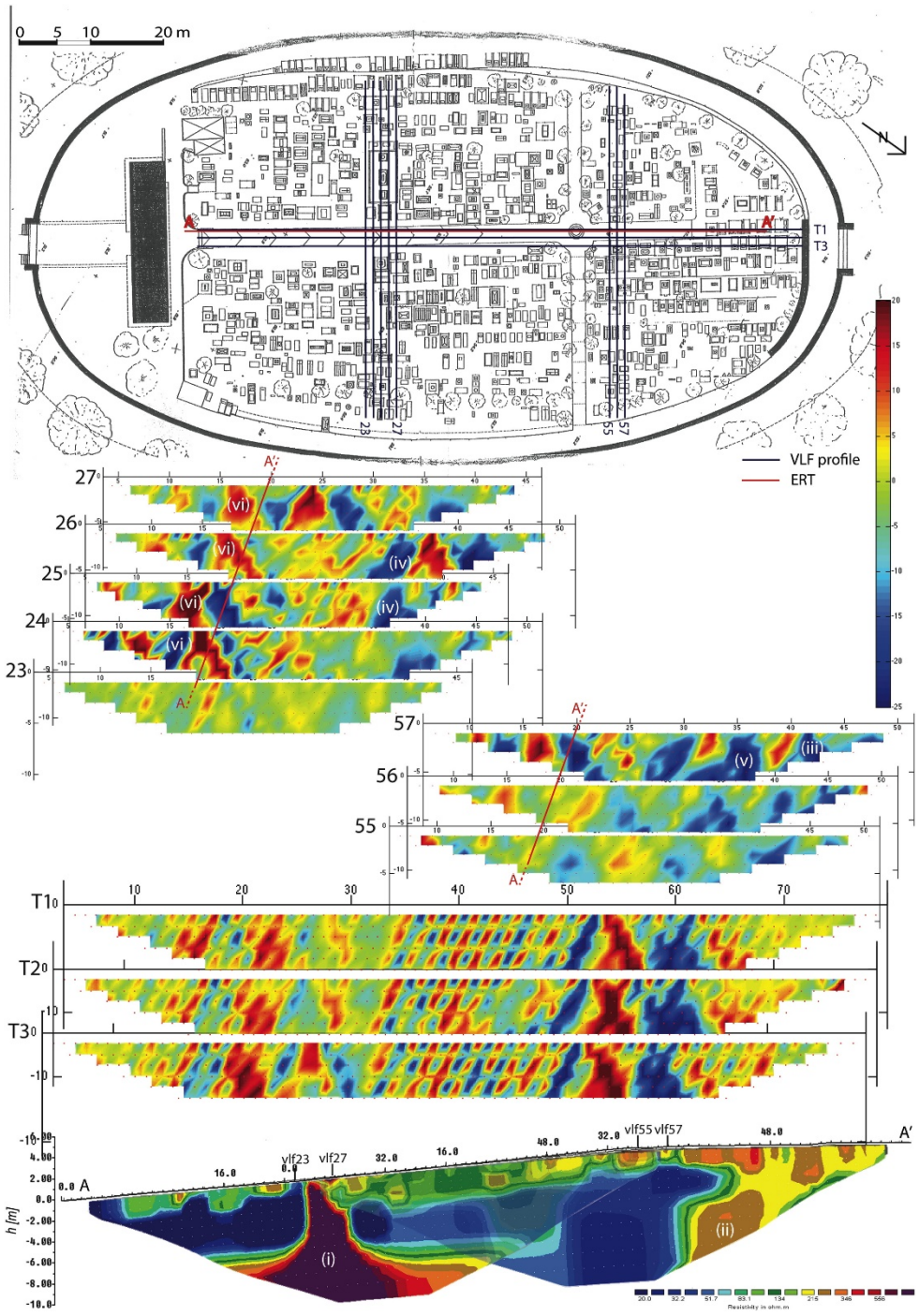

Figure 27 Pseudo-sections of current density from VLF-EM profiles orthogonal to the AA′ ERT profile (red line top; reported as resistivity section at the bottom) and parallel profiles to the ERT. Reproduced with permission from Pazzi et al., 2016.

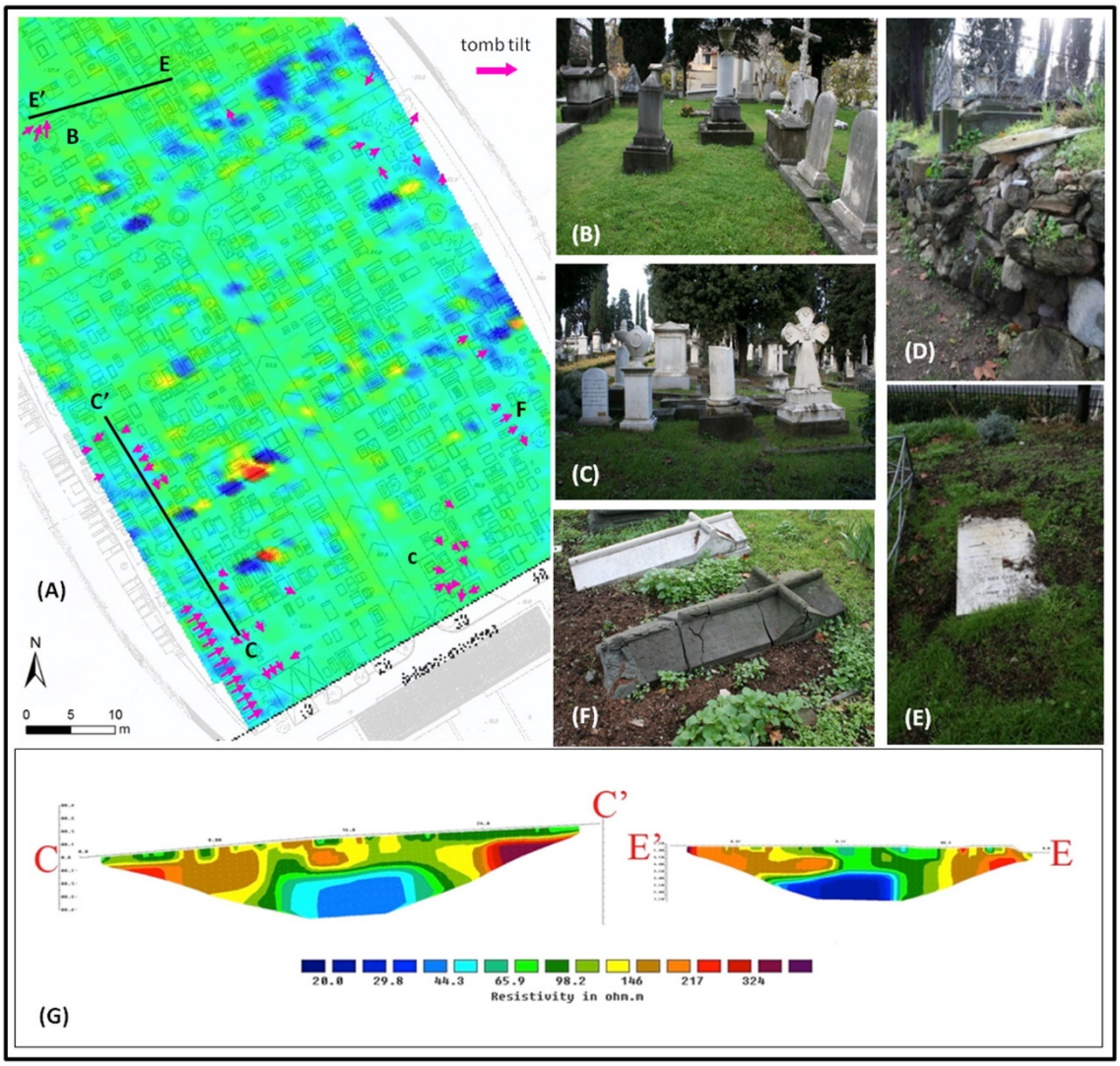

Figure 28 (A) Tilt pattern map of the Cemetery onto the Karous-Hjelt filtered in-phase component of the VLF-EM survey. (B–C) clusters of tilted tombs; (D–E) gravestones displaced along the slope and (F) damaged at an extent that the sarcophagi are severely broken; (G) CC′ and EE′ ERTs. Reproduced with permission from Pazzi et al., 2016.

3.3. Geophysical techniques commonly used in geomorphological research

In this section we have included two tables that can serve as quick reference guides that can aid in the selection of geophysical methods for geomorphological research. Table 4 builds on the work published by NASEM (2020) and summarizes the applicability of surface geophysical methods to answer research questions (second column) related to geomorphic environments and processes (first column). The rest of the columns indicate if the method is effective and commonly used to answer the research question (primary application) or if the method is used to obtain direct or indirect information relevant for the investigation (secondary application). As previously mentioned, geophysical techniques are not process-dependent and are used to study a variety of processes across geomorphic environments. The reader should interpret the term "across" listed in the first column as a research question related to most geomorphic environments and processes.

Table 4 Applicability of geophysical methods. P=Primary application; S=Secondary application; Across = across processes-environments; AN= anthropogenic landforms; CZ= Critical Zone studies; F=fluvial; G=glacial; K=karst processes-environment; MM= mass movement processes; T=tectonic processes-environment. After NASEM (2020).

Geomorphic environment-processes	**Research question**	**Seismic Refraction**	**Seismic Reflection**	**Refraction Tomography**	**Surface Wave**	**Resistivity**	**IP**	**SP**	**GPR**	**FDEM**	**TDEM**	**Magnetic**	**Gravity**
Across	Determine rock depth	P	P	P	P	P	S	-	P	S	S	-	S
Across	Determine rock topography	P	P	P	S	P	S	-	P	S	S	-	S
T	Detect fracture/fault zones	S	P	P	S	P	P	S	P	S	S	S	-
T	Characterize fractures/faults	-	P	-	-	S	-	-	P	S	-	-	-
AN	Determine rippability	P	-	P	S	-	-	-	-	-	-	-	-
MM, AN	Map weak zones in rock	P	S	P	S	P	-	-	S	S	S	S	-
Across	Map lithology	S	S	S	S	P	S	-	S	S	S	S	-
MM, AN, T	Determine rock mass stiffness	P	-	P	P	-	-	-	-	-	-	-	-
MM, AN, T	Determine rock mass density	-	-	-	-	-	-	-	-	-	-	-	S
Across	Map sands, clays, gravels	S	-	S	S	P	P	-	S	P	P	-	-
CZ, AN	Map organic materials	S	S	S	S	P	P	-	S	S	S	-	-
AN	Map landfills	S	-	S	S	P	P	-	S	P	P	P	-

Table 4 Continued. After NASEM (2020).

Geomorphic environment-processes	Research question	Seismic Refraction	Seismic Reflection	Refraction Tomography	Surface Wave	Resistivity	IP	SP	GPR	FDEM	TDEM	Magnetic	Gravity
MM, AN	Determine soil stiffness	P	-	P	P	-	-	-	-	-	-	-	-
MM, AN	Determine soil density	-	-	-	-	-	-	-	-	-	-	-	-
Across	Map groundwater table	P	S	S	-	P	P	-	P	P	P	-	-
Across	Map groundwater flow	-	-	-	-	-	-	P	-	-	-	-	-
MM, AN	Map landslide extent	P	S	P	S	P	S	-	S	S	S	-	-
MM, AN	Identify landslide slip surface	-	S	S	-	S	-	-	S	-	-	-	-
K, AN	Detect voids, cavities	S	P	P	S	P	S	-	P	S	S	-	P
F, G	Image scour features	-	P	-	-	-	-	-	P	-	-	-	-
MM, AN	Estimate clay content	-	-	-	-	P	P	-	S	S	S	-	-

The reader is encouraged to consult the chapter on near-surface geophysics written by Kruse (2013) as well as the chapter on field techniques used in geomorphology by Schrott et al. (2013) found in the first edition of the *Treatise on Geomorphology*. The key references mentioned in the introduction of this section are also listed in Table 5. This table is organized by geophysical method (first column), the key references that provide extensive information about the methods are listed in the second column, while the third column provides relevant references to consult if interested in the application of the method in a particular setting. Some of the references provided under the geomorphological research column use or mention a single type of geophysical method, whereas the ones marked with a star (*) use multiple geophysical methods. The use of a single geophysical method does not imply the approach is not a multiple-method approach as it has been discussed in the introduction, it refers specifically to the use of one or more geophysical methods in combination with other methodologies.

Table 5 Geophysical techniques commonly used in geomorphological research. For in depth information about the geophysical method consult the key references. Case studies illustrating the use of each method in geomorphological research are compiled in the last column. References marked with a * exemplify multiple geophysical methods.

Geophysical method	Key references	Geomorphological research
Ground Penetrating Radar (GPR)	Davis and Annan (1989) Jol (2009) Jol and Bristow (2003) van der Kruk (2015) Robinson et al. (2013) Schrott et al. (2013)	•Periglacial processes (rock glaciers, permafrost, active layer) (Degenhardt and Giardino, 2003) (Colombo et al., 2018)*(Monnier et al., 2014) (Schrott et al., 2013) •Volcanic processes (Kruse et al., 2010)(Ettinger and Kruse, 2007) •Coastal processes (Wegmann et al., 2012) •Aeolian processes (Van Dam, 2012) •Erosion and mass movement processes (Bernatek-Jakiel and Kondracka, 2016)* (Brody et al., 2015)* •Karst processes (Bottari et al., 2017)* (Kaufmann and Romanov, 2017)* (Artugyan et al., 2015)* (Carbonel et al., 2015)*

Table 5 continued

Geophysical method	Key references	Geomorphological research
Electrical resistivity tomography (ERT)	Loke and Barker (1996) Barker and Loke (1996) Binley (2015) Schrott et al. (2013)	•Periglacial processes (rock glaciers, permafrost, periglacial blockfields, active layer) (Colombo et al., 2018)* (Scapozza and Laigre, 2014) (Hauck and Kneisel, 2008) (Stan et al., 2017)* (Doetsch et al., 2015)* •Karst processes (Bottari et al., 2017)* (Siart et al., 2013)* (Billi et al., 2016) (Kaufmann and Romanov, 2017)* (Kaufmann and Romanov, 2016)* (Carbonel et al., 2015)* (Margiotta et al., 2012)* •Coastal environment (Margiotta et al., 2012)* •Aeolian processes (Bristow et al., 2010) •Hydrogeological research (Robinson et al., 2008)* (Khalil et al., 2018)* •Cave system mapping in urban areas (Lazzari et al., 2010)* •Critical Zone research (Leopold et al., 2013) •Erosion and mass movement processes (Bottari et al., 2018)* (Kasprzak et al., 2019) (Naudet et al., 2008)*, (Perrone et al., 2014) (Bernatek-Jakiel and Kondracka, 2016)*(Pánek et al., 2010) (Solberg et al., 2016)* (Marescot et al., 2008)* (Brody et al., 2015)* •Anthropogenic landforms (Pazzi et al., 2016)* •Impact structures (Bobée et al., 2010)* •Volcanic processes (Brothelande et al., 2016)* •Tectonic processes (Carrasco et al., 2018)*

Table 5 continued

Geophysical method	Key references	Geomorphological research
Electromagnetic (EM) methods Time domain Electromagnetic induction (TDEM) Frequency domain Electromagnetic induction (FDEM) Very low frequency electromagnetic (VLF-EM)	Ward and Hohmann (1988) Spies (1989) Everett (2012) Fitterman (2015)	TDEM •Impact structures (Bobée et al., 2010)* •Coastal environment (Paine et al., 2015)* •Tectonic processes (Pavan Kumar et al., 2019) •Hydrogeological research (Robinson et al., 2008)* (Rapti-Caputo et al., 2009)* •Volcanic processes (Brothelande et al., 2016)* FDEM •Karst processes (Bottari et al., 2017)* •Coastal environment (Paine et al., 2015)* (Weymer et al., 2015) (Wernette et al., 2018) •Impact structures (Bobée et al., 2010)* •Mass movement processes (Solberg et al., 2016)* (Gallistl et al., 2018)* VLF •Anthropogenic landforms (Pazzi et al., 2016)* •Hydrogeological research (Khalil et al., 2018)* •Potential subsidence zone detection (Dindi, 2015)* •Subsurface structure of a mud volcano (Lin and Jeng, 2010) •Tracing buried faults (Gürer et al., 2009)

Table 5 continued

Geophysical method	Key references	Geomorphological research
Induced polarization (IP)	Binley (2015)	•Hydrogeological research (Robinson et al., 2008)* (Ntarlagiannis et al., 2016)* •Geothermal areas (Van Dam, 2012) •Mass movement processes (Marescot et al., 2008)* (Gallistl et al., 2018)* (Sastry and Mondal, 2013)* •Mineral prospecting (Binley, 2015) •Periglacial processes (Doetsch et al., 2015)* (Grimm and Stillman, 2015)
Self-potential or Spontaneous potential (SP)	Jackson (2015)	•Mass movement and erosion processes (Naudet et al., 2008)* (Santoso et al., 2019)* (Wang et al., 2018a) (Wang et al., 2018b)* (Heinze et al., 2019) •Periglacial processes (Colombo et al., 2018)* •Volcanic processes (Brothelande et al., 2016)* (Mauri et al., 2018)* •Karst processes (Kaufmann and Romanov, 2017)* (Kaufmann and Romanov, 2016)* (Artugyan et al., 2015)* (Giampaolo et al., 2016)
Seismic reflection	Steeples and Miller (1998)	•Submarine geomorphological studies (Acosta et al., 2003) (Andreassen et al., 2008) (Santos et al., 2019) (Fierens et al., 2019) (Maestro et al., 2013) •Coastal geomorphology (Raimbault et al., 2018) •Fluvial geomorphology (Calvès et al., 2019) •Submarine landslides (Teixeira et al., 2019) •Geological landform assemblage study (Bellwald et al., 2019)

Table 5 continued

Geophysical method	Key references	Geomorphological research
Seismic refraction	Knapp and Steeples (1986a) Knapp and Steeples (1986b) Schrott et al. (2013)	•Critical Zone studies (Befus et al., 2011) (Wang et al., 2019) (Flinchum et al., 2018)* •Mass movement processes (Brody et al., 2015)* (Chen et al., 2019)* •Tectonic processes (Carrasco et al., 2018)*
Seismic surface-wave analysis	Nazarian et al. (1983) Nazarian and Stokoe (1986) Park et al. (1999) Socco and Strobbia (2004) Socco et al. (2010)	•Mass movement processes (Huntley et al., 2019)* •Soil mapping (Kruse, 2013) •Karst systems and landforms (Kruse, 2013) (Van Dam, 2012) •Liquefaction potential studies (Kruse, 2013) •Determination of soil/material properties (Van Dam, 2012)
Gravity method	Phillips (2015)	•Potential subsidence zone detection (Dindi, 2015)* •Impact structures (Bobée et al., 2010)* •Volcanic processes (Brothelande et al., 2016)* •Karst processes (Kaufmann and Romanov, 2017)* (Kaufmann and Romanov, 2016)* •Mapping salt beds (Phillips, 2015)

Table 5 continued

Geophysical method	Key references	Geomorphological research
Nuclear Magnetic Resonance (NMR)	Dlugosch et al. (2011) Müller-Petke and Yaramanci (2015) Grombacher et al. (2017)	•Periglacial processes (Keating et al., 2018)* •Hydrogeophysics (Grombacher et al., 2017) (Lin et al., 2018) (Kirkland and Codd, 2018) (Hull et al., 2019)* •Critical Zone Hydrology (Flinchum et al., 2018)* •Environmental research (Spurlin et al., 2019) • Tectonic processes (Carrasco et al., 2018)*

3.4. Using geophysical methods to address cutting-edge geomorphological questions

As previously mentioned, traditional methods used in geomorphology tend to be invasive, typically using outcrops, trenching, or boring to collect the necessary data. Technologic advances in near surface non-invasive geophysical methods, can now be utilized for a variety of applications, including planetary geomorphology. The versatile nature of methods such as GPR has made it possible to further exploration of the Moon and Mars. GPR systems bear vital characteristics for the scientific payload on a mission, including its convenient size, light weight, high data resolution, and simple operation (Ali and Shieh, 2014). The Chang'e-3 (2013) and Chang'e-4 (2018) missions launched by the China National Space Administration (CNSA) have explored the subsurface of the Moon using Lunar Penetrating Radar (LPR). Chang'e-3 landed in the Mare Imbrium region of the Moon, a large crater with a vast lava plain, and was able to characterize nine subsurface layers suggesting the region is compositionally distinct from other landing sites (Xiao et al., 2015). The following CNSA mission, Chang'e-4, landed on the far side of the Moon in the Von Kármán crater. Implementing the Lunar Penetrating Radar (LPR) resulted in the first high resolution image of a lunar ejecta sequence thickness and internal architecture (Li et al., 2020). Figure 29 corresponds with an example of LPR data and interpretations.

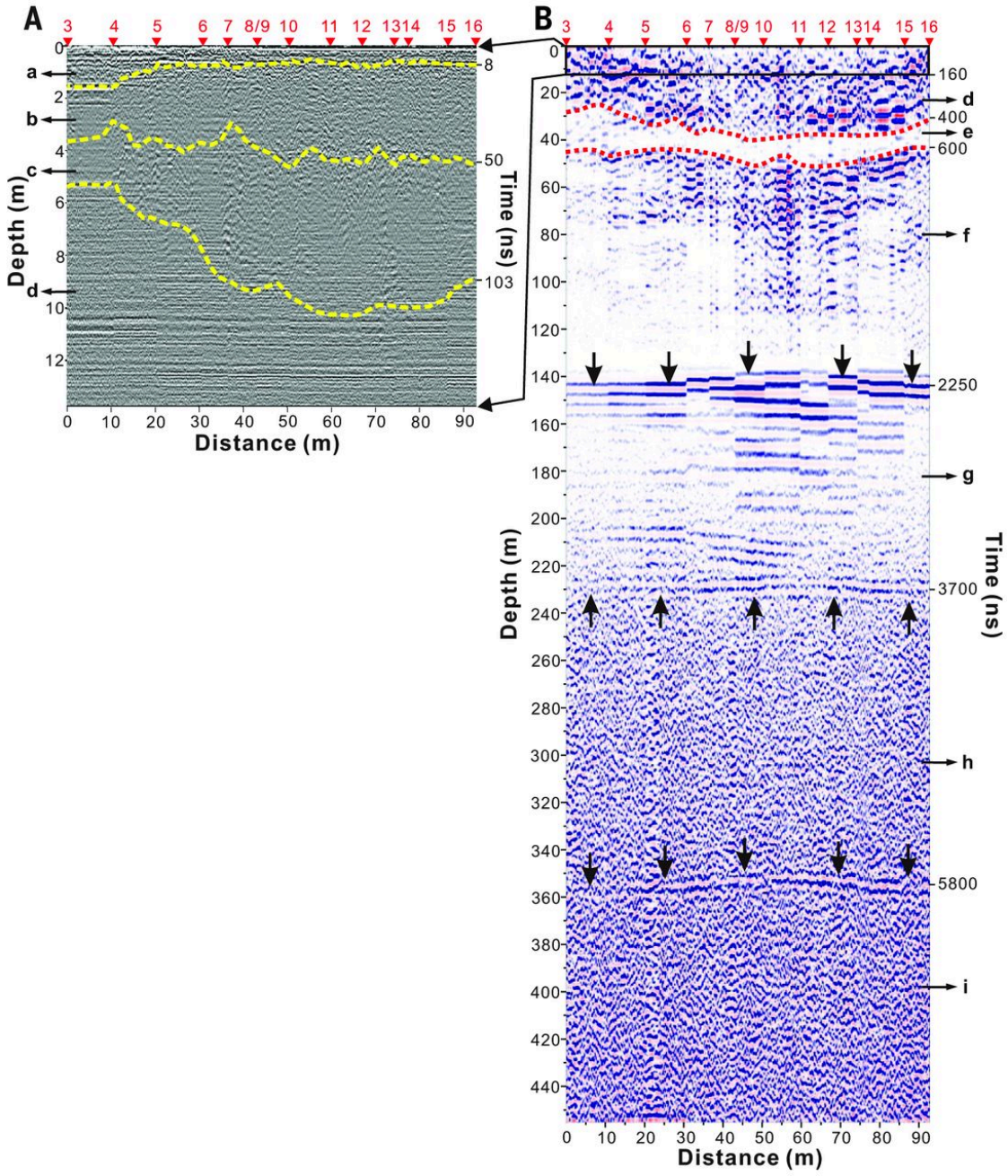

Figure 29 Results and interpretations (dashed lines and arrows) of the data from LPR Channel-2B and Channel-1. (A) Channel-2B. (B) Channel-1. Reprinted from Li et al., 2020.

Future missions deploying GPR include NASA's Mars 2020 rover and the European Space Agency's (ESA) ExoMars mission (2022). The Mars 2020 mission will carry the Radar Imager for Mars' Subsurface Experiment (RIMFAX) with the goal of imaging subsurface structure and to acquire information regarding subsurface composition (Hamran et al., 2016). The scientific payload for the ExoMars mission includes the GPR for the "Water Ice and Subsurface Deposit Observations on Mars" (WISDOM) experiment. The goals for WISDOM are to characterize the geologic environment by identifying sedimentary layers and to determine the distribution of water in the shallow subsurface (Dorizon et al., 2016; Plettemeier et al., 2009). By utilizing GPR future missions can elucidate the present state and understand the past evolution of Mars.

Collaborative work between diverse scientific disciplines allows the modern geomorphologist to access information about previously inaccessible areas, as demonstrated by recent advances on remote sensing and geophysical techniques used for planetary exploration. Geomorphological studies of extraterrestrial bodies are exemplified by publications such as Rodriguez et al. (2015) which provided high-resolution geomorphic mapping and insights on the developmental processes associated with Simud, Tiu and Ares Valles (i.e., some of the largest Martian outflow channels), and Smith et al. (2015) which combined surface and sub-surface data to study the evolution of landforms controlled by aeolian processes in Mars.

Expanding our research boundaries (Vitek and Giardino, 1993) and gathering high resolution data leads to the generation of large data sets. In some cases,

heterogeneous scientific data (i.e., GPS data, imagery, text and numerical values) are compiled in vast databases (up to 1 trillion gigabytes) which are referred to as Big Data (Spina, 2019). With A growing understanding of form-process relationships and increasing improvement of available technology, we seek to automate time-consuming tasks such as landform identification, processing remotely sensed data, Big Data analysis, and interpretation of geophysical data, employing Machine Learning Algorithms (MLAs) and Artificial Intelligence (AI) approaches. Spina (2019) discusses the use of MLAs (complex algorithms that can be taught decision making) and AI (computer systems resembling some functions of the human brain) in geosciences.

The application of AI and MLA approaches to geophysical interpretations is exemplified by Cracknell and Reading (2014) in their study of supervised geologic maps generated from remotely sensed geophysical data. The authors evaluate five MLAs in terms of the sensitivity to changes in the spatial distribution (clustering) of inputs used for training, as well as the introduction of explicit coordinates. Goetz et al. (2015) aid the user select appropriate approaches as concluded from their assessment of MLAs and statistical prediction methods. Their study applies MLAs and statistical methods for modeling landslide susceptibility in three geologically and geomorphologically distinct areas. Rahmati et al. (2017) compared the performance of seven MLAs in the predictive mapping of gully erosion susceptibility. The authors report robust and accurate results from their models. Infante-Paez and Marfurt (2019) used a workflow to determine the appropriate attributes to input in MLAs to assist seismic geomorphology interpretations. Jia and Ma (2017) developed an application for interpolation and reconstruction of

seismic data from under-sampled or missing traces, which is based on the method of support vector regression (SVR), a prevailing MLA.

The use of complex methodologies, multiple instruments, interdisciplinary teams, and large data sets is required to appropriately assess the relationships between the many components of complex geomorphic systems. Studies of geomorphological interest can now be conducted in remote and previously inaccessible areas. Geophysical methods used in combination with other techniques are increasingly promising, demonstrating the vast potential for exploration and thus the advancement of our understanding of geomorphological processes on Earth and other planetary bodies.

3.5. Concluding thoughts

The use of multiple-method approaches prevails in geomorphological studies pertaining complex processes and environments. Using multiple methodologies allows researchers access to information about the surface and subsurface at varying scales. Data collection and processing are increasingly carried out by interdisciplinary teams of researchers. The creation of open access information (i.e., databases) allows for faster data analysis and validation.

Increasing interest in non-invasive methods to study subsurface-surface interactions is evident in recent literature. Non-invasive methods are ideal for studies in remote locations, where access to the site(s) of interest is restricted, as well as in urban or culturally relevant areas (i.e., archaeological sites). Advances in geomorphological research across all geomorphic environments in recent years are accomplished with the

aid of remote sensing methods and non-invasive geophysics, typically validated using traditional invasive methodologies.

Examples of geomorphological studies carried out using geophysical methods were described this section to illustrate successful methodologies applied in varying geomorphic environments, as well as to highlight the potential uses in other environments. The techniques are not process-dependent, which allows for a wide range of new applications. With continuous advancements in methodologies and instrumentation, one can argue that geomorphological studies could be carried out using exclusively non-invasive techniques in the near future.

3.6. References

Acosta, J., Canals, M., López-Martínez, J., Muñoz, A., Herranz, P., Urgeles, R., Palomo, C., Casamor, J.L., 2003. The Balearic Promontory geomorphology (western Mediterranean): morphostructure and active processes. Geomorphology 49, 177–204. https://doi.org/10.1016/S0169-555X(02)00168-X

Aguilar, R.G., Owens, R., Giardino, J.R., 2020. The expanding role of anthropogeomorphology in critical zone studies in the Anthropocene. Geomorphology 366, 107165. https://doi.org/10.1016/j.geomorph.2020.107165

Ali, W., Shieh, S.R., 2014. Exploring Shallow Subsurface of Mars and Introducing the GPR Technique for Planetary Sciences(Exploring Mars beyond the Surface Features). J. Geol. Geosci. 03, 3–7. https://doi.org/10.4172/2329-6755.1000142

Andreassen, K., Laberg, J.S., Vorren, T.O., 2008. Seafloor geomorphology of the SW Barents Sea and its glaci-dynamic implications. Geomorphology 97, 157–177. https://doi.org/10.1016/j.geomorph.2007.02.050

Annan, A., 2005. The principals of ground penetrating radar in near-surface geophysics, in: Butler, D. (Ed.), Investigations in Geophysics No 13 - Near-Surface Geophysics. Society of Exploration Geophysicists, Tulsa, OK.

Artugyan, L., Ardelean, A., Urdea, P., 2015. Characterization of Karst Terrain Using Geophysical Methods Based on Sinkhole Analysis: A Case Study of the Anina Karstic Region (Banat Mountains, Romania), in: Sinkholes and the Engineering and

Environmental Impacts of Karst: Proceedings of the Fourteenth Multidisciplinary Conference. University of South Florida Tampa Library, pp. 387–398. https://doi.org/10.5038/9780991000951.1044

Azócar, G.F., Brenning, A., 2010. Hydrological and geomorphological significance of rock glaciers in the dry Andes, Chile (27°-33°S). Permafr. Periglac. Process. 21, 42–53. https://doi.org/10.1002/ppp.669

Befus, K.M., Sheehan, A.F., Leopold, M., Anderson, S.P., Anderson, R.S., 2011. Seismic constraints on critical zone architecture, Boulder Creek Watershed, Front Range, Colorado. Vadose Zo. J. 10, 915–927. https://doi.org/10.2136/vzj2010.0108

Bellwald, B., Planke, S., Lebedeva-Ivanova, N., Piasecka, E.D., Andreassen, K., 2019. High-resolution landform assemblage along a buried glacio-erosive surface in the SW Barents Sea revealed by P-Cable 3D seismic data. Geomorphology 332, 33–50. https://doi.org/10.1016/j.geomorph.2019.01.019

Bernatek-Jakiel, A., Kondracka, M., 2016. Combining geomorphological mapping and near surface geophysics (GPR and ERT) to study piping systems. Geomorphology 274, 193–209. https://doi.org/10.1016/j.geomorph.2016.09.018

Billi, A., De Filippis, L., Poncia, P.P., Sella, P., Faccenna, C., 2016. Hidden sinkholes and karst cavities in the travertine plateau of a highly-populated geothermal seismic territory (Tivoli, central Italy). Geomorphology 255, 63–80. https://doi.org/10.1016/j.geomorph.2015.12.011

Binley, A., 2015. Tools and Techniques: Electrical Methods, in: Treatise on Geophysics: Second Edition. pp. 233–259. https://doi.org/10.1016/B978-0-444-53802-4.00192-5

Binley, A., Ullah, S., Heathwaite, A.L., Heppell, C., Byrne, P., Lansdown, K., Trimmer, M., Zhang, H., 2013. Revealing the spatial variability of water fluxes at the groundwater-surface water interface. Water Resour. Res. 49, 3978–3992. https://doi.org/10.1002/wrcr.20214

Bobée, C., Schmutz, M., Camerlynck, C., Robain, H., 2010. An integrated geophysical study of the western part of the Rochechouart-Chassenon impact structure, Charente, France. Near Surf. Geophys. 8, 259–270. https://doi.org/10.3997/1873-0604.2010011

Bodin, X., Rojas, F., Brenning, A., 2010. Status and evolution of the cryosphere in the Andes of Santiago (Chile, 33.5°S.). Geomorphology 118, 453–464. https://doi.org/10.1016/j.geomorph.2010.02.016

Bottari, C., Albano, M., Capizzi, P., D'Alessandro, A., Doumaz, F., Martorana, R., Moro, M., Saroli, M., 2018. Recognition of Earthquake-Induced Damage in the

Abakainon Necropolis (NE Sicily): Results From Geomorphological, Geophysical and Numerical Analyses. Pure Appl. Geophys. 175, 133–148. https://doi.org/10.1007/s00024-017-1653-4

Bottari, C., Aringoli, D., Carluccio, R., Castellano, C., D'Ajello Caracciolo, F., Gasperini, M., Materazzi, M., Nicolosi, I., Pambianchi, G., Pieruccini, P., Sepe, V., Urbini, S., Varazi, F., 2017. Geomorphological and geophysical investigations for the characterization of the Roman Carsulae site (Tiber basin, Central Italy). J. Appl. Geophys. 143, 74–85. https://doi.org/10.1016/j.jappgeo.2017.03.021

Bristow, C., 2013. 14.16 Ground Penetrating Radar, in: Treatise on Geomorphology. Elsevier, pp. 183–194. https://doi.org/10.1016/B978-0-12-374739-6.00383-3

Bristow, C.S., Jol, H.M., Augustinus, P., Wallis, I., 2010. Slipfaceless "whaleback" dunes in a polar desert, Victoria Valley, Antarctica: Insights from ground penetrating radar. Geomorphology 114, 361–372. https://doi.org/10.1016/j.geomorph.2009.08.001

Brody, A.G., Pluhar, C.J., Stock, G.M., Greenwood, W.J., 2015. Near-Surface Geophysical Imaging of a Talus Deposit in Yosemite Valley, California. Environ. Eng. Geosci. 21, 111–127. https://doi.org/10.2113/gseegeosci.21.2.111

Brothelande, E., Lénat, J.-F., Chaput, M., Gailler, L., Finizola, A., Dumont, S., Peltier, A., Bachèlery, P., Barde-Cabusson, S., Byrdina, S., Menny, P., Colonge, J., Douillet, G.A., Letort, J., Letourneur, L., Merle, O., Di Gangi, F., Nakedau, D., Garaebiti, E., 2016. Structure and evolution of an active resurgent dome evidenced by geophysical investigations: The Yenkahe dome-Yasur volcano system (Siwi caldera, Vanuatu). J. Volcanol. Geotherm. Res. 322, 241–262. https://doi.org/10.1016/j.jvolgeores.2015.08.021

Calkin, P.E., Rutford, R.H., 1974. The sand dunes of Victoria Valley, Antarctica. Geogr. Rev. 64, 189–216.

Calvès, G., Calderon, Y., Roso, V., Bonnel, C., Roddaz, M., Brusset, S., Baby, P., Clift, P.D., 2019. Past Amazon Basin fluvial systems, insight into the Cenozoic sequences using seismic geomorphology (Marañón Basin, Peru). J. South Am. Earth Sci. 90, 440–452. https://doi.org/10.1016/j.jsames.2018.12.019

Carbonel, D., Rodríguez-Tribaldos, V., Gutiérrez, F., Galve, J.P., Guerrero, J., Zarroca, M., Roqué, C., Linares, R., McCalpin, J.P., Acosta, E., 2015. Investigating a damaging buried sinkhole cluster in an urban area (Zaragoza city, NE Spain) integrating multiple techniques: Geomorphological surveys, DInSAR, DEMs, GPR, ERT, and trenching. Geomorphology 229, 3–16. https://doi.org/10.1016/j.geomorph.2014.02.007

Carrasco, R.M., Turu, V., Pedraza, J., Muñoz-Martín, A., Ros, X., Sánchez, J., Ruiz-Zapata, B., Olaiz, A.J., Herrero-Simón, R., 2018. Near surface geophysical analysis of the Navamuño depression (Sierra de Béjar, Iberian Central System): Geometry, sedimentary infill and genetic implications of tectonic and glacial footprint. Geomorphology 315, 1–16. https://doi.org/10.1016/j.geomorph.2018.05.003

Chamorro, A., Giardino, J.R., Granados-Aguilar, R., Price, A.E., 2015. A Terrestrial Landscape Ecology Approach to the Critical Zone, in: Developments in Earth Surface Processes. https://doi.org/10.1016/B978-0-444-63369-9.00007-0

Chen, Q., Zhang, S., Chang, S., Liu, B., Liu, J., Long, J., 2019. Geophysical Interpretation of a Subsurface Landslide in the Southern Qinshui Basin. J. Environ. Eng. Geophys. 24, 433–449. https://doi.org/10.2113/JEEG24.3.433

Church, M., 2010. The trajectory of geomorphology. Prog. Phys. Geogr. Earth Environ. 34, 265–286. https://doi.org/10.1177/0309133310363992

Colombo, N., Sambuelli, L., Comina, C., Colombero, C., Giardino, M., Gruber, S., Viviano, G., Vittori Antisari, L., Salerno, F., 2018. Mechanisms linking active rock glaciers and impounded surface water formation in high-mountain areas. Earth Surf. Process. Landforms 43, 417–431. https://doi.org/10.1002/esp.4257

Conyers, L.B., Leckebusch, J., 2010. Geophysical Archaeology Research Agendas for the Future: Some Ground-penetrating Radar Examples. Archaeol. Prospect. 17, 117–123. https://doi.org/10.1002/arp.379

Cracknell, M.J., Reading, A.M., 2014. Geological mapping using remote sensing data: A comparison of five machine learning algorithms, their response to variations in the spatial distribution of training data and the use of explicit spatial information. Comput. Geosci. 63, 22–33. https://doi.org/10.1016/j.cageo.2013.10.008

Davis, J.L., Annan, A.P., 1989. Ground-Penetrating Radar for High-Resolution Mapping of Soil and Rock Stratigraphy. Geophys. Prospect. 37, 531–551. https://doi.org/10.1111/j.1365-2478.1989.tb02221.x

Degenhardt, J.J., 2009. Development of tongue-shaped and multilobate rock glaciers in alpine environments - Interpretations from ground penetrating radar surveys. Geomorphology 109, 94–107. https://doi.org/10.1016/j.geomorph.2009.02.020

Degenhardt, J.J., Giardino, J.R., 2003. Subsurface investigation of a rock glacier using ground-penetrating radar: Implications for locating stored water on Mars. J. Geophys. Res. E Planets 108, 1–17. https://doi.org/10.1029/2002je001888

Dindi, E., 2015. An assessment of the performance of the geophysical methods as a tool for the detection of zones of potential subsidence in the area southwest of Nakuru

town, Kenya. Environ. Earth Sci. 73, 3643–3653. https://doi.org/10.1007/s12665-014-3647-1

Dlugosch, R., Mueller-Petke, M., Günther, T., Costabel, S., Yaramanci, U., 2011. Assessment of the potential of a new generation of surface nuclear magnetic resonance instruments. Near Surf. Geophys. 9, 89–102. https://doi.org/10.3997/1873-0604.2010063

Doetsch, J., Ingeman-Nielsen, T., Christiansen, A. V., Fiandaca, G., Auken, E., Elberling, B., 2015. Direct current (DC) resistivity and induced polarization (IP) monitoring of active layer dynamics at high temporal resolution. Cold Reg. Sci. Technol. 119, 16–28. https://doi.org/10.1016/j.coldregions.2015.07.002

Dorizon, S., Ciarletti, V., Plettemeier, D., Benedix, W.S., 2016. Performance validation of the ExoMars 2018 WISDOM GPR in ice caves, Austria. Planet. Space Sci. 120, 1–14. https://doi.org/10.1016/j.pss.2015.10.008

El-Mowafy, H.Z., Marfurt, K.J., 2016. Quantitative seismic geomorphology, south Texas, United States. Am. Assoc. Pet. Geol. Bull. 100, 537–564. https://doi.org/10.1306/02011615136

Ettinger, S., Kruse, S., 2007. Using ground penetrating radar to help delineate lahar hazard zones at Cotopaxi Volcano, Ecuador, in: EOS Transactions of AGU.

Everett, M.E., 2013. Near-Surface Applied Geophysics. Cambridge University Press.

Everett, M.E., 2012. Theoretical Developments in Electromagnetic Induction Geophysics with Selected Applications in the Near Surface. Surv. Geophys. 33, 29–63. https://doi.org/10.1007/s10712-011-9138-y

Fierens, R., Droz, L., Toucanne, S., Raisson, F., Jouet, G., Babonneau, N., Miramontes, E., Landurain, S., Jorry, S.J., 2019. Late Quaternary geomorphology and sedimentary processes in the Zambezi turbidite system (Mozambique Channel). Geomorphology 334, 1–28. https://doi.org/10.1016/j.geomorph.2019.02.033

Fisk, H.N., 1959. Padre Island and the Laguna Madre flats, coastal south Texas, in: Proceedings 2nd Coastal Geography Conference. Louisiana State University, Baton Rouge, LA, pp. 103–151.

Fitterman, D.V., 2015. Tools and Techniques: Active-Source Electromagnetic Methods, in: Treatise on Geophysics. Elsevier, pp. 295–333. https://doi.org/10.1016/B978-0-444-53802-4.00193-7

Flinchum, B.A., Holbrook, W.S., Grana, D., Parsekian, A.D., Carr, B.J., Hayes, J.L., Jiao, J., 2018. Estimating the water holding capacity of the critical zone using near-

surface geophysics. Hydrol. Process. 32, 3308–3326. https://doi.org/10.1002/hyp.13260

Gallistl, J., Weigand, M., Stumvoll, M., Ottowitz, D., Glade, T., Orozco, A.F., 2018. Delineation of subsurface variability in clay-rich landslides through spectral induced polarization imaging and electromagnetic methods. Eng. Geol. 245, 292–308. https://doi.org/10.1016/j.enggeo.2018.09.001

Gance, J., Grandjean, G., Samyn, K., Malet, J.P., 2012. Quasi-Newton inversion of seismic first arrivals using source finite bandwidth assumption: Application to subsurface characterization of landslides. J. Appl. Geophys. 87, 94–106. https://doi.org/10.1016/j.jappgeo.2012.09.008

Giampaolo, V., Capozzoli, L., Grimaldi, S., Rizzo, E., 2016. Sinkhole risk assessment by ERT: The case study of Sirino Lake (Basilicata, Italy). Geomorphology 253, 1–9. https://doi.org/10.1016/j.geomorph.2015.09.028

Goetz, J.N., Brenning, A., Petschko, H., Leopold, P., 2015. Evaluating machine learning and statistical prediction techniques for landslide susceptibility modeling. Comput. Geosci. 81, 1–11. https://doi.org/10.1016/j.cageo.2015.04.007

Goudie, A., 2013. Arid and Semi-Arid Geomorphology. Cambridge University Press, Cambridge. https://doi.org/10.1017/CBO9780511794261

Grimm, R.E., Stillman, D.E., 2015. Field test of detection and characterisation of subsurface ice using broadband spectral-induced polarisation. Permafr. Periglac. Process. 26, 28–38. https://doi.org/10.1002/ppp.1833

Grombacher, D., Fiandaca, G., Behroozmand, A.A., Auken, E., 2017. Comparison of stabiliser functions for surface NMR inversions. Near Surf. Geophys. 15, 533–544. https://doi.org/10.3997/1873-0604.2017027

Gürer, A., Bayrak, M., Gürer, Ö.F., 2009. A VLF survey using current gathering phenomena for tracing buried faults of Fethiye–Burdur Fault Zone, Turkey. J. Appl. Geophys. 68, 437–447. https://doi.org/10.1016/j.jappgeo.2009.03.011

Hamran, S.-E., Amundsen, H.E.F., Asak, L., Berger, T., Brovoll, S., Buskenes, J.I., Damsgård, L., Diaz, C., Ghent, R., Helleren, Ø., Kohler, J., Mellon, M., Paige, D., Plettemeier, D., Rowe, K., Russell, P., Sagsveen, B., Ødegaard, N., Øyan, M.J., Geophysical, V., 2016. the Rimfax Gpr Instrument Development for the Mars 2020 Rover Mission. 3rd Int. Work. Instrum. Planet. Mission. 4–5.

Hauck, C., Kneisel, C., 2008. Applied geophysics in periglacial environments, Applied Geophysics in Periglacial Environments. https://doi.org/10.1017/CBO9780511535628

Heinze, T., Limbrock, J., Pudasaini, S., Kemna, A., 2019. Relating mass movement with electrical self-potential signals. Geophys. J. Int. 216, 55–60. https://doi.org/10.1093/gji/ggy418

Hull, R.., Johnson, C.D., Stone, B.D., LeBlanc, D.R., McCobb, T.D., Phillips, S.N., Pappas, K.L., Lane, J.W., 2019. Lithostratigraphic, geophysical, and hydrogeologic observations from a boring drilled to bedrock in glacial sediments near Nantucket sound in East Falmouth, Massachusetts: U.S. Geological Survey Scientific Investigations Report. https://doi.org/https://doi.org/10.3133/sir20195042

Huntley, D., Bobrowsky, P., Hendry, M., Macciotta, R., Best, M., 2019. Multi-technique Geophysical Investigation of a Very Slow-moving Landslide near Ashcroft, British Columbia, Canada. J. Environ. Eng. Geophys. 24, 87–110. https://doi.org/10.2113/JEEG24.1.87

Infante-Paez, L., Marfurt, K.J., 2019. Using machine learning as an aid to seismic geomorphology, which attributes are the best input? Interpretation 7, SE1–SE18. https://doi.org/10.1190/INT-2018-0096.1

Jackson, M.D., 2015. Tools and Techniques: Self-Potential Methods, in: Treatise on Geophysics. Elsevier, pp. 261–293. https://doi.org/10.1016/B978-0-444-53802-4.00208-6

Jia, Y., Ma, J., 2017. What can machine learning do for seismic data processing? An interpolation application. GEOPHYSICS 82, V163–V177. https://doi.org/10.1190/geo2016-0300.1

Jol, H.M., 2009. Ground Penetrating Radar Theory and Applications. Elsevier. https://doi.org/10.1016/B978-0-444-53348-7.X0001-4

Jol, H.M., Bristow, C.S., 2003. GPR in sediments: Advice on data collection, basic processing and interpretation, a good practice guide. Geol. Soc. Spec. Publ. 211, 9–27. https://doi.org/10.1144/GSL.SP.2001.211.01.02

Jongmans, D., Bièvre, G., Renalier, F., Schwartz, S., Beaurez, N., Orengo, Y., 2009. Geophysical investigation of a large landslide in glaciolacustrine clays in the Trièves area (French Alps). Eng. Geol. 109, 45–56. https://doi.org/10.1016/j.enggeo.2008.10.005

Kasprzak, M., Jancewicz, K., Różycka, M., Kotwicka, W., Migoń, P., 2019. Geomorphology- and geophysics-based recognition of stages of deep-seated slope deformation (Sudetes, SW Poland). Eng. Geol. 260, 105230. https://doi.org/10.1016/j.enggeo.2019.105230

Kaufmann, G., Romanov, D., 2017. The Jettencave, Southern Harz Mountains,

Germany: Geophysical observations and a structural model of a shallow cave in gypsum/anhydrite-bearing rocks. Geomorphology 298, 20–30. https://doi.org/10.1016/j.geomorph.2017.09.027

Kaufmann, G., Romanov, D., 2016. Structure and evolution of collapse sinkholes: Combined interpretation from physico-chemical modelling and geophysical field work. J. Hydrol. 540, 688–698. https://doi.org/10.1016/j.jhydrol.2016.06.050

Keating, K., Binley, A., Bense, V., Van Dam, R.L., Christiansen, H.H., 2018. Combined Geophysical Measurements Provide Evidence for Unfrozen Water in Permafrost in the Adventdalen Valley in Svalbard. Geophys. Res. Lett. 45, 7606–7614. https://doi.org/10.1029/2017GL076508

Khalil, M.A., Bobst, A., Mosolf, J., 2018. Utilizing 2D Electrical Resistivity Tomography and Very Low Frequency Electromagnetics to Investigate the Hydrogeology of Natural Cold Springs Near Virginia City, Southwest Montana. Pure Appl. Geophys. 175, 3525–3538. https://doi.org/10.1007/s00024-018-1865-2

Kirkland, C.M., Codd, S.L., 2018. Low-Field Borehole NMR Applications in the Near-Surface Environment. Vadose Zo. J. 17. https://doi.org/10.2136/vzj2017.01.0007

Knapp, R.W., Steeples, D.W., 1986a. High-resolution common-depth-point seismic reflection profiling: instrumentation. Geophysics 51, 276–282. https://doi.org/10.1190/1.1442087

Knapp, R.W., Steeples, D.W., 1986b. High-resolution common-depth-point reflection profiling: Field acquisition parameter design Ralph 51, 283–294.

Koruk, K., Yilmaz, K.K., Akyurek, Z., Binley, A., 2020. A multi-technique approach to determine temporal and spatial variability of groundwater-stream water exchange. Hydrol. Process. 34, 2612–2627. https://doi.org/10.1002/hyp.13754

Kruse, S., 2013. Near-Surface Geophysics in Geomorphology, in: Treatise on Geomorphology. Elsevier, pp. 103–129. https://doi.org/10.1016/B978-0-12-374739-6.00047-6

Kruse, S., Mora-Amador, R., Ramírez, C., Alvarado, G.E., 2010. Ground penetrating radar imaging of tephra stratigraphy on Poás and Irazú volcanoes , Department of Geology , University of South Florida Escuela Centroamericana de Geología , Centro de Investigaciones en Ciencias Área de Amenazas y Auscultación Sísmica y. Rev. Geol. Am. Cent. 43, 119–135.

Lazzari, M., Loperte, A., Perrone, A., 2010. Near surface geophysics techniques and geomorphological approach to reconstruct the hazard cave map in historical and urban areas. Adv. Geosci. 24, 35–44. https://doi.org/10.5194/adgeo-24-35-2010

Leopold, M., Völke, J., Huber, J., Dethier, D., 2013. Subsurface architecture of the boulder creek critical zone observatory from electrical resistivity tomography. Earth Surf. Process. Landforms 38, 1417–1431. https://doi.org/10.1002/esp.3420

Li, C., Su, Y., Pettinelli, E., Xing, S., Ding, C., Liu, J., Ren, X., Lauro, S.E., Soldovieri, F., Zeng, X., Gao, X., Chen, W., Dai, S., Liu, D., Zhang, G., Zuo, W., Wen, W., Zhang, Z., Zhang, X., Zhang, H., 2020. The Moon's farside shallow subsurface structure unveiled by Chang'E-4 Lunar Penetrating Radar. Sci. Adv. 6, 1–9. https://doi.org/10.1126/sciadv.aay6898

Li, Q., Yu, S., Wu, W., Tong, L., Kang, H., 2017. Detection of a deep-water channel in 3D seismic data using the sweetness attribute and seismic geomorphology: a case study from the Taranaki Basin, New Zealand. New Zeal. J. Geol. Geophys. 60, 199–208. https://doi.org/10.1080/00288306.2017.1307230

Lin, M.J., Jeng, Y., 2010. Application of the VLF-EM method with EEMD to the study of a mud volcano in southern Taiwan. Geomorphology 119, 97–110. https://doi.org/10.1016/j.geomorph.2010.02.021

Lin, T., Yang, Y., Teng, F., Müller-Petke, M., 2018. Enabling surface nuclear magnetic resonance at high-noise environments using a pre-polarization pulse. Geophys. J. Int. 212, 1463–1467. https://doi.org/10.1093/gji/ggx490

Lissak, C., Maquaire, O., Malet, J.P., Bitri, A., Samyn, K., Grandjean, G., Bourdeau, C., Reiffsteck, P., Davidson, R., 2014. Airborne and ground-based data sources for characterizing the morpho-structure of a coastal landslide. Geomorphology 217, 140–151. https://doi.org/10.1016/j.geomorph.2014.04.019

Loke, M. H., Barker, R.D., 1996. Rapid least-squares inversion of apparent resistivity pseudosections by a quasi-Newton method. Geophys. Prospect. 44, 131–152. https://doi.org/10.1111/j.1365-2478.1996.tb00142.x

Loke, M.H., Barker, R.D., 1996. Practical techniques for 3D resistivity surveys and data inversion. Geophys. Prospect. 44, 499–523.

Maestro, A., López-Martínez, J., Llave, E., Bohoyo, F., Acosta, J., Hernández-Molina, F.J., Muñoz, A., Jané, G., 2013. Geomorphology of the Iberian Continental Margin. Geomorphology 196, 13–35. https://doi.org/10.1016/j.geomorph.2012.08.022

Marescot, L., Monnet, R., Chapellier, D., 2008. Resistivity and induced polarization surveys for slope instability studies in the Swiss Alps. Eng. Geol. 98, 18–28. https://doi.org/10.1016/j.enggeo.2008.01.010

Margiotta, S., Negri, S., Parise, M., Valloni, R., 2012. Mapping the susceptibility to sinkholes in coastal areas, based on stratigraphy, geomorphology and geophysics.

Nat. Hazards 62, 657–676. https://doi.org/10.1007/s11069-012-0100-1

Mauri, G., Saracco, G., Labazuy, P., Williams-Jones, G., 2018. Correlating hydrothermal system dynamics and eruptive activity – A case-study of Piton de la Fournaise volcano, La Réunion. J. Volcanol. Geotherm. Res. 363, 23–39. https://doi.org/10.1016/j.jvolgeores.2018.08.009

Monnier, S., Kinnard, C., Surazakov, A., Bossy, W., 2014. Geomorphology, internal structure, and successive development of a glacier foreland in the semiarid Chilean Andes (Cerro Tapado, upper Elqui Valley, 30°08′ S., 69°55′ W.). Geomorphology 207, 126–140. https://doi.org/10.1016/j.geomorph.2013.10.031

Müller-Petke, M., Yaramanci, U., 2015. Tools and Techniques: Nuclear Magnetic Resonance, in: Treatise on Geophysics. Elsevier, pp. 419–445. https://doi.org/10.1016/B978-0-444-53802-4.00206-2

NASEM, 2020. Advancements in Use of Geophysical Methods for Transportation Projects, National Academies of Sciences, Engineering, and Medicine. The National Academies Press, Washington, DC. https://doi.org/10.17226/25809

National Research Council, N., 2001. Basic Research Opportunities in Earth Science, Basic Research Opportunities in Earth Science. https://doi.org/10.17226/9981

Naudet, V., Lazzari, M., Perrone, A., Loperte, A., Piscitelli, S., Lapenna, V., 2008. Integrated geophysical and geomorphological approach to investigate the snowmelt-triggered landslide of Bosco Piccolo village (Basilicata, southern Italy). Eng. Geol. 98, 156–167. https://doi.org/10.1016/j.enggeo.2008.02.008

Nazarian, S., Stokoe, K.H., 1986. Use of Surface Waves in Pavement Evaluation. Transp. Res. Rec. 132–144.

Nazarian, S., Stokoe, K.H., Hudson, W.R., 1983. Use of Spectral Analysis of Surface Waves Method for Determination of Moduli and Thicknesses of Pavement Systems. Transp. Res. Rec. 38–45.

Ntarlagiannis, D., Robinson, J., Soupios, P., Slater, L., 2016. Field-scale electrical geophysics over an olive oil mill waste deposition site: Evaluating the information content of resistivity versus induced polarization (IP) images for delineating the spatial extent of organic contamination. J. Appl. Geophys. 135, 418–426. https://doi.org/10.1016/j.jappgeo.2016.01.017

Obodovsky, A., 2019. Impact Craters in Seismic Data 44, 32–36.

Paine, J.G., Collins, E.W., Costard, L., 2015. Discriminating Quaternary depositional units on the Texas Coastal Plain using airborne lidar and near-surface geophysics,

in: Gulf Coast Association of Geological Societies Transactions. Society of Exploration Geophysicists and Environment and Engineering Geophysical Society, pp. 313–322. https://doi.org/10.4133/SAGEEP.28-010

Pánek, T., Margielewski, W., Tábořík, P., Urban, J., Hradecký, J., Szura, C., 2010. Gravitationally induced caves and other discontinuities detected by 2D electrical resistivity tomography: Case studies from the Polish Flysch Carpathians. Geomorphology 123, 165–180. https://doi.org/10.1016/j.geomorph.2010.07.008

Park, C.B., Miller, R.D., Xia, J., 1999. Multichannel analysis of surface waves. Geophysics 64, 800–808. https://doi.org/10.1190/1.1444590

Parsekian, A.D., Singha, K., Minsley, B.J., Holbrook, W.S., Slater, L., 2015. Multiscale geophysical imaging of the critical zone. Rev. Geophys. 53, 1–26. https://doi.org/10.1002/2014RG000465

Pavan Kumar, G., Nagar, M., Choudhary, V., Prasad, A.D., 2019. Shallow subsurface imaging of the Wagad active fault system (Kachchh, northwestern India) by time domain electromagnetic studies. J. Earth Syst. Sci. 128, 65. https://doi.org/10.1007/s12040-019-1090-0

Paxman, G.J.G., Jamieson, S.S.R., Ferraccioli, F., Jordan, T.A., Bentley, M.J., Ross, N., Forsberg, R., Matsuoka, K., Steinhage, D., Eagles, G., Casal, T.G., 2019. Subglacial Geology and Geomorphology of the Pensacola-Pole Basin, East Antarctica. Geochemistry, Geophys. Geosystems 20, 2786–2807. https://doi.org/10.1029/2018GC008126

Pazzi, V., Tapete, D., Cappuccini, L., Fanti, R., 2016. An electric and electromagnetic geophysical approach for subsurface investigation of anthropogenic mounds in an urban environment. Geomorphology 273, 335–347. https://doi.org/10.1016/j.geomorph.2016.07.035

Perrone, A., Lapenna, V., Piscitelli, S., 2014. Electrical resistivity tomography technique for landslide investigation: A review. Earth-Science Rev. 135, 65–82. https://doi.org/10.1016/j.earscirev.2014.04.002

Phillips, J.D., 2015. Tools and Techniques: Gravitational Method, in: Treatise on Geophysics: Second Edition. pp. 393–418. https://doi.org/10.1016/B978-0-444-53802-4.00197-4

Plettemeier, D., Ciarletti, V., Hamran, S.E., Corbel, C., Cais, P., Benedix, W.S., Wolf, K., Linke, S., Röddecke, S., 2009. Full polarimetric GPR antenna system aboard the ExoMars rover. IEEE Natl. Radar Conf. - Proc. https://doi.org/10.1109/RADAR.2009.4977120

Rahmati, O., Tahmasebipour, N., Haghizadeh, A., Pourghasemi, H.R., Feizizadeh, B., 2017. Evaluation of different machine learning models for predicting and mapping the susceptibility of gully erosion. Geomorphology 298, 118–137. https://doi.org/10.1016/j.geomorph.2017.09.006

Raimbault, C., Duperret, A., Le Gall, B., Authemayou, C., 2018. Structural inheritance and coastal geomorphology in SW Brittany, France: An onshore/offshore integrated approach. Geomorphology 306, 141–154. https://doi.org/10.1016/j.geomorph.2018.01.018

Rapti-Caputo, D., Bratus, A., Santarato, G., 2009. Strategic groundwater resources in the Tagliamento River basin (northern Italy): hydrogeological investigation integrated with geophysical exploration. Hydrogeol. J. 17, 1393–1409. https://doi.org/10.1007/s10040-009-0459-6

Revil, A., Jardani, A., 2013. The Self-Potential Method: Theory and Applications in Environmental Geosciences. Cambridge University Press. https://doi.org/10.1017/CBO9781139094252

Riebe, C.S., Hahm, W.J., Brantley, S.L., 2017. Controls on deep critical zone architecture: a historical review and four testable hypotheses. Earth Surf. Process. Landforms 42, 128–156. https://doi.org/10.1002/esp.4052

Robinson, D.A., Binley, A., Crook, N., Day-Lewis, F.D., Ferré, T.P.A., Grauch, V.J.S., Knight, R., Knoll, M., Lakshmi, V., Miller, R., Nyquist, J., Pellerin, L., Singha, K., Slater, L., 2008. Advancing process-based watershed hydrological research using near-surface geophysics: a vision for, and review of, electrical and magnetic geophysical methods. Hydrol. Process. 22, 3604–3635. https://doi.org/10.1002/hyp.6963

Robinson, M., Bristow, C., Mckinley, J., Ruffell, A., 2013. Ground Penetrating Radar, in: Cook, S.J., Clarke, L.E., Nield, J.M. (Eds.), Geomorphological Techniques (Online Edition). British Society for Geomorphology, London, pp. 1–26.

Rodriguez, J.A.P., Platz, T., Gulick, V., Baker, V.R., Fairén, A.G., Kargel, J., Yan, J., Miyamoto, H., Glines, N., 2015. Did the martian outflow channels mostly form during the Amazonian Period? Icarus 257, 387–395. https://doi.org/10.1016/j.icarus.2015.04.024

Santos, R., Quartau, R., Brum da Silveira, A., Ramalho, R., Rodrigues, A., 2019. Gravitational, erosional, sedimentary and volcanic processes on the submarine environment of Selvagens Islands (Madeira Archipelago, Portugal). Mar. Geol. 415, 105945. https://doi.org/10.1016/j.margeo.2019.05.004

Santoso, B., Hasanah, M.U., Setianto, 2019. Landslide investigation using self potential

method and electrical resistivity tomography (Pasanggrahan, South Sumedang, Indonesia). IOP Conf. Ser. Earth Environ. Sci. 311, 012068. https://doi.org/10.1088/1755-1315/311/1/012068

Sastry, R.G., Mondal, S.K., 2013. Geophysical Characterization of the Salna Sinking Zone, Garhwal Himalaya, India. Surv. Geophys. 34, 89–119. https://doi.org/10.1007/s10712-012-9206-y

Scapozza, C., Laigre, L., 2014. The contribution of Electrical Resistivity Tomography (ERT) in Alpine dynamics geomorphology: case studies from the Swiss Alps. Géomorphologie Reli. Process. Environ. 20, 27–42. https://doi.org/10.4000/geomorphologie.10474

Schrott, L., Otto, J.-C., Götz, J., Geilhausen, M., 2013a. Fundamental Classic and Modern Field Techniques in Geomorphology: An Overview, in: Treatise on Geomorphology. Elsevier, pp. 6–21. https://doi.org/10.1016/B978-0-12-374739-6.00369-9

Schrott, L., Otto, J.C., Götz, J., Geilhausen, M., 2013b. Fundamental Classic and Modern Field Techniques in Geomorphology: An Overview, in: Treatise on Geomorphology. pp. 6–21. https://doi.org/10.1016/B978-0-12-374739-6.00369-9

Schrott, L., Sass, O., 2008. Application of field geophysics in geomorphology: Advances and limitations exemplified by case studies. Geomorphology 93, 55–73. https://doi.org/10.1016/j.geomorph.2006.12.024

Selby, M.J., Rains, R.B., Palmer, R.W.P., 1974. Eolian deposits of the ice free Victoria Valley, southern Victoria Land, Antarctica. New Zeal. J. Geol. Geophys. 17, 543–562.

Siart, C., Forbriger, M., Nowaczinski, E., Hecht, S., Höfle, B., 2013. Fusion of multi-resolution surface (terrestrial laser scanning) and subsurface geodata (ERT, SRT) for karst landform investigation and geomorphometric quantification. Earth Surf. Process. Landforms 38, 1135–1147. https://doi.org/10.1002/esp.3394

Slim, M., Perron, J.T., Martel, S.J., Singha, K., 2015. Topographic stress and rock fracture: A two-dimensional numerical model for arbitrary topography and preliminary comparison with borehole observations. Earth Surf. Process. Landforms 40, 512–529. https://doi.org/10.1002/esp.3646

Smith, I.B., Spiga, A., Holt, J.W., 2015. Aeolian processes as drivers of landform evolution at the South Pole of Mars. Geomorphology 240, 54–69. https://doi.org/10.1016/j.geomorph.2014.08.026

Socco, L.V., Foti, S., Boiero, D., 2010. Surface-wave analysis for building near-surface

velocity models - Established approaches and new perspectives. Geophysics 75. https://doi.org/10.1190/1.3479491

Socco, L.V., Strobbia, C., 2004. Surface-wave method for near-surface characterization: a tutorial. Near Surf. Geophys. 2, 165–185. https://doi.org/10.3997/1873-0604.2004015

Solberg, I.-L., Long, M., Baranwal, V.C., Gylland, A.S., Rønning, J.S., 2016. Geophysical and geotechnical studies of geology and sediment properties at a quick-clay landslide site at Esp, Trondheim, Norway. Eng. Geol. 208, 214–230. https://doi.org/10.1016/j.enggeo.2016.04.031

Spies, B.R., 1989. Depth of investigation in electromagnetic sounding methods. GEOPHYSICS 54, 872–888.

Spina, R., 2019. Big Data and Artificial Intelligence Analytics in Geosciences: Promises and Potential. GSA Today 29, 42–43. https://doi.org/10.1130/GSATG372GW.1

Spurlin, M.S., Barker, B.W., Cross, B.D., Divine, C.E., 2019. Nuclear magnetic resonance logging: Example applications of an emerging tool for environmental investigations. Remediat. J. 29, 63–73. https://doi.org/10.1002/rem.21590

St. Clair, J., Moon, S., Holbrook, W.S., Perron, J.T., Riebe, C.S., Martel, S.J., Carr, B., Harman, C., Singha, K., Richter, D. d., 2015. Geophysical imaging reveals topographic stress control of bedrock weathering. Science (80-.). 350, 534–538. https://doi.org/10.1126/science.aab2210

Stan, D., Stan-Kłeczek, I., Kania, M., 2017. Geophysical approach to the study of a periglacial blockfield in a mountain area (Ztracené kameny, Eastern Sudetes, Czech Republic). Geomorphology 293, 380–390. https://doi.org/10.1016/j.geomorph.2016.12.004

Steeples, D.W., Miller, R.D., 1998. Avoiding pitfalls in shallow seismic reflection surveys. Geophysics 63, 1213–1224. https://doi.org/10.1190/1.1444422

Teixeira, M., Terrinha, P., Roque, C., Rosa, M., Ercilla, G., Casas, D., 2019. Interaction of alongslope and downslope processes in the Alentejo Margin (SW Iberia) – Implications on slope stability. Mar. Geol. 410, 88–108. https://doi.org/10.1016/j.margeo.2018.12.011

Tucker, G.E., 2015. Landscape Evolution, in: Treatise on Geophysics. Elsevier, pp. 593–630. https://doi.org/10.1016/B978-0-444-53802-4.00124-X

Van Dam, R.L., 2012. Landform characterization using geophysics—Recent advances, applications, and emerging tools. Geomorphology 137, 57–73.

https://doi.org/10.1016/j.geomorph.2010.09.005

van der Kruk, J., 2015. Tools and Techniques: Ground-Penetrating Radar, in: Treatise on Geophysics. Elsevier, pp. 209–232. https://doi.org/10.1016/B978-0-444-53802-4.00195-0

Viles, H., 2016. Technology and geomorphology: Are improvements in data collection techniques transforming geomorphic science? Geomorphology 270, 121–133. https://doi.org/10.1016/j.geomorph.2016.07.011

Vitek, J.D., 2013. Geomorphology: Perspectives on observation, history, and the field tradition. Geomorphology 200, 20–33. https://doi.org/10.1016/j.geomorph.2012.10.021

Vitek, J.D., Giardino, J.R., 1993. Preface: a perspective on getting to the frontier, in: Vitek, J.D., Giardino, J.R. (Eds.), Geomorphology: The Research Frontier and Beyond. Elsevier Science, pp. vii–xii.

Wang, F., Dai, Z., Okeke, C.A.U., Mitani, Y., Yang, H., 2018a. Experimental study to identify premonitory factors of landslide dam failures. Eng. Geol. 232, 123–134. https://doi.org/10.1016/j.enggeo.2017.11.020

Wang, F., Okeke, A.C.-U., Kogure, T., Sakai, T., Hayashi, H., 2018b. Assessing the internal structure of landslide dams subject to possible piping erosion by means of microtremor chain array and self-potential surveys. Eng. Geol. 234, 11–26. https://doi.org/10.1016/j.enggeo.2017.12.023

Wang, W., Chen, P., Keifer, I., Dueker, K., Lee, E.-J., Mu, D., Jiao, J., Zhang, Y., Carr, B., 2019. Weathering front under a granite ridge revealed through full-3D seismic ambient-noise tomography. Earth Planet. Sci. Lett. 509, 66–77. https://doi.org/10.1016/j.epsl.2018.12.038

Ward, S.H., Hohmann, G.W., 1988. Electromagnetic Theory for Geophysical Applications, Nabighian,. ed, Electromagnetic Methods in Applied Geophysics. SEG Press. https://doi.org/10.1190/1.9781560802716.ch2a

Wegmann, K.W., Bohnenstiehl, D.R., Bowman, J.D., Homburg, J.A., Windingstad, J.D., Beery, D., 2012. Assessing Coastal Landscape Change for Archaeological Purposes: Integrating ShallowGeophysics, Historical Archives andGeomorphology at Port Angeles,Washington, USA. Archaeol. Prospect. 19, 229–252. https://doi.org/10.1002/arp

Wernette, P., Houser, C., Weymer, B.A., Everett, M.E., Bishop, M.P., Reece, B., 2018. Influence of a spatially complex framework geology on barrier island geomorphology. Mar. Geol. 398, 151–162.

https://doi.org/10.1016/j.margeo.2018.01.011

Weymer, B.A., Everett, M.E., de Smet, T.S., Houser, C., 2015. Review of electromagnetic induction for mapping barrier island framework geology. Sediment. Geol. 321, 11–24. https://doi.org/10.1016/j.sedgeo.2015.03.005

Xiao, L., Zhu, P., Fang, G., Xiao, Z., Zou, Y., Zhao, J., Zhao, N., Yuan, Y., Qiao, L., Zhang, X., Zhang, H., Wang, J., Huang, J., Huang, Q., He, Q., Zhou, B., Ji, Y., Zhang, Q., Shen, S., Li, Y., 2015. A young multilayered terrane of the northern Mare Imbrium revealed by Chang'E-3 mission. Science (80-.). 347, 1226–1229. https://doi.org/10.1126/science.1259866

4. USING ELECTROMAGNETIC INDUCTION TO MODEL THE INTERNAL STRUCTURE-HYDROLOGICAL FLOW CONNECTION: UPPER CAMP BIRD ROCK GLACIER, SAN JUAN MOUNTAINS, COLORADO

4.1. Synopsis

Climatic variability affects the timing, frequency, and intensity of precipitation events. In periglacial areas, this variability could result in a decrease in the amount of rainfall, the depth of the snowpack, and the length of the snow seasons. Thus, decreasing the window for recharge for three water sources in periglacial environments: glaciers, aquifers, and rock glaciers. Rock glaciers occur in areas that favor permafrost formation and preservation. Poorly sorted rock fragments of varying sizes (gravel – fines) and ice makeup a rock glacier. Internally, they can be ice-cemented or ice-cored. Externally, a blanket of debris insulates the ice, preventing rapid melting in response to short-term temperature increases. A rock glacier constitutes a highly porous and heterogeneous reservoir that collects, stores, and discharges water. Complex relationships between inputs and outputs, ground and surface water, as well as phase changes occurring within a rock glacier, complicate the pathways for water flow. The Upper Camp Bird rock glacier, located on level 3 of Camp Bird Mine in Ouray County, Colorado, is the rock glacier of interest. This research used non-invasive methods, and integrated geomorphological, geological, and geophysical information to characterize the internal structure of the selected rock glacier, while evaluating the suitability of two controlled-source electromagnetic induction systems. Geophysical surveys using electromagnetic induction, employing both time-domain and frequency-domain systems, were interpreted

to determine the internal structure of the rock glacier. The electromagnetic induction methods employed include the new G-TEM™ equipment by Geonics Ltd., as well as the Profiler EMP-400™ by GSSI to create a profile of the internal structure of the rock glacier. The G-TEM™ is a time domain instrument that measures a decaying electromagnetic signal to determine apparent-resistivity, whereas the Profiler EMP-400™ is a frequency domain instrument that measures apparent-conductivity using multiple frequencies. The G-TEM™ was used on a central loop configuration along a 7x5 grid with 25 m spaced stations transversally and 50 m longitudinally. The G-TEM™ data was fitted using 1D manual models and expressed as resistivity depth profiles. The Profiler EMP-400™ recorded measurements using discrete data points every 5 m along the profiling lines, at the following frequencies: 1,000 Hz, 8,000 Hz, and 15,000 Hz. Lastly, local weather information including snowfall, rainfall, and temperature were analyzed, and integrated in a conceptual model for the hydrology of the Upper Camp Bird rock glacier.

4.2. Introduction

4.2.1. Problem

The World Economic Forum ranked catastrophes caused by climate change as the biggest threat to economy. In September 2016, the amount of CO_2 in the atmosphere went above 400 ppm, this makes it extremely difficult to prevent global temperatures from rising more than 2 °C (~35 °F) in the following years (IPCC, 2013). Although all environments are sensitive to impacts of climate change, alpine environments are

especially vulnerable to the effects of increasing temperatures (i.e. diminishing snowpack, longer droughts).

The timing and amount of runoff in creeks and rivers in mountainous regions will be affected by changes in snowfall. If these changes lead to the reduction of runoff, the availability of water supply in mountain communities is compromised and can further impact the more populated lowland regions that benefit from alpine river basins. A potential consequence of diminished availability of essential water resources globally is an increase in conflicts not only between countries, such as the United States and Mexico, but within the United States in locations like California.

The wide distribution of rock glaciers in major mountain ranges of the world make them significant for water supply. Rock glaciers provide the seasonal water that maintains the summer water flow of many alpine streams (Janke et al., 2013). Many cities in Europe and Asia depend on water supply from rivers originating in alpine areas. Melt water from rock glaciers contributes to the water supply for various cities, agriculture, and industrial water supplies. In the state of Colorado, the municipal water for the city of Boulder is supplied by melt water provided by the Arapaho glacier and rock glacier (City of Boulder Colorado, 2002).

Global warming is having a detrimental impact on water resources supplied by ice glaciers because they are melting rapidly (Haddeland et al., 2014). Rock glaciers, on the other hand, have a cover of rock and debris that serves as a blanket and insulates the internal ice from direct solar radiation, preventing rapid melting (Jones et al., 2019). Rock glaciers that develop in north facing slopes in the Northern Hemisphere remain

mostly shaded, potentially allowing further ice preservation. Thus, knowing the extent and makeup of rock glaciers is important for evaluating future water resources.

4.2.2. Purpose

The purpose of this study was to characterize the hydrological importance of a rock glacier in an alpine area using a non-invasive methodology, as well as to assess the applicability of two geophysical instruments on a highly heterogeneous landform.

To assess the contribution of rock glaciers to water supply requires determining 1) the spatial extent (Irham, 2016; Degenhardt, 2002); 2) the hydrologic characteristics, and 3) the internal structure of the rock glaciers. The composition and internal structure of rock glaciers remains understudied (Duguay et al., 2015). Thus, a clear understanding of the processes and fluid-mass pathways on and within a rock glacier has yet to be achieved.

4.2.3. Rock glaciers

Rock glaciers are ubiquitous forms found in the Arctic, Antarctic and almost any alpine environment on Earth. Rock glaciers consist of unconsolidated poorly sorted rock debris shell, supported by an ice interior (i.e., permafrost; Duguay et al., 2015). Mountain permafrost is heterogeneous and non-continuous, and accretion of permafrost is influenced by local climatic regimens (French, 2013). Permafrost is extensive in areas where the mean annual temperature is below -2 °C (28.4 °F). High latitude and/or high-elevation mountain ranges with cold dry climates support permafrost features. Thus, permafrost can occur at lower elevation than glaciers and below tree line in mid-latitude mountains (Eamer et al. 2007).

In periglacial regions, permafrost can occur in steep headwalls, rock glaciers, glacial till (moraines), and in vegetated soils. Permafrost distribution and ice-content vary in response to changes in conditioning factors such as topography, snowfall and cover, shaping processes, aspect, and mean-annual ground and air temperatures. Such changes can occur over short distances at high elevations (Eamer et al. 2007).

In areas where the mean-annual temperature is marginally below freezing (0 °C or 32 °F), permafrost only forms in shaded or sheltered areas. Thus, permafrost is mostly discontinuous to sporadic in mid-latitude mountains. North-facing slopes in the Northern Hemisphere receive less sunlight; thus, favoring the accretion of mountain permafrost. According to Heginbottom et al. (2012), mountain permafrost is considered continuous when it occurs above 3,600 m (11,811 ft) of elevation, discontinuous between 3,200 m (10,500 ft) – 3,600 m (11,811 ft), and sporadic between 2,700 m (8,858 ft) – 3,200 m (10,500 ft). Seasonally frozen ground occurs below 2,700 m (8,858 ft) of elevation (Heginbottom et al. 2012; fig. 30).

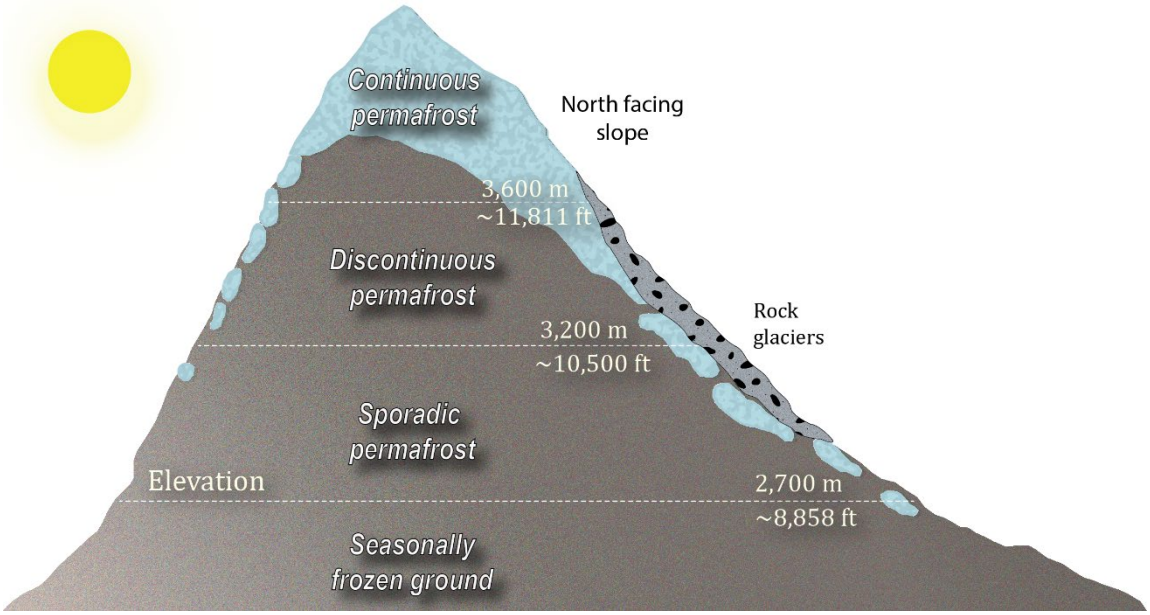

Figure 30 Classification of the type of permafrost occurrence based on elevation shown on a North-facing slope in the Northern Hemisphere. Modified from Heginbottom et al., 2012 and Rowley et al., 2015.

Malehmir et al. (2016) attribute the origin of rock glaciers to permafrost creep, highlighting rock glacier occurrence in high-alpine periglacial areas. Rock glaciers tend to form where the average angle of a slope is between 35° and 60° (Janke et al. 2013) and in areas where permafrost is present, leading some researchers to map rock glaciers as an alternative to mapping less obvious surficial expressions of permafrost (Irham, 2016; Riffle, 2018). Eamer et al. (2007), suggest a connection between the rate of movement (i.e., active/inactive status) of rock glaciers with the changing climate. The authors argue that inactive or fossil rock glaciers are indicative of past colder climates that allowed for permafrost formation.

Geomorphic processes that form and shape alpine environments are complex and operate as a trifecta through commencement, transfer, and accumulation of debris. Giardino and Vitek (1988) estimate that 20%-60% of the total debris transport in alpine areas is carried out by rock glaciers. Because rock glaciers are the major component of the fluid-mass cascade, they serve as transporters and storages for debris movement, and as a source and pathway for meltwater.

The rock glacier is a transitional form (Giardino and Vitek, 1988), that can have a glacial or periglacial origin, and that can evolve as time progresses into distinct terminal forms (Knight et al., 2019). Figure 31 illustrates this concept of the periglacial landscape continuum proposed by Giardino and Vitek (1988). Rock glaciers are frequently misidentified especially when looking at the surface alone, but fabric can be used to differentiate between phenomena such as glacial till and rock glaciers (Giardino and Vitek, 1985).

Rock glaciers contain either an ice core (Potter, 1972; Whalley, 1974; Whalley et al., 1994; Whalley, 2020) or an ice-rock matrix (Johnson, 1981; Haeberli, 1985; Gardner and Bajewsky, 1987; Bajewsky and Gardner, 1989; Giardino et al., 1992; Haeberli and Vonder Müehll, 1996; Schrott, 1996). The frozen core of the rock glacier allows for plastic deformation and enables the structure to function similarly to an ordinary ice glacier, exhibiting movement downslope (Wahrhaftig and Cox, 1959; Haeberli, 1985; Barsch, 1996; Giardino et al., 1992).

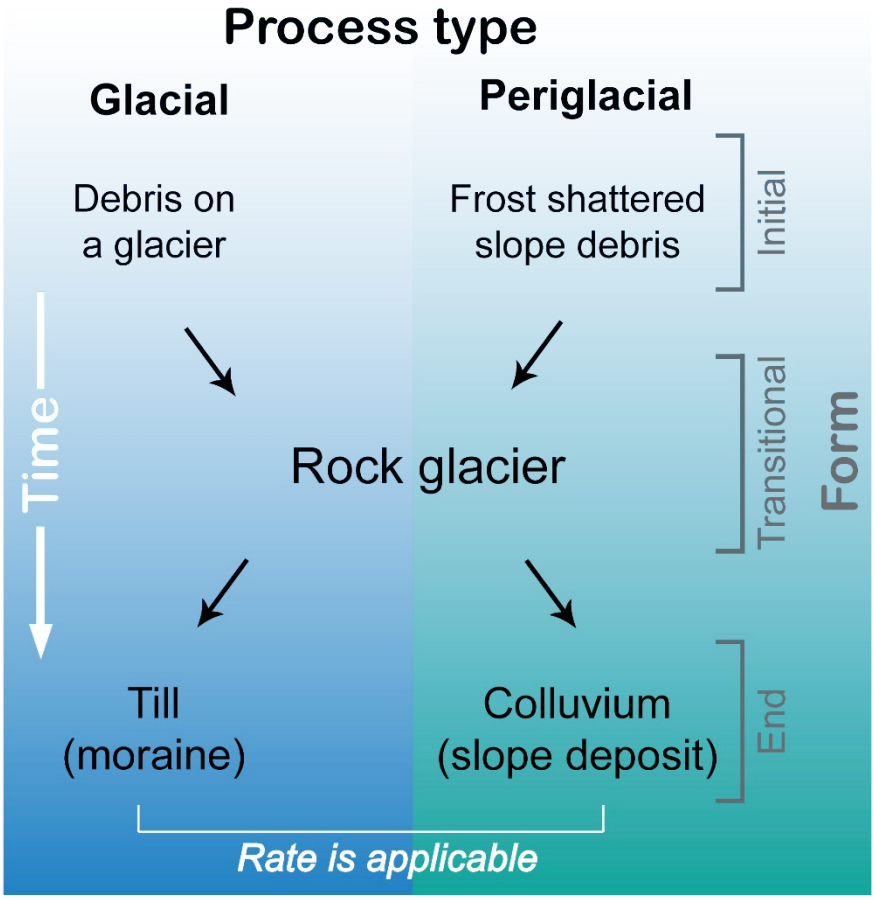

Figure 31 Time, space and processes are part of the concept of the periglacial landscape continuum. Rock glaciers are transitional forms that can develop from glacial or periglacial processes that with time can result in distinct end-members. The applicable rate of movement is related to the process, not the form. Modified from Giardino and Vitek, 1988.

Conditioning factors for rock glacier development, in addition to environmental conditions favoring permafrost formation, include rock supply from a surrounding cirque headwall (source) which is steep and susceptible to failure resulting in rock fall (Giardino, 1979). Rock glacier classifications include those based on origin (i.e., glacial/glaciogenic or periglacial/talus-derived), morphological characteristics (i.e., the

shape of the main body: lobate, tongue-shaped, spatulate, or complex), type of ice (i.e., massive or interstitial), ice/rock ratio (see Janke et al., 2015), and state of activity (i.e., active, inactive, or relict).

Seasonal freeze-thaw processes characterize the near-surface layer, known as the active layer, of permafrost features. Therefore, a transient boundary exists between frozen and unfrozen ground (Rowley et al., 2015). Active rock glaciers can exhibit an active layer of up to 7 m (~23 ft) of thickness (Haeberli et al, 2006), whereas inactive rock glaciers can have a 10 m (32.8 ft) thick active layer (Barsch, 1996).

Cheng and Jin (2013) have studied the role of permafrost on the hydrology of mountain basins. The authors concluded the presence of permafrost restricts the connection of surface water and the groundwater found below the frozen ground, which they call subpermafrost groundwater. As expected, the hydraulic conductivity of frozen soils can be significantly lower than that of unfrozen soils, which results in a perched water table within the active layer, above the frozen ground boundary (Kane et al., 2013).

Authors such as Corte (1976, 1978), Giardino and Vick (1987), and Barsch (1988), discuss rock glaciers as potential water storage or water reservoirs in mountainous regions. Janke et al. (2015) combine field observations with coring data to relate the surface morphology of rock glaciers to their internal structure (i.e., ice and rock content) and use this as an indicator of water resource availability.

The significance of rock glaciers as water resources is at watershed scale. Thus, looking at a singular rock glacier as a unique source of water supply is not practical. In a

study by Geiger et al. (2014), significant differences were observed between the hydrographs of adjacent alpine basins, only one of which hosts a rock glacier. The rock glacier basin produced discharge patterns analogous to those observed from ice glaciers but differing in magnitude, characterized by high discharge rates resulting from snowmelt in the spring, weather-driven diurnal fluctuations, and storm-driven flood peaks. Internal melting of rock glacier ice provides the summer baseflow, and the discharge from the toe progressively lessens through the warm summer months (Geiger et al., 2014). The authors add their observations to the vast pool of evidence that prove the insulating effect of the debris mantle that allows rock glaciers to respond slower to temperature variations.

Giardino et al., (1992) use a systems approach to study rock glaciers, describing interrelated geomorphic processes observed in alpine watersheds. The authors refer to rock glaciers as alpine aquifers. In rock glacier systems, hydrological inputs consist of rainfall, snowfall, hail and ice. These inputs enter the subsystems and are subjected to varying processes such as phase changes, and follow diverse pathways through the rock glacier. Part of the inputs remain stored as ice or water for varying periods of time. Outputs occur in the form of evaporation, sublimation, runoff, discharge and springs (Giardino et al., 1992; fig. 32).

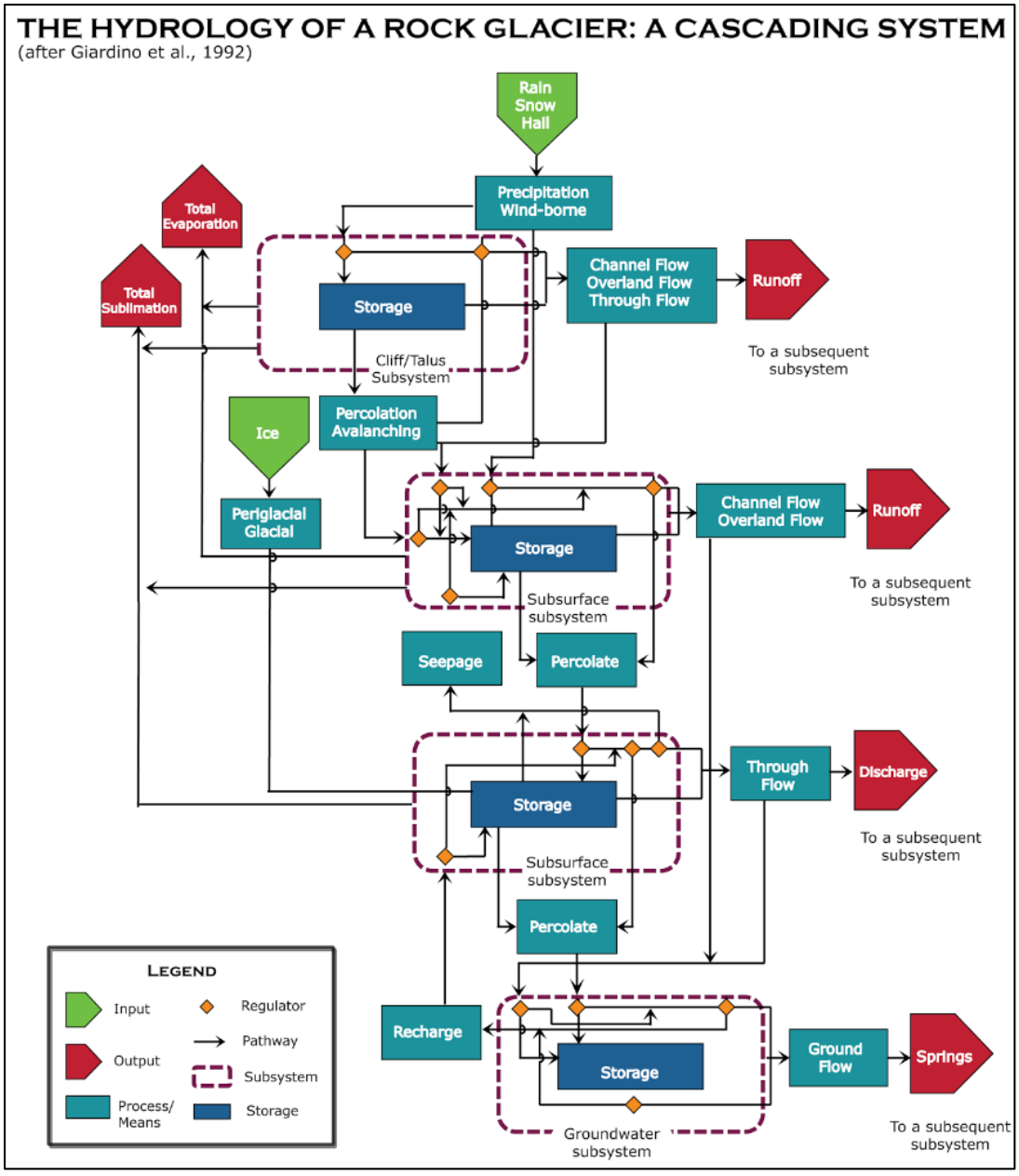

Figure 32 Conceptual model of the hydrology of a rock glacier. Modified from Giardino et al., 1992.

4.2.4. Area of study

The area of study is located in Ouray County, in the San Juan Mountains in southwestern Colorado. According to Baars (1992), during the past two million years

over a dozen glacial advances have occurred in the San Juan Mountains. The same author indicates the cirques in the area have remained ice-free for about 15,000 years, based on to C-14 dating.

Orogenic events caused alteration of intrusive igneous rock into mineral rich, hydrothermal fluids which were deposited as economically valuable minerals in the region known as the Ouray Mining District in the San Juan Mountains. The Ouray Mining District is recognized mostly for its gold resources. One of the most productive mines in Ouray was the Camp Bird Mine, producing gold, silver, lead, copper, and zinc (Rosemeyer, 1999), from the 1890s until the early 2000s. The Camp Bird Mine is the namesake for the rock glacier of interest.

The selected rock glacier is located near the third level of Camp Bird Mine (Fig. 33) and is herein referred to as the Upper Camp Bird rock glacier. The access to the region is by the San Juan Skyway, whereas access to the Camp Bird rock glacier is through county road 869 also known as Camp Bird road.

The Upper Camp Bird rock glacier, located in the headwaters of the Imogene Basin, is part of the Uncompahgre River Watershed, which extends over seven counties in the San Juan Mountains and is part of the Upper Colorado River Basin. The Upper Uncompahgre Watershed in Ouray county collects snowmelt from the high-elevation areas, where the Uncompahgre River flows from prominent peaks through rugged terrain and steep canyons (UWP, 2019).

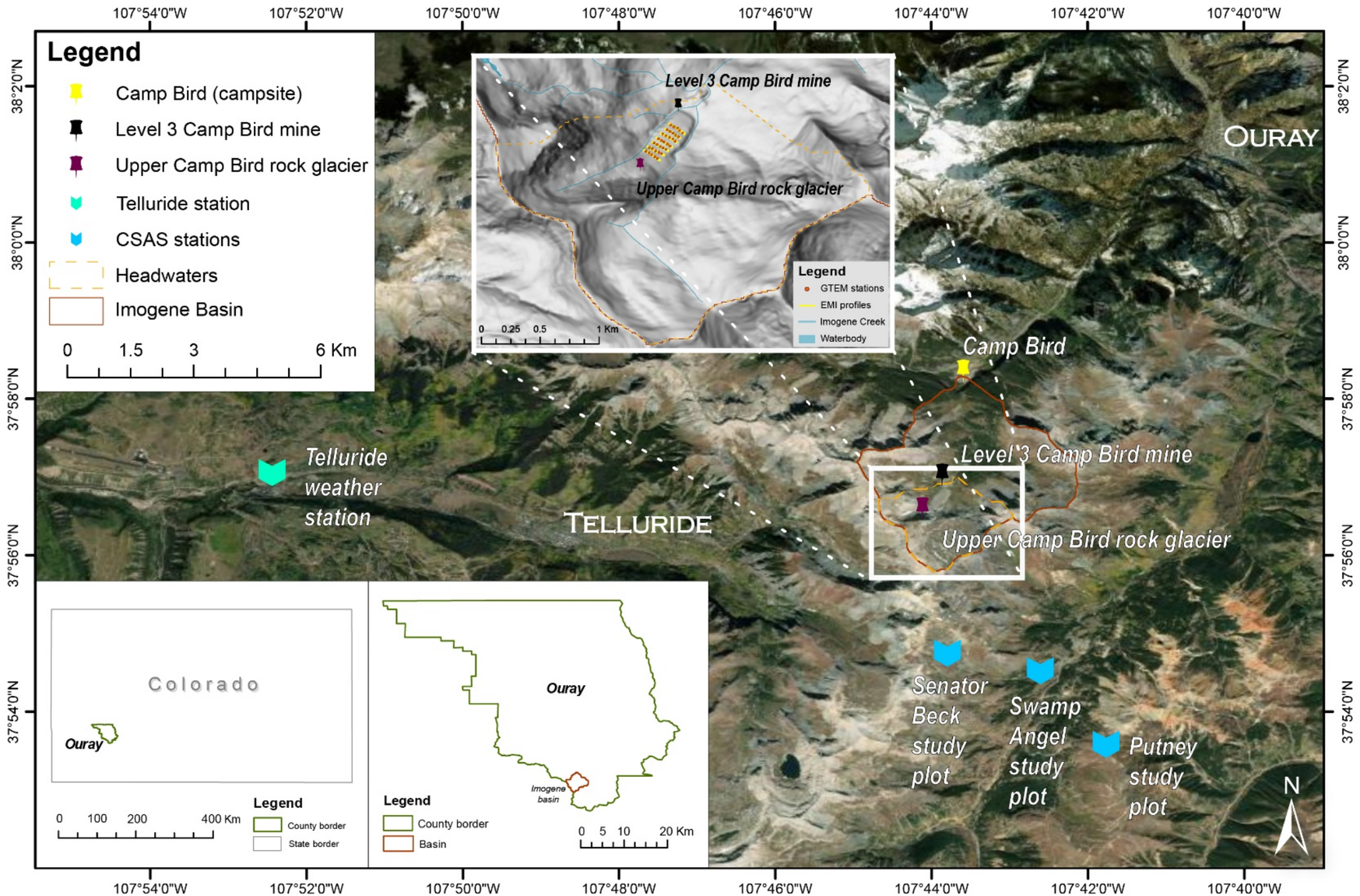

Figure 33 General location map of the Imogene Basin, San Juan Mountains, Colorado. The dashed with lines indicate the extent of the detailed hill shade map. Coordinate System: GCS WGS 1984. DEMs harvested from 1/3rd arc-second Digital Elevation Models (DEMs) - USGS National Map 3DEP Downloadable Data Collection Hydrography harvested from USGS, National Geospatial Program, 20200615, NHD 20200615 for Colorado State or Territory Shapefile Model Version 2.2.1: USGS. Index maps harvested from ArcGis online. Service Layer Credits: Source: Esri, Maxar, GeoEye, Earthstar Geographics, CNES/Airbus DS, USDA, USGS, AeroGRID, IGN, and the GIS User Community Esri, HERE, Garmin, (c) OpenStreetMap contributors, and the GIS user community.

4.2.5. Weather

4.2.5.1. The San Juan Mountains, Colorado

The San Juan Mountains have defined seasons, as expected in the northern hemisphere, with an average minimum temperature of -18.8 ℃ (-1.84 °F) that allows for snow to accumulate during autumn and winter, and melt during the spring and summer (average maximum temperatures reach 23 ℃ or 73.4 °F) (County, 2015; Ménard et al., 2019).

4.2.5.2. The Imogene Basin, San Juan Mountains, Colorado

Weather information is available from two sources in the vicinity of Imogene Basin, a weather station near the regional airport in Telluride, and instrumentation corresponding with the Senator Beck Basin Study Area. Table 6 shows the coordinates of each location in decimal degrees, the elevation above sea level, as well as the distance to the reference point in the Imogene Basin.

Table 6 Location of the meteorological stations near the area of study.

Name		Latitude	Longitude	Elevation	
Imogene Basin		37.943832	-107.727905	Mean 3,802 m ~12,474 ft	Reference point
Telluride 4 WNW Weather Station		37.949258	-107.873481	2,635 m ~8,645 ft	~11 km away from Imogene Basin; ~1000 m elevation difference
Senator Beck Basin Study Area	Senator Beck Study Plot	37.906883	-107.726265	3,714 m ~12,185 ft	~4 km away from Imogene Basin; ~90 m elevation difference
	Swamp Angel Study Plot	37.906914	-107.711322	3,371 m ~11,060	~4 km away from Imogene Basin; ~430 m elevation difference

Weather information collected at the Telluride 4 WNW Station since 1901 can be requested from the National Centers for Environmental Information (NCEI), formerly the National Climatic Data Center (NCDC). The Telluride weather station is about 11 km away from the Imogene Basin, at an elevation of 2,635 m (~8,645 ft). The total annual precipitation and the total annual snowfall in millimeters for the period 1901-2020 is represented in figure 34. The data plotted in figure 34 suggest a decrease in the annual snowfall between 1901-2020, whereas the rainfall seems to have a steady trend.

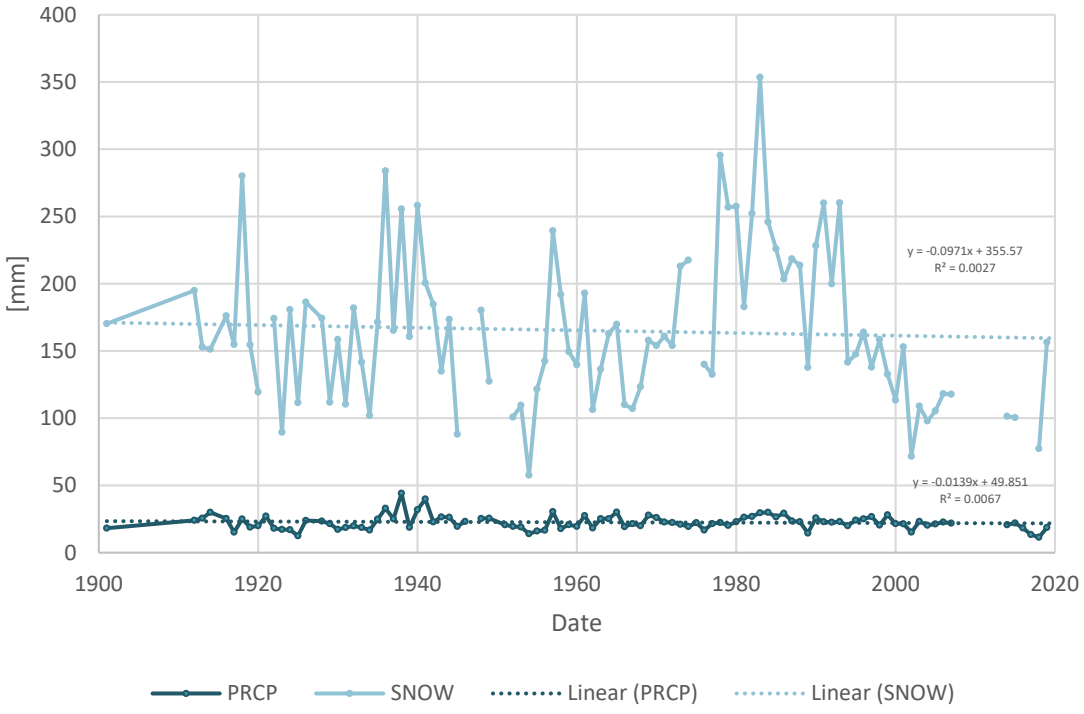

Figure 34 Total precipitation and snowfall over time at the Telluride station. Note there are gaps in the data. Data source NCEI (2020).

The Center for Snow and Avalanche Studies (CSAS) located in Silverton, Colorado, established the Senator Beck Basin Study Area (SNBSA) in 2003. The Senator Beck Study Plot (SNB) and the Swamp Angel Study Plot (SWA) are part of the SNBSA. The SNB is characterized by thin soil and exposed bedrock, the vegetation type corresponds to alpine tundra, the snow cover is classified as alpine, and Köppen climate classification corresponds with polar and alpine (montane) climates.

The SWA is located at a lower elevation in a clearing in the subalpine forest, with soil consisting of colluvium, with a snow cover classified as alpine, and a subarctic climate according to the Köppen climate classification (Ménard et al., 2019).

The Senator Beck Basin is part of the Uncompahgre River Basin and is located about 4 km away from Imogene Basin. Since the establishment of the SNBSA, the CSAS has conducted integrative year-long mountain system monitoring. The CSAS makes datasets, graphs and publications available for researchers.

A paper published by Ménard et al. (2019) uses meteorological data from 10 reference sites in cold regions around the world. Datasets from the SNBSA, specifically the SNB and SWA, were included in the snow modelling study along with three other mid-latitude alpine sites, three boreal, one maritime and one arctic (Ménard et al., 2019). The authors used datasets from the selected ten sites for assessing models taking part in the Earth System Model-Snow Model Intercomparison Project (ESM-SnowMIP). The in-situ datasets were bias-corrected with data derived from the Global Soil Wetness Project Phase 3 (GSWP3). Figure 35 shows the annual-mean air temperature for the in situ and bias-corrected GSWP3 data at SNB and SWA between 1981 and 2016, whereas figure 36 shows snowfall variations at the same sites.

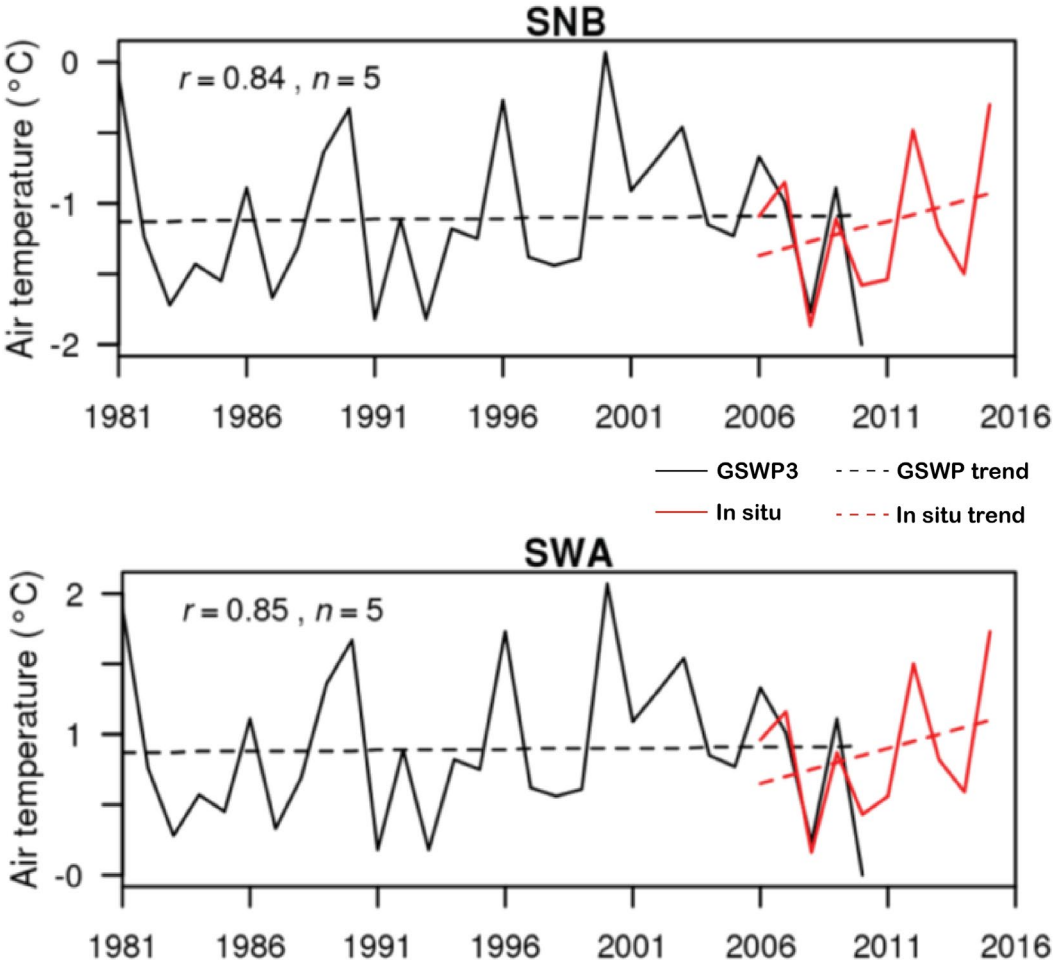

Figure 35 Annual mean temperatures and fitted trends at SNB and SWA from GSWP3 (in black) and in-situ data (in red). Numbers show correlation (*r*) between GSWP3 and in situ air temperature for the *n* complete years of overlap. Reprinted from Ménard et al., 2019.

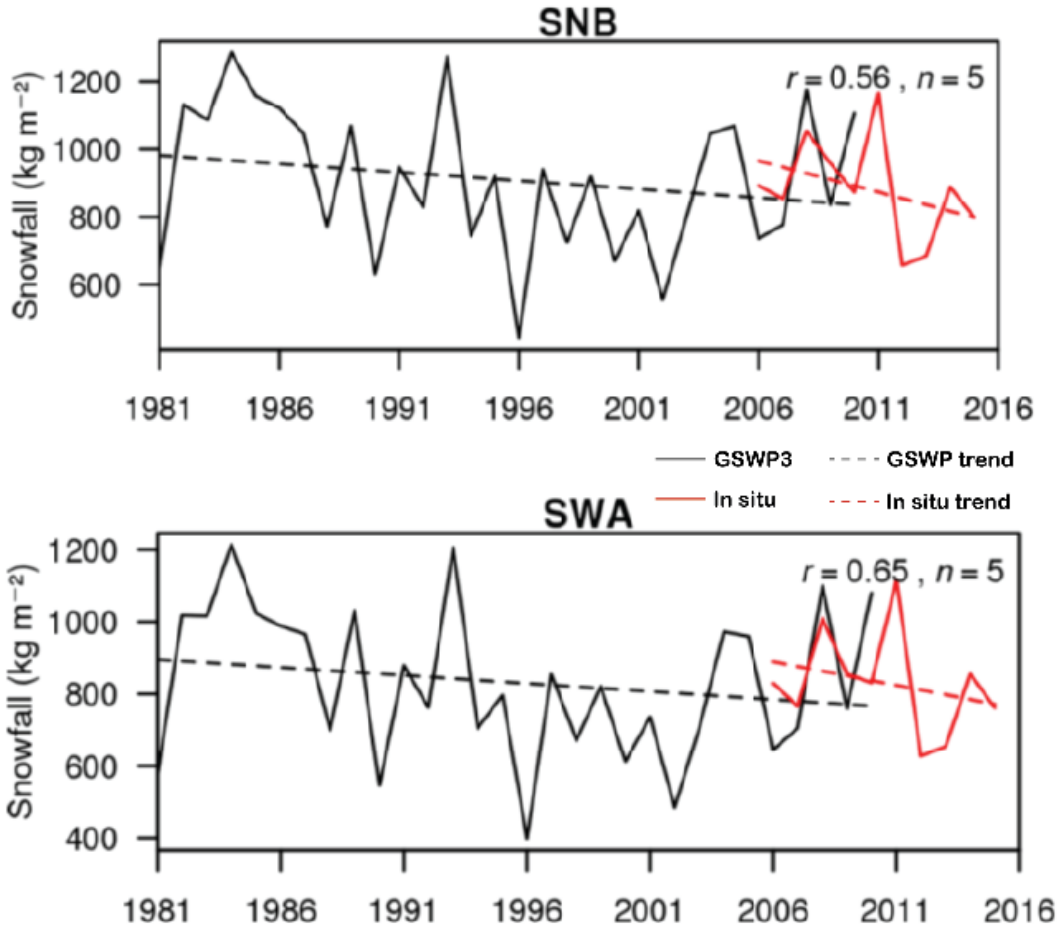

Figure 36 Annual snowfall and fitted trends at SNB and SWA from GSWP3 (in black) and in-situ data (in red). Numbers show correlation (*r*) between GSWP3 and in situ air temperature for the *n* complete years of overlap. Reprinted from Ménard et al., 2019.

Ménard et al. (2019) noted that the SNB is the only reference site at which the annual mean temperature is below freezing (around-1 °C or 30.2 °F). The alpine sites represented in their study experienced the most snowfall, with SNB and SWA in second and third place. Figure 37 shows the fraction of precipitation falling as snow with respect to air temperature at SNB. The minimum and maximum peak yearly snow depth reported for SNB are 1.52 m (4.98 ft) and 2.37 m (7.77 ft), whereas the numbers for

SWA are 1.66 m (5.44 ft) and 2.66 m (8.72 ft). The SNB site experiences an average of 4 times the wind speeds recorded at the SWA (Ménard et al., 2019).

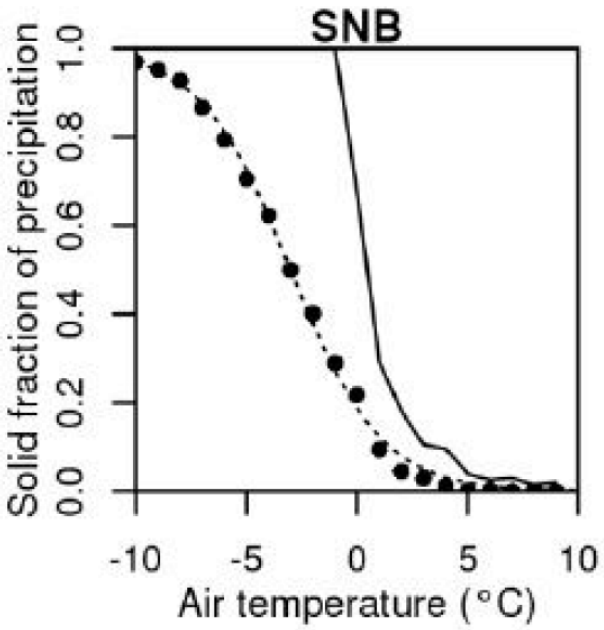

Figure 37 Solid fraction of precipitation falling at different temperatures, as imposed on the in-situ data and fitted to the GSWP3 data. Reprinted from Ménard et al., 2019.

The daily climatological averages of surface temperature at SNB range between 10° C and -19 °C (50 °F and – 2.2 °F), whereas SWA exhibits a range between 13 °C and -20 °C (55.4 °F and – 4 °F). Daily climatological averages of soil temperature at 10 cm (~3.94 inches) depth are reported to range between -2 °C and 9 °C (28.4 °F and 48.2 °F) at SNB, and 0 °C and 15 °C (32 °F and 59 °F) at SWA. All this information along with the daily climatological averages of air-soil temperature differences is presented in figure 38.

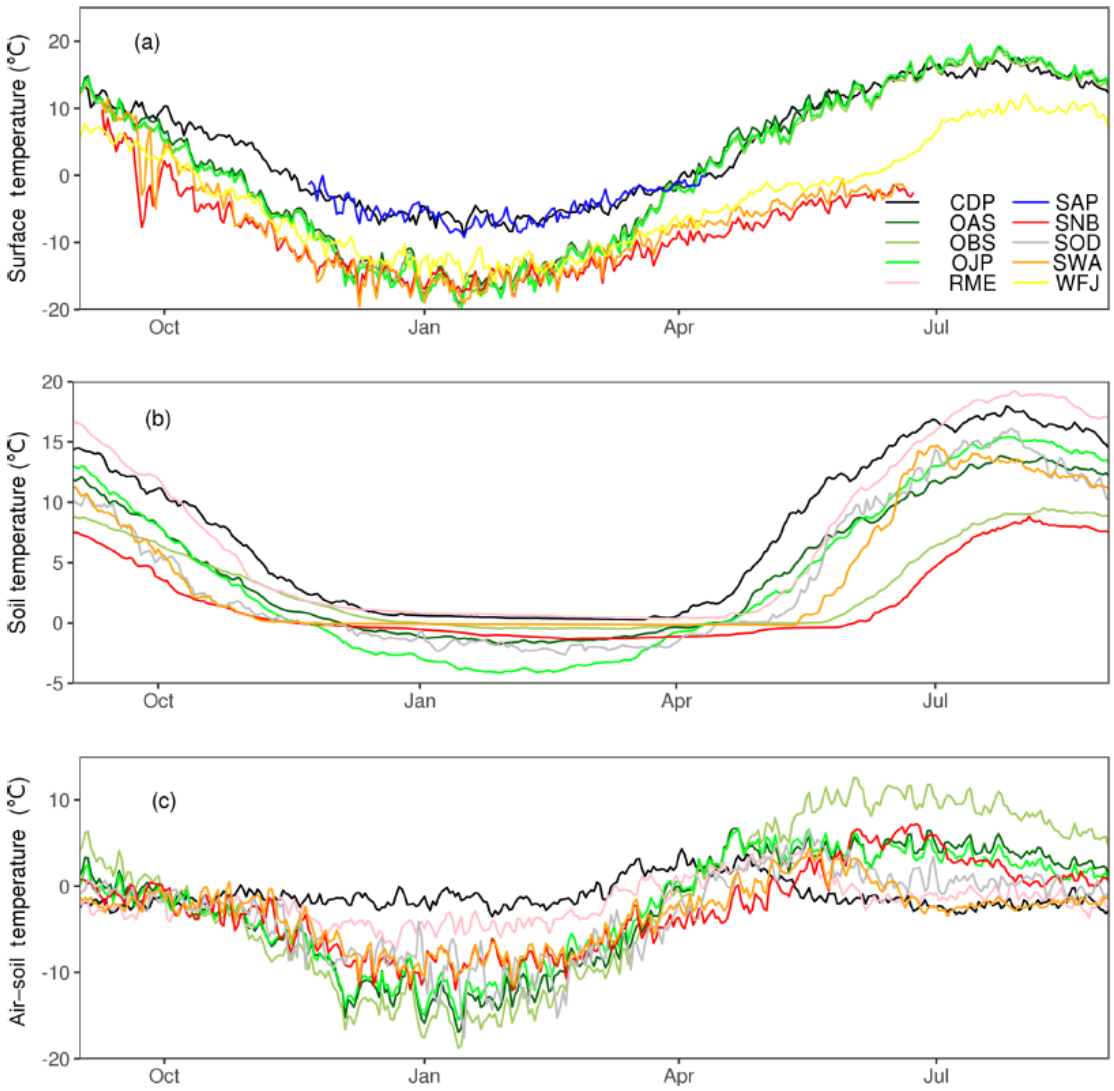

Figure 38 Daily climatological averages of (a) surface temperature, (b) soil temperature (at 10 cm depth, RME at 30 cm depth), and (c) differences between air and soil temperatures. As shown in the legend in (A), SNB and SWA are shown in red and orange, respectively, whereas the other colors correspond with the other reference sites studied by Ménard et al. (2019). Reprinted from Ménard et al., 2019.

The data published by Ménard et al. (2019) show that the in situ annual mean temperature trends upward for SNB and SWA, and the annual snowfall for the same locations shows a downward trend. The annual snowfall reported for the Telluride station also suggests a downward trend. The data from the monitoring stations close to Imogene Basin show that overall, the temperatures are rising, and the snowfall is decreasing. However, the SNB site, which is the closest to the Imogene Basin in elevation and distance, maintains a mean annual temperature below freezing and records the second highest snowfall of the ten reference sites studied by Ménard et al. (2019). Considering the Environmental Lapse Rate (ELR), one expects the temperatures at Imogene Basin to decrease about 0.5 °C per 100 m or 3.5 °F per 1,000 ft with respect to the monitoring stations located at lower elevations. The weather conditions in the area are considered favorable for permafrost formation and preservation.

4.2.6. Geology

4.2.6.1. The San Juan Mountains, Colorado

The geologic history of the San Juan Mountains begins with a metamorphic basement of Proterozoic age. The geologic record is missing for part of the Paleozoic. Limestones, dolomites and other marine sedimentary rocks (Devonian and Mississippian) overlay the basement in an angular unconformity. Marine transitional to continental rocks including conglomerates, sandstones, and shales with interbedded fossiliferous limestones of Pennsylvanian and Permian age follow the sequence. Another angular unconformity exists in which Mesozoic shales, mudstones, sandstones, limestones, breccias, and conglomerates overlay the Paleozoic section. Orogeny events

have affected the region, including the Laramide uplifts (late Cretaceous, Gonzales & Karlstrom, 2011) with associated ore deposits. Volcanism occurred in the Cenozoic covering the region with andesites, rhyolites, and tuff breccias of intermediate composition (Luedke and Burbank, 1963; Steven et al., 1974; Lipman 1976).

Multiple glaciations have occurred in the area and post-glacial processes have shaped the landscape. Glacial deposits in the area are Pleistocene events whereas alluvial deposits are of Holocene age (Burbank and Luedke, 1984; Huffman, 1995; Blair, 1996).

4.2.6.2. The Imogene Basin, San Juan Mountains, Colorado

Figure 39 shows a regional map of the major volcanotectonic structures associated with the Silverton and San Juan Calderas, as well as the geology of the Imogene Basin. Hydrothermal alteration associated with the orogeny events deposited economically valuable minerals along preferential pathways (i.e., fractures) in the region. As a result, the Ouray Mining District is known for its silver, copper, lead, zinc, and most importantly gold resources (Rosemeyer, 1999). One of the most prolific mines in Ouray was the Camp Bird mine in Imogene Basin, producing for over a century. The predominant lithologies in the area of study are Cenozoic.

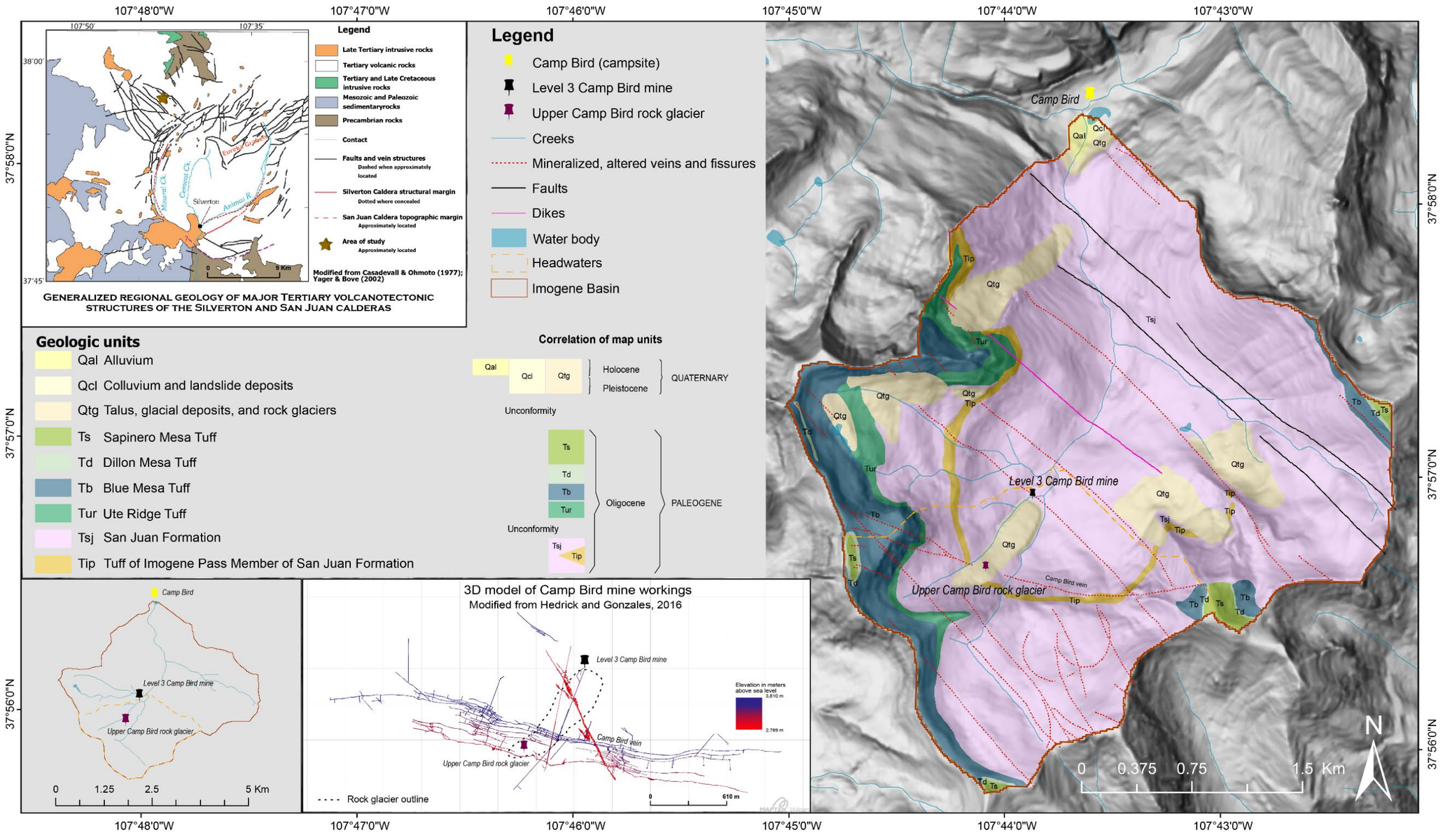

Figure 39 Generalized Geologic Map of the Imogene Basin, Ouray, Colorado. Geology harvested and modified from: Yager and Bove, 2002 and Casadevall and Ohmoto, 1977. DEMs harvested from 1/3rd arc-second USGS National Map. Hydrography harvested from USGS, NHD 20200615. Coordinate System: GCS WGS 1984. 3D model of Camp Bird mine modified from Hedrick and Gonzales, 2016.

The San Juan Formation (Tsj, Lower Oligocene) comprises the oldest lava flows (intermediate-composition) and volcaniclastic deposits, consisting of mudflow breccias with volcanic, conglomerate, and sandstone clasts (Yager and Bove, 2002). The Tuff of Imogene Pass Member (Tip) of the San Juan Formation corresponds with a dark-brown, andesitic-dacitic tuff, formed from ash-flows resulting from a stratovolcano collapse (Yager and Bove, 2002). This tuff is mapped as the Eureka Member of Sapinero Mesa Tuff (Tse, Oligocene) by Burbank and Luedke (1964).

The Ute Ridge (Tur, dacitic), Blue Mesa (Tb), Dillon Mesa (Td, rhyolitic), and Sapinero Mesa (Ts, rhyolitic) Tuff are all resulting from Oligocene ash-flows originating at Ute Creek, Lost Lake, Uncompahgre caldera, and San Juan and Uncompahgre caldera, respectively. These units range from nonwelded grayish to densely welded red-brown dacitic to rhyolitic tuffs (Yager and Bove, 2002).

Talus, glacial deposits, and rock glaciers (Qtg, Holocene and Pleistocene) are grouped as a geologic unit on the map (fig. 39) and correspond with the most predominant Quaternary deposit in the area of study. The Upper Camp Bird rock glacier is identified with a push-pin symbol in purple in figure 39. Colluvium and landslide deposits (Qcl, Holocene and Pleistocene) and Alluvium (Qal, Holocene) are only evident in the lower elevation areas near the camp site (yellow push-pin symbol).

4.2.7. Geomorphology

4.2.7.1. The San Juan Mountains, Colorado

The San Juan Mountain Range of southwestern Colorado is part of the north-south trending major mountain range known as the Rocky Mountains. In the State of

Colorado, the San Juan Mountains extend for ~32,000 km^2 (~12,355 mi^2) encompassing a variety of microclimates and vegetation types, and characterized by rugged terrain and prominent peaks, over a dozen of which rise to over 4,000 m (~13,123 ft) above sea level (Southwest, 2016).

Geomorphic features present in the San Juan Mountains include steep-walled mountain peaks with cirques, rocky hills, avalanche tracks, talus, landslides, rock fall, u-shaped and incised valleys, floodplains, lakes, as well as alluvial deposits, rock glaciers, and glacial deposits comprising diverse types of moraines (Blair, 1996b).

4.2.7.2. The Imogene Basin, San Juan Mountains, Colorado

The Imogene Basin has a drainage area of ~2.85 km^2 (~1.1 mi^2) with a mean basin slope of ~25° (47%) computed from a Digital Elevation Model (DEM) with 10 m resolution (USGS, 2016). The minimum basin elevation corresponds to 3,444 m (~11,300 ft), whereas the maximum basin elevation reaches 4,084 m (13,399 ft), with a mean elevation of 3,802 m (12,473.75 ft). A mean annual precipitation of 1,188.46 mm (46.8 in) is reported at Imogen Basin (USGS, 2016). Figure 40 corresponds with the slope map and figure 41 with the aspect map calculated for the headwaters of Imogene Basin.

The Upper Camp Bird rock glacier in Imogene Basin is, according to Brenning et. al (2007, p. 2) “typical of rock glaciers in the San Juan Mountains in plan, size, and location relative to tree line”. Extending from an elevation of 3,475 m (~11, 400 ft) above sea level at the toe, to 3,901 m (~12,798 ft) at the head, the Upper Camp Bird rock glacier is located at an elevation that favors the formation of discontinuous permafrost.

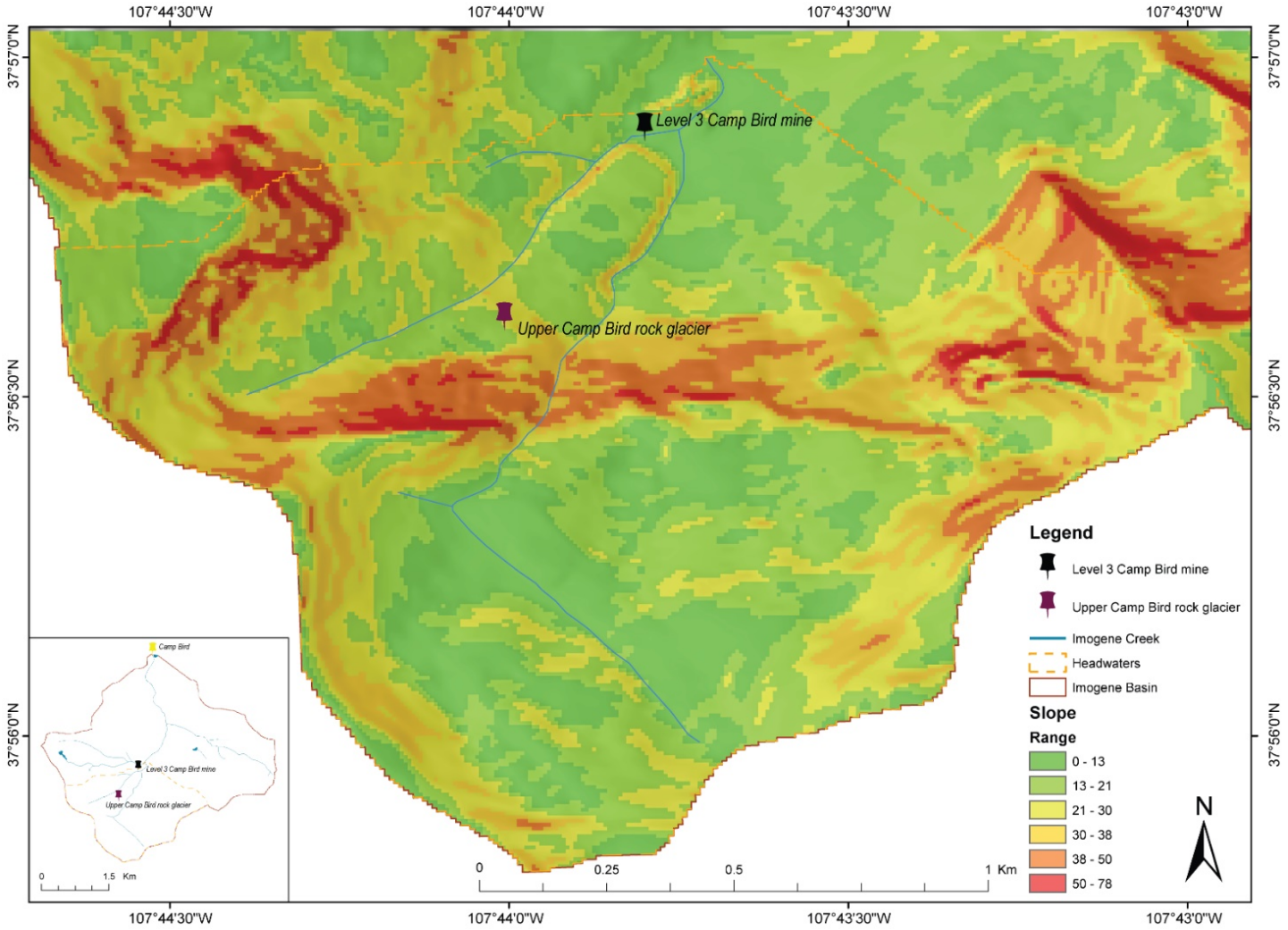

Figure 40 Slope map of the Imogene Basin, San Juan Mountains, Colorado. DEMs harvested from 1/3rd arc-second USGS National Map. Hydrography harvested from USGS, NHD 20200615. Coordinate System: GCS WGS 1984.

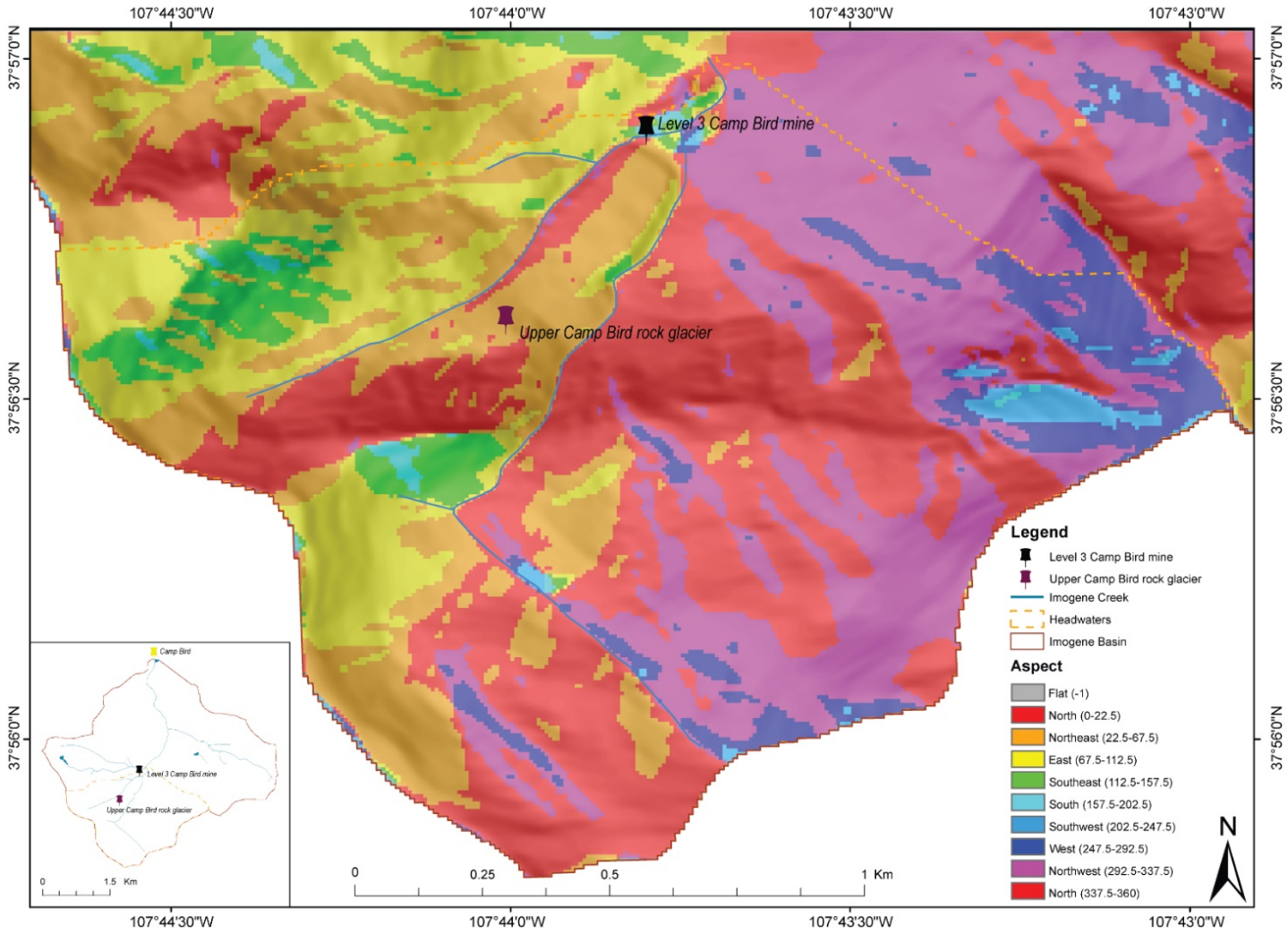

Figure 41 Aspect map of the Imogene Basin, San Juan Mountains, Colorado. DEMs harvested from 1/3rd arc-second USGS National Map. Hydrography harvested from USGS, NHD 20200615. Coordinate System: GCS WGS 1984.

The slope ranges between 38° and 78° at the headwall cliffs of the Upper Camp Bird rock glacier, whereas the rock glacier body exhibits slope ranges between 13°-21° with small segments of <13°. The toe and side slopes range between 21°-38° (fig. 40). The headwall slopes predominantly face north, and most of the rock glacier body faces northeast – north (fig. 41). The Upper Camp Bird rock glacier is a singular form, approximately 780 m long and 215 m wide (~2,559 ft by ~705 ft), that extends over an area of 167,700 m^2 (0.1677 km^2 or 0.06475 mi^2).

The toe slope of the Upper Camp Bird rock glacier is at the angle of repose, and is free of vegetation and lichen, exhibiting a noticeable lighter tone than the main body (fig. 42b). From an oblique view, the surface of the rock glacier is at a sharp angle with the front slope, as indicated with white lines in figure 42c. The micro-relief (microform or surface relief) observed at the Upper Camp Bird rock glacier suggests recent movement. The above characteristics indicate the active status of the Upper Camp Bird rock glacier (Giardino and Vick, 1987; Imhof, 1996).

The rock glacier of interest can also be identified as a class 4 or "proper" rock glacier, characterized by well-defined transverse and longitudinal ridges and furrows, as well as by a clearly differentiated toe slope (Janke et al., 2015). Characteristics of class 4 rock glaciers include being fully covered by a thick layer of debris, containing 25%-45% internal ice in the form of a massive core (i.e., solid ice), permafrost (i.e., interstitial ice; a mixture of ice and coarse to fine sediment), and ice lenses (i.e., segregated ice) (Janke et al., 2015, Janke et al., 2013). Table 7 lists the characteristics of the Upper Camp Bird rock glacier according to the classification by Corte (1987).

Table 7 Corte's (1987) rock glacier classification criteria for the Upper Camp Bird rock glacier. The criteria are listed in order of importance. Modified from Degenhardt (2002).

Form-based classification criteria	
Source of Material	Talus
Location	Talus Rock Glacier Valley head, including cirques
Connection to Source Area	Direct
Surface Relief (micro-relief)	Very well developed
Form	Singular
Shape	Tongue (Length > Width) Mature landform
Size	Medium (10^4 - 10^5 m^2)

Rock glaciers are described by Giardino (1979) and Giardino et al. (1992) as a cascading system of water, ice, and debris, with interrelated subsystems that provide inputs and outputs to each other if the rock glacier flows slowly enough for the subsystems to remain interconnected. The headwall cliffs merge gently with the talus cones or slopes, at the base of which a transition zone (i.e., rooting zone) where permafrost accretion occurs, separates the source of debris (i.e., erosion zone) from the depositional zone (i.e., main body of the rock glacier) (Vitek and Giardino, 1987; Haeberli, 1985; Frauenfelder et al., 2008; Brardinoni et al., 2019).

Figure 42a outlines the location of the erosional zone or headward talus zone (i.e., headwall cliffs, talus slopes and rooting zone) and the depositional zone (i.e., main body, scarps) on a satellite image of the Upper Camp Bird rock glacier. The distinct transversal

and longitudinal ridges and furrows (micro-relief) are delineated over still-frames obtained from drone footage in figure 42b, whereas the variation in slope of the main body, the side scarps, and the toe are outlined in figure 42c.

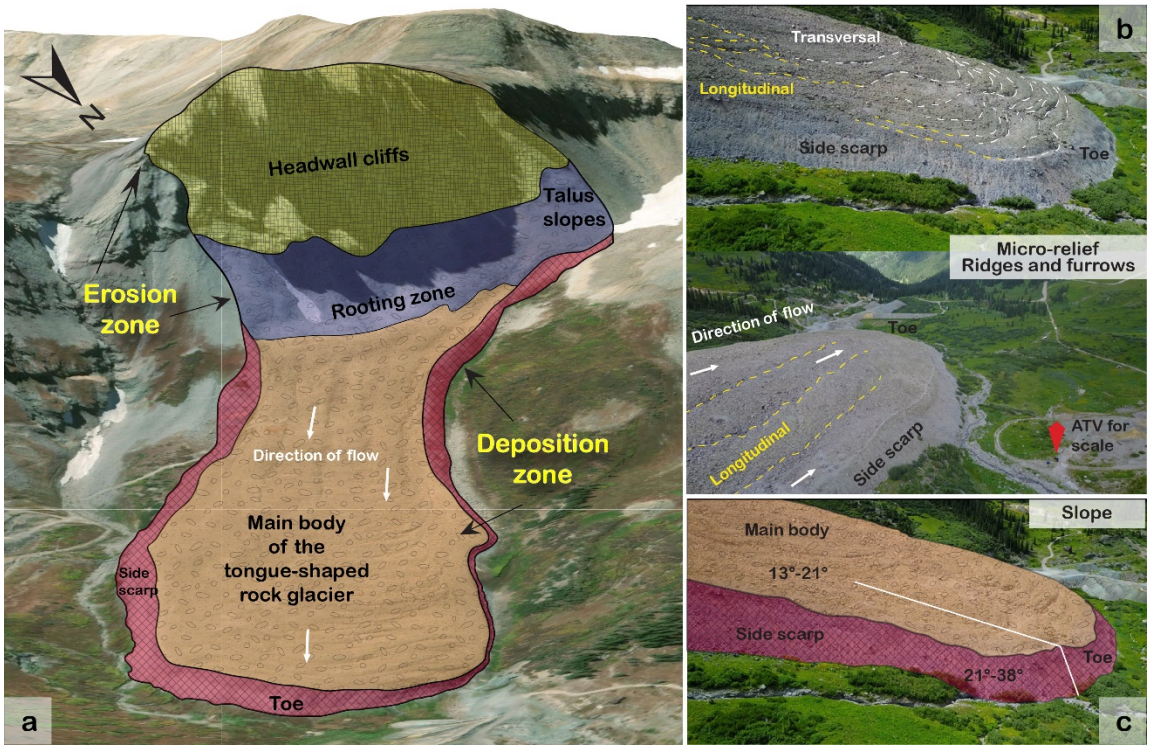

Figure 42 a) Satellite image of the Upper Camp Bird rock glacier from ArcGisPro shows delineation of the geomorphic zones in color-filled polygons; white arrows indicate the direction of flow b) still-frame extracted from drone footage showing the micro-relief (transversal and longitudinal ridges and furrows) c) still-frame extracted from drone footage indicating the variation in slope of the main body, the side and the toe scarps.

The development of ridges and furrows transverse to the flow of the rock glacier (fig. 42b) is attributed to compressive forces that increase as the slope declines (Giardino,

1979; Haeberli, 1985; Degenhardt, 2002). The layered materials found within the rock glacier can exhibit differential movement, and variations in debris content or supply can also influence transverse ridge and furrow development (Janke et al., 2013; Janke et al., 2015). The longitudinal ridges highlighted near the side scarp of the rock glacier in figure 42b (top), likely result from extensional flow or resistance to flow (Janke et al., 2015). Drainage or the melting of internal ice can cause the meandering longitudinal furrows shown in 42b (bottom) (Janke et al., 2015).

At the Upper Camp Bird rock glacier, sizes of rock range from ~10 cm long to 2 m (fig. 43a) . Less frequently encountered boulders are ~ 7 m to 10 m long. Rock fragments exhibit grayish (i.e., 5Y 3/2 olive gray, 5Y 7/2 yellowish gray), reddish (i.e., 5R 4/6 moderate red, 10R 2/2 very dusky red), brownish (i.e., 5YR 5/6 light brown, 10R 4/6 moderate reddish brown), and greenish (i.e., 5G 7/2 pale green, 5G 7/4 light green, 10Y 6/6 pale olive, 10Y 8/2 pale greenish yellow) colorations, corresponding to Tsj, Tip, Tur and Tb. Quartz vein fragments are occasionally found. In some areas, an arrangement or alignment of the clasts is evident. I refer to these as debris supply chains (fig. 43b). Some supply chains seem to maintain a similar rock size, whereas others consist of a range of sizes. The characteristic platy shapes of the weathered rock fragments as described by Giardino and Vitek (1985) are evident in figure 43b.

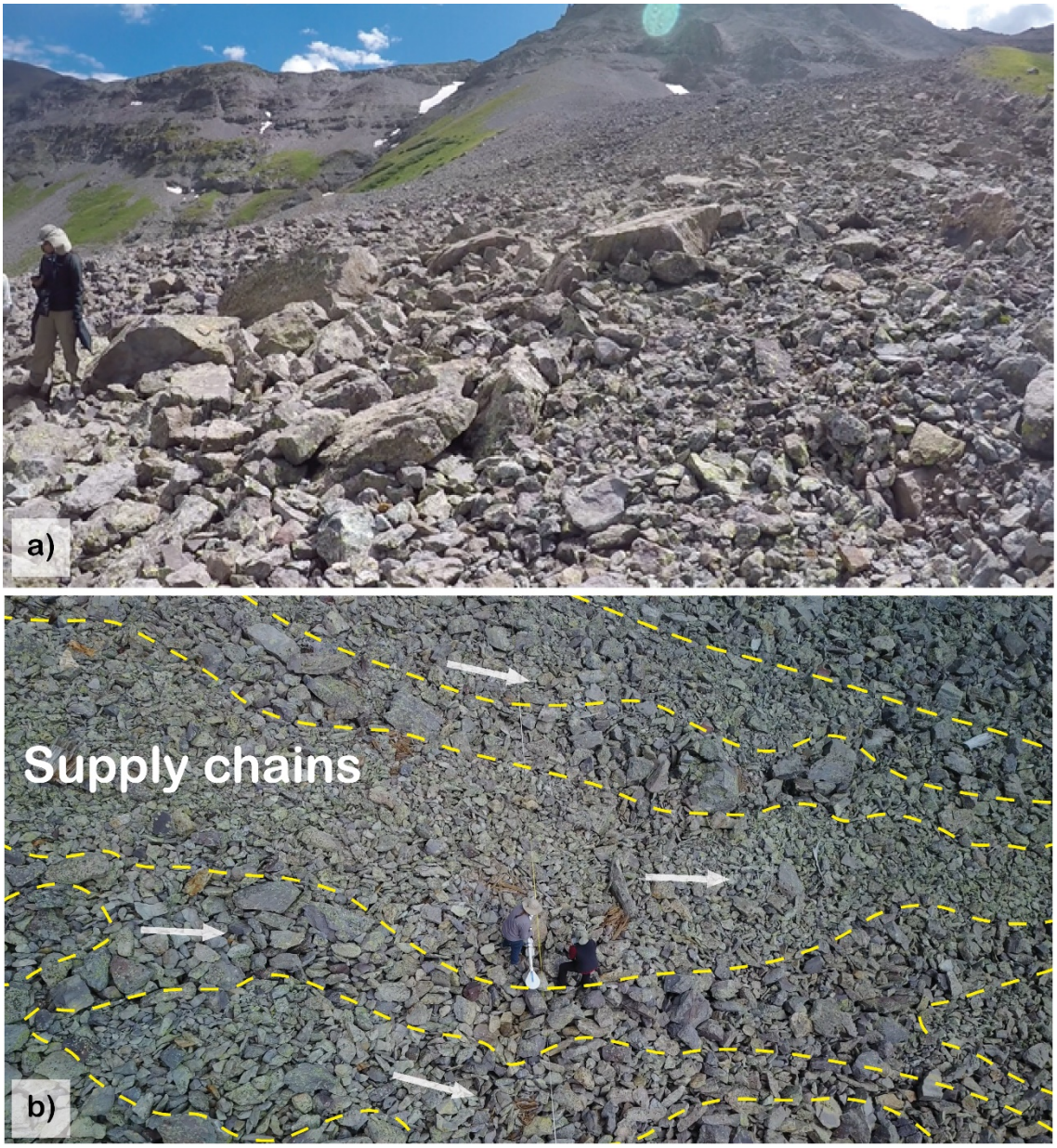

Figure 43 a) Sizes of rock fragments b) Some of the debris supply chains are delineated in this still-frame obtained from drone footage.

4.3. Methods

At the beginning of the 20th century, direct methods (i.e. invasive or destructive methods such as drilling, trenching and excavating) were the main technique used to

access rock glaciers. Brown (1925) studied a “fossil glacier” from a tunnel carved through the landform. As technology advanced and became more available, researchers started incorporating indirect geophysical methods in geomorphological studies, usually ground-truthing geophysical interpretations with borehole information (Maurer and Hauk, 2007; Monnier and Kinnard, 2013; Riffle, 2018).

Invasive methods are costly, time-consuming, and sometimes not feasible (i.e., restricted/protected areas, urban settings) even for ground-truthing purposes. Geophysical investigations allow for continuous subsurface characterization of extensive areas, in contrast with the localized point-scale information obtained from costly boreholes, all of which have led researchers to increasingly rely on geophysics (Hauck and Kneisel, 2008). The applicability of geophysical methods in studies in the periglacial environment has been validated by many scholars, and ground-truthing is far less common in 21st century investigations (Maurer and Hauk, 2007; Hauck and Kneisel, 2008; Monnier and Kinnard, 2013; Riffle, 2018).

The subsurface characterization of the Upper Camp Bird rock glacier presented in this study was carried out using non-invasive geophysical methods, as follows:

1. Performed near-surface geophysical explorations to map the distribution of the electrical resistivity in the subsurface and interpret the corresponding materials.
2. Collected geophysical data with two instruments with different resolution.
3. Local meteorological, geological, geomorphological, and geophysical data were combined to analyze the rock glacier system.

The surface characteristics of the Upper Camp Bird rock glacier were determined by analyzing satellite imagery as well as high-resolution drone imagery. The DJI Mavic Pro UAV (unmanned aerial vehicle) was employed recording at DCI 4K (4096 x 2160) and 24 frames per second, a bit rate of 60 Mbps and 8-bit color depth. Neutral density filters with polarization (ND8/PL, ND16/PL, and ND32/PL) were used at the site. Still-frames were extracted from the footage and are used throughout this section to highlight features that are not evident at the resolution of the satellite imagery.

4.3.1. Near-surface geophysics

Many studies have been conducted using several geophysical methods, such as seismic refraction (Wagner, 1996), gravimetry (Vonder Müehll and Klingelé, 1994), resistivity (King et al., 1987; Wagner, 1996), radio-echo surveys (King et al., 1987), GPR (Degenhardt and Giardino, 2009; Jorgensen, 2007) and EM profilers to study the internal structure of rock glaciers. Recently, authors such as Guglielmin et al. (2018) used a combination of geophysical surveys and borehole investigations to determine the internal structure and origin of several rock glaciers in Antarctica, and Killingbeck et al. (2020) used transient electromagnetics (TDEM) to characterize subglacial water on the terminus of an ice glacier.

Croce and Milana (2002) studied the internal structure of a rock glacier with the implicit purpose to assess and monitor the availability of water resources in the landform. The authors used a combination of geophysical methods to accomplish their objectives. They used seismic refraction to investigate the upper layer and vertical electrical resistivity surveys to study the thickness of permafrost.

Winkler et al. (2016) used seismic refraction and natural tracers to study the hydrogeological system and the internal structure of a relict rock glacier, concluding the landform is a layered heterogeneous aquifer that resembles the complexity of a karst aquifer. The authors observed a rapid response to recharge (about two hours) as well as a large storage component which lead to large base flow rates long after the recharge event.

Colombo et al. (2018) used waterborne geophysical methods combined with heat tracing, to study the connectivity between an active rock glacier and a marginal pond system. The investigation concluded the rock glacier advance had created the pond, and intense precipitation events yielded a larger contribution of cold and mineralized groundwater from the rock glacier.

Everett (2013) discussed the applicability of electromagnetic induction methods in groundwater resource evaluation and characterization of aquifer heterogeneity. This study employed controlled-source electromagnetic induction methods. Namely, the novel G-TEM system, which is time-domain electromagnetic induction instrumentation, and the EMP-400 Profiler, which corresponds to a frequency-domain electromagnetic induction system.

4.3.1.1. Electromagnetic Induction

The presence and distribution of different materials in the subsurface can be determined based on physical parameters such as electrical resistivity or inversely, electrical conductivity. Electromagnetic (EM) methods are commonly used to measure the electrical resistivity of the subsurface. Time-varying currents from a transmitter

induce electric currents in the ground, and their associated secondary magnetic field is picked up by a receiver. Depending on the operating principle of the system (i.e., variation of the transmitter current), EM methods can be divided into time-domain (TDEM or TEM) or frequency-domain (FDEM or EMI) electromagnetics (Hauck and Kneisel, 2008; Kruse, 2013; Riffle, 2018).

4.3.1.1.1. Time-Domain Electromagnetic Induction

To conduct a Time-Domain Electromagnetic Induction survey in a central loop configuration, a transmitter coil is placed on the surface, commonly as a square loop and a receiver coil is placed in the center of the loop (fig. 44). A constant current is run through the square loop, generating a primary magnetic field. If the source of the magnetic field is discontinued (i.e., the current is shut off), secondary currents appear initially shallow as an image of the source, and quickly start to decay. As time progresses, these induced currents diffuse away from the transmitter, reaching greater depths and propagating outwards. The decaying current induces voltage pulses that are measured by the receiver coil at progressively later times. The subsurface resistivity structure can be interpreted from the rate of decay of the magnetic field (Hersir and Flóvenz, 2013; Everett, 2013; Kruse, 2013; Riffle, 2018; Pondthai et al., 2020).

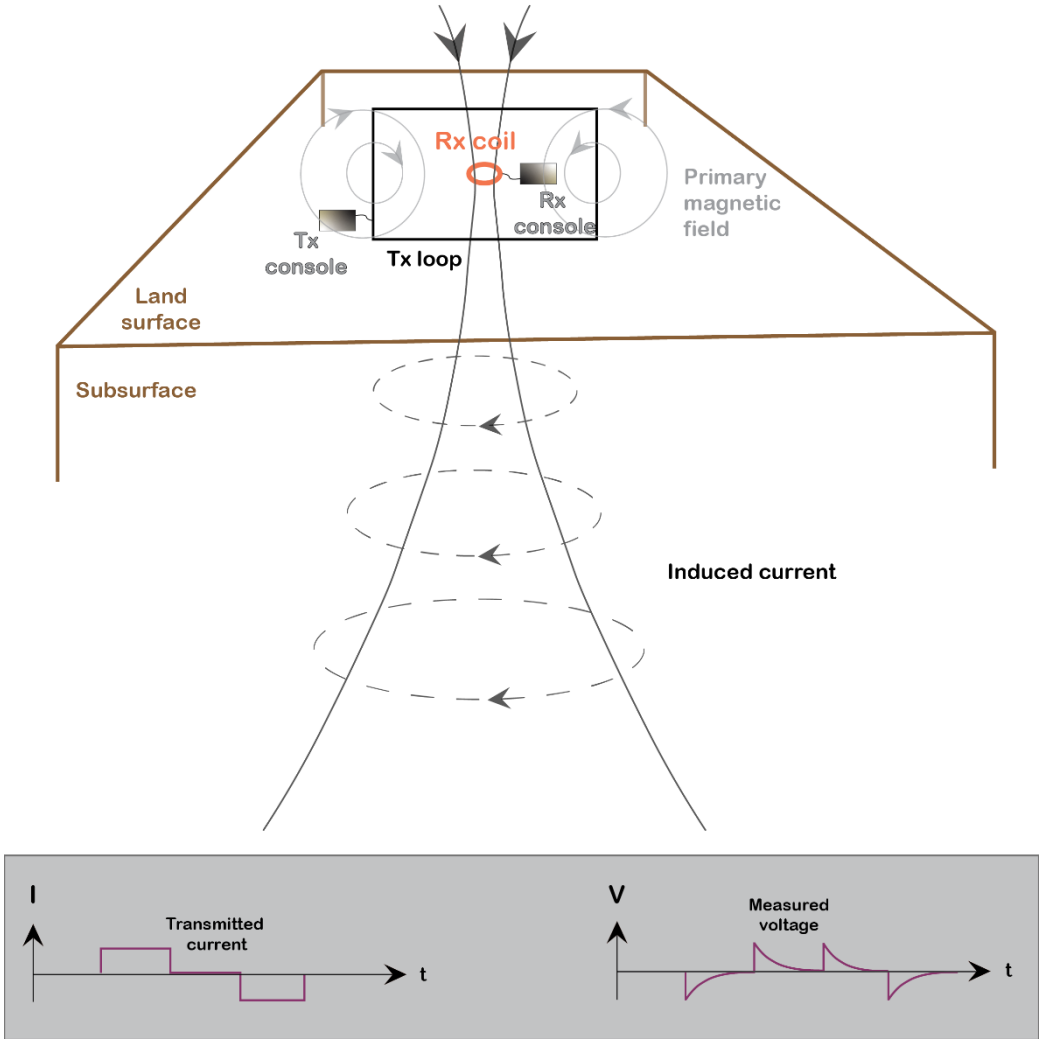

Figure 44 Diagram of a TDEM sounding setup in a central loop configuration. Tx=transmitter, Rx=receiver. A schematic representation of the transmitted current, as well as of the measured transient voltage, is included in the gray box. Diagram modified from USGS (public domain) and Hersir and Flóvenz, 2013.

In my study, the TDEM system employed was the G-TEM™ developed by Geonics Limited. The G-TEM™ poses a number of advantages over other geophysical methods, including deep subsurface penetration, a realistic data collection model as it uses a layered-earth model, detailed and stable data collection, and capabilities to

perform 1D inversion of the data on site. The suitability of the G-TEM™ for aquifer characterization is demonstrated by Pondthai et al., 2020.

4.3.1.1.2. Frequency-Domain Electromagnetic Induction

In the Frequency-Domain Electromagnetic method, a sinusoidal current (alternating current or AC) is generated in the transmitter coil at a set frequency. Thus, a time-varying magnetic field is induced, which excites currents in the subsurface and/or conductive objects in the subsurface. A secondary magnetic field associated with the subsurface currents is picked up by the receiver (passive coil). The frequency of operation is defined by the user depending on the desired depth of investigation. The higher the frequency, the shallower the investigation (Hauck and Kneisel, 2008; Kruse, 2013; GSSI). Figure 45 is a schematic representation of the operating principles of the Profiler EMP-400™.

EMI surveys (FDEM) are used mostly for reconnaissance because they can only resolve shallow depths but are easy to carry out. Instrumentation is user friendly and portable, allowing the user to cover relatively large areas in reasonable time investigation (Hauck and Kneisel, 2008; Kruse, 2013).

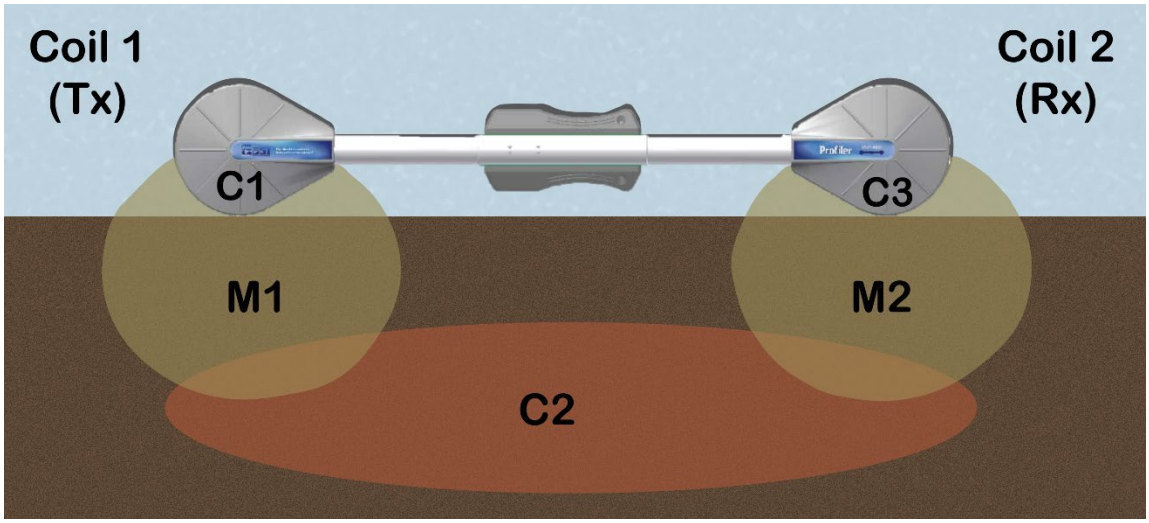

Figure 45 The transmitter (Tx) -or Coil 1- creates a current (C1), which induces a magnetic field (M1) that induces C2 in the subsurface and/or objects in the subsurface. C2 induces M2, which induces C3 in the Rx (Coil 2, receiver). Modified from GSSI.

The Profiler EMP-400™ was used with the intention to validate the G-TEM™ data, as it was employed along the same profiles.

4.3.2. Field data collection

The electromagnetic induction soundings carried out at the Upper Camp Bird rock glacier were conducted at a safe distance from the unstable sides and frontal scarps. The characteristic rugged terrain and abrupt slope changes encountered on the surface of the Upper Camp Bird rock glacier are almost imperceptible at the scale of the satellite image shown in figure 46. This figure shows the location of the Level 3 of Camp Bird mine, the headwaters of the Imogene Creek basin as well as the creek are also highlighted, along with the distribution of the geophysical soundings that was recorded using a handheld GPS.

The data collection design for the G-TEM™ consisted of a grid of 7 lines with 5 stations per line. The spacing between stations is 25 m whereas the lines are 50 m apart, except for lines 7 and 6, which are only 40 m apart. Figure 47 corresponds with a diagram of the Upper Camp Bird rock glacier showing the data collection design, as well as the approximate location of relevant surrounding features. Markers are exaggerated to show the distribution of the data collection stations (i.e., orange circles represent G-TEM™ stations, yellow lines EMI profiles) in this diagram. Note that EMI profile line 1 is missing in the diagram (fig. 47) but not in figure 46 where the planned data collection is shown. An instrument failure prevented data collected along line 1 from being saved.

Line 1 is closest to the toe scarp whereas station 1 is opposite the entrance to level 3 Camp Bird Mine. The locations of the surveying lines and stations were strategic in terms of slope changes and stability of the landform, as well as in terms of the likelihood of ice presence and detection. The area near the toe exhibits well developed ridges and furrows which, as discussed in a previous section, has been linked to processes that result in decreasing ice. Therefore, measurements were conducted in areas that were both safer and more relevant to the purpose of this study.

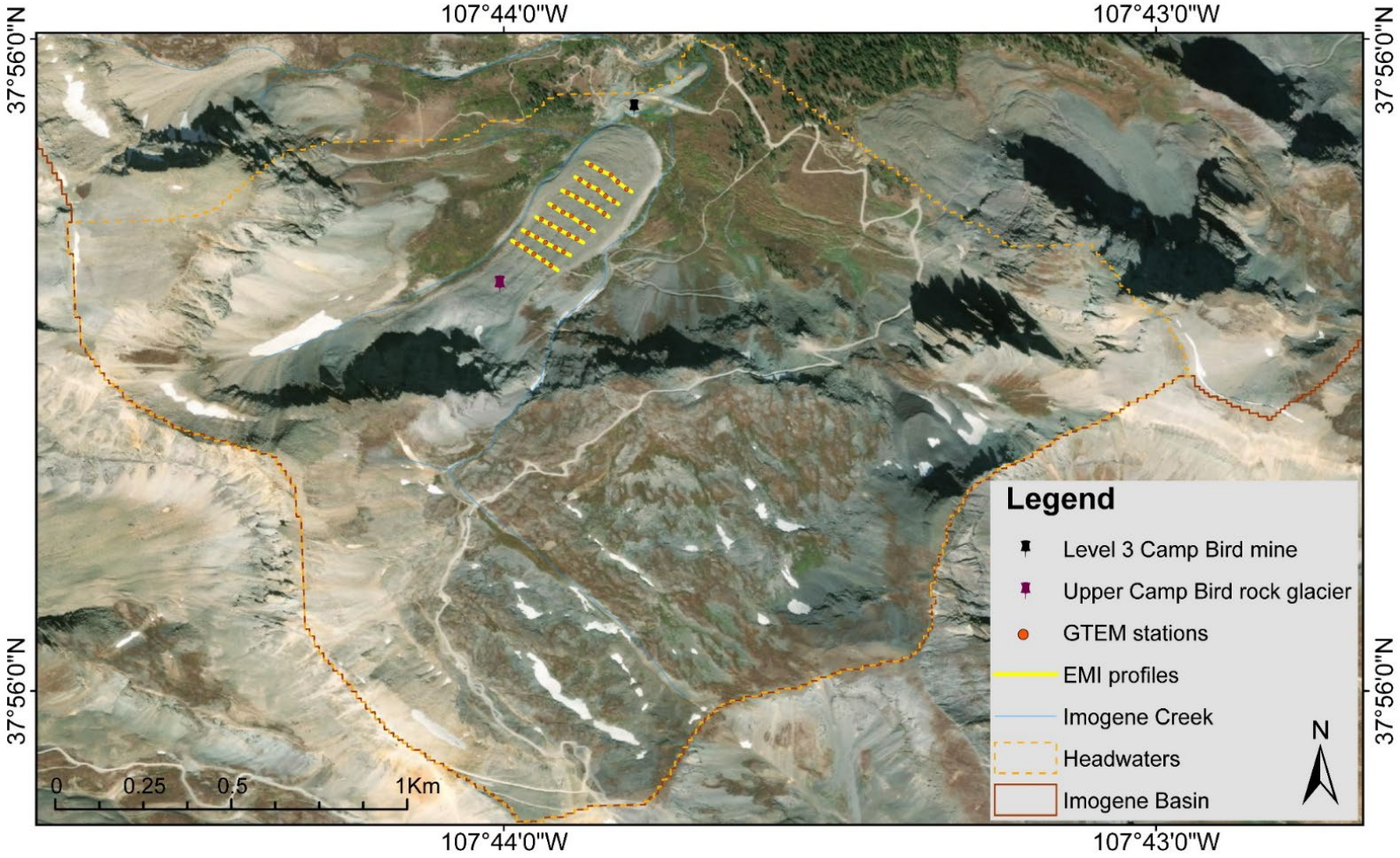

Figure 46 Data collection map. Headwaters of the Imogene Basin, Ouray, Colorado. Hydrography harvested from USGS, NHD 20200615. Coordinate System: GCS WGS 1984. Service Layer Credits: Source: Esri, Maxar, GeoEye, Earthstar Geographics, CNES/Airbus DS, USDA, USGS, AeroGRID, IGN, and the GIS User Community Esri, HERE, Garmin, (c) OpenStreetMap contributors, and the GIS user community.

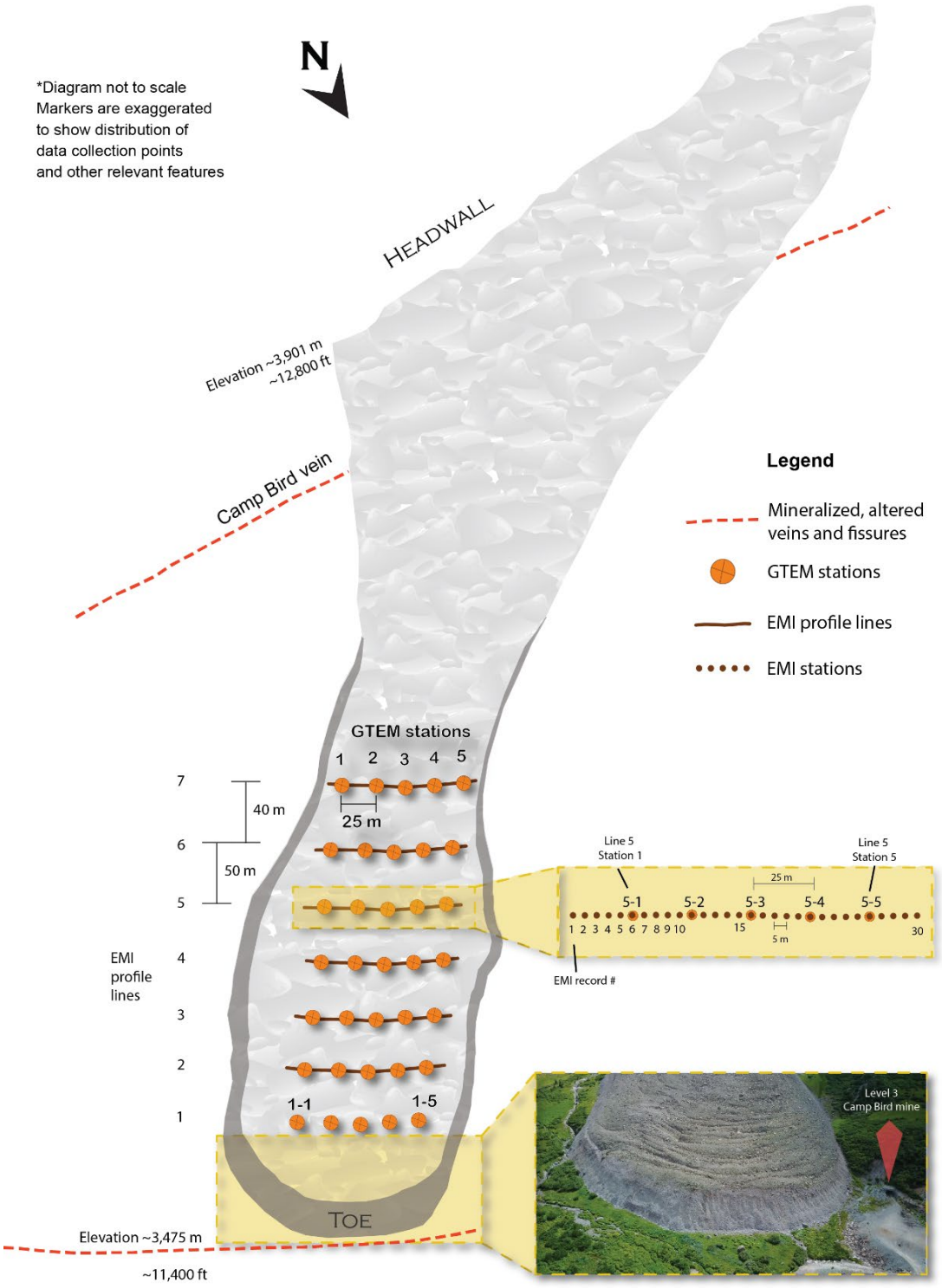

Figure 47 Diagram of the Upper Camp Bird rock glacier showing the data collection design, as well as the approximate location of relevant surrounding features. This diagram is not drawn to scale. Markers are exaggerated to show the distribution of the stations used for data collection.

4.3.2.1. TDEM

The G-TEM™ system consists of a transmitter coil (Tx; loop of wire), a Tx console, a high-frequency receiver coil (Rx), and a Rx console. Measurements were conducted using a central loop configuration (i.e., Rx in the center of the loop) within a 10 m x 10 m square loop (4 turns) at the Upper Camp Bird rock glacier (fig. 48). The rugged surface of the rock glacier presented a challenge in terms of data collection. The equipment was carried from station to station by a team of 5 people. The G-TEM™ measurements were conducted at a total of 35 stations (5 stations per line) over 3 consecutive days.

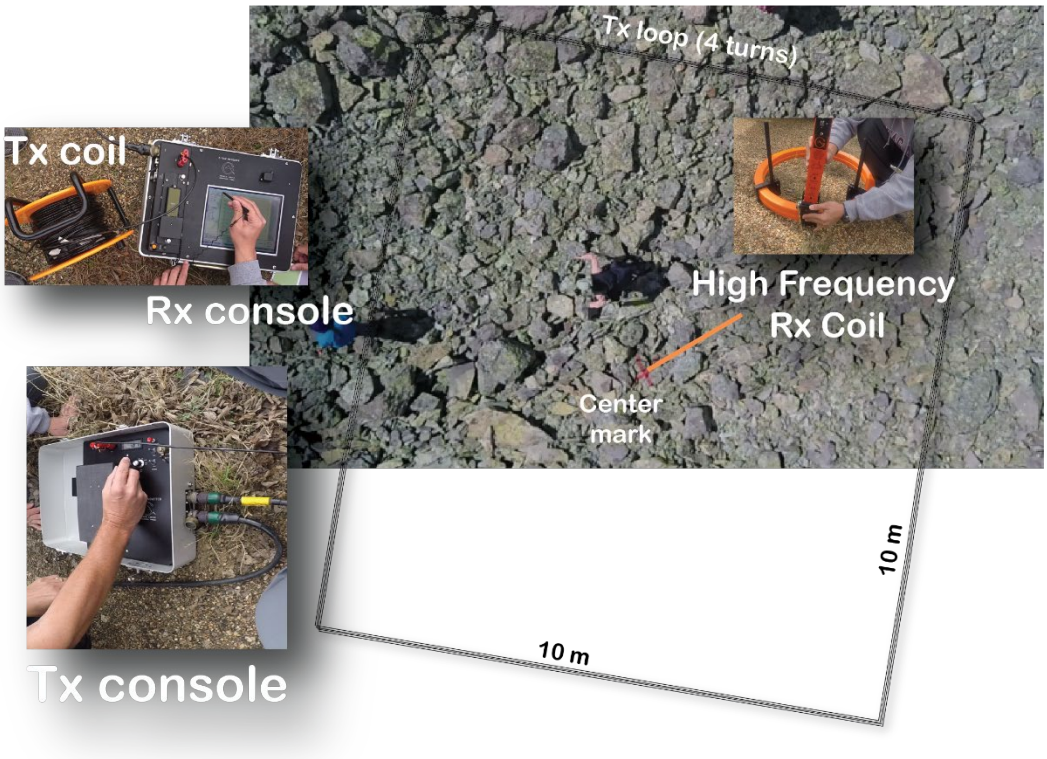

Figure 48 G-TEM system components and deployment at the Upper Camp Bird rock glacier. Drone image.

The field parameters used to operate the G-TEM™ at the Upper Camp Bird rock glacier are presented in Table 8.

Table 8 Field parameters of TDEM measurements.

G-TEM field parameters	
TX Current [I]	2A
TX Moment [A]	400 m²
Ground Conductivity [σ]	10 S/m
Repetition Rate [f]	285 Hz
Averaging Time [t]	15 s
Stacking Number [s#]	4

An effective penetration depth of 96 m was achieved for the soundings, as shown by equation 1. The G-TEM features standard and smart integration (stacking) for low-noise data acquisition. Equation 2 details the resulting stacking per sounding.

(Eq. 1) Effective Penetration Depth

$$d \approx 40 \times (I \times A / \sigma)^{1/5}$$

$$d \approx 40 \times (2 \times 400 / 10)^{1/5}$$

$$d \approx 96$$

(Eq. 2) Stacks / Sounding

$$S/_S = f \times t \times s\#$$

$$S/_S = 285 \times 15 \times 4$$

$$S/_S = 17100$$

4.3.2.2. FDEM

The Profiler EMP-400™ is a portable, digital multi-frequency FDEM system with a Horizontal Co-Planar (HCP) coil configuration (GSSI, 2017). The EMI measurements were carried out using the Profiler EMP-400™ on the discrete mode along the profile lines shown in figure 46 and 47, recording measurements at three different frequencies. The Profiler EMP-400™ can be carried and operated by a single user, but the surface of the Upper Camp Bird rock glacier required two operators (fig. 49). Each profiler line represents 30 discrete and equally spaced measurements (i.e., data points, record #).

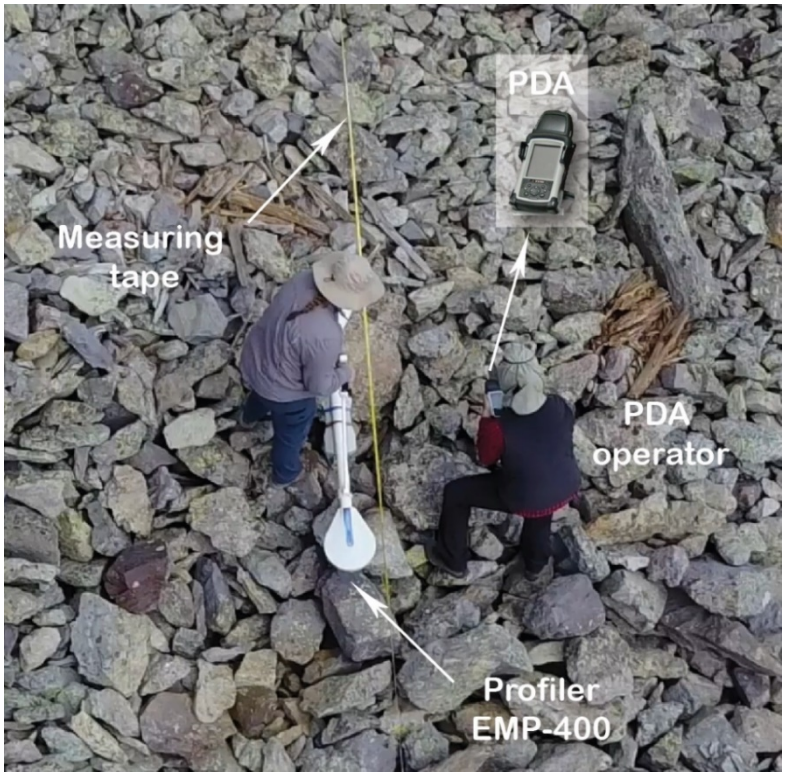

Figure 49 EMI measurements at the Upper Camp Bird rock glacier using the Profiler EMP-400. From drone image.

The field parameters of the EMI data collection are presented in Table 9.

Table 9 Field parameters of EMI measurements.

Profiler field parameters	
Collection mode	Stationary
Grid type*	xLTZ
Line spacing	50 m
Station spacing	5 m
Mark spacing	25 m
Instrument orientation	Vertical Dipole Moment (I)

Table 9 continued

Profiler field parameters	
Frequency 1	1,000 Hz
Frequency 2	8,000 Hz
Frequency 3	15,000 Hz
Number of stacks	16

* xLTZ: X-axis profiling starting in the left top (LT) corner of the survey grid with lines collected in a zigzag (Z) fashion.

The Profiler was operated using the low carry handle, as recommended by the manufacturer to collect apparent conductivity data. A 15,000 Hz frequency was selected because the algorithm that converts the Quadrature values to apparent conductivity is optimized for this frequency for the Profiler coil spacing (GSSI, 2017).

4.3.3. Data Analysis and Processing

4.3.3.1. TDEM

The G-TEM™ measurements of apparent resistivity over time were analyzed using the IXG-TEM™ software by Interpex Limited. This software allowed the generation of 1D inversion models that show the variation of the electrical resistivity of the subsurface in depth. The user can create manual or smooth models with the IXG-TEM™. The smooth models are estimated using Occam's Inversion (fig. 50).

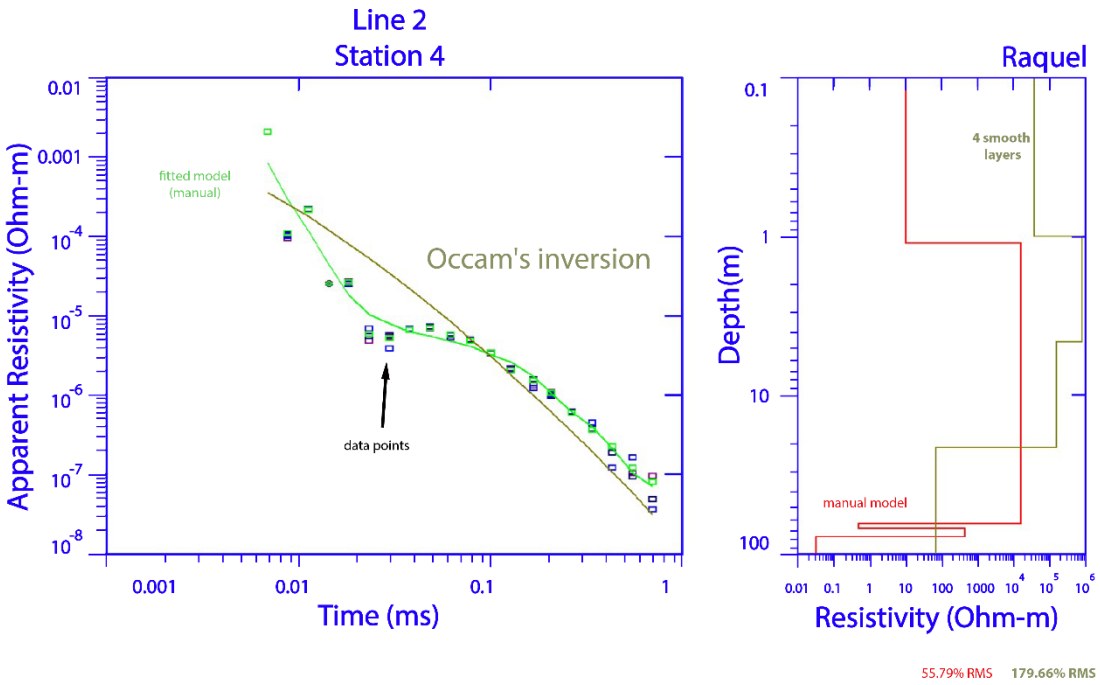

Figure 50 Example of G-TEM data collected at station 4, line 2 and 1D inversion models.

In this study, the manual models were determined by adjusting the thickness and the number of layers that best fit the data. Once the 1D models were determined for all the stations, the data were interpretated using geological information as well as comparing the resistivity values with known values for geologic materials (fig. 51). The 1D models for all 35 G-TEM™ stations are included in Appendix A.

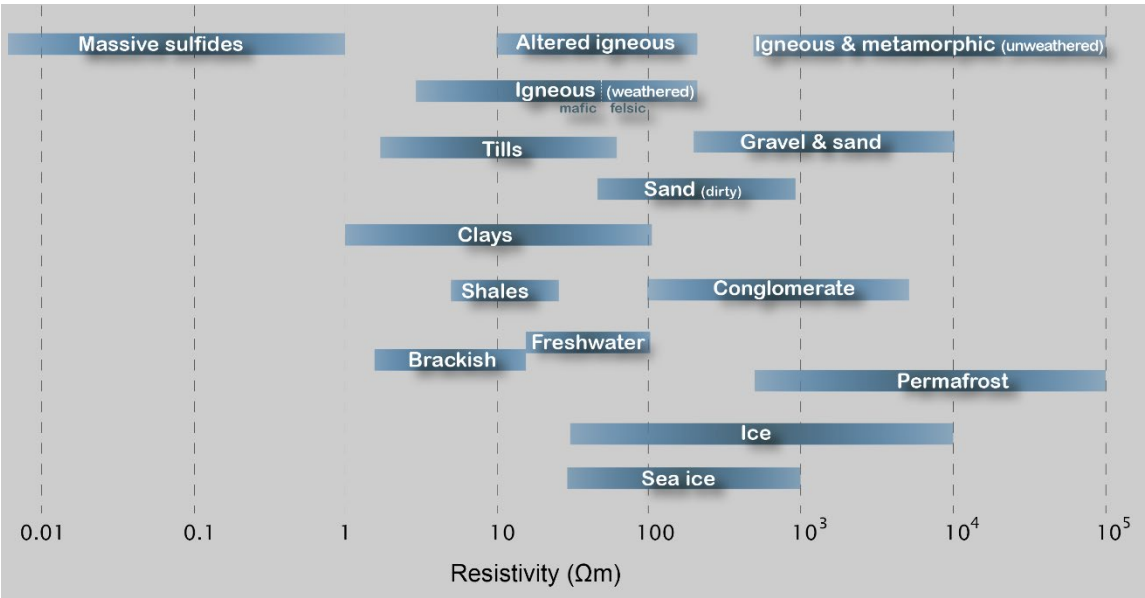

Figure 51 Ranges of resistivity values expected in near-surface geophysical investigations. Modified from Palacky (1987) and Fitterman (2015).

The importance of understanding the geological setting of the area of study is heightened by the similar electrical resistivity values that can be associated to different materials. As shown in figure 51, there is some overlap between the expected resistivity of most subsurface materials. Interpretations are, thus, driven by local geological information.

4.3.3.2. FDEM

The EMI data for each profiler line were plotted using Microsoft Excel. Figure 52 shows the apparent conductivity of each of the 30 records conforming line 3. Note that the apparent conductivity values are negative, which could indicate that the signal is becoming lost in the subsurface in response to environmental conditions.

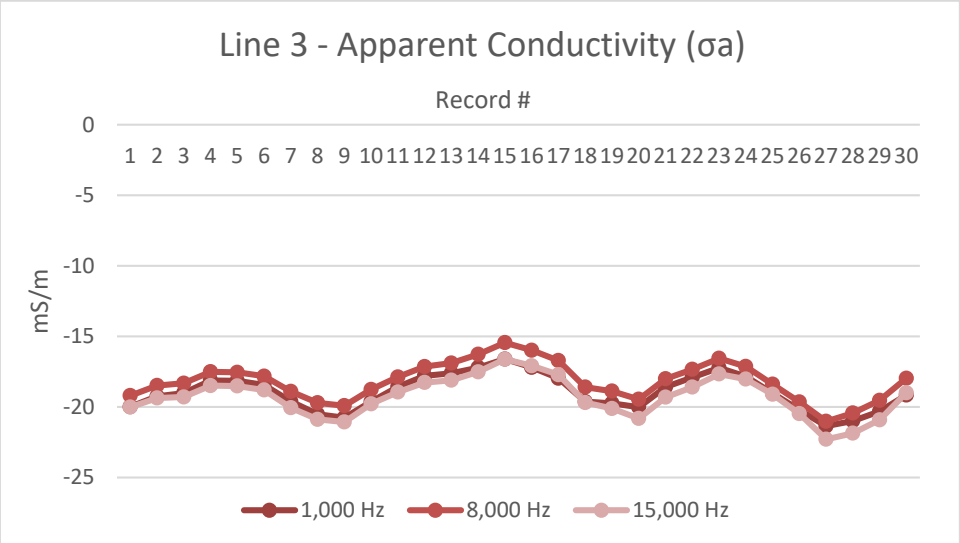

Figure 52 Apparent conductivity measured using FDEM along profiler line 3.

Examination of plots of individual profiler lines makes it difficult to identify and trace the presence of potential anomalies that could be causing the loss of the EMI signals. DPlot software by Hydesoft Computing, LLC was used to create a 2D surface-interpolating data from all the surveyed lines. Measurements were conducted along line 1; however, the instrument failed to save the data for this line. Thus, the apparent conductivity values presented in figure 53 correspond to lines 2 -7.

The patterns of distribution of the apparent conductivity values observed in figure 53 suggest the presence of objects or disturbances in the near-surface that are interfering with the EMI signals. At the Upper Camp Bird rock glacier, one could potentially encounter discarded mining equipment (i.e., mine carts), lamp posts, or tunnel tracks, that are not visible on the surface where the measurements are conducted.

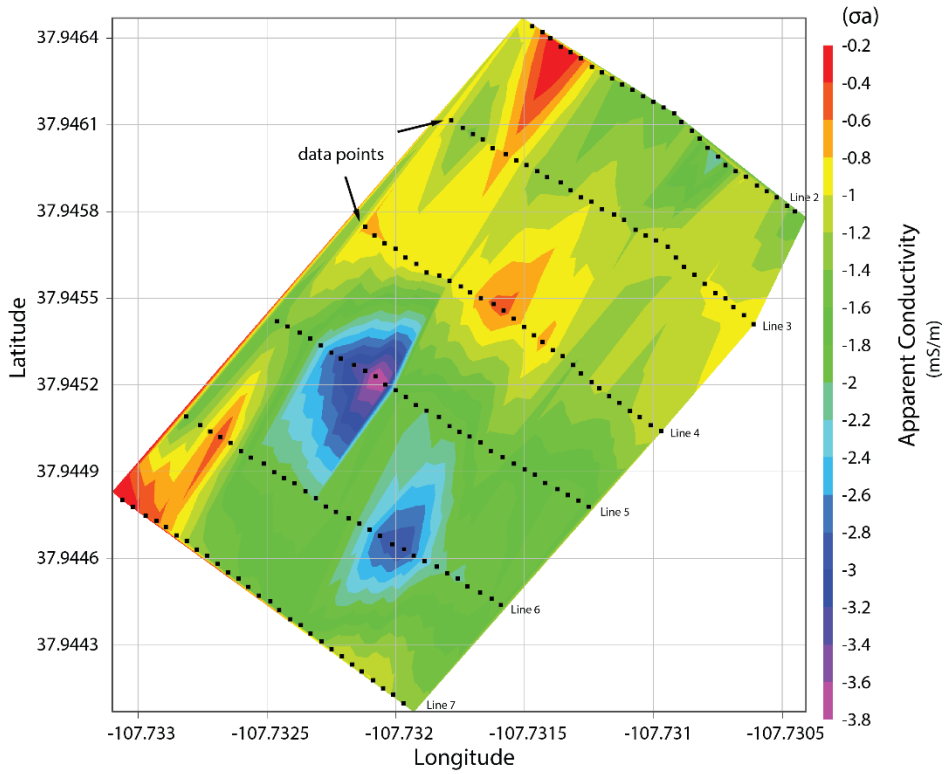

Figure 53 Distribution of the apparent conductivity values measured using FDEM along profiler lines 2 -7.

Detailed information about Camp Bird mine is not publicly available, thus, determining the location of potential mine tunnels and tracks was challenging. Hedrick and Gonzales (2016) created a 3D model of the Camp Bird mine (fig. 39). The authors shared their information such as planes and maps that allowed for an approximate location of the mine tunnels. The results of the integration of the mine and EMI data are discussed in the next section.

The Profiler EMP-400™ data files are included in Appendix C, and all the graphs are included in Appendix D. The locations of the G-TEM™ stations along the profiler lines are presented in Appendix E.

4.4. Results and Discussion

4.4.1. TDEM

Variations in measured resistivity values result from the presence of different materials in the subsurface. In a highly heterogeneous medium, such as a rock glacier, variations over several orders of magnitude are expected in all directions. Figures 54 – 60 correspond with the 1D inversion models of 7 of the 35 stations (i.e., a station from each of the 7 lines is shown). The TDEM measurements are represented in logarithmic scale and the characteristic decaying curve over time is evident across the models. The number of layers varies from 4 to 6 layers over the depth represented by the 1D models. Note that some models seem to extend beyond 100 m depth; however, the effective penetration of the soundings was calculated to reach 96 m. The uppermost layer is not resolved by the G-TEM™. Thus, the 1D models presented in this study are considered more reliable from ~1 m to ~100 m depth. The description of the 7 selected stations that follows, includes the entire resistivity depth profile shown. A detailed interpretation of the 1D models generated at each station per line is provided at the end of this section.

In figure 54, the resistivity depth profile of station 3 in line 1 shows two layers of around 10 Ωm up to 1.5 m depth. A highly resistive layer, in the order of 10^4 Ωm, extends from ~ 1.5 m to 30 m deep. A drop in the resistivity of 5 orders of magnitude is

observed beneath the highly resistive layer, followed by a 15 m - 20 m thick 500 Ωm layer. The resistivity around 60 m - 100 m depth drops to its lowest value at <0.01 Ωm.

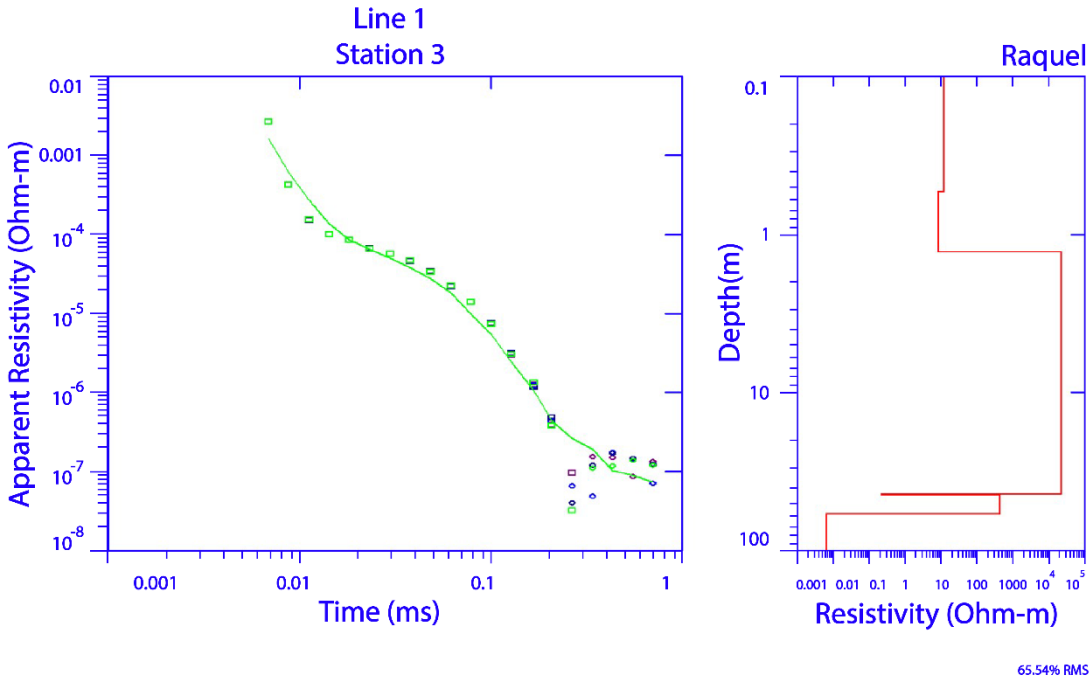

Figure 54 Apparent resistivity (Ωm) vs. time (ms) on the left and the resistivity (Ωm) vs. depth (m) on the right for station 3, line 1.

Examination of station 1 in line 2 (fig. 55), shows a 10 Ωm layer extending down to 1.5 m depth. The underlaying 45.5 m corresponds to a layer with a high resistivity (i.e., in the order of 10^5 Ωm), followed by a 0.02 Ωm layer <10 m thick. The resistivity is 50 Ωm in the layer located between 45 m and 65 m depth, dropping to around 0.05 Ωm for the next 35 m.

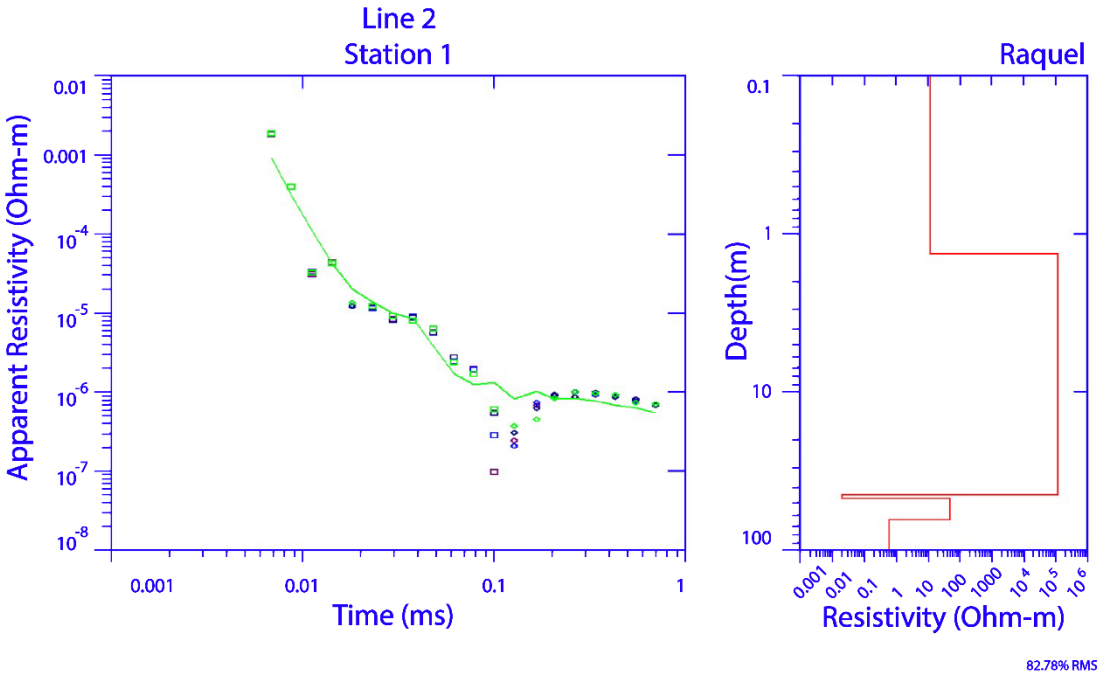

Figure 55 Apparent resistivity (Ωm) vs. time (ms) on the left and the resistivity (Ωm) vs. depth (m) on the right for station 1, line 2.

The resistivity-depth profile of station 3 in line 3 (fig. 56) consists of a 40 Ωm layer extending to 4 m of depth, followed by a 30 m thick layer with a resistivity value in the order of 10^4 Ωm. A thin, low resistivity (~0.5 Ωm) layer is observed at ~ 40 m depth. An approximately 10 m thick layer with a resistivity around 400 Ωm is below. The resistivity is reduced to nearly 0.001 Ωm for the remaining ~45 m.

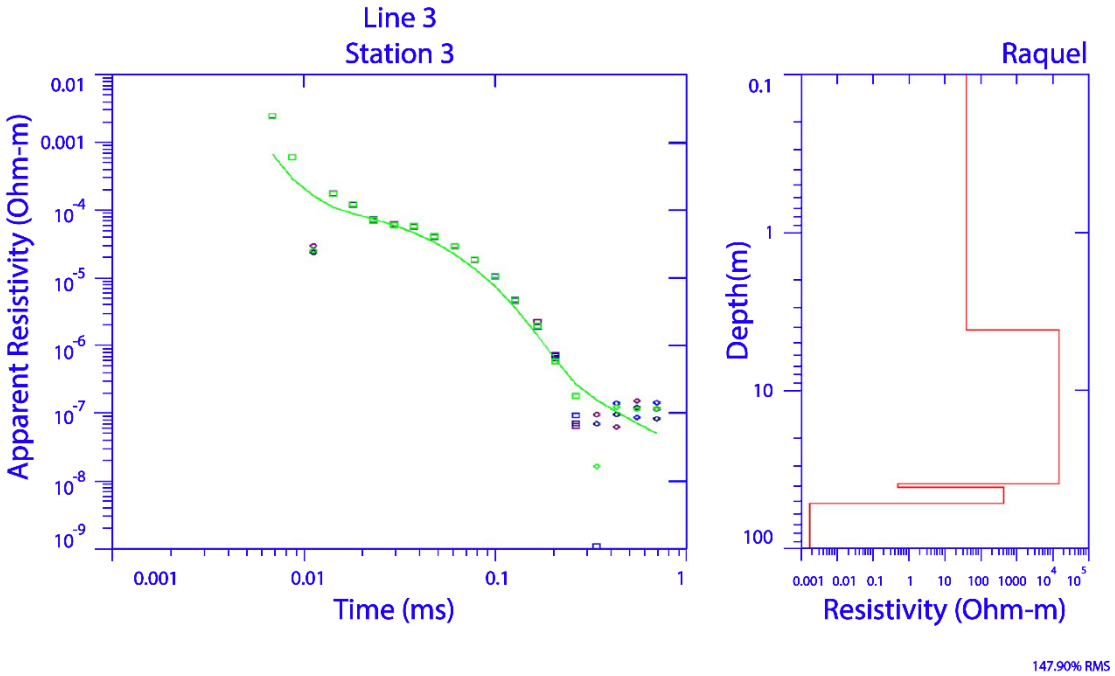

Figure 56 Apparent resistivity (Ωm) vs. time (ms) on the left and the resistivity (Ωm) vs. depth (m) on the right for station 3, line 3.

At station 5 in line 4 (fig. 57), the resistivity ranges between 10 Ωm and 40 Ωm in the first 1.5 m of depth. A highly resistive layer (in the order of 10^5 Ωm) extends to 80 m deep, followed by a ~45 Ωm layer of 20 m thickness.

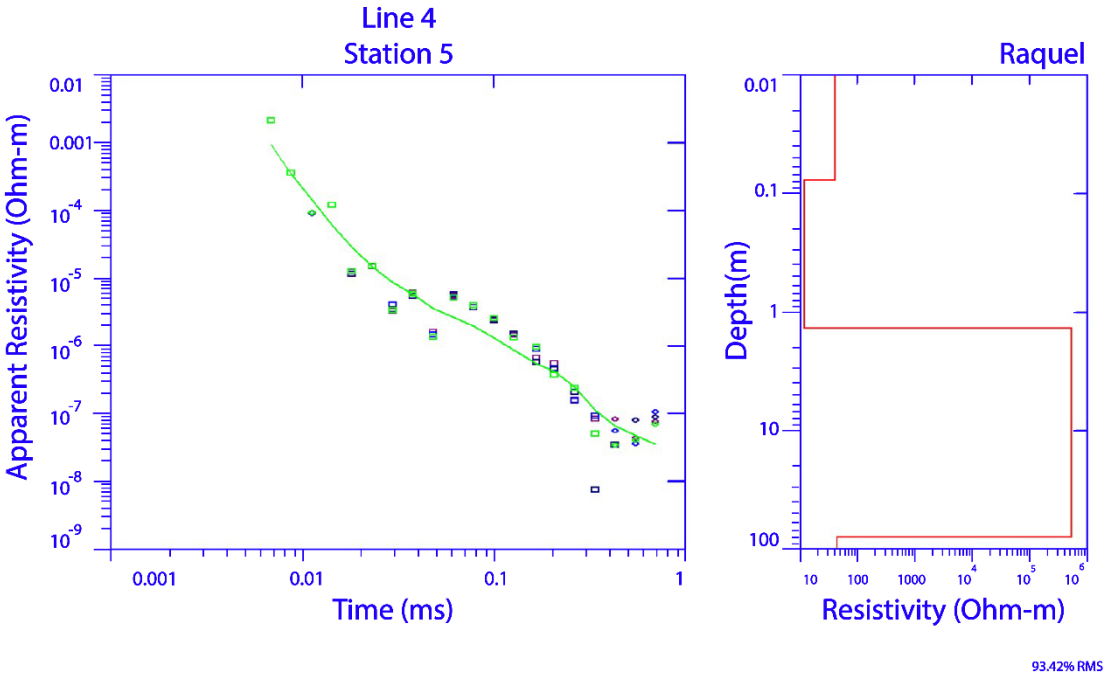

Figure 57 Apparent resistivity (Ωm) vs. time (ms) on the left and the resistivity (Ωm) vs. depth (m) on the right for station 5, line 4.

In figure 58, a 10 Ωm extends to 1.5 m depth, underlain by a layer of high resistivity (in the order of 10^5 Ωm) that extends to a depth of ~45 m. A 50 Ωm layer is evident in the remaining section of the 100 m resistivity-depth profile at station 5 in line 5.

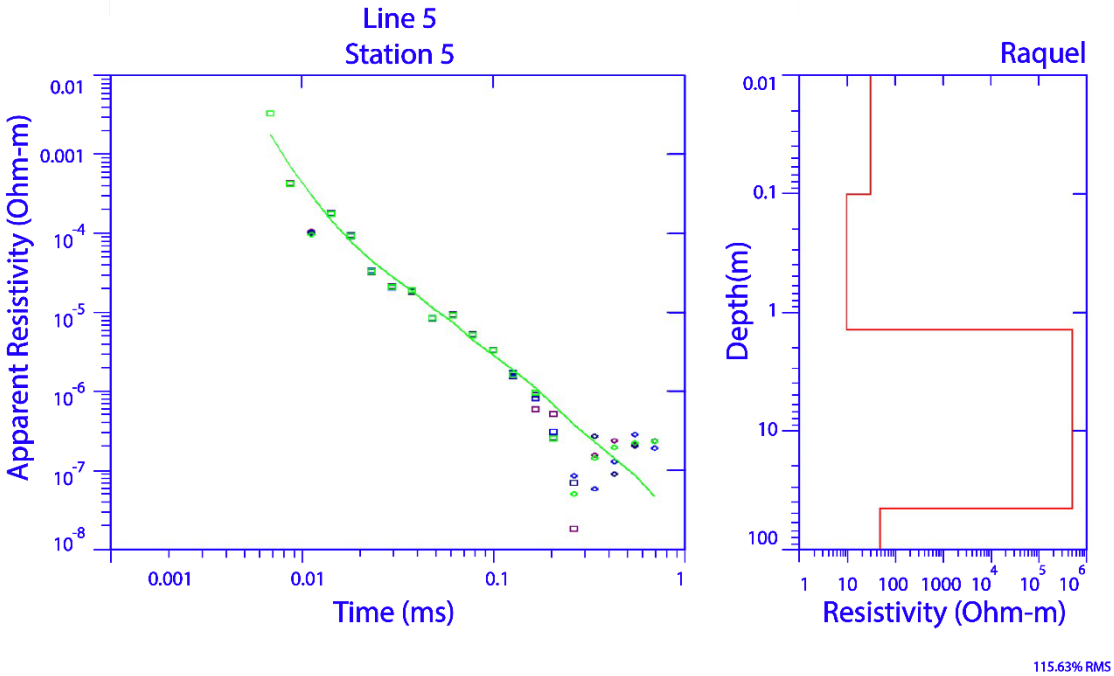

Figure 58 Apparent resistivity (Ωm) vs. time (ms) on the left and the resistivity (Ωm) vs. depth (m) on the right for station 5, line 5.

The resistivity-depth profile shown in figure 59, corresponds to station 5 in line 6. The top 0.7 m show a resistivity value around 500 Ωm, followed by a layer of ~ 150 Ωm extending to 2 m depth. Between 2 m and 5.5 m depth, the resistivity is 35 Ωm. A 55-m thick layer shows a resistivity value of ~ 1,500 Ωm, which is underlain by a 35 Ωm extending to 100 m in depth.

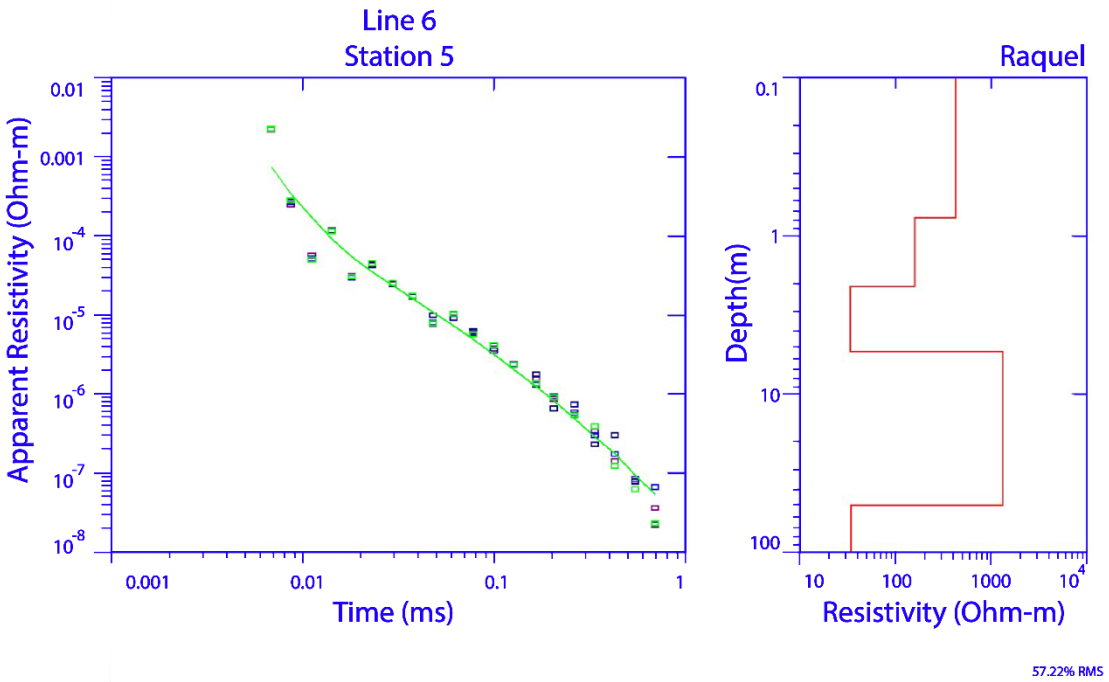

Figure 59 Apparent resistivity (Ωm) vs. time (ms) on the left and the resistivity (Ωm) vs. depth (m) on the right for station 1, line 6.

At station 4 in line 7 (fig. 60), the resistivity to 0.07 m depth is ~ 20 Ωm, followed by a sharp increase to 10^5 Ωm extending to 0.8 m deep. Between 0.8 m – 80 m, the resistivity remains ~ 200 Ωm. A 20-m thick 10 Ωm layer is present at the end of this profile.

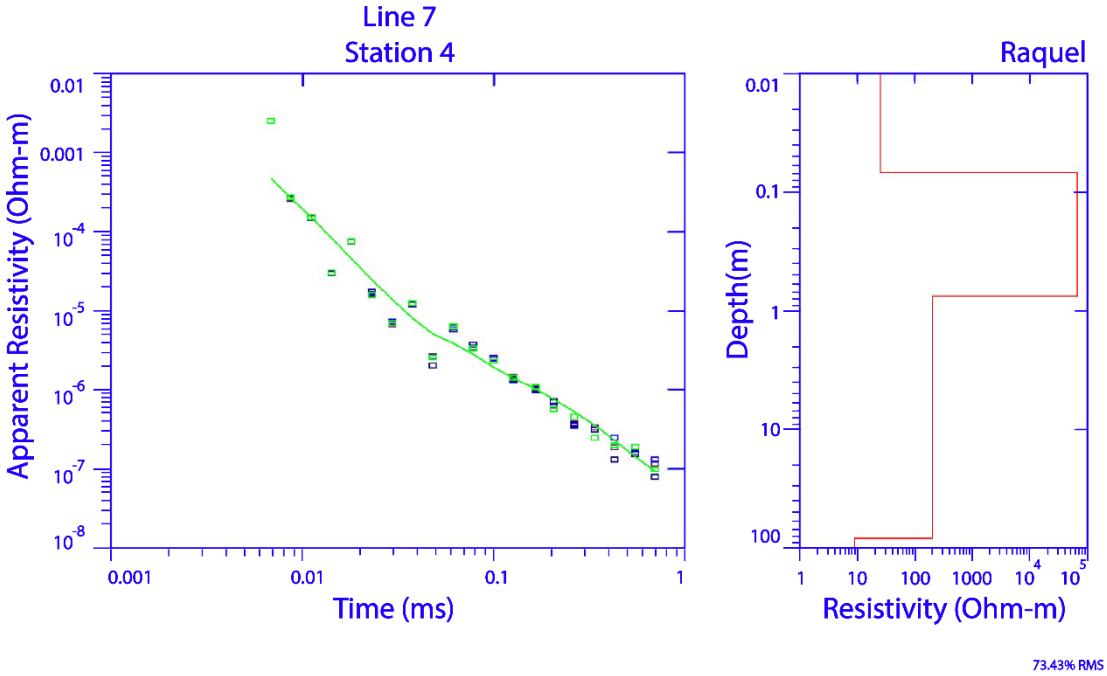

Figure 60 Apparent resistivity (Ωm) vs. time (ms) on the left and the resistivity (Ωm) vs. depth (m) on the right for station 4, line 7.

According to the morphological characteristics discussed in section 4.2.7.2, the Upper Camp Bird rock glacier is a class 4 rock glacier. An outer layer of angular rocks extends over the entire rock glacier body, and ice is absent on its surface. A core of ice (i.e., remnant glaciogenic ice), ice lenses (i.e., segregated ice), and interstitial ice (i.e., talus ice), can be found in the matrix of class 4 rock glaciers (Giardino, 1979; Giardino et al., 1987; Janke et al. 2013; Janke et al 2015). Researchers (Croce and Milana, 2002; Degenhardt and Giardino, 2009; Winkler et al., 2016; Janke et al. 2013; Janke et al 2015) report highly heterogeneous internal make ups for comparable rock glaciers where layers are differentiated by variations in ice and water content.

Volcanic rocks of the Paleogene constitute the outer shell of the Upper Camp Bird rock glacier (fig. 39). The presence of mineralized veins is likely to produce a significant resistivity contrast with unaltered volcanic rocks in the matrix and at the base of the rock glacier (fig. 39 and 47). The integration of geological information with the 1D G-TEM™ models, using the resistivity ranges for subsurface materials shown in figure 51, resulted in the interpretations presented in figures 61 – 68.

The interpretation of the 1D models produced for each station is presented per line in this section based on the resolution and effective depth of penetration achieved with the G-TEM™. The spacing between stations is 25 m; lines 1-6 are 50 m apart and 6-7 40 m apart (fig. 47). The interpretations for lines 1 – 7 are included as a single figure in appendix B.

Resistivity values of <1 Ωm are reported for materials such as massive sulfides (fig. 51). At the Upper Camp Bird rock glacier, such materials can be interpreted as the hydrothermally altered rocks of economic value. In this case, possibly associated with the vein mapped near the toe of the rock glacier. Materials exhibiting resistivity values between 1 Ωm -100 Ωm are interpreted as volcanic rocks in accordance with reported values for weathered and altered igneous rocks (fig. 51). Layers with resistivities ranging from 100 Ωm -1,000 Ωm are considered thawing zones. There is significant overlap in the reported resistivity values for massive ice and permafrost shown in figure 51, which makes it difficult to distinguish between the two types of ice. In this study, resistivity values in the order of 10^4 Ωm or higher, are interpreted as permafrost rather than as solid ice.

Along line 1 (stations 1 – 5, fig. 61), a layer of 1.5 m thickness with resistivity values ranging between 1 Ωm -100 Ωm (mostly 10 Ωm -100 Ωm) corresponds with the outer debris layer of volcanic rocks. The highly resistive layer that varies between 50 m and 80 m in thickness, is interpreted as permafrost storage (10^4 Ωm – 10^5 Ωm). A much less resistant (500 Ωm) layer ~ 45 m thick at station 1 and 10 m – 15m thick at stations 2-5, is present at depths of 45 m - 80 m. This layer is interpreted as a thawing zone, where water contents could be higher, causing the resistivity to drop significantly with respect to the ice-bearing layer above. Lastly, low resistivity materials (<1 Ωm) near the bottom of soundings 2-5 are interpreted as hydrothermally altered rocks.

In line 2 (fig. 62), the volcanic debris layer (1 Ωm -100 Ωm) extends to a depth of 5 m at the center station (station 3) but extends to only the upper 1 m – 1.5 m at the other stations. The permafrost layer (10^4 Ωm – 10^5 Ωm) is 45 m to 60 m thick. The underlying thawing zone is only evident in stations 3 – 5, ranging in thickness from 10 m – 20 m and looks to be <10 m thick at stations 1 and 2. The hydrothermally-altered rocks extend from 30 m - 48 m (<1 Ωm). The interpretations for lines 1 and 2 suggest continuity of the layers along each line (i.e., from station to station), as well as between the lines with slight variations in thickness.

Variations within and between lines are more frequent as we move up rock glacier from the toe. Stations 1 and 2, differ significantly from other stations along line 3 (fig. 63) because a high resistivity layer (i.e., in the range of the permafrost layer) seems to occur outside and near the instrument resolution (≤1 m depth). A layer with values at the cut off between resistivity ranges associated with volcanic rocks (1 Ωm -

100 Ωm) and thawing zones (100 Ωm -1,000 Ωm), extends to a depth of 10 m in station 1. It is common to encounter water bearing materials within the active layer. Therefore, finding a thawing zone at this depth is as likely as finding the volcanic debris layer. At station 2, the debris cover (1 Ωm -100 Ωm) extends from ~ 1.5 m to 7 m, most likely from the surface, whereas at stations 3-5 this layer extends to a depth of 1.5 m to 5 m deep. The thickness of the permafrost layer ($\geq 10^3$ Ωm) varies between 50 m and 80 m, with the top of the layer at ~ 10 m depth in stations 1 and 2, and between 2 m and 4 m at stations 3 -5. The 1D models reach a depth of 1,000 m at stations 1 and 2, but as stated before, readings less than 1 m deep and beyond 100 m are considered unreliable in this study. The models for stations 3 and 5 have a thin (~10 m thick) thawing zone (100 Ωm -1,000 Ωm) within the hydrothermally-altered layer (<1 Ωm); this thin layer needs to be investigated further. At station 4, the permafrost layer is underlain by ~ 20 m of altered igneous rocks (1 Ωm -100 Ωm), and in turn, it is underlain by ~ 30 m of mineralized igneous rocks (<1 Ωm).

Stations 1 and 2 along line 4 present the same sequence as above with some variations in thickness. The volcanic-debris cover (1 Ωm -100 Ωm) extends to a depth of 2 m – 4 m, underlain by a 30 m – 40 m thick thawing zone (100 Ωm -1,000 Ωm). The permafrost layer ($\geq 10^3$ Ωm) varies from ~55 m to ~90 m in thickness, underlain by a ~40 m thick layer of altered igneous rocks (1 Ωm -100 Ωm). The outer volcanic-rock layer (1 Ωm -100 Ωm) extends to a depth of 5 m at station 3, and it is at just below 1 m at stations 4 and 5. The permafrost layer ($\geq 10^3$ Ωm) extends to 100 m, 70 m, and 80 m depth, respectively. Beneath the permafrost layer, a ~30-m thick layer of

hydrothermally-altered rocks (<1 Ωm) is present at station 4, whereas ~ 20 m of altered igneous rocks (1 Ωm -100 Ωm) complete the sequence at station 5. From this point on, description of the interpreted materials along the lines will be restricted to the area between 1 m and 100 m depth.

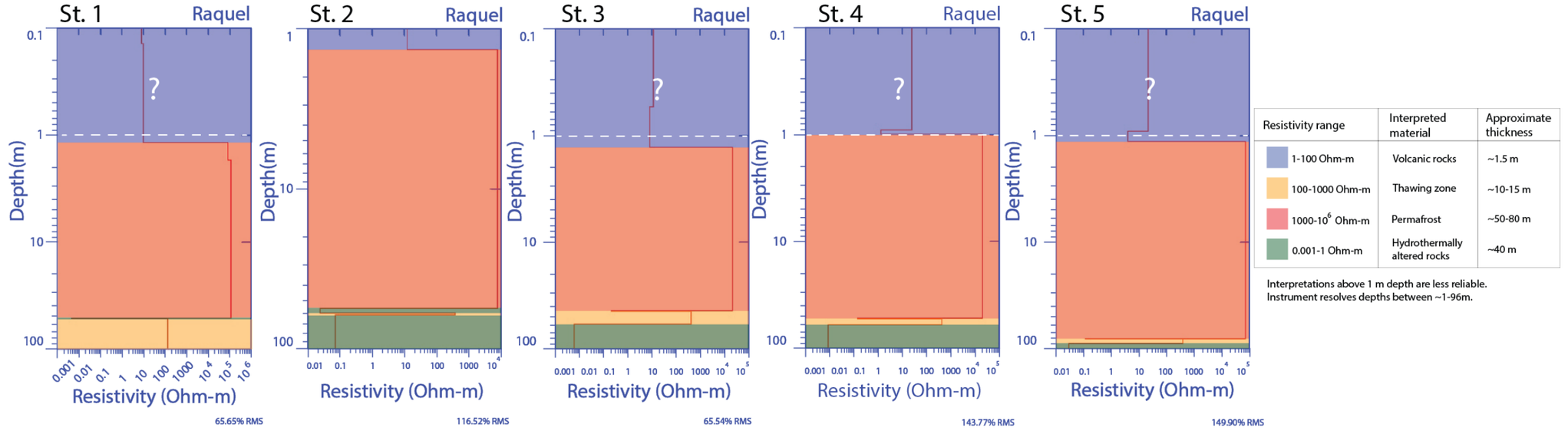

Figure 61 Interpretation of the resistivity values in depth for stations 1-5, line 1. Approximate thickness shown for each interpreted layer represents the range of thickness along the line.

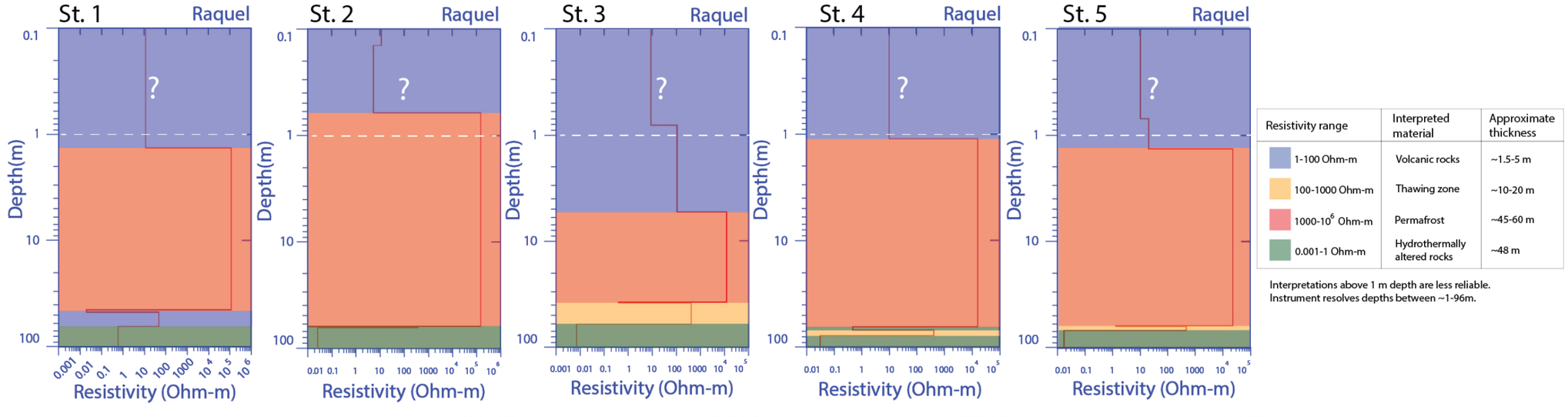

Figure 62 Interpretation of the resistivity values in depth for stations 1-5, line 2. Approximate thickness shown for each interpreted layer represents the range of thickness along the line.

Line 3

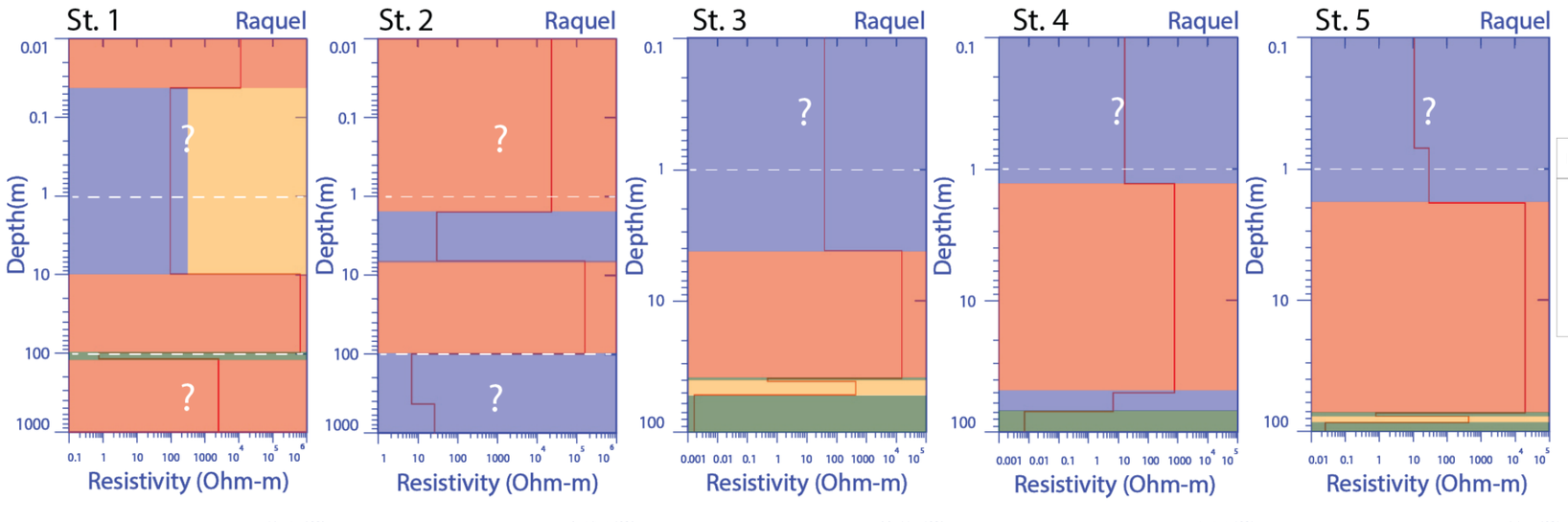

Resistivity range	Interpreted material	Approximate thickness
1-100 Ohm-m	Volcanic rocks	~1.5-5 m
100-1000 Ohm-m	Thawing zone	~10 m
1000-10^6 Ohm-m	Permafrost	~50-80 m
0.001-1 Ohm-m	Hydrothermally altered rocks	~10-60 m

Interpretations above 1 m depth are less reliable.
Instrument resolves depths between ~1-96m.

Figure 63 Interpretation of the resistivity values in depth for stations 1-5, line 3. Approximate thickness shown for each interpreted layer represents the range of thickness along the line.

Line 4

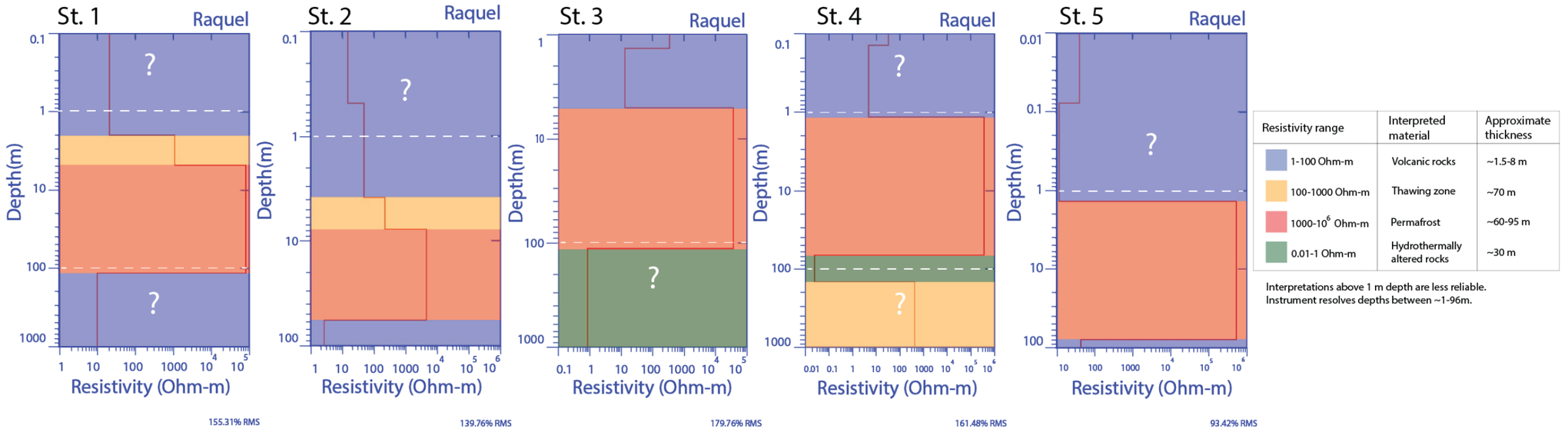

Resistivity range	Interpreted material	Approximate thickness
1-100 Ohm-m	Volcanic rocks	~1.5-8 m
100-1000 Ohm-m	Thawing zone	~70 m
1000-10^6 Ohm-m	Permafrost	~60-95 m
0.01-1 Ohm-m	Hydrothermally altered rocks	~30 m

Interpretations above 1 m depth are less reliable.
Instrument resolves depths between ~1-96m.

Figure 64 Interpretation of the resistivity values in depth for stations 1-5, line 4. Approximate thickness shown for each interpreted layer represents the range of thickness along the line.

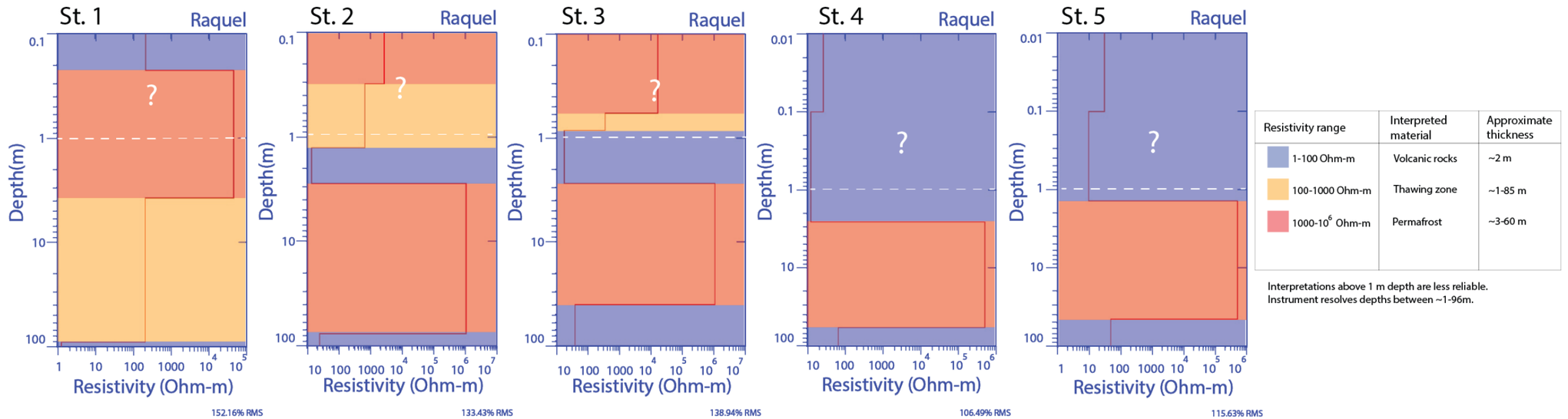

Figure 65 Interpretation of the resistivity values in depth for stations 1-5, line 5. Approximate thickness shown for each interpreted layer represents the range of thickness along the line.

Line 6

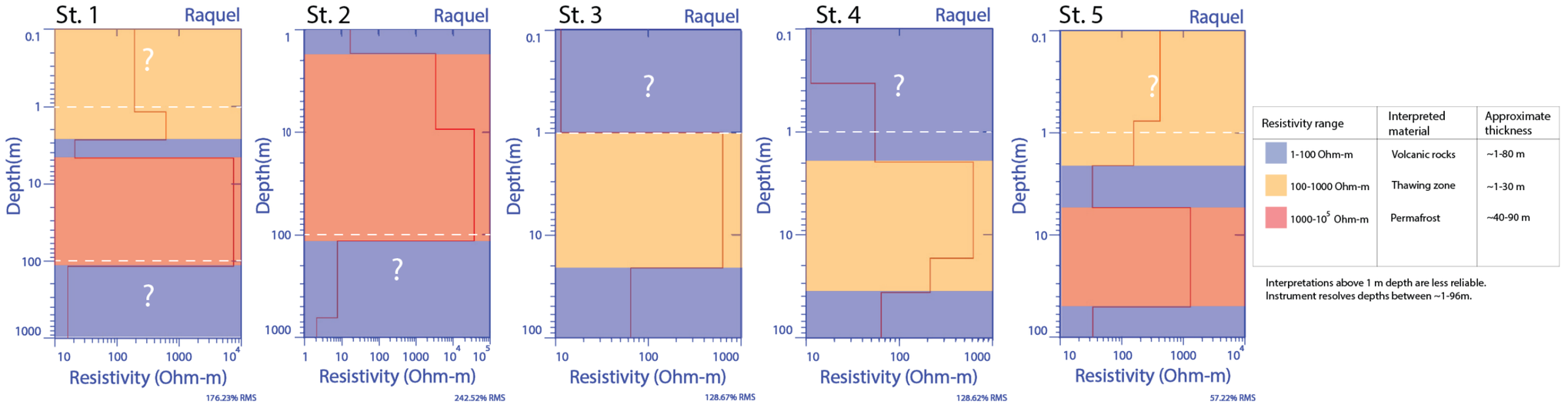

Resistivity range	Interpreted material	Approximate thickness
1-100 Ohm-m	Volcanic rocks	~1-80 m
100-1000 Ohm-m	Thawing zone	~1-30 m
1000-10^5 Ohm-m	Permafrost	~40-90 m

Interpretations above 1 m depth are less reliable.
Instrument resolves depths between ~1-96m.

Figure 66 Interpretation of the resistivity values in depth for stations 1-5, line 6. Approximate thickness shown for each interpreted layer represents the range of thickness along the line.

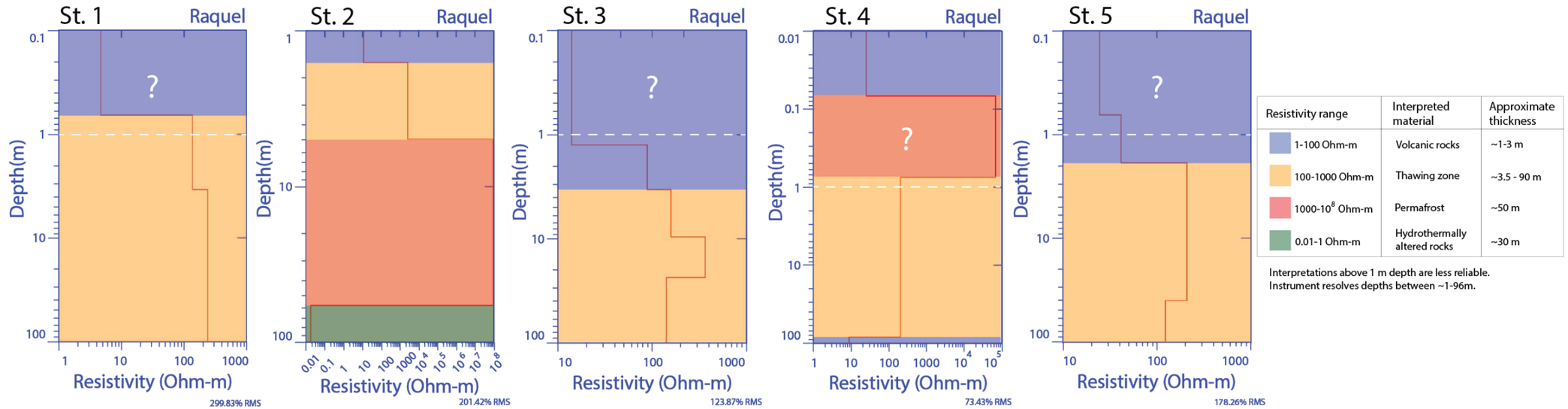

Figure 67 Interpretation of the resistivity values in depth for stations 1-5, line 7. Approximate thickness shown for each interpreted layer represents the range of thickness along the line.

Along line 5, station 1 is uncharacteristic with an apparent permafrost layer ($\geq 10^4$ Ωm) extending from 1 m to ~ 4m depth, underlain by a thick thawing zone (100 Ωm - 1,000 Ωm) down to 90 m, a 10 m thick altered igneous rock layer (1 Ωm -100 Ωm) is at the bottom of this model. Stations 2 – 5 exhibit similar profiles to all others, with a 1.5 m to 2 m thick volcanic debris cover (1 Ωm -100 Ωm), underlain by a ~37 m – 60 m thick permafrost layer ($\geq 10^5$ Ωm), subsequently followed by a 20 m - ~ 55 m thick layer corresponding to altered igneous rocks (1 Ωm -100 Ωm).

The active layer at stations 1 and 5, in line 6 includes a 1.5 m – 2 m thick thawing zone (100 Ωm -1,000 Ωm), followed by 2 m – 3 m of volcanic debris (1 Ωm - 100 Ωm). At station 2, the debris cover is about 1.5 m thick. The permafrost layer ($\geq 10^3$ Ωm) extends down to 100 m deep at stations 1 and 2, and to 50 m at station 5. The debris cover covers the first meter of the sequence at station 4. Stations 3 and 4 have a thawing zone to a 20 m – 30 m depth, respectively. The altered igneous rocks (10 Ωm - 100 Ωm) are found beneath the thawing zone at stations 3 and 4, with a thickness of 80 m to 65 m.

The resistivity values at stations 1, 4 and 5 in line 7, correspond mostly with the range associated with the thawing zone (100 Ωm -1,000 Ωm). This layer consists most of the resistivity depth profile at stations 1 and 5, at the latter the altered igneous rocks (1 Ωm -100 Ωm) is present in the bottom ~15 m. The debris cover (10 Ωm -100 Ωm) is about 2.5 m thick at station 3, which is underlain by the thawing zone (100 Ωm -1,000 Ωm). The model for station 2 shows a very different sequence. The uppermost 1.5 m correspond to a volcanic debris cover (1 Ωm -100 Ωm). The thawing zone (100 Ωm -

1,000 Ωm) extends down to 5 m depth, which is underlain by the permafrost layer (10^8 Ωm) that extends down to ~ 60 m depth. The bottom of the sequence is composed of mineralized igneous rocks (<1 Ωm).

4.4.2. FDEM

The Profiler EMP-400™ data were collected in zigzag mode (see section 4.3.2.2). Thus, the axis was flipped so that the measurements are seen from left to right as if looking at the rock glacier from the toe (fig. 47). Figures 68 – 73 correspond with the graphs of the apparent conductivity values measured with the FDEM system along profile lines 2 – 7. The curves for the three frequencies employed at the Upper Camp Bird rock glacier follow each other closely, suggesting good agreement. However, the negative apparent conductivity values, as well as the pronounced peaks could indicate the presence of objects of disturbances that cause the EMI signal to dissipate, such as tunnels or voids.

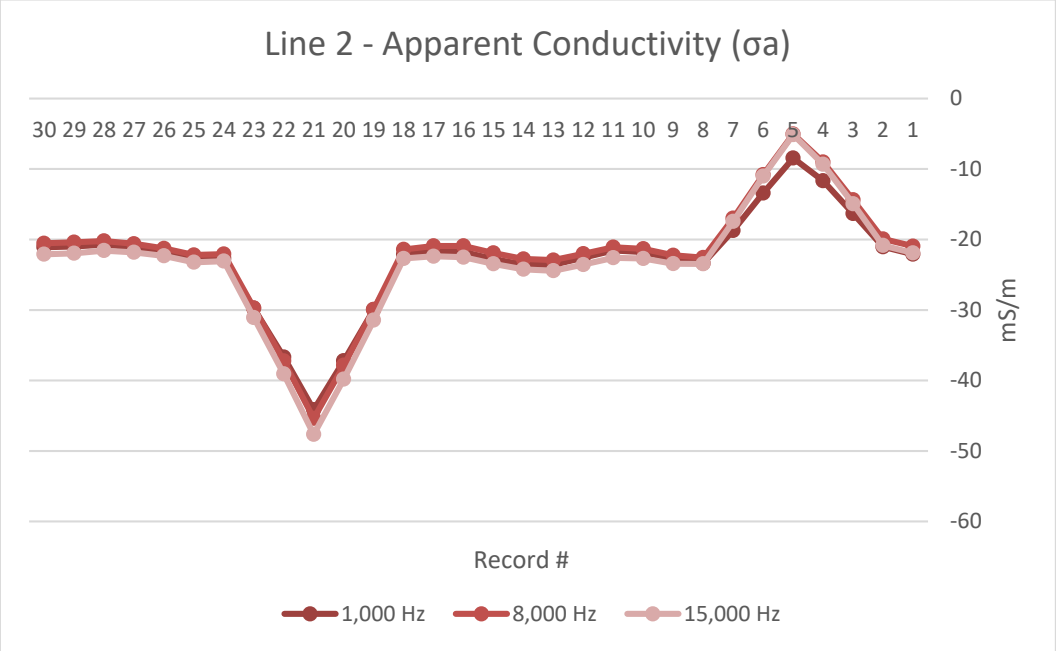

Figure 68 Apparent conductivity measured using FDEM along profiler line 2.

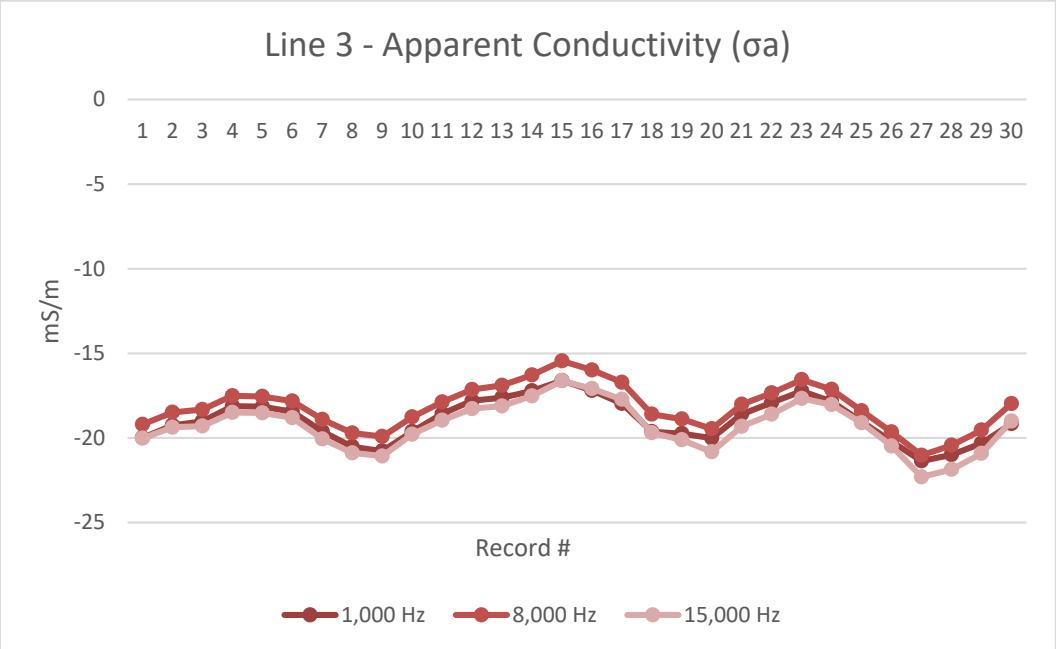

Figure 69 Apparent conductivity measured using FDEM along profiler line 3.

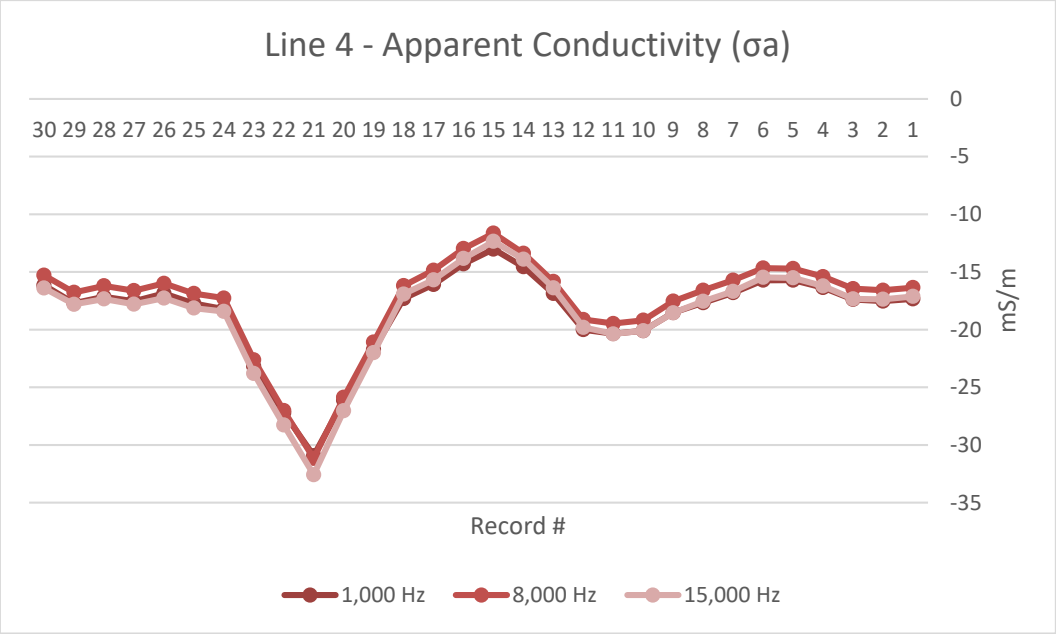

Figure 70 Apparent conductivity measured using FDEM along profiler line 4.

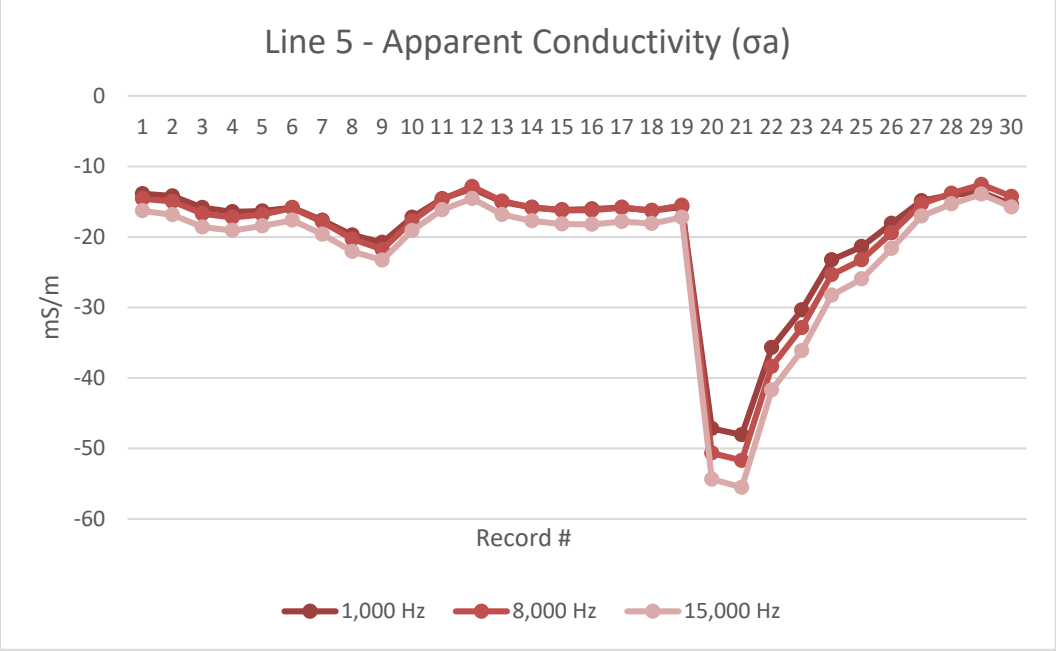

Figure 71 Apparent conductivity measured using FDEM along profiler line 5.

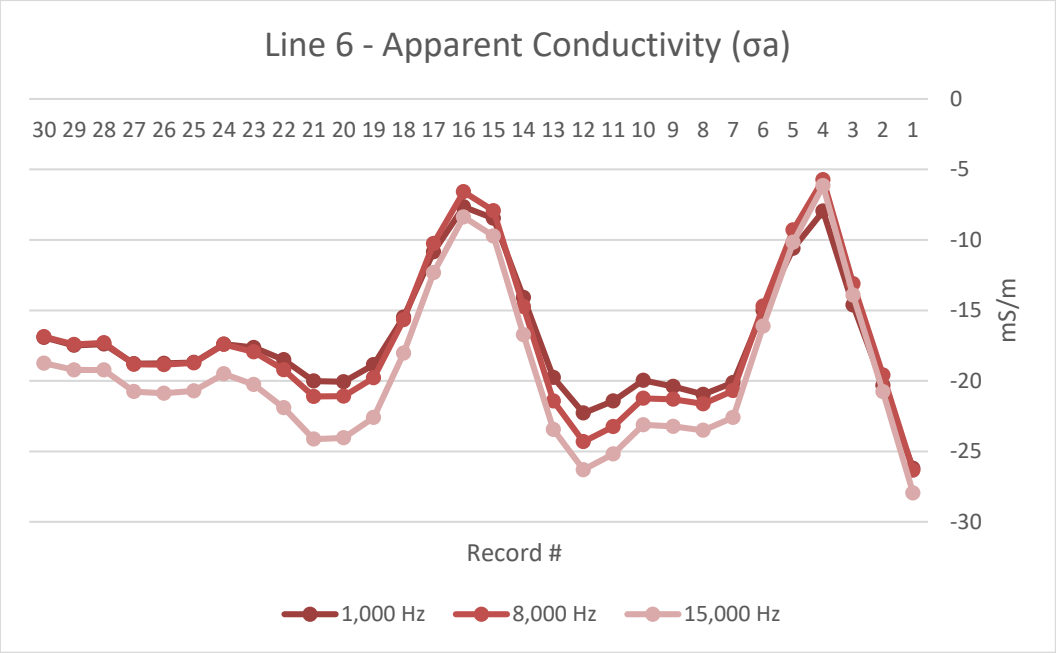

Figure 72 Apparent conductivity measured using FDEM along profiler line 6.

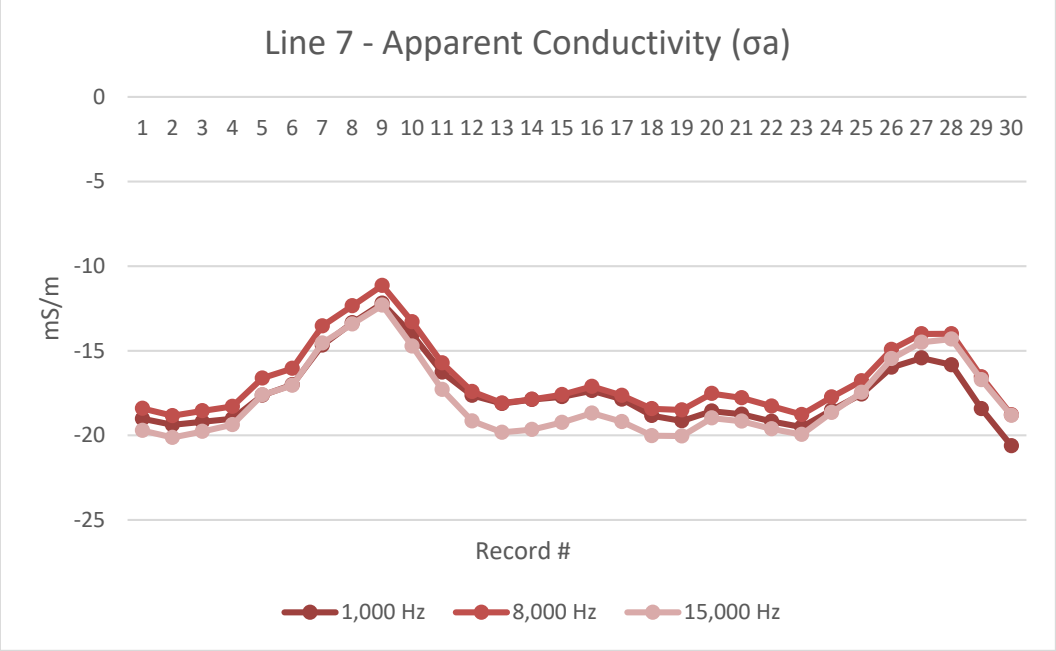

Figure 73 Apparent conductivity measured using FDEM along profiler line 7.

A possible explanation for the anomalous negative-conductivity values observed in figures 68-73, could be the presence of objects related to historic mining activities within the rock glacier. Several mining-related items were observed on the surface of the Upper Camp Bird rock glacier such as an overturned mine cart, remains of wooden lamp posts and several glass lamps, as well as cabling on the side scarp. Along the profiling lines, pieces of wood were observed. However, other remains could be buried unnoticeable in the near-surface.

Highly conductive materials such as mining carts, rail tracks, and metal support structures, are possibly buried under the outer rock layer. The characteristic heterogenous makeup of the rock glacier with the added contrasts produced by anthropogenic objects could violate the operating principles of the EMI methods. EMI profilers are generally used for high-resolution shallow investigations but are susceptible to environmental noise (Hauck and Kneisel, 2008; Kruse, 2013). Unfortunately, the principles are not satisfied to compute the apparent conductivity at the Upper Camp Bird rock glacier.

The distribution of the apparent conductivity values measured using FDEM along profiler lines 2 -7, as well as a Diagram of the Upper Camp Bird rock glacier showing the approximate location of some of the mine shafts and tunnels at Camp Bird mine Level 3 is shown in figure 74. The maps and diagrams used to determine the approximate location of the shafts and tunnels are from 1980's. Therefore, the use of GPS when the maps where drawn is unlikely and the accuracy of the locations shown is

not certain. Discrepancies were observed between the contour lines from the mine maps and USGS maps, possibly caused by changes in map projections, inaccurate mapping, and the availability of higher-resolution data through the years.

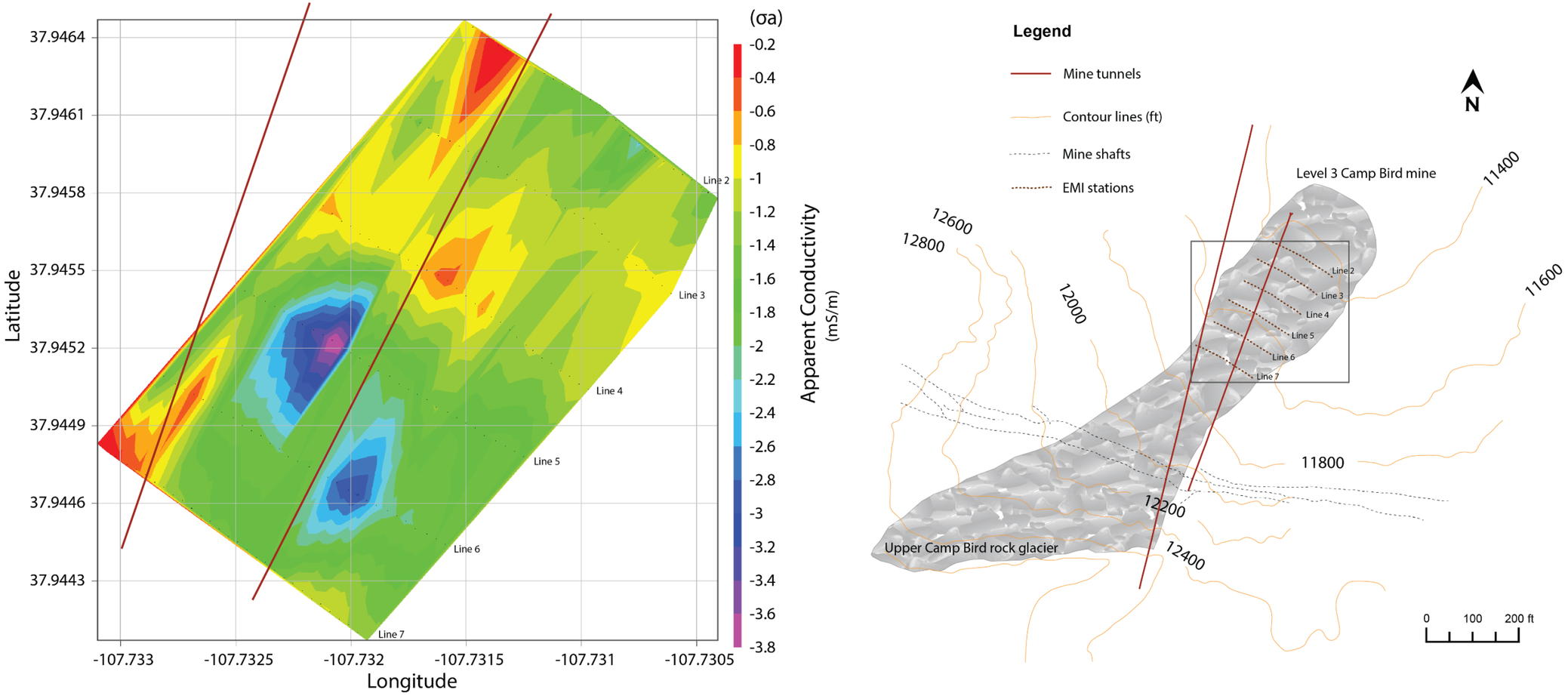

Figure 74 Left: Distribution of the apparent conductivity values measured using FDEM along profiler lines 2 -7. Right: Diagram of the Upper Camp Bird rock glacier showing the approximate location of some of the mine shafts and tunnels at Camp Bird mine Level 3. The black square shows the approximate extent of the apparent conductivity map.

4.4.3. Hydrology model

Benedict (1975, personal communication to J. Schroder in Giardino, 1979) has facetiously indicated “researchers are fortunate to have so few data, so that they can all enjoy themselves in this speculation”. The internal structure of rock glaciers is complex, and data are not only limited in terms of availability, but it is challenging to collect and analyze (Degenhardt, 2002; Riffle, 2018).

Active rock glaciers such as the Upper Camp Bird rock glacier are characterized by heterogeneity in the interior composition. Sediment sizes vary from very fine to coarse in the matrix, and large rock fragments and ice are also part of this complex mixture. Layers of varying ice and water contents are described in geophysical investigations of rock glaciers. Researchers report that more than one permafrost layer (i.e., frozen sediments layer) can be found within a rock glacier, with ice-free and water-bearing layers in between (Haeberli, 1985; Giardino et al., 1992; Guglielmin et al., 1994; Degenhardt, 2002).

The heterogeneity of the interior makeup of a rock glacier complicates their hydrology. Varying grain sizes and ice contents result in varying porosity, permeability, and interconnectivity, making it challenging to define pathways for water flow. A model for water flow through a rock glacier by Giardino et al., 1992 and Haeberli, 1985 is presented in figure 75. Part of the water will flow along the surface of the rock glacier, and part will percolate down into the active layer. Near subsurface flow, occurs within the active layer. Some of the water can flow through and discharge at various points, frequently at the toe, and areas of lower permeability can temporarily retain pockets of

water. A portion of the water can freeze and remain stored as part of the permafrost layer, and beneath the frozen layer deep subsurface aquifers are commonly encountered.

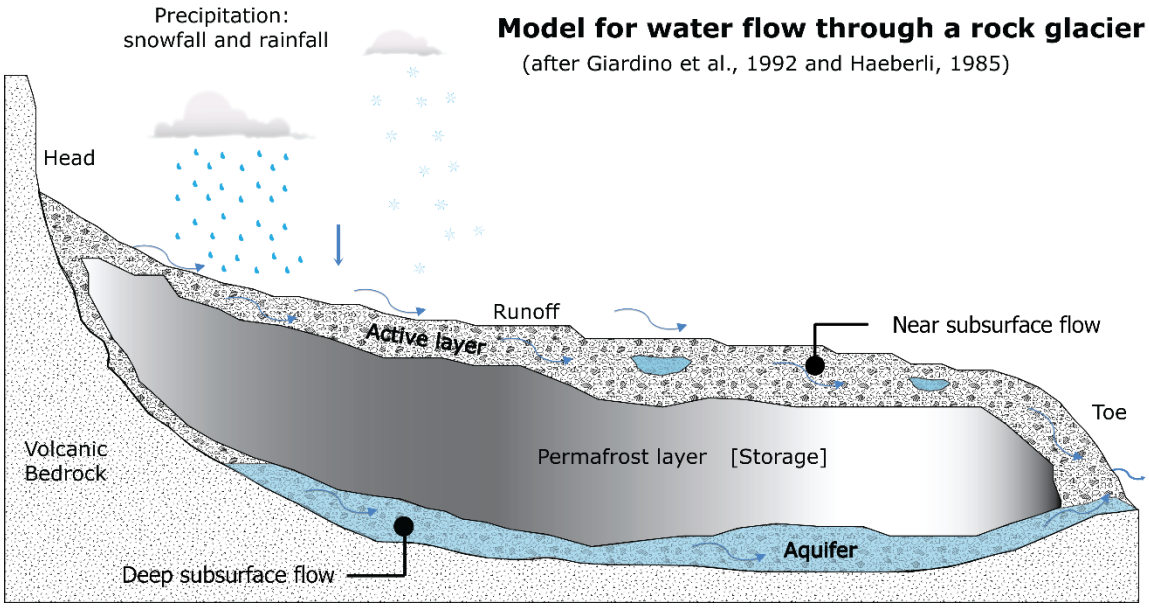

Figure 75 Model for water flow through a rock glacier. Diagram shows a profile view. Modified from Giardino et al., 1992 and Haeberli, 1985.

At the Upper Camp Bird rock glacier, a thawing zone is observed at varying depths. This potentially water-bearing layer is encountered beneath the frozen layer along the lines that are closer to the toe (i.e., lines 1-3). Moving away from the toe, the variability increases, and the thawing zone is observed over the permafrost layer in most cases. Layers of unfrozen, dry sediments are encountered, which occur at varying depths, in some cases separating the frozen from the water-bearing layers. The highly mineralized bedrock is observable at several stations, particularly those that are closer to the toe.

The active layer consists of a volcanic debris cover and a thawing zone encountered above the permafrost layer. Some areas interpreted as thawing zones could correspond with pockets of water that can exist within the active layer. Variations in the thickness of the active layer occur as expected. Internal variations in the ice/sediment ratio within the permafrost layer are likely responsible for the different resistivity ranges recorded. The thawing zones present beneath the ice-rich layer, could correspond with the aquifer beneath the permafrost layer.

4.5. Conclusions and future work

Local conditions such as elevation, weather, slope, and aspect, favor the preservation of permafrost at the Imogene Basin. The Upper Camp Bird rock glacier is connected to the debris source, which favors further ice preservation by maintain a thick, insulating debris cover. This tongue-shaped rock glacier is active and is characterized by a highly heterogeneous internal structure.

The use of non-invasive methods allowed for a detailed interpretation of surface characteristics (i.e., drone and satellite imagery), as well as of the internal composition and hydrology (i.e., near-surface geophysics). The suitability of two types of controlled-source electromagnetic inductions system was evaluated at the study site. The frequency-domain system (EMI or profiler) is portable, easy to operate, and allows the user to obtain high-resolution measurements at shallow depths. The operating principles of the EMI assume a homogeneous subsurface, and large conductivity contrasts prevent the equipment from computing apparent-conductivity values, yielding negative readings.

The intrinsic heterogeneity of the rock glacier was exacerbated by the site disturbances resulting from historic mining operations. The site conditions necessary for the profiler EMP-400™ to compute the apparent-conductivity of the subsurface were not satisfied at the Upper Camp Bird rock glacier. Thus, the EMI is not an appropriate instrument to resolve the internal structure of the Upper Camp Bird rock glacier.

The time-domain instrument (G-TEM™) is more challenging to operate. Moving the equipment from one station to the next requires a team of people on the rugged surface of a rock glacier. The minimal disadvantages associated with the use of this system are outweighed by numerous advantages. The G-TEM™ uses a layered Earth model and reaches great depths of penetration. These characteristics are particularly important to determine the internal composition of a highly heterogeneous feature. Additionally, the instrument seems to be averaging out the small-scale environmental conditions that affected the EMI readings, providing promising results even with the initial 1D models presented in this study. The G-TEM™ proved to be an adequate instrument to map the distribution of the electrical resistivity at depth at the Upper Camp Bird rock glacier.

Data collected using the G-TEM™ system can be used to produce 2D and 3D models. The 2D and 3D models are more complex, and heavily reliant on mathematical skills. In a 3D environment such as a rock glacier, 3D models could provide more accurate interpretations. Thus, future work should involve an interdisciplinary team of researchers to produce a 3D model of the Upper Camp Bird rock glacier.

4.6. References

Aguilar, R.G., Owens, R., Giardino, J.R., 2020. The expanding role of anthropogeomorphology in critical zone studies in the Anthropocene. Geomorphology 366, 107165. https://doi.org/10.1016/j.geomorph.2020.107165

Baars, D.L., 1992. The American Alps: The San Juan Mountains of Southwest Colorado. University of New Mexico Press. Albuquerque, 204 p.

Bajewski, I., Gardner, J. S., 1989. Discharge and sediment-load characteristics of the Hilda rock-glacier stream, Canadian Rocky Mountains, Alberta. Physical Geography 10, 295-306.

Barsch, D., 1988. Rockglaciers. In: Clark, M. J., (Ed.), Advances in Periglacial Geomorphology. Wiley, Chichester, West Sussex, 69-90.

Barsch, D., 1996. Rock Glaciers – Indicators for the Present and Former Geoecology in High Mountain Environments. Springer-Verlag, Berlin, 331 pp.

Benedict, J.B.,1975 personal communication to Schroder in Giardino, J. R., 1979. Rock glacier mechanics and chronologies: Mount Mestas, Colorado, unpublished Ph.D. dissertation, University of Nebraska, Lincoln, Nebraska, 244 pp.

Blair, R., 1996a. Geology of the Western San Juan Mountains and a Tour of the San Juan Skyway, Southwestern Colorado. Colorado Geological Survey, Department of Natural Resources.

Blair, R., 1996b. The Western San Juan Mountains: Their Geology, Ecology, and Human History. University Press of Colorado.

Brardinoni, F., Scotti, R., Sailer, R., Mair, V., 2019. Evaluating sources of uncertainty and variability in rock glacier inventories. Earth Surface Processes and Landforms, 44(12), pp.2450-2466.

Brenning, A., Grasser, M., Friend, D. A., 2007. Statistical estimation and generalized additive modeling of rock glacier distribution in the San Juan Mountains, Colorado, United States. Journal of Geophysical Research: Earth Surface, 112(F2).

Brown, W. H., 1925. A probable fossil glacier. Journal of Geology 33, 464-66.

Burbank, W. S., Luedke, R. G., 1984. Geology and ore deposits of the Uncompahgre (Ouray) mining district, southwestern Colorado (No. 1753). US Government Printing Office.

Cheng, G., Jin, H., 2013. Permafrost and groundwater on the Qinghai-Tibet Plateau and in northeast China. Hydrogeology Journal, 21(1), 5-23.

City of Boulder Colorado, 2002 https://www-static.bouldercolorado.gov/docs/boulder-watershed-map-1-201304161145.pdf?_ga=2.159501181.1147060098.1515803599-493358221.1515803599

Colombo, N., Sambuelli, L., Comina, C., Colombero, C., Giardino, M., Gruber, S., Viviano, G., Vittori Antisari, L., Salerno, F., 2018. Mechanisms linking active rock glaciers and impounded surface water formation in high-mountain areas. Earth Surface Processes and Landforms, 43(2), 417-431.

Corte, A. E., 1976. The hydrological significance of rock glaciers. Journal of Glaciology, 17, 157-158.

Corte, A. E., 1978. Rock glaciers as permafrost bodies with debris cover as an active layer. A hydrological approach. Andes of Mendoza, Argentina. Proceedings of the Third International Conference on Permafrost, Edmonton, Alberta, Canada, 1, 262-269.

County, S. J., 2015. The Official Website of San Juan County Colorado. Retrieved from http://sanjuancountycolorado.us/index.html

Croce, F. A., Milana, J. P., 2002. Internal structure and behaviour of a rock glacier in the arid Andes of Argentina. Permafrost and Periglacial Processes 13(4):289–299.

Degenhardt, J. J., 2002. A model for the development of a lobate alpine rock glacier in southwest Colorado, USA: implications for water on Mars. Doctoral dissertation, Texas A&M University.

Degenhardt, J.J., Giardino, J.R., 2003. Subsurface investigation of a rock glacier using ground-penetrating radar: Implications for locating stored water on Mars. Journal of Geophysical Research: Planets, 108(E4).

Duguay, M. A., Edmunds, A., Arenson, L. U., Wainstein, P. A., 2015. Quantifying the significance of the hydrological contribution of a rock glacier–A review. In GEOQuébec 2015: Challenges from North to South, Québec, Canada.

Eamer, J., Ahlenius, H. and Prestrud, P., 2007. Global outlook for ice & snow. Division of Early Warning and Assessment (DEWA), United Nations Environmental Programme.

Everett, M. E., 2013. Near-surface applied geophysics. Cambridge University Press.

Fitterman, D.V., 2015. Tools and techniques: Active-source electromagnetic methods. In Resources in the Near-Surface Earth, Treatise on Geophysics; Slater, L., Ed.; Elsevier B. V.: Amsterdam, The Netherlands, 2015; Volume 11, pp. 295–333.

Frauenfelder R, Schneider B, Kääb A., 2008. Using dynamic modelling to simulate the distribution of rock glaciers. Geomorphology 93: 130–143.

French, H.M., 2013. The Periglacial Environment. John Wiley & Sons, p. 478.

Gardner, J. S., Bajewsky, I., 1987. Hilda rock glacier stream discharge and sediment load characteristics, Sunwapta Pass area, Canadian Rocky Mountains. In: Giardino, J. R., Shroder, J. F. Jr., Vitek, J. D. (Eds.), Rock Glaciers. Allen and Unwin, London, pp. 161-174.

Geiger, S. T., J. M. Daniels, S. N. Miller, Nicholas, J. W., 2014. Influence of rock glaciers on stream hydrology in the La Sal Mountains, Utah. Arctic, Antarctic, and Alpine Research 46 (3):645–658.

Geonics. G-TEM Operating Manual; Geonics Limited: Mississauga, ON, Canada, 2016.

Geophysical Survey Systems, Inc (GSSI), 2017. ProfilerTM EMP-400 Manual, online https://www.geophysical.com/ accessed on 12/15/2018.

Giardino, J. R., Vitek, J. D., 1985. A statistical interpretation of the fabric of a rock glacier. Arctic and Alpine Research, 165-177.

Giardino, J. R., 1979. Rock glacier mechanics and chronologies: Mount Mestas, Colorado, unpublished Ph.D. dissertation, University of Nebraska, Lincoln, Nebraska, 244 pp.

Giardino, J. R., Shroder, J. F., Vitek, J. D., 1987. Rock Glaciers. London: Allen & Unwin, 416 pp.

Giardino, J. R., Vitek, J. D., 1985. A statistical study of the fabric of a rock glacier. Arctic and Alpine Research 17, 165-177.

Giardino, J. R., Vitek, J. D., 1988. The significance of rock glaciers in the glacial-periglacial landscape continuum. Journal of Quaternary Science 3 (1), 97-103.

Giardino, J. R., Vitek, J. D., Demorett, J. L., 1992. A model of water movement in rock glaciers and associated water characteristics. In: Dixon, J. C., Abrahams, A. D. (Eds.), Periglacial Geomorphology. Wiley, Chichester, West Sussex, pp. 159-184.

Gonzales, D.A. Karlstrom, K.E., 2011. A legacy of mountains past and present in the San Juan Region. The Eastern San Juan Mountains: Their Ecology, Geology, and Human History, p.3.

Guglielmin, M., Lozej, A. Tellini, C., 1994. Permafrost distribution and rock glaciers in the Livigno Area (Northern Italy). Permafrost and Periglacial Processes, 5(1), pp.25-36.

Guglielmin, M., Ponti, S., Forte, E., 2018. The origins of Antarctic rock glaciers: periglacial or glacial features? Earth Surface Processes and Landforms.

Haddeland, I., Heinke, J., Biemans, H., Eisner, S., Flörke, M., Hanasaki, N., Konzmann, M., Ludwig, F., Masaki, Y., Schewe, J. Stacke, T., 2014. Global water resources affected by human interventions and climate change. Proceedings of the National Academy of Sciences, 111(9), pp.3251-3256.

Haeberli, W., 1985. Creep of mountain permafrost: Internal structure and flow of alpine rock glaciers: Mitteilungen der Versuchsanstalt fur Wasserbau, Hydrologie und Glaziologie Nr. 77, Zurich, 142 pp.

Haeberli, W., B. Hallet, L. Arenson, R. Elconin, O. Humlum, A. Kaab, V. Kaufmann, B. Ladanyi, N. Matsuoka, S. Springman, Mühll, D. V., 2006. Permafrost creep and rock glacier dynamics. Permafrost and Periglacial Processes 17:189–214.

Haeberli, W., Mühll, D. V., 1996. On the characteristics and possible origins of ice in rock glacier permafrost. Zeitschrift für Geomorphologie (Supplement 104), 43-57.

Hauck, C., Kneisel, C., 2008. Applied geophysics in periglacial environments. Cambridge University Press. https://doi.org/10.1017/CBO9780511535628

Hedrick, E. A., Gonzales, D.A., 2016. Data Compellation, Multi-Source Integration, and Three-Dimensional (3D) Modelling of Camp Bird Mine, Colorado. Geological Society of America Abstracts with Programs. Vol. 48, No. 6. doi: 10.1130/abs/2016RM-275797

Heginbottom, J.A., Brown, J., Humlum, O., Svensson, H., 2012. Permafrost and periglacial environments. In Williams, R.S., Jr., and Ferrigno, J.G., eds., 2012, State of the Earth's cryosphere at the beginning of the 21st century–Glaciers, global snow cover, floating ice, and permafrost and periglacial environments: U.S. Geological Survey Professional Paper 1386–A, 546 p.

Hersir, G.P., Flóvenz, Ó.G., 2013. Resistivity surveying and electromagnetic methods. Global Environment. 14 pages

Huffman Jr, A. C., 1995. San Juan Basin Province (022). Gautier, DL, Dolton, GL, Takahashi, KI, and Varnes, KL, eds.

Imhof M., 1996. Modelling and verification of the permafrost distribution in the Bernese Alps (Western Switzerland). Permafrost and Periglacial Processes 7: 267–280.

IPCC (International Panel on Climate Change)., 2013: Summary for policymakers. Climate Change 2013: The Physical Science Basis. Contribution of Working Group I to the Fifth Assessment Report of the Intergovernmental Panel on Climate Change: 33.

Irham, M., 2016. The Impact of Temperature, Elevation, and Aspect on the Potential Distribution of Permafrost in San Juan Mountains, Colorado (Doctoral dissertation).

Janke, J. R., Bellisario, A. C., Ferrando, F. A., 2015. Classification of debris-covered glaciers and rock glaciers in the Andes of central Chile. Geomorphology, 241, 98-121.

Janke, J. R., Regmi, N. R., Giardino, J. R., Vitek, J. D., 2013. Rock Glaciers. Treatise on Geomorphology 8, 238-273.

Johnson, P. G., 1981. The structure of a talus-derived rock glacier as deduced from its hydrology. Canadian Journal of Earth Science 18 (9), 1,422-1,430.

Jones, D.B., Harrison, S., Anderson, K., Whalley, W.B., 2019. Rock glaciers and mountain hydrology: A review. Earth-Science Reviews, 193, pp.66-90.

Jorgensen, W. R., 2007. A validation of ground penetrating radar for reconstructing the internal structure of a rock glacier: Mount Mestas, Colorado, USA. Master's thesis, Texas A&M University.

Kane, D. L., Yoshikawa, K., McNamara, J. P., 2013. Regional groundwater flow in an area mapped as continuous permafrost, NE Alaska (USA). Hydrogeology Journal, 21(1), 41-52.

Killingbeck, S.F., Booth, A.D., Livermore, P.W., Bates, C.R. West, L.J., 2020. Characterisation of subglacial water using a constrained transdimensional Bayesian transient electromagnetic inversion. *Solid Earth*, 11(1), pp.75-94. https://doi.org/10.5194/se-11-75-2020

King, L., Fisch, W. W., Haeberli, W., Waechter, H. P., 1987. Comparison of resistivity and radio-echo soundings on rock glacier permafrost. Zeitschrift für Gletscherkunde und Glazialgeologie 23 (1), 77-97.

Knight, J., Harrison, S., Jones, D.B., 2019. Rock glaciers and the geomorphological evolution of deglacierizing mountains. Geomorphology, 324, pp.14-24.

Kruse, S., 2013. Near-surface geophysics in geomorphology. Treatise on Geomorphology. Elsevier, pp. 103–129. https://doi.org/10.1016/B978-0-12-374739-6.00047-6.

Lipman, P.W., 1976, Geologic map of the Lake City caldera area, western San Juan Mountains, southwestern Colorado: U.S. Geological Survey Miscellaneous Investigations Series Map 1-962, scale 1:48,000.

Luedke, R.G, Burbank, W.S, 1963. Tertiary volcanic stratigraphy in the western San Juan Mountains, Colorado, in Short papers in geology and hydrology: U.S. Geological Survey Professional Paper 475-C, p. C39-C44.

Malehmir, A., Socco, L. V., Bastani, M., Krawczyk, C. M., Pfaffhuber, A. A., Miller, R. D., Maurer, H., Frauenfelder, R., Bazin, S., Merz, K., Dahlin, T., 2016. Near-surface geophysical characterization of areas prone to natural hazards: a review of the current and perspective on the future. In Advances in Geophysics (Vol. 57, pp. 51-146). Elsevier.

Maurer, H., C. Hauck., 2007. Instruments and methods: Geophysical imaging of alpine rock glaciers. Journal of Glaciology 53 (180):110–120.

Ménard, C.B., Essery, R., Barr, A., Bartlett, P., Derry, J., Dumont, M., Fierz, C., Kim, H., Kontu, A., Lejeune, Y., Marks, D., 2019. Meteorological and evaluation datasets for snow modelling at 10 reference sites: description of in situ and bias-corrected reanalysis data. Earth System Science Data, 11(2), pp.865-880.

Monnier, S., Kinnard, C., 2013. Internal structure and composition of a rock glacier in the Andes (upper Choapa valley, Chile) using borehole information and ground penetrating radar. Annals of Glaciology 54 (64):61–72.

National Centers for Environmental Information (NCEI), 2020. TELLURIDE 4 WNW, CO US. https://www.ncei.noaa.gov/

Palacky, G.J., 1988. Resistivity characteristics of geologic targets. Electromagnetic methods in applied geophysics, 1, pp.53-129.

Pondthai, P., Everett, M.E., Micallef, A., Weymer, B.A., Faghih, Z., Haroon, A., Jegen, M., 2020. 3D characterization of a coastal freshwater aquifer in SE Malta (Mediterranean Sea) by time-domain electromagnetics. Water, 12(6), p.1566.

Potter, N., 1972. Ice-cored rock glacier, Galena Creek, Northern Absaroka Mountains, Wyoming. Geological Society of America Bulletin, 83(10), 3025-3058.

Riffle, A., 2018. Internal composition, structure, and hydrological significance of rock glaciers in the Eastern Cascades, Washington. Masters Thesis. Central Washington University.

Rosemeyer, T., 1990. Camp Bird Mine Ouray County, Colorado. Rocks & Minerals, 65(2), pp.114-149.

Rowley, T., Giardino, J. R., Granados-Aguilar, R., Vitek, J. D., 2015. Periglacial Processes and Landforms in the Critical Zone. In Developments in Earth Surface Processes (Vol. 19, pp. 397-447). Elsevier.

Schrott, L., 1996. Some geomorphological-hydrological aspects of rock glaciers in the Andes (San Juan, Argentina). Zeitschrift für Geomorphologie Supplement 104, 161- 173.

Southwest, T. A., 2016. The American Southwest. Retrieved from http://www.americansouthwest.net/colorado/san_juan_mountains/

Steven, T.A., Lipman, P.W., Hall, W.J., Jr., Barker, F., Luedke, R.G., 1974. Geologic map of the Durango quadrangle, southwestern Colorado: U.S. Geological Survey Miscellaneous Investigations Series Map I-764 , scale l:250,000.

U.S. Geological Survey (USGS), 2016. The StreamStats program for Colorado, online at http://water.usgs.gov/osw/streamstats/colorado.html, accessed on (give date of access).

Uncompahgre Watershed Partnership (UWP), 2019. The Uncompahgre River Watershed in Ouray County: The Basics & A Little Bit More, online at https://www.uncompahgrewatershed.org/, accessed on September, 2020.

USGS, https://www.usgs.gov/media/images/time-domain-electromagnetic-method-diagrams

Vitek, J. D., Giardino, J.R., 1987. Rock glaciers: a review of the knowledge base. pp.1-26. In Giardino, J. R., Shroder, J. F., and Vitek, J. D. (1987). Rock Glaciers. London: Allen & Unwin, 416 pp.

Vonder Mühll, D.S., Klingelé, E.E., 1994. Gravimetrical investigation of ice-rich permafrost within the rock glacier Murtèl-Corvatsch (upper Engadin, swiss alps). Permafrost and Periglacial Processes, 5(1), pp.13-24.

Wagner, S., 1996. DC resistivity and seismic refraction soundings on rock glacier permafrost in northwestern Svalbard. Norsk Geografisk Tidsskrift 50, 25-36.

Wahrhaftig C., Cox, A., 1959. Rock glaciers in the Alaska Range. Geological Society of America Bulletin 70, 383-436.

Whalley, W. B., 1974. Rock glaciers and their formation as part of a glacier debris transport system, Geographic Papers, No. 27, University Reading, England, 48 pp.

Whalley, W. B., 2020. Gruben glacier and rock glacier, Wallis, Switzerland: glacier ice exposures and their interpretation. Geografiska Annaler: Series A, Physical Geography, 102(2), pp.141-161.

Whalley, W. B., Palmer, C. F., Hamilton, S. J., Gordon, J. E., 1994. Ice exposures in rock glaciers. Journal of Glaciology 40, 427.

Winkler G, Wagner T, Pauritsch M, Birk S, Kellerer-Pirklbauer A, Benischke R, Leis A, Morawetz R, Schreilechner MG, Hergarten S (2016) Identification and assessement of groundwater flow and storage components of the relict Schöneben Rock Glacier, Niedere Tauern Range, Eastern Alps (Austria). Hydrogeol J 24:937–953.

5. CONCLUSION

5.1. Anthropogeomorphology, Critical Zone and the Anthropocene

A new framework for geomorphology is required as rapidly increasing human population pushes anthropic-geomorphic processes to a dominant role in the Anthropocene. Understanding these processes requires new conceptual frameworks, interdisciplinarity, and a strong technology-assisted approach. Thus, geomorphology has progressed from a predominantly descriptive discipline to a largely quantitative science.

The Critical Zone provides a useful conceptual framework in studies of Anthropocene geomorphology. A soil-centered focus prevails on Anthropocene studies. Soils are generally considered the unifying thread of the Critical Zone; however, a water-centered approach is a more appropriate (Giardino and Houser, 2015).

The extent of the Critical Zone is from the top of the canopy to the base of the groundwater system. Thus, this concept permits a systems approach to geomorphology across scales, addressing the extensive role of human impact on terrestrial surface processes.

Land-cover changes and climatic variability impact the delivery of water to the Critical Zone. Land-cover alteration is decreasing infiltration, armoring surfaces, increasing surface runoff, enhancing erosion rates, and causing an expansion of arid lands. The rate at which humans are altering the surface continues to grow. Thus, the benefit of using the Critical Zone as a lens to study geomorphology will result in a broad, unified interdisciplinary study of the Anthropocene.

Anthropogeomorphology studies can be aided by modern technology, including the use of unmanned aerial vehicles, artificial intelligence, and machine-learning applications. The trend toward technology-driven studies will continue in the geosciences, and geomorphology will be well-assisted by its use.

A focus on the Critical Zone in anthropogenic geomorphology allows a framework for interdisciplinary research that incorporates effects of multiple Earth spheres, modification of systems, and feedback mechanisms resulting from past and current human influence.

5.2. Non-invasive multiple-method approaches to geomorphology

The use of multiple-method approaches prevails in geomorphological studies pertaining complex processes and environments. Using multiple methodologies allows researchers access to information about the surface and subsurface at varying scales. Data collection and processing are increasingly carried out by interdisciplinary teams of researchers. The creation of open access information (e.g. databases) allows for faster data analysis and validation.

Increasing interest in non-invasive methods to study subsurface-surface interactions is evident in recent literature. Non-invasive methods are ideal for studies in remote locations, where access to the site(s) of interest is restricted, as well as in urban or culturally relevant areas (i.e. archaeological sites). Advances in geomorphological research across all geomorphic environments in recent years are accomplished with the aid of remote sensing methods and non-invasive geophysics, typically validated using traditional invasive methodologies.

Examples of geomorphological studies carried out using geophysical methods were described in this section to illustrate successful methodologies applied in varying geomorphic environments, as well as to highlight the potential uses in other environments. The techniques are not process-dependent, which allows for a wide range of new applications. With continuous advancements in methodologies and instrumentation, one can argue that geomorphological studies could be carried out using exclusively non-invasive techniques in the near future.

5.3. Water storage in the periglacial Critical Zone: The Upper Camp Bird rock glacier

Local conditions such as elevation, weather, slope, and aspect, favor the preservation of permafrost at the Imogene Basin. The Upper Camp Bird rock glacier is connected to the debris source, which favors further ice preservation by maintain a thick, insulating debris cover. This tongue-shaped rock glacier is active and is characterized by a highly heterogeneous internal structure.

The use of non-invasive methods allowed for a detailed interpretation of surface characteristics (i.e., drone and satellite imagery), as well as of the internal composition and hydrology (i.e., near-surface geophysics). The suitability of two types of controlled-source electromagnetic inductions system was evaluated at the study site. The frequency-domain system (EMI or profiler) is portable, easy to operate, and allows the user to obtain high-resolution measurements at shallow depths. The operating principles of the EMI assume a homogeneous subsurface, and large conductivity contrasts prevent the equipment from computing apparent-conductivity values, yielding negative readings.

The intrinsic heterogeneity of the rock glacier was exacerbated by the site disturbances resulting from historic mining operations. The site conditions necessary for the profiler EMP-400™ to compute the apparent-conductivity of the subsurface were not satisfied at the Upper Camp Bird rock glacier. Thus, the EMI is not an appropriate instrument to resolve the internal structure of the Upper Camp Bird rock glacier.

The time-domain instrument (G-TEM™) is more challenging to operate. Moving the equipment from one station to the next requires a team of people on the rugged surface of a rock glacier. The minimal disadvantages associated with the use of this system are outweighed by numerous advantages. The G-TEM™ uses a layered Earth model and reaches great depths of penetration. These characteristics are particularly important to determine the internal composition of a highly heterogeneous feature. Additionally, the instrument seems to be averaging out the small-scale environmental conditions that affected the EMI readings, providing promising results even with the initial 1D models presented in this study. The G-TEM™ proved to be an adequate instrument to map the distribution of the electrical resistivity at depth at the Upper Camp Bird rock glacier.

Data collected using the G-TEM™ system can be used to produce 2D and 3D models. The 2D and 3D models are more complex, and heavily reliant on mathematical skills. In a 3D environment such as a rock glacier, 3D models could provide more accurate interpretations. Thus, future work should involve an interdisciplinary team of researchers to produce a 3D model of the Upper Camp Bird rock glacier.

5.4. References

Giardino, J. R., Houser, C. (Eds.), 2015. Principles and dynamics of the Critical Zone (Vol. 19). Elsevier.

APPENDIX A

G-TEM 1D models for all stations

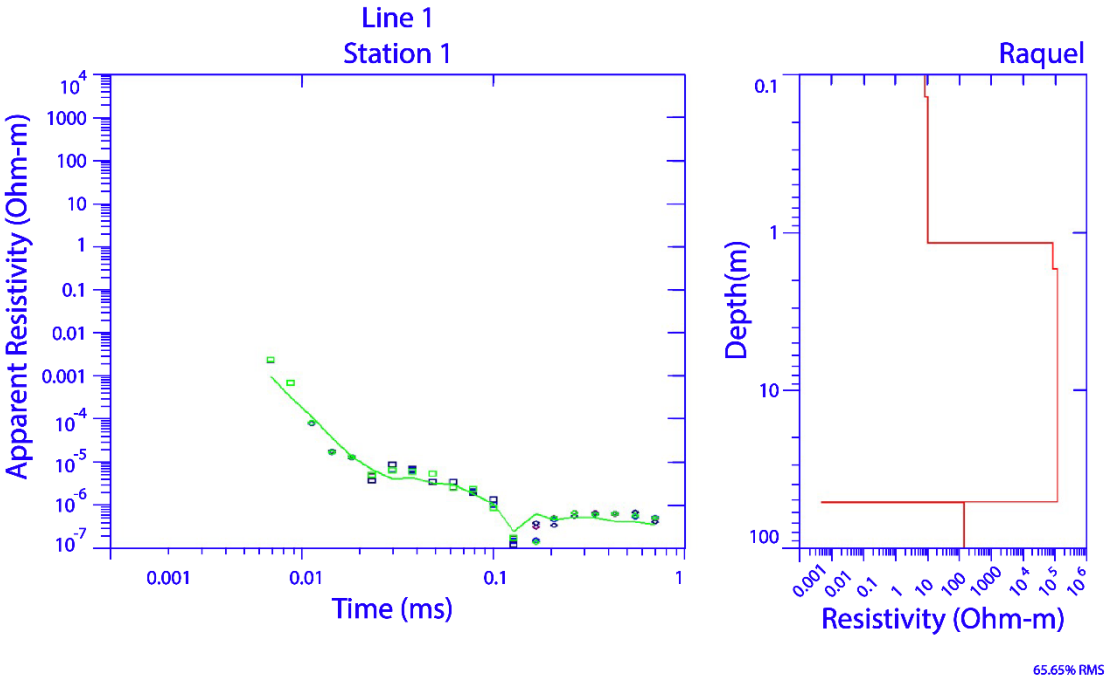

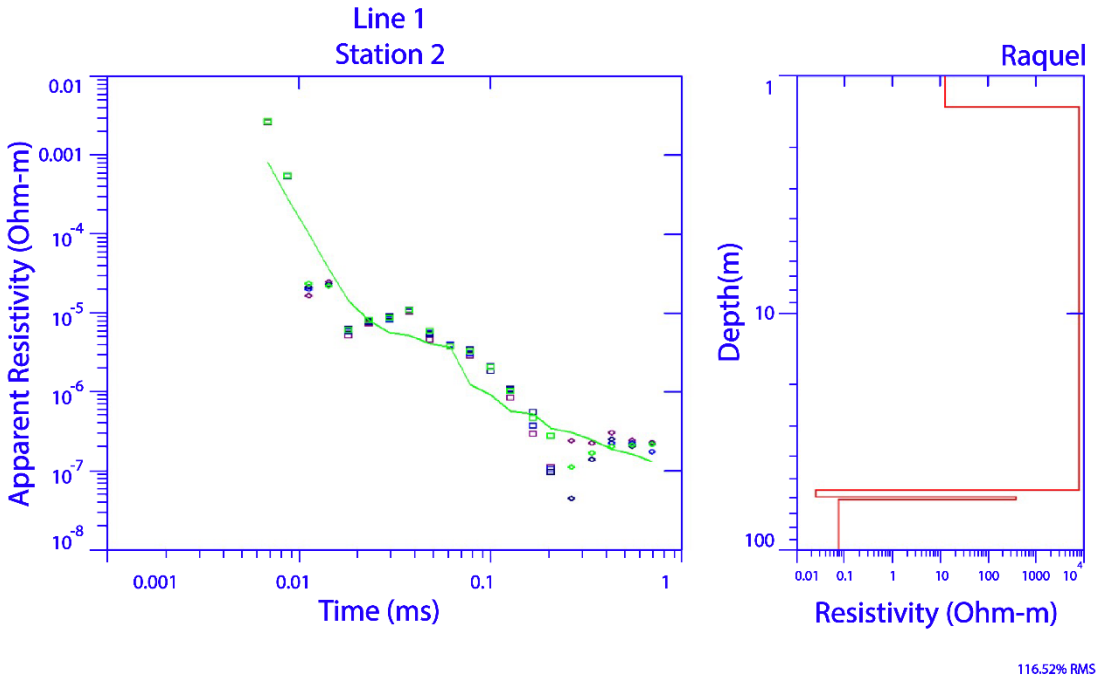

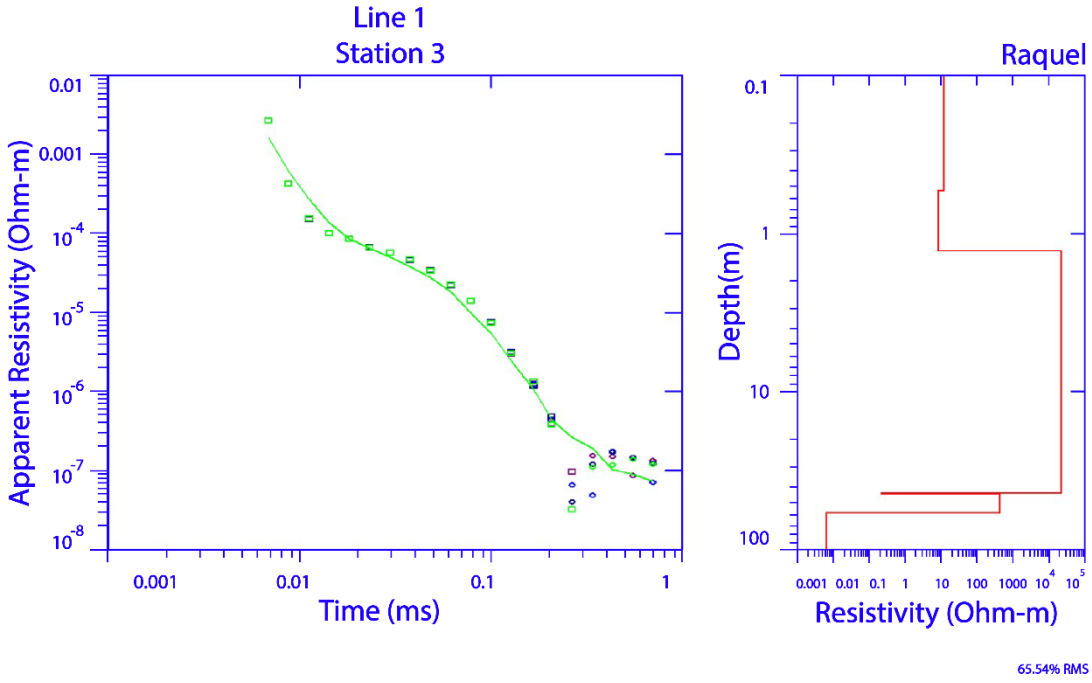
Line 1
Station 3
Raquel
Apparent Resistivity (Ohm-m)
Time (ms)
Depth(m)
Resistivity (Ohm-m)
65.54% RMS

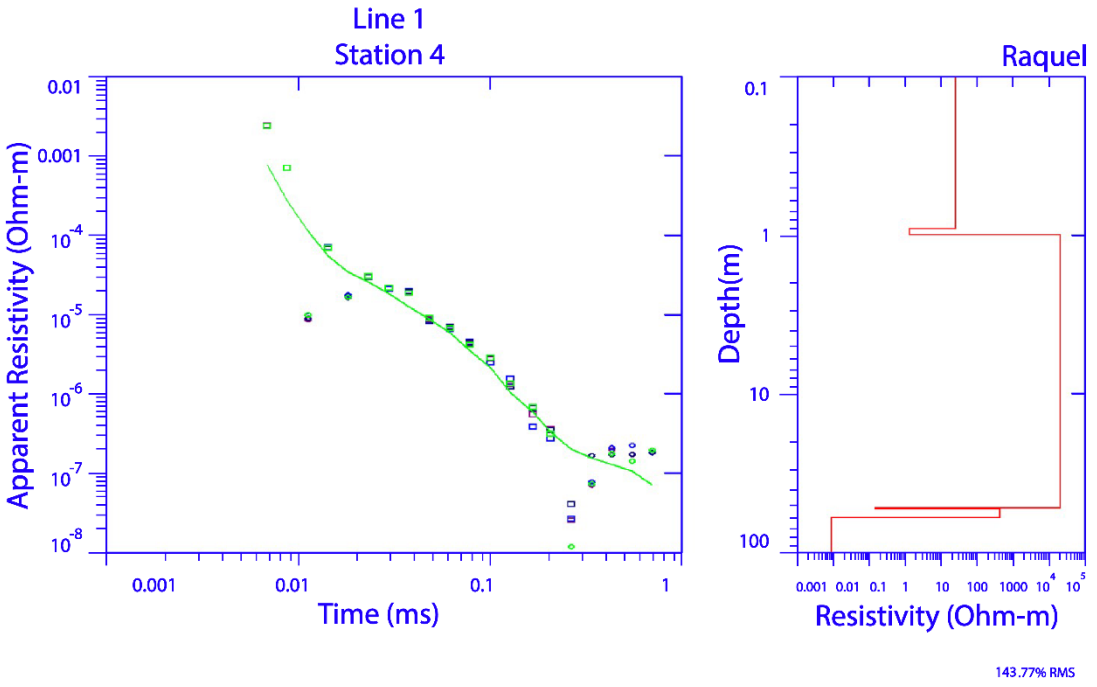
Line 1
Station 4
Raquel
Apparent Resistivity (Ohm-m)
Time (ms)
Depth(m)
Resistivity (Ohm-m)
143.77% RMS

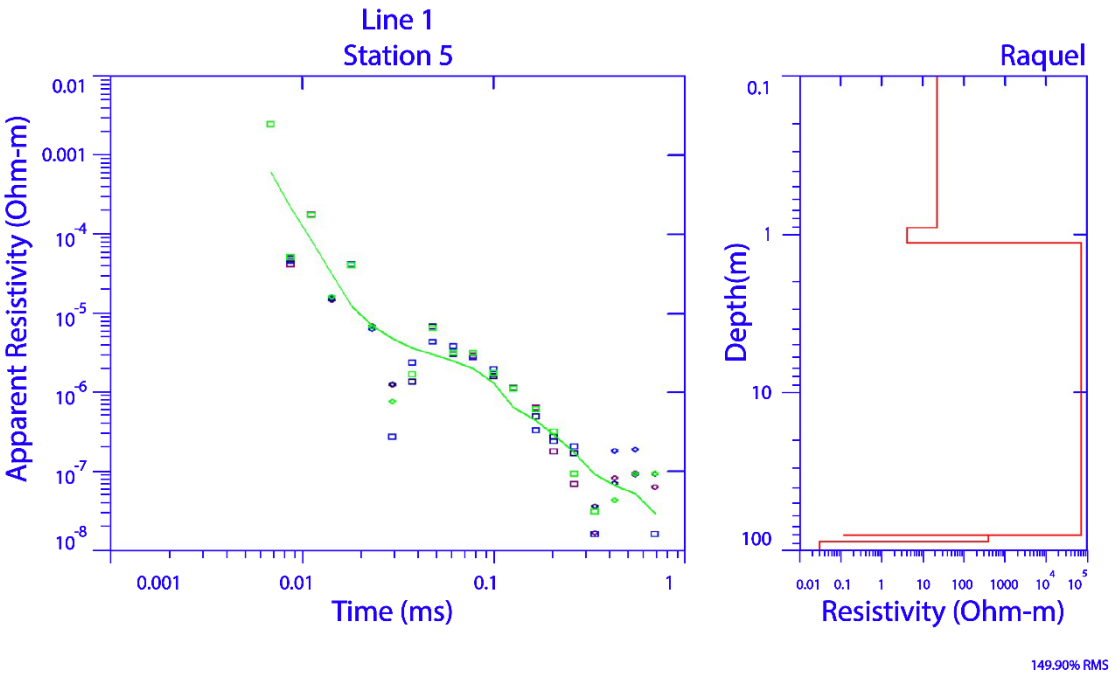
Line 1
Station 5
Raquel
Apparent Resistivity (Ohm-m)
Time (ms)
Depth(m)
Resistivity (Ohm-m)
149.90% RMS

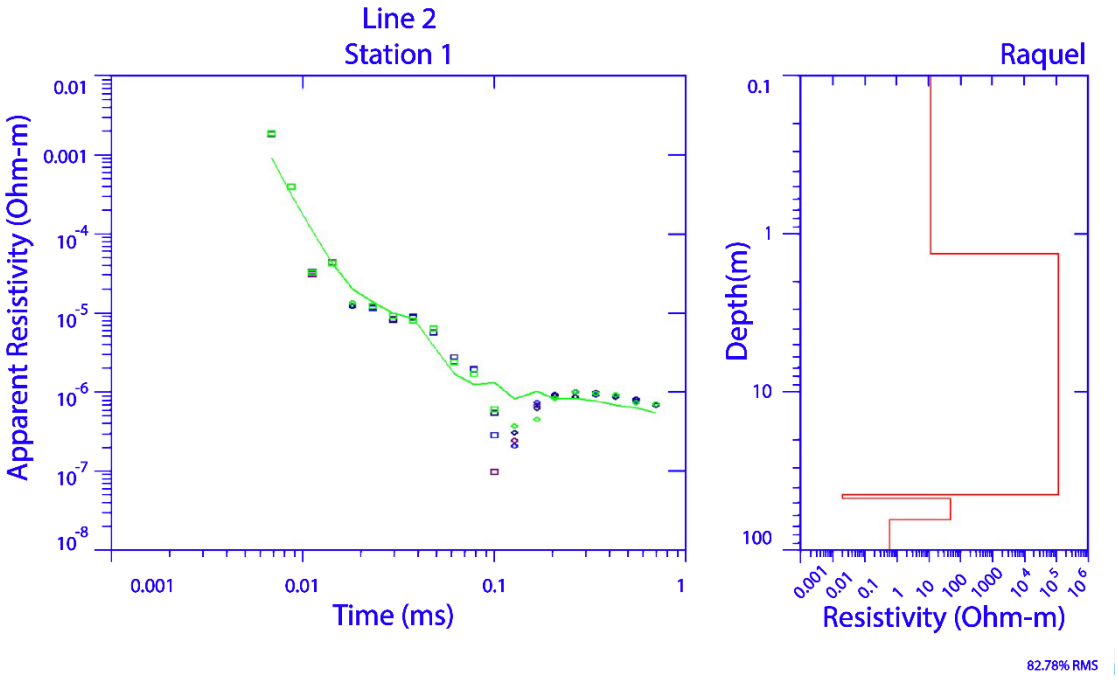
Line 2
Station 1
Raquel
Apparent Resistivity (Ohm-m)
Time (ms)
Depth(m)
Resistivity (Ohm-m)
82.78% RMS

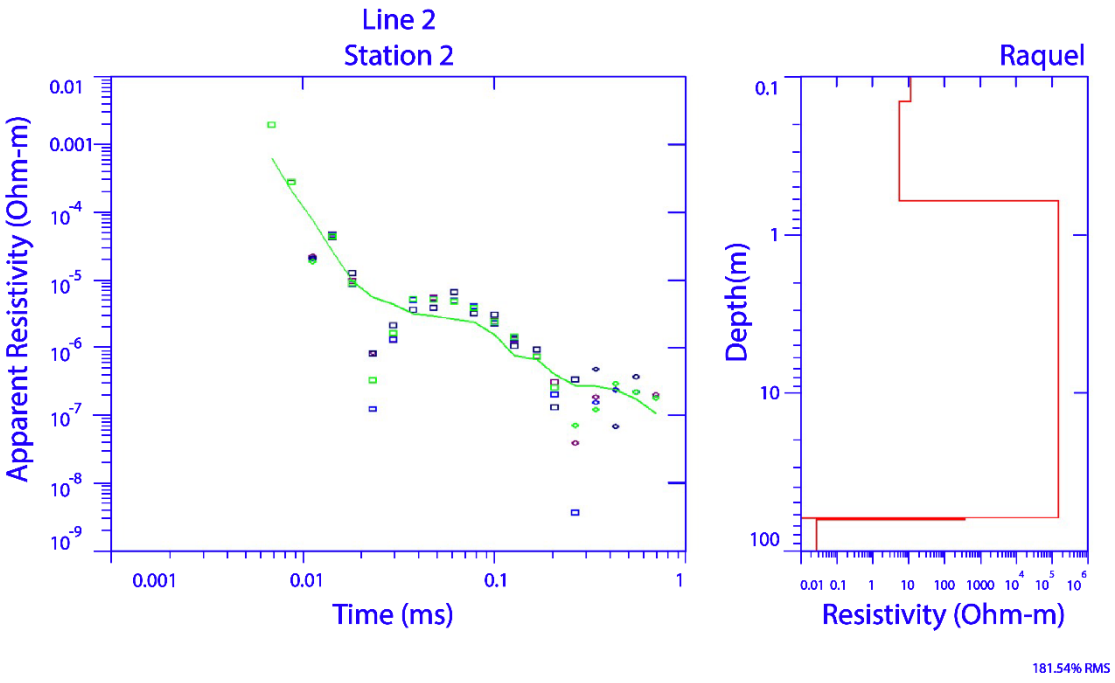
Line 2
Station 2
Raquel
Apparent Resistivity (Ohm-m)
Time (ms)
Depth(m)
Resistivity (Ohm-m)
181.54% RMS

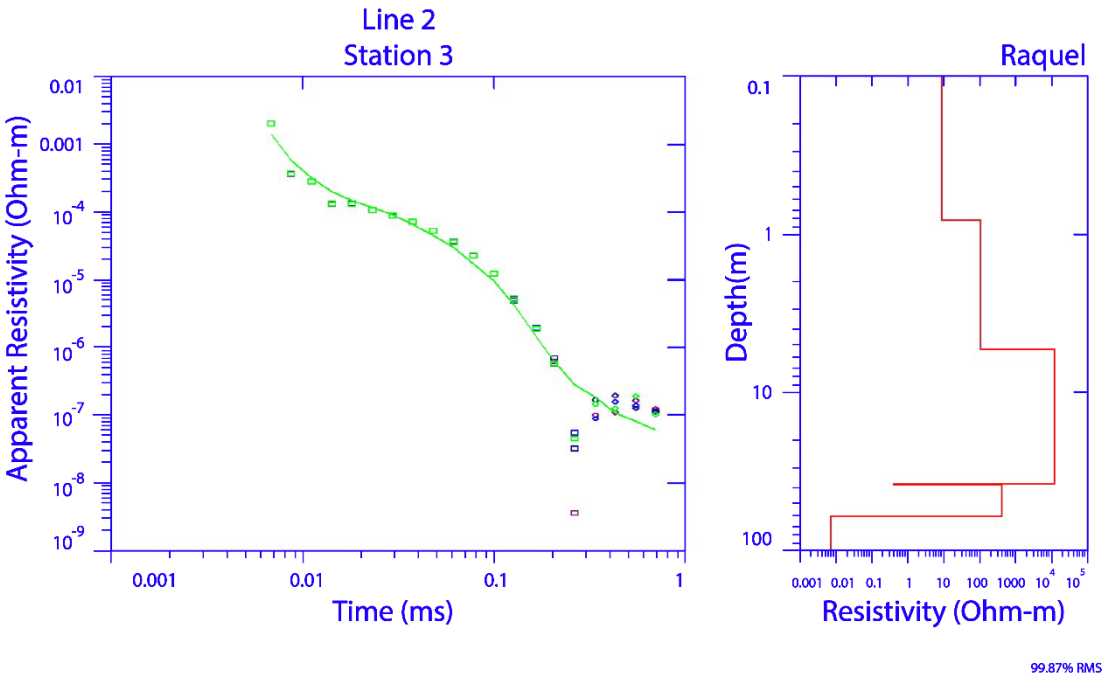
Line 2
Station 3
Raquel
Apparent Resistivity (Ohm-m)
Time (ms)
Depth(m)
Resistivity (Ohm-m)
99.87% RMS

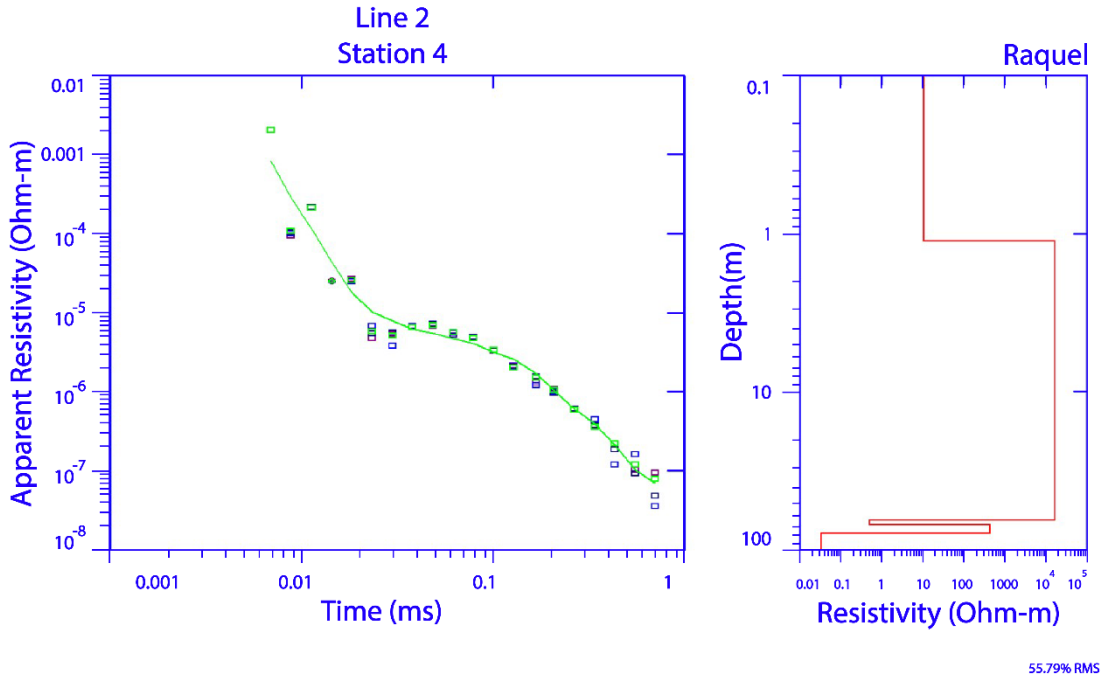
Line 2
Station 4
Raquel
Apparent Resistivity (Ohm-m)
Time (ms)
Depth(m)
Resistivity (Ohm-m)
55.79% RMS

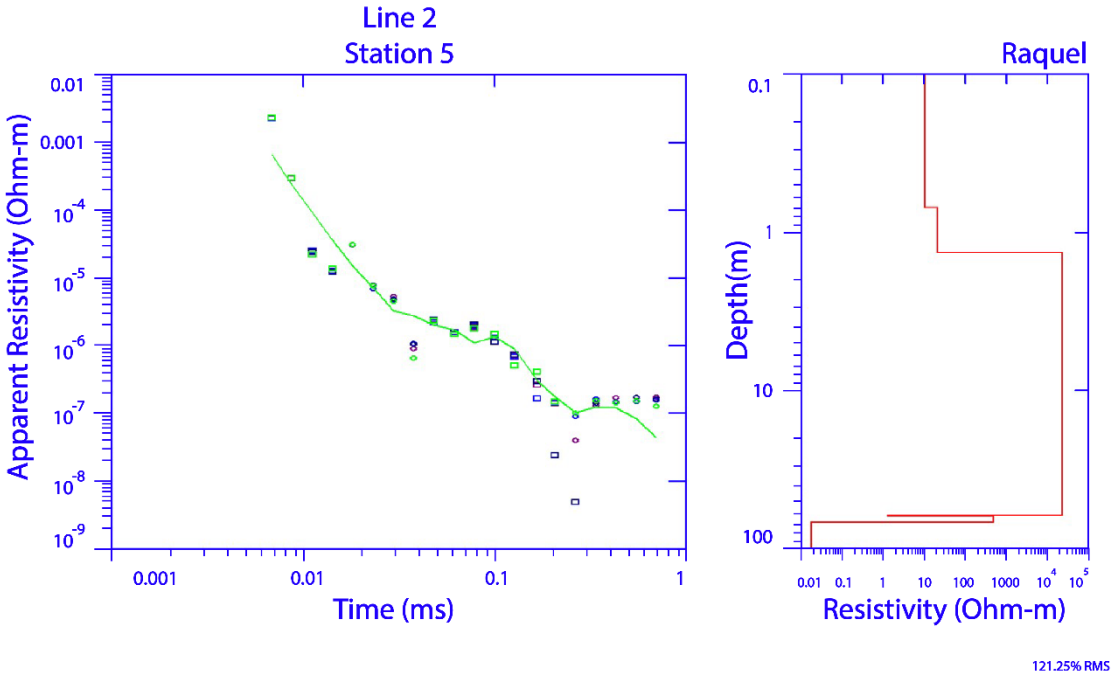
Line 2
Station 5
Raquel
Apparent Resistivity (Ohm-m)
Time (ms)
Depth(m)
Resistivity (Ohm-m)
121.25% RMS

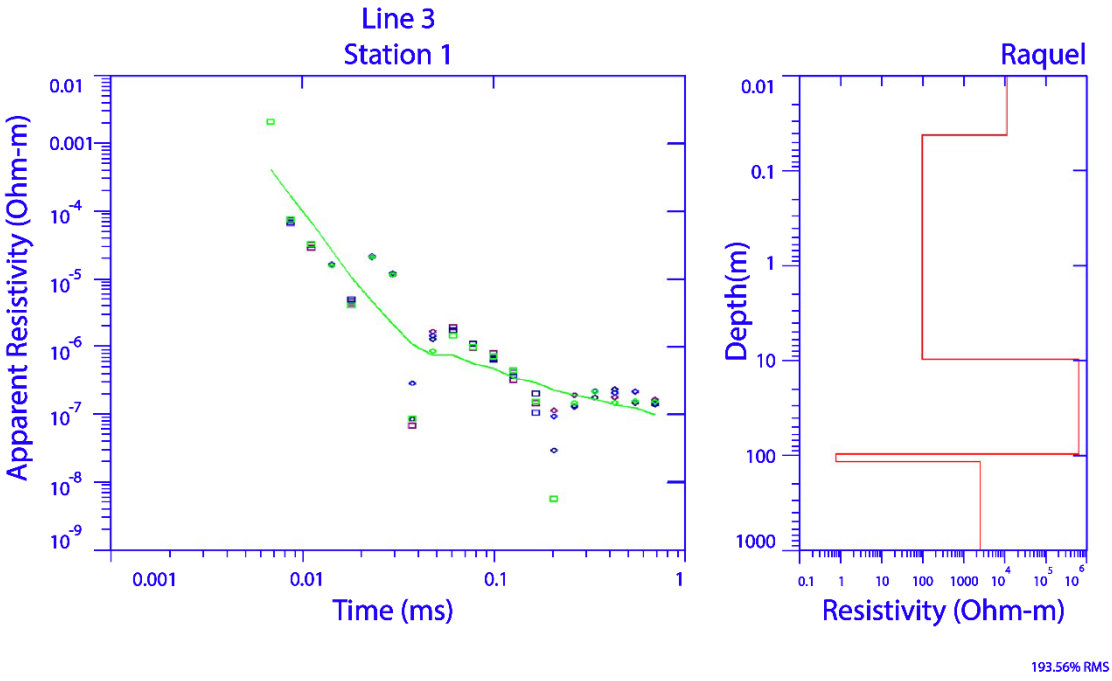
Line 3
Station 1
Raquel
Apparent Resistivity (Ohm-m)
Time (ms)
Depth(m)
Resistivity (Ohm-m)
193.56% RMS

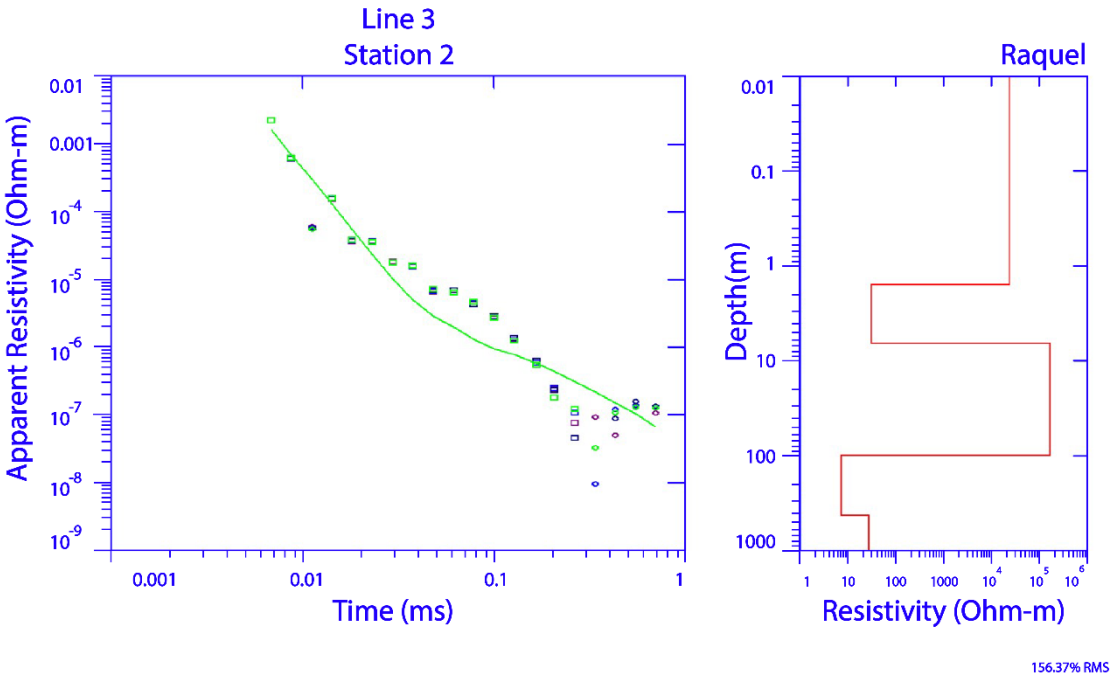
Line 3
Station 2
Raquel
Apparent Resistivity (Ohm-m)
Time (ms)
Depth(m)
Resistivity (Ohm-m)
156.37% RMS

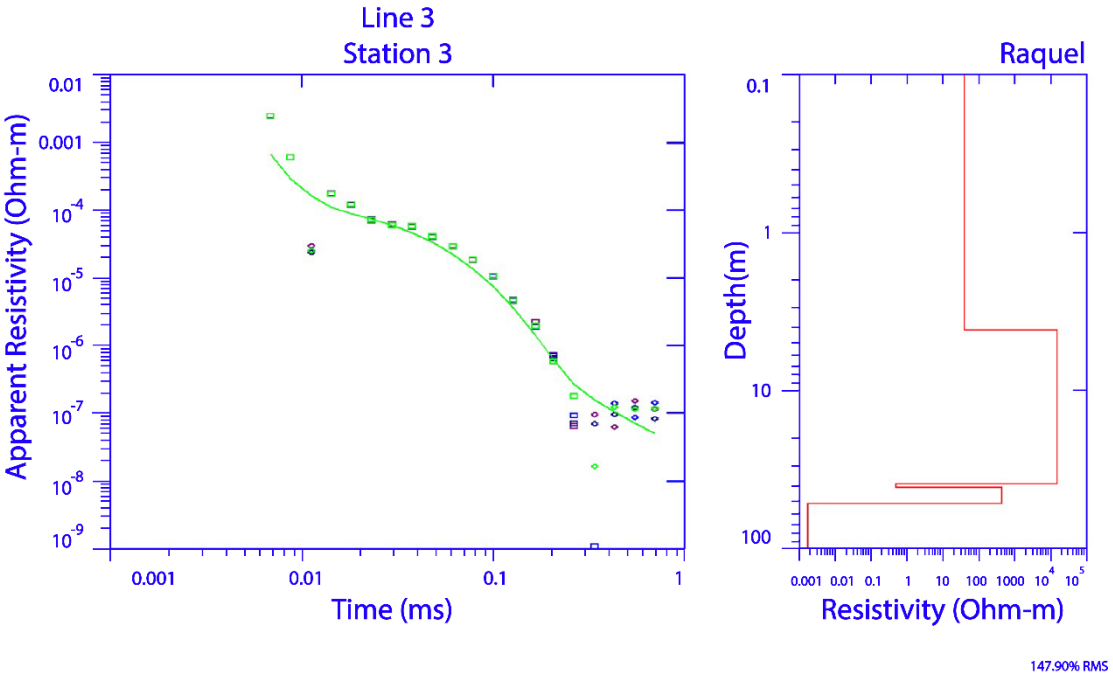
Line 3
Station 3
Raquel
Apparent Resistivity (Ohm-m)
Time (ms)
Depth(m)
Resistivity (Ohm-m)
147.90% RMS

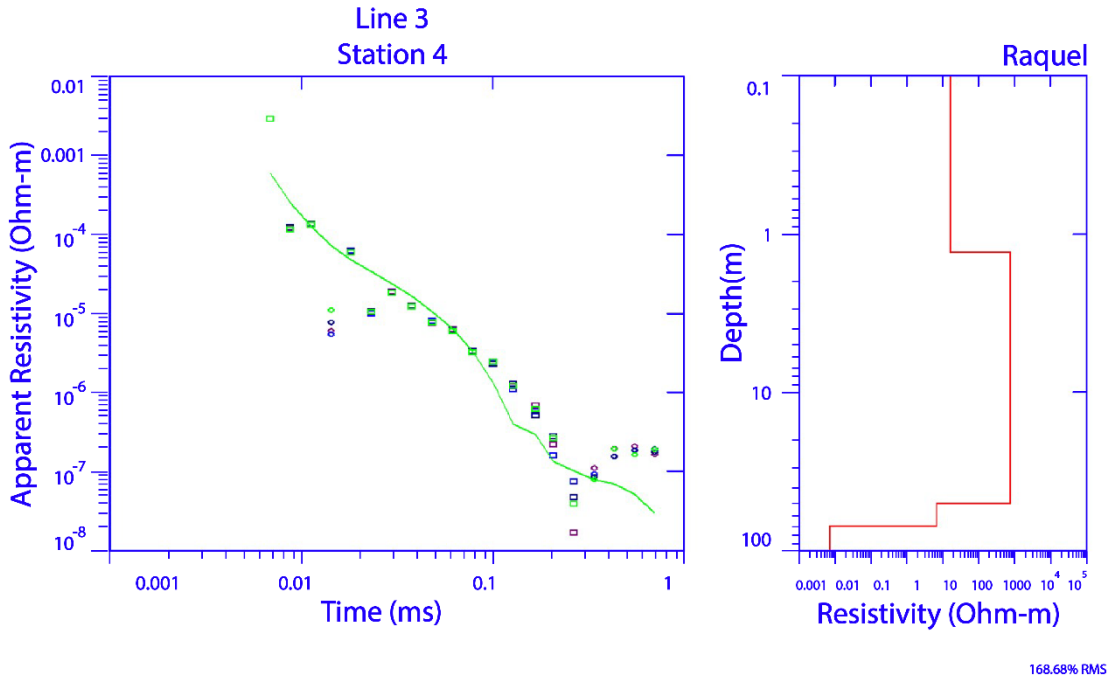
Line 3
Station 4
Raquel
Apparent Resistivity (Ohm-m)
Time (ms)
Depth(m)
Resistivity (Ohm-m)
168.68% RMS

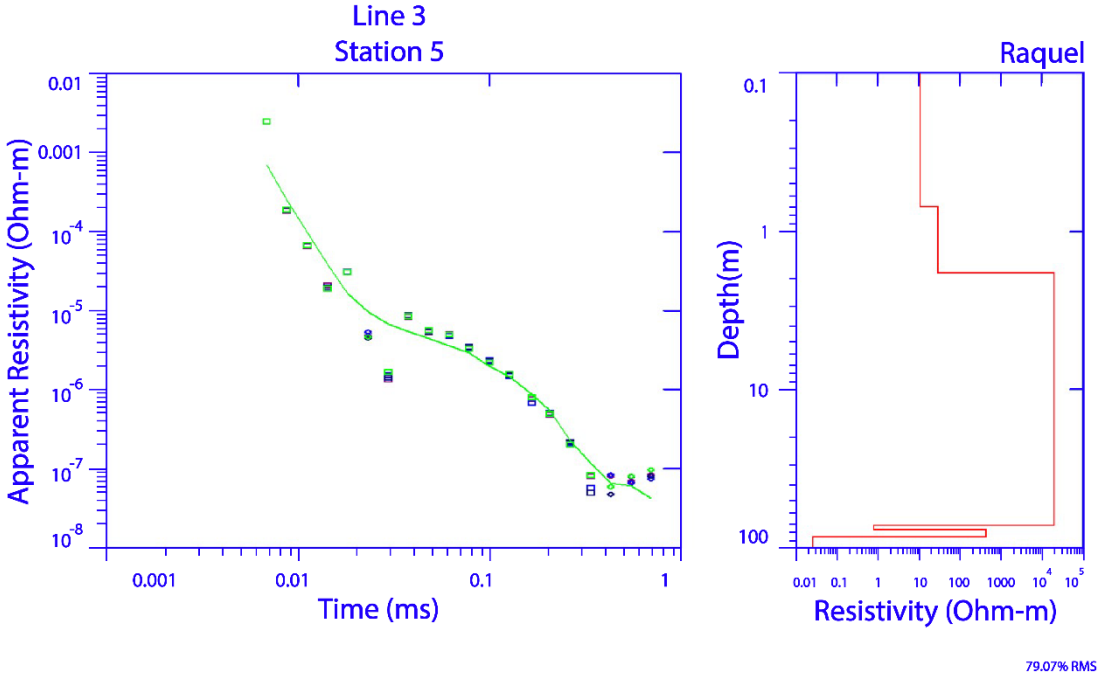
Line 3
Station 5
Raquel
Apparent Resistivity (Ohm-m)
Time (ms)
Depth(m)
Resistivity (Ohm-m)
79.07% RMS

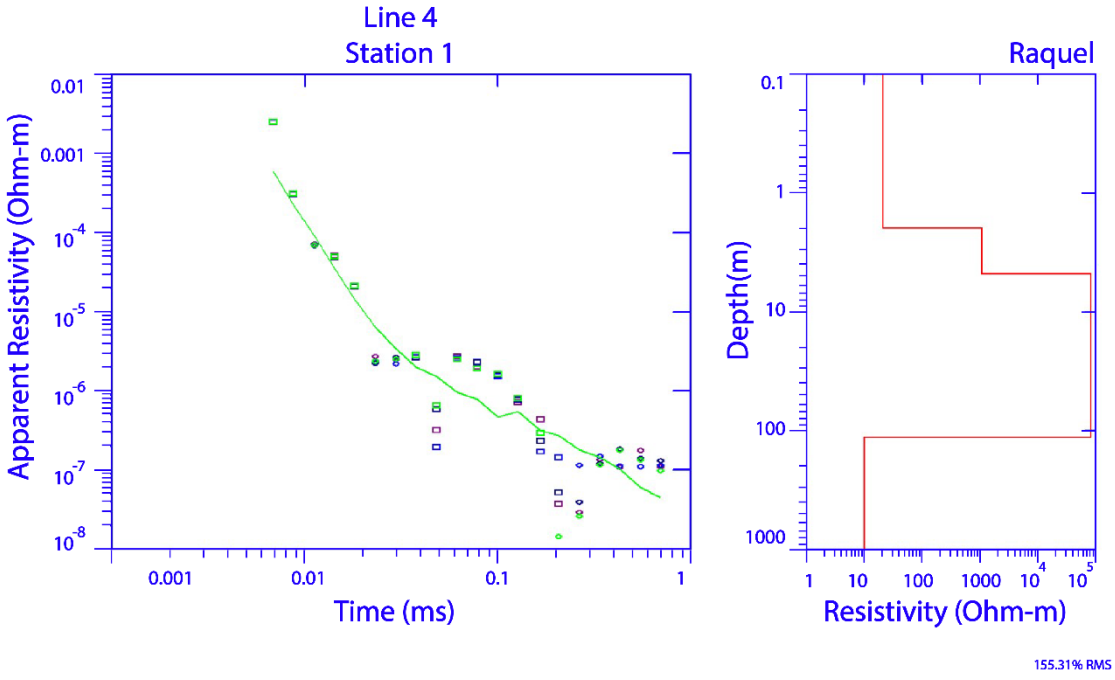
Line 4
Station 1
Raquel
Apparent Resistivity (Ohm-m)
Time (ms)
Depth(m)
Resistivity (Ohm-m)
155.31% RMS

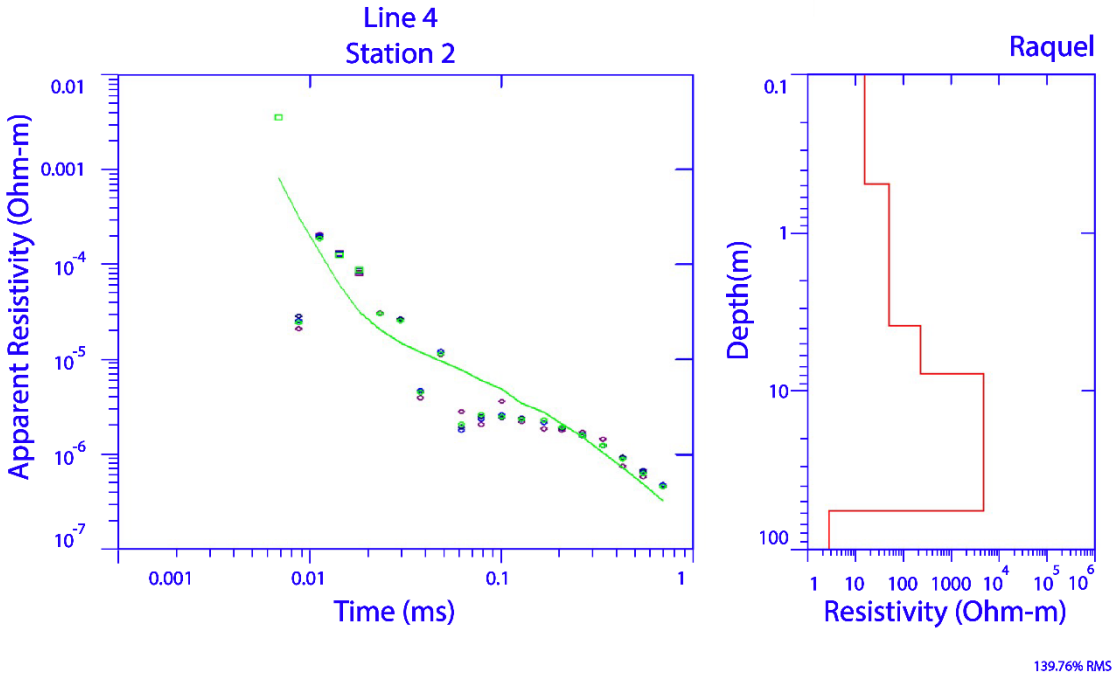
Line 4
Station 2
Raquel
Apparent Resistivity (Ohm-m)
Time (ms)
Depth(m)
Resistivity (Ohm-m)
139.76% RMS

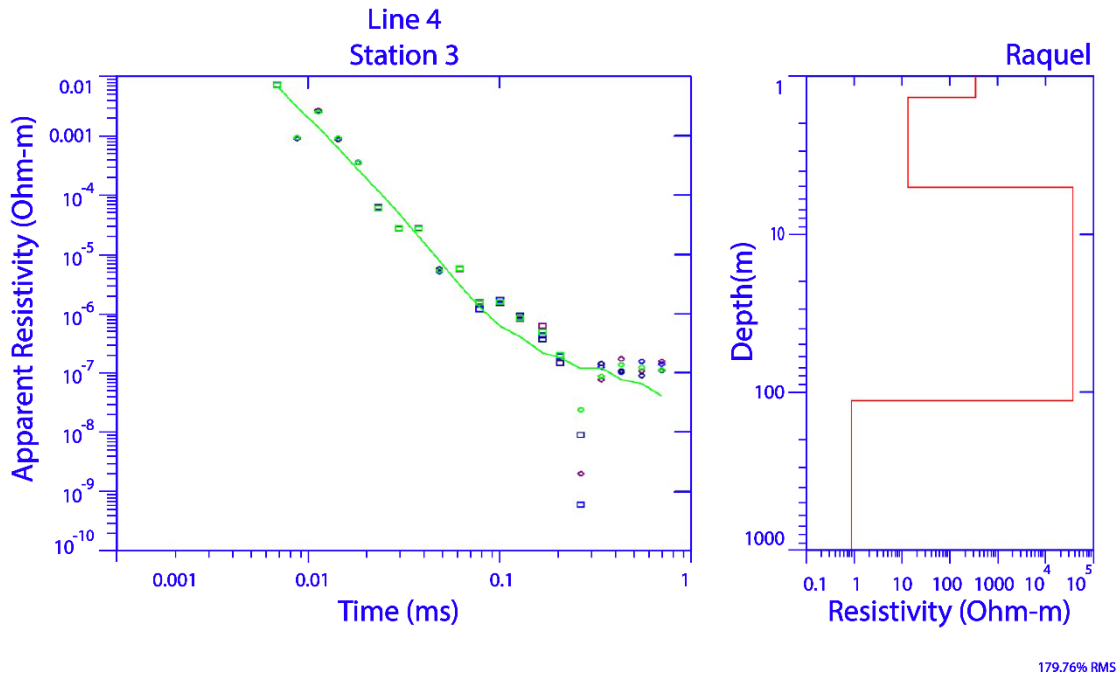
Line 4
Station 3
Raquel
Apparent Resistivity (Ohm-m)
Time (ms)
Depth(m)
Resistivity (Ohm-m)
179.76% RMS

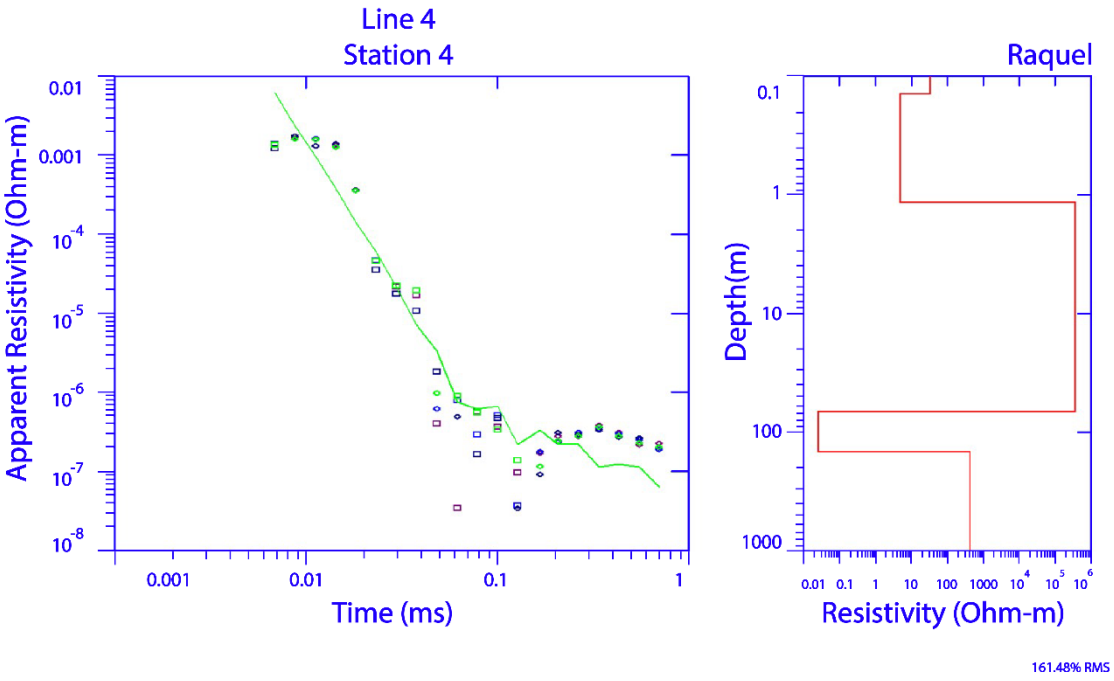
Line 4
Station 4
Raquel
Apparent Resistivity (Ohm-m)
Time (ms)
Depth(m)
Resistivity (Ohm-m)
161.48% RMS

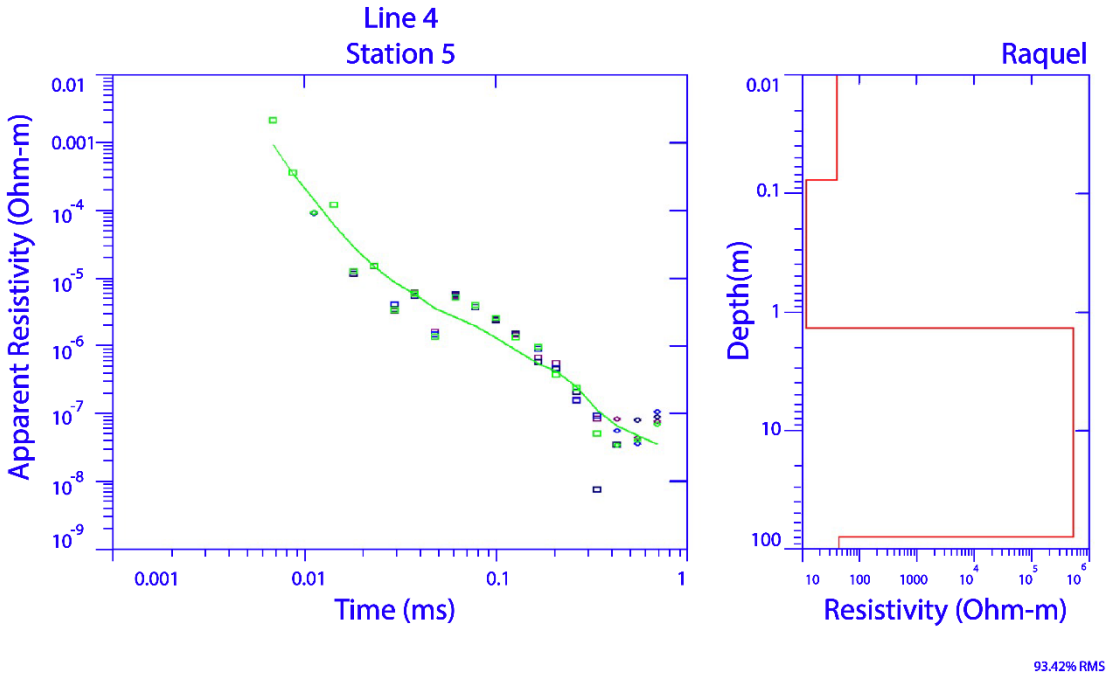
Line 4
Station 5
Raquel
Apparent Resistivity (Ohm-m)
Time (ms)
Depth(m)
Resistivity (Ohm-m)
93.42% RMS

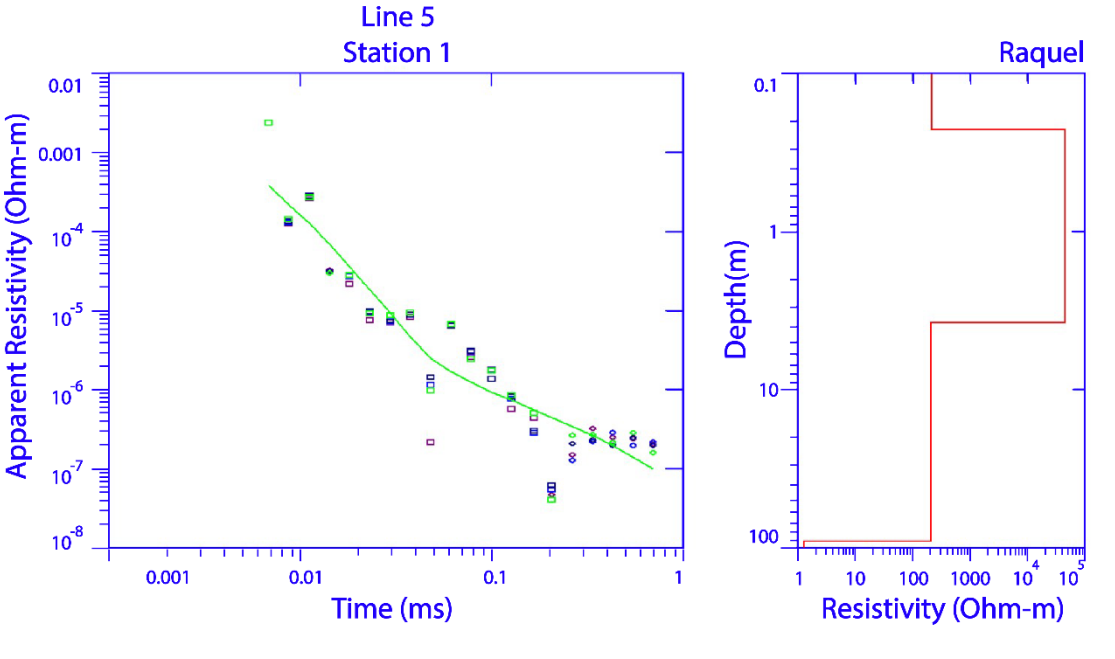
Line 5
Station 1
Raquel
Apparent Resistivity (Ohm-m)
Time (ms)
Depth(m)
Resistivity (Ohm-m)
152.16% RMS

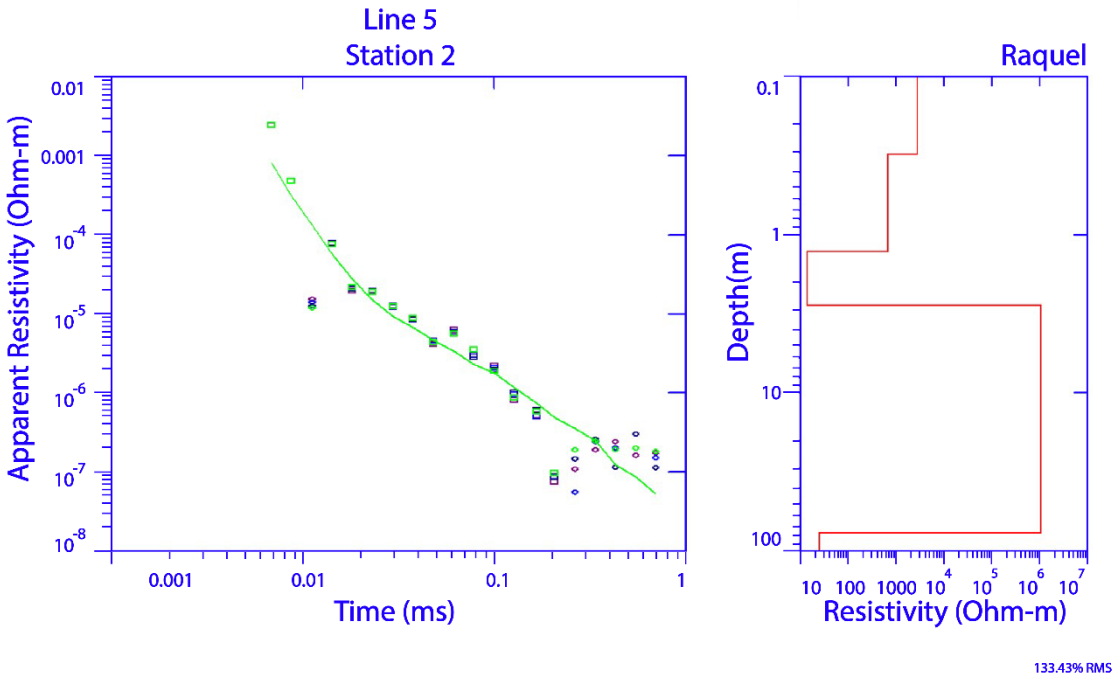
Line 5
Station 2
Raquel
Apparent Resistivity (Ohm-m)
Time (ms)
Depth(m)
Resistivity (Ohm-m)
133.43% RMS

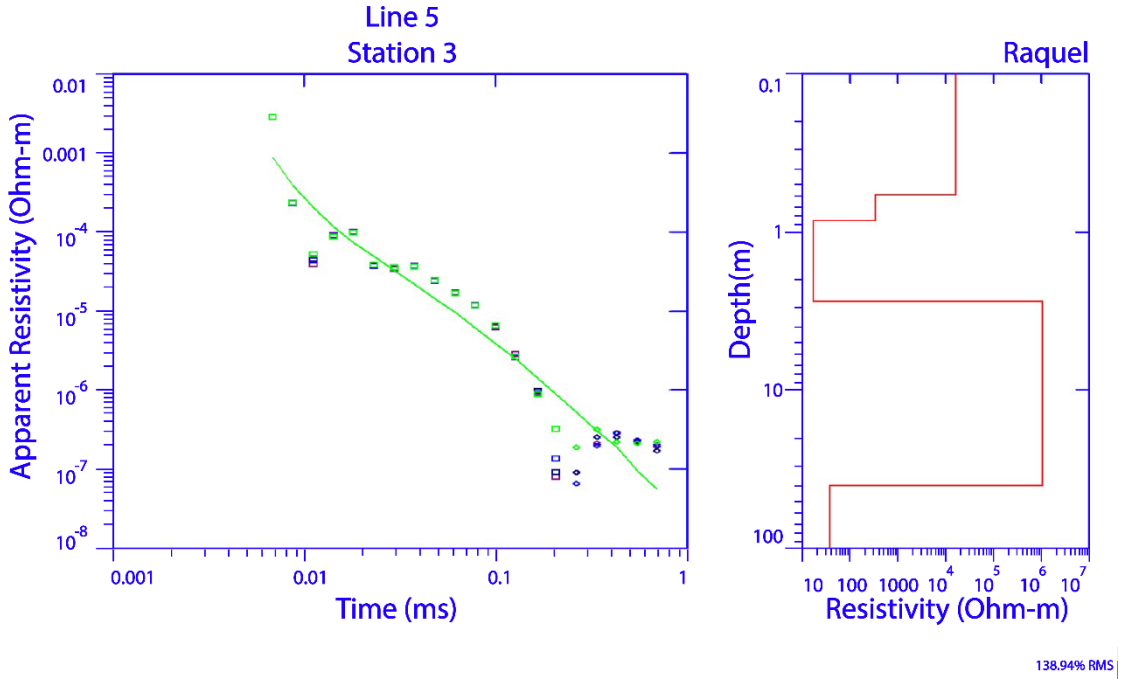
Line 5
Station 3
Raquel
Apparent Resistivity (Ohm-m)
Time (ms)
Depth(m)
Resistivity (Ohm-m)
138.94% RMS

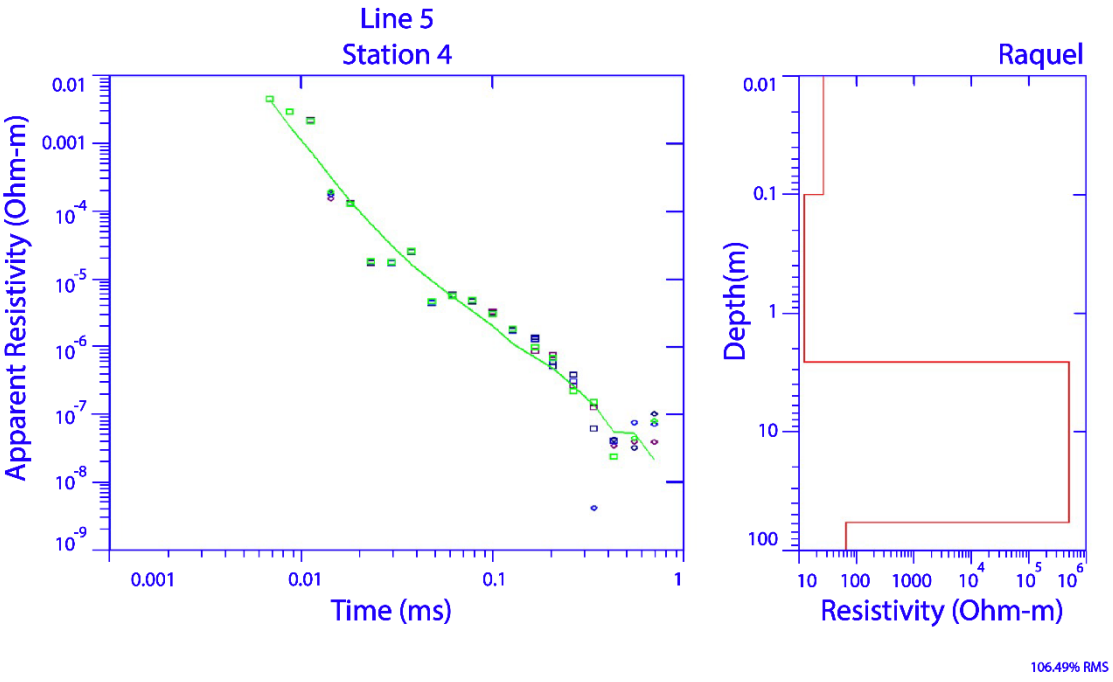
Line 5
Station 4
Raquel
Apparent Resistivity (Ohm-m)
Time (ms)
Depth(m)
Resistivity (Ohm-m)
106.49% RMS

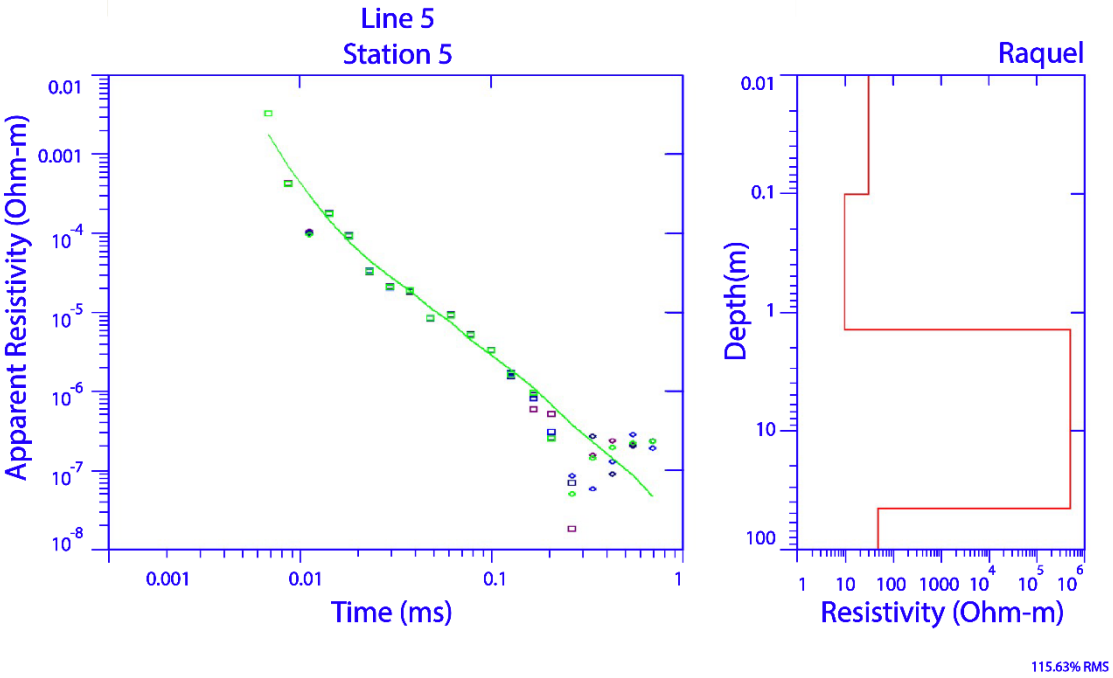
Line 5
Station 5
Raquel
Apparent Resistivity (Ohm-m)
Time (ms)
Depth(m)
Resistivity (Ohm-m)
115.63% RMS

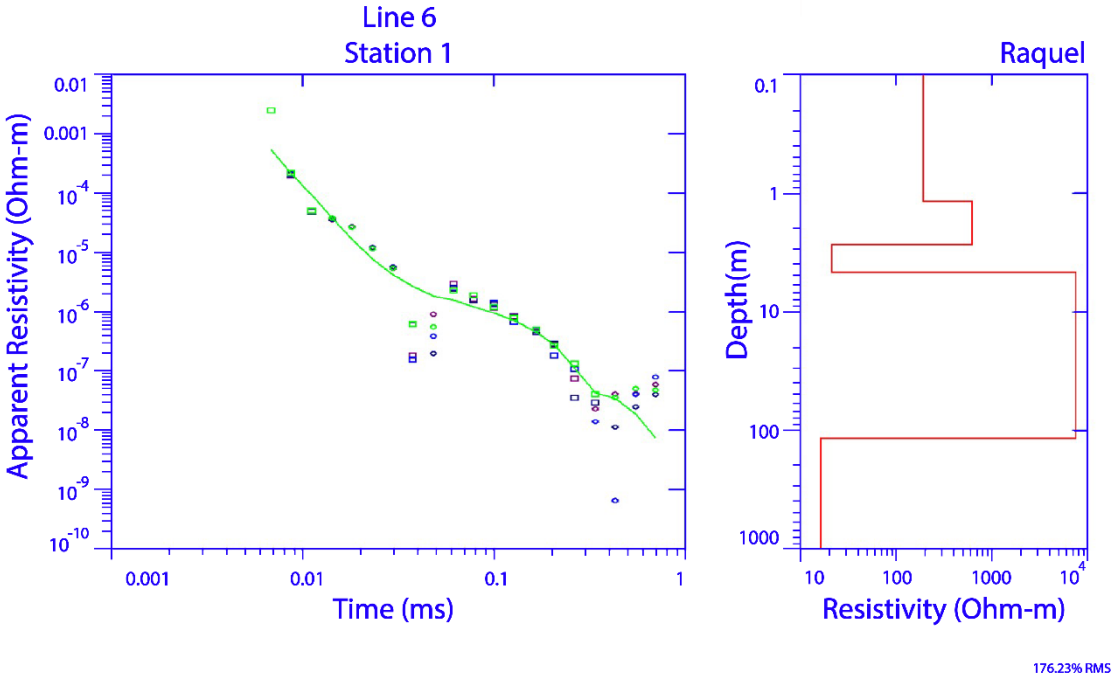
Line 6
Station 1
Raquel
Apparent Resistivity (Ohm-m)
Time (ms)
Depth(m)
Resistivity (Ohm-m)
176.23% RMS

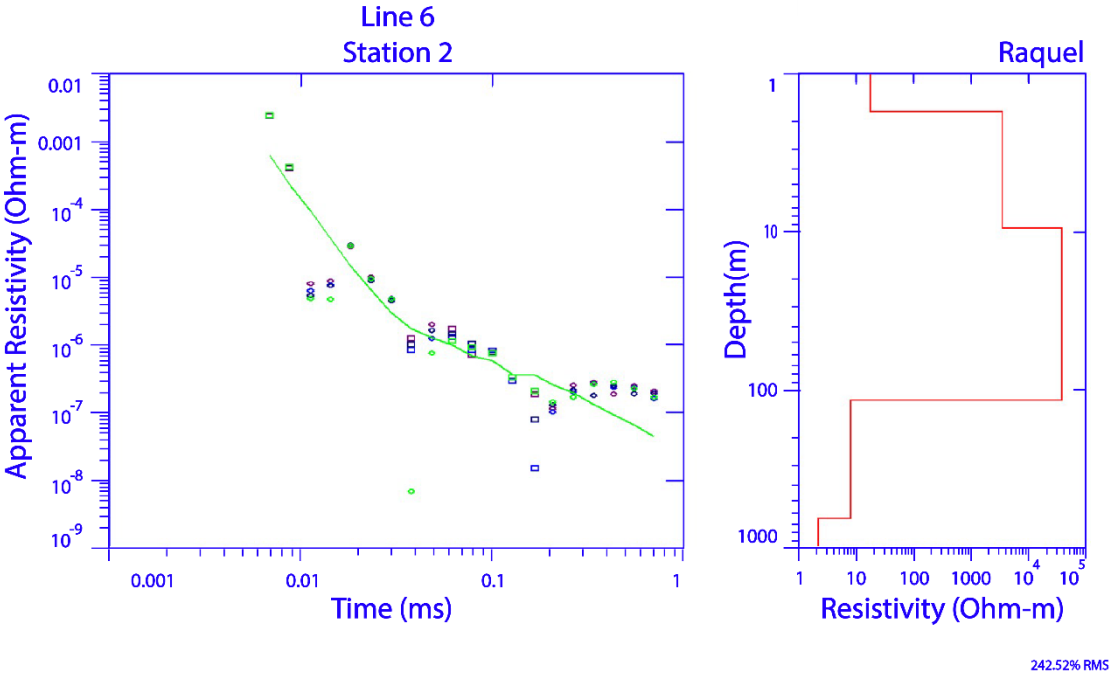
Line 6
Station 2
Raquel
Apparent Resistivity (Ohm-m)
Time (ms)
Depth(m)
Resistivity (Ohm-m)
242.52% RMS

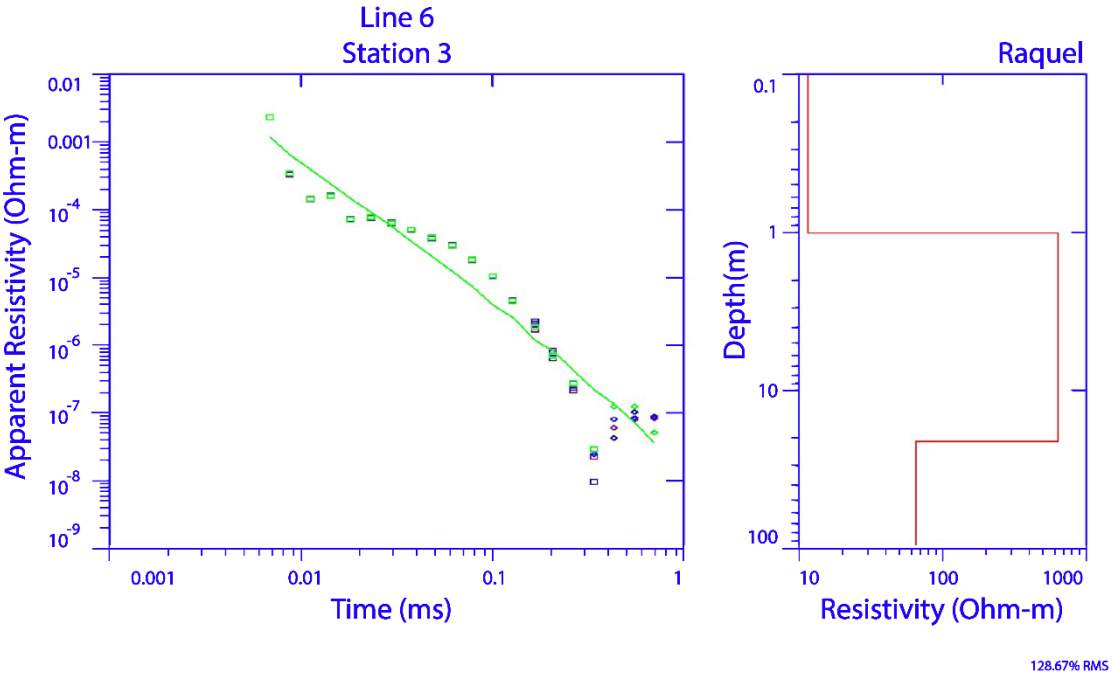
Line 6
Station 3
Raquel
Apparent Resistivity (Ohm-m)
Time (ms)
Depth(m)
Resistivity (Ohm-m)
128.67% RMS

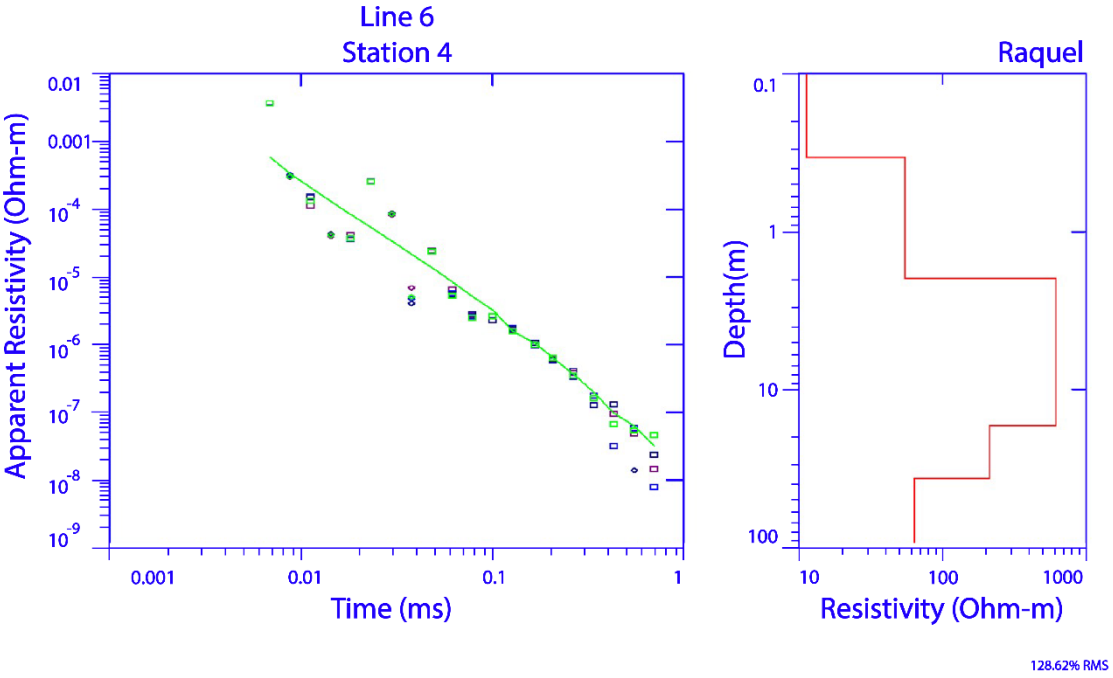
Line 6
Station 4
Raquel
Apparent Resistivity (Ohm-m)
Time (ms)
Depth(m)
Resistivity (Ohm-m)
128.62% RMS

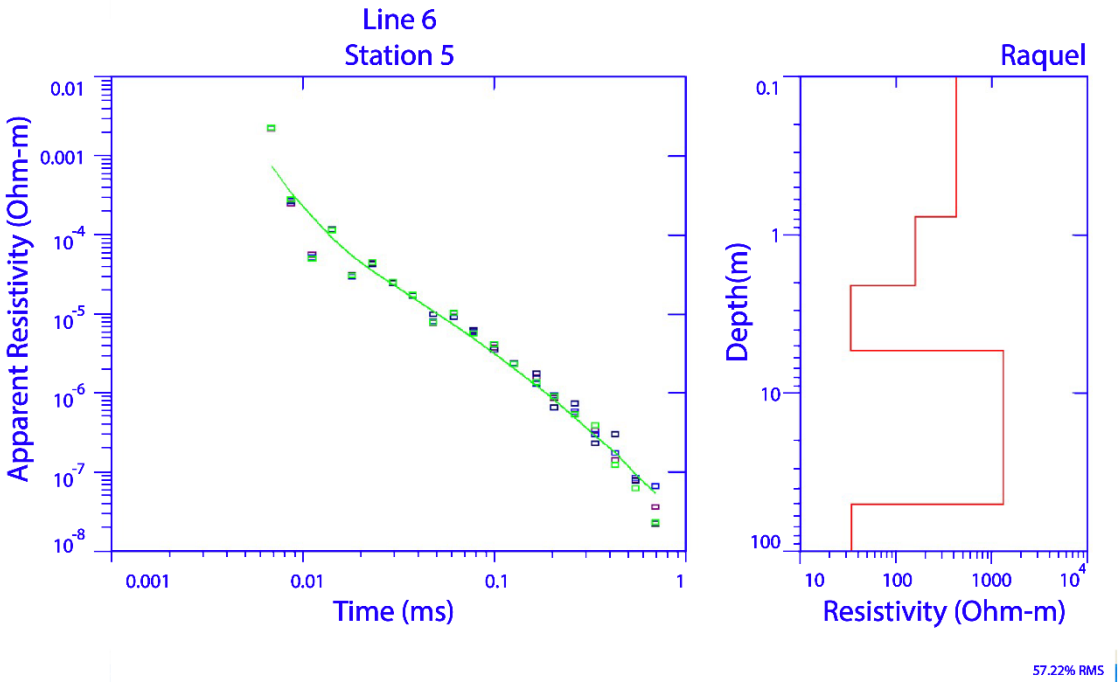
Line 6
Station 5
Raquel
Apparent Resistivity (Ohm-m)
Time (ms)
Depth(m)
Resistivity (Ohm-m)
57.22% RMS

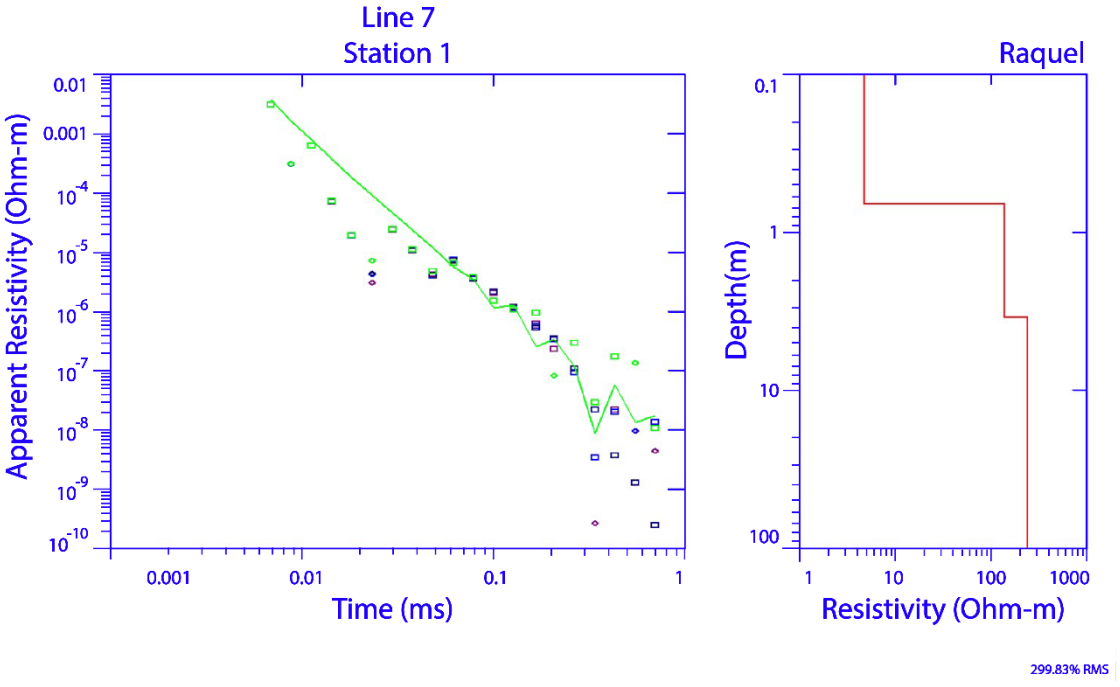
Line 7
Station 1
Raquel
Apparent Resistivity (Ohm-m)
Time (ms)
Depth(m)
Resistivity (Ohm-m)
299.83% RMS

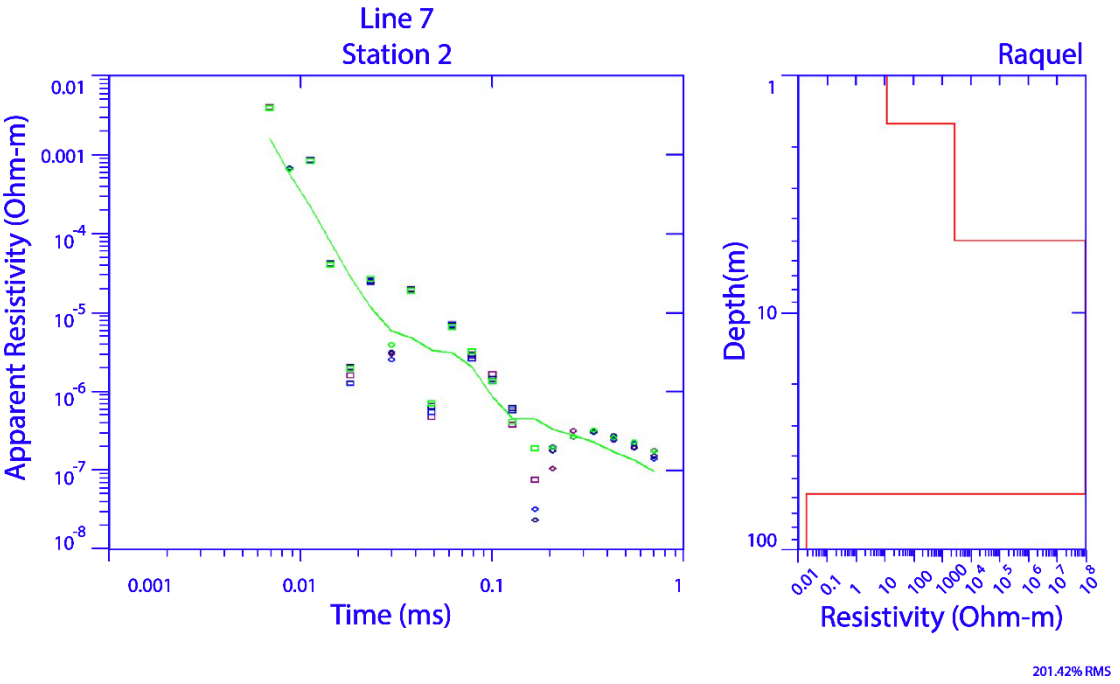
Line 7
Station 2
Raquel
Apparent Resistivity (Ohm-m)
Time (ms)
Depth(m)
Resistivity (Ohm-m)
201.42% RMS

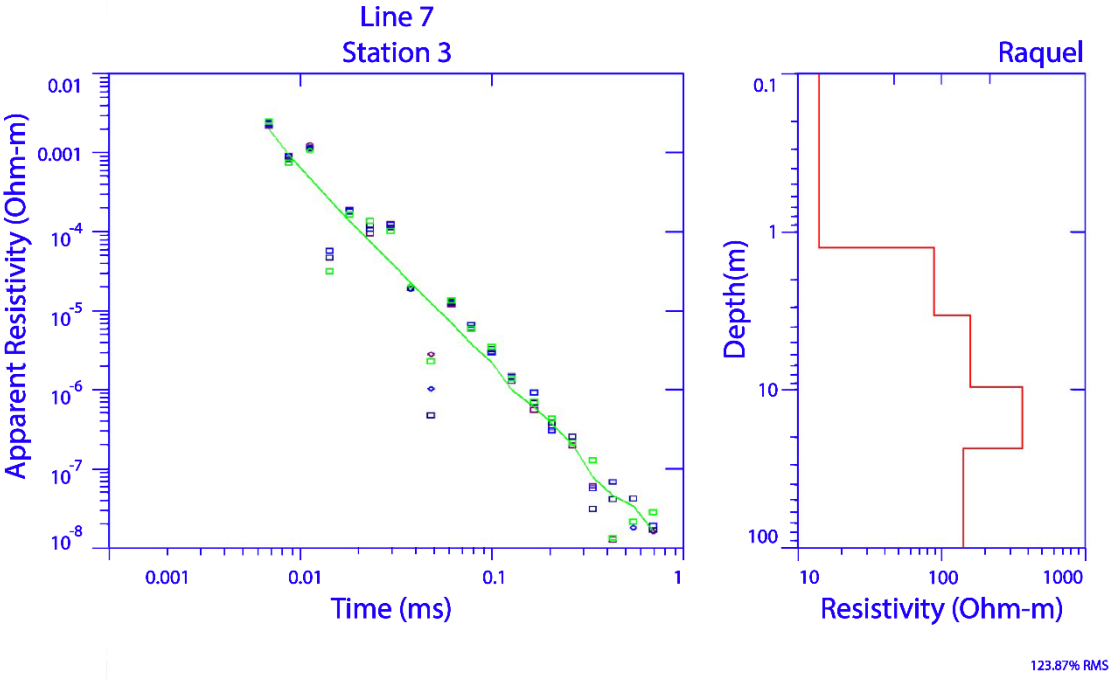
Line 7
Station 3
Raquel
Apparent Resistivity (Ohm-m)
Time (ms)
Depth(m)
Resistivity (Ohm-m)
123.87% RMS

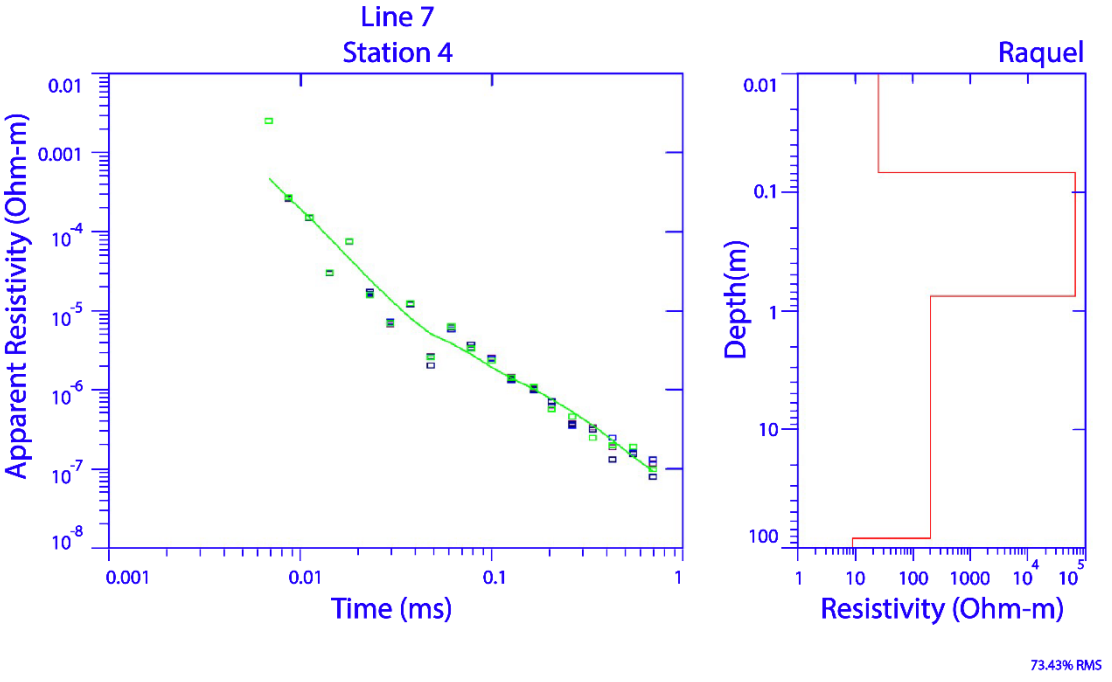
Line 7
Station 4
Raquel
Apparent Resistivity (Ohm-m)
Time (ms)
Depth(m)
Resistivity (Ohm-m)
73.43% RMS

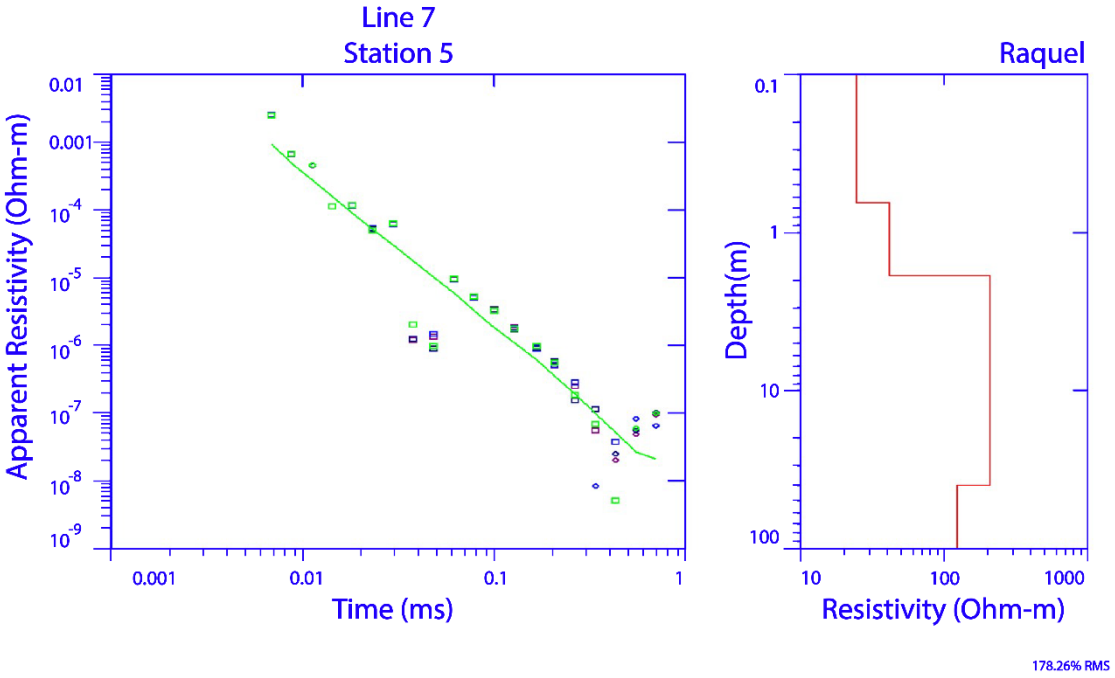
Line 7
Station 5
Raquel
Apparent Resistivity (Ohm-m)
0.01
0.001
10-4
10-5
10-6
10-7
10-8
10-9
0.001
0.01
0.1
1
Time (ms)
Depth(m)
0.1
1
10
100
10
100
1000
Resistivity (Ohm-m)
178.26% RMS

APPENDIX B

G-TEM 1D models for all stations

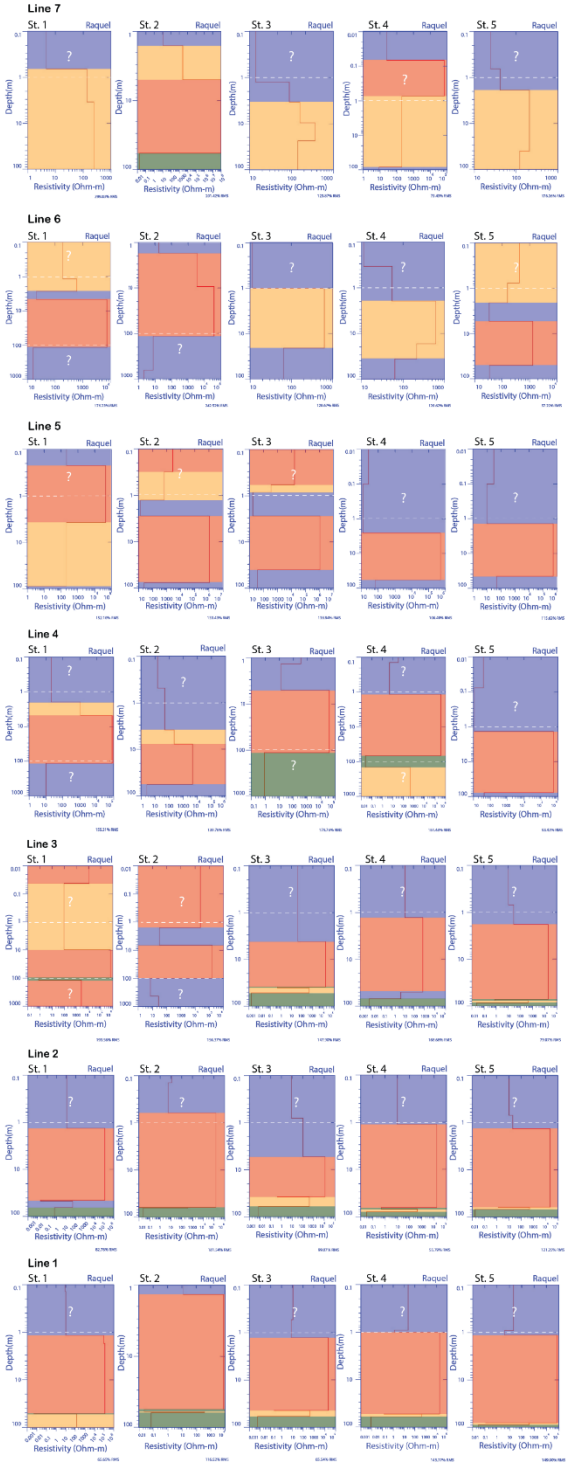

Legend

Resistivity ranges	Interpreted material
1-100 Ohm-m	Volcanic rocks
100-1000 Ohm-m	Thawing zone
10^3-10^6 Ohm-m	Permafrost
0.001-1 Ohm-m	Hydrothermally altered rocks

Interpretations above 1 m depth are less reliable.
Instrument resolves depths between ~1-96m.

Diagram showing the location of the lines and stations

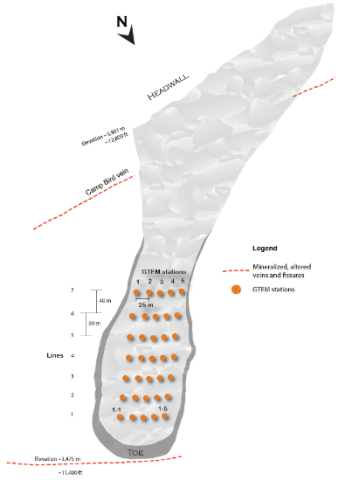

APPENDIX C

Profiler EMP-400 data for all lines

Instrument settings	**Data collected**									
Line 2										
GSSI Profiler Ver.#, 1 0 8 9	**Record #**	**InPhase[1000]**	**Quad[1000]**	**Conductivity [1000]**	**InPhase[8000]**	**Quad[8000]**	**Conductivity [8000]**	**InPhase[15000]**	**Quad[15000]**	**Conductivity[15000]**
GSSI Profiler Firmware Ver.#, 1060	1	-426	-64	-22.094	-608	27	1.146	-654	-42	-0.968
Project Name, rock_glacier	2	-393	-61	-21.04	-579	26	1.113	-624	-40	-0.926
Date, 08/18/2017 14:07:52.000	3	-350	-47	-16.317	-486	45	1.942	-509	-23	-0.555
Units, METRIC	4	-215	-33	-11.678	-286	62	2.664	-296	-13	-0.325
Gps Status, Disabled	5	-94	-24	-8.452	-95	80	3.409	-90	-3	-0.084
Collection Mode, Stationary	6	19	-38	-13.429	-40	61	2.616	-69	-8	-0.208
Grid Type, xLTZ	7	36	-54	-18.72	-93	41	1.735	-140	-19	-0.462
Line Spacing, 50.000	8	69	-67	-23.373	-124	19	0.805	-200	-38	-0.887
Station Spacing, 5.000	9	83	-66	-22.793	-104	13	0.546	-155	-51	-1.192
Mark Spacing, 25.000	10	178	-63	-21.779	-1	11	0.455	-44	-60	-1.378
Xmin, 0.000	11	238	-62	-21.548	53	11	0.453	31	-65	-1.496
Ymin, 240.000	12	293	-65	-22.587	102	13	0.565	80	-66	-1.534
Xmax, 150.000	13	296	-68	-23.601	100	16	0.679	82	-65	-1.512
Ymax, 240.000	14	276	-68	-23.549	83	18	0.789	53	-64	-1.473
Instrument Orientation, VDM (I)	15	249	-66	-22.773	64	20	0.859	20	-67	-1.546
Frequencies:,1000,8000, 15000,	16	203	-63	-21.763	26	20	0.853	-26	-70	-1.605

InPhase Zero Levels:,499,7027,-1,	17	192	-63	-21.715	19	19	0.797	-31	-63	-1.465
Quad Zero Levels:, N/A	18	175	-64	-22.133	-6	17	0.713	-52	-55	-1.28
Number of Stacks:, 16	19	259	-87	-29.947	7	0	0.012	-45	-65	-1.511
Data Smoothing:, ON	20	305	-108	-37.206	-12	-14	-0.64	-81	-85	-1.963
Calibration Height, 0.25	21	353	-128	-44.149	-20	-28	-1.236	-100	-99	-2.265
Power Line Frequency, 60	22	229	-106	-36.675	-78	-12	-0.561	-144	-79	-1.831
	23	110	-86	-29.762	-128	1	0.041	-165	-59	-1.361
	24	58	-65	-22.659	-108	14	0.585	-123	-43	-0.996
	25	105	-65	-22.705	-46	12	0.508	-50	-44	-1.031
	26	206	-63	-21.747	60	11	0.48	46	-45	-1.052
	27	212	-61	-21.132	57	12	0.522	50	-53	-1.219
	28	188	-60	-20.742	20	12	0.525	16	-58	-1.352
	29	143	-60	-20.985	-28	14	0.587	-8	-67	-1.557
	30	128	-61	-21.097	-41	13	0.552	-11	-67	-1.552
Line 3										
GSSI Profiler Ver.#, 1 0 8 9	Record #	InPhase[1000]	Quad[1000]	Conductivity[1000]	InPhase[8000]	Quad[8000]	Conductivity[8000]	InPhase[15000]	Quad[15000]	Conductivity[15000]
GSSI Profiler Firmware Ver.#, 1060	1	400	-58	-19.989	173	18	0.786	191	-35	-0.815
Project Name, rock_glacier	2	378	-55	-19.255	169	18	0.766	176	-38	-0.882
Date, 08/18/2017 13:23:26.000	3	422	-55	-19.018	219	16	0.696	215	-42	-0.977
Units, METRIC	4	440	-52	-18.122	246	14	0.613	227	-42	-0.986
Gps Status, Disabled	5	489	-52	-18.151	289	14	0.6	268	-42	-0.969
Collection Mode, Stationary	6	924	-53	-18.447	715	15	0.622	693	-42	-0.982
Grid Type, xLTZ	7	1381	-56	-19.616	1169	17	0.707	1135	-50	-1.152

Line Spacing, 50.000	8	1833	-59	-20.521	1614	19	0.81	1546	-51	-1.175
Station Spacing, 5.000	9	1435	-60	-20.773	1238	20	0.857	1124	-50	-1.157
Mark Spacing, 25.000	10	1014	-56	-19.621	822	20	0.859	670	-44	-1.024
Xmin, 0.000	11	585	-53	-18.577	393	16	0.699	228	-46	-1.076
Ymin, 190.000	12	545	-51	-17.802	326	16	0.662	171	-49	-1.134
Xmax, 150.000	13	487	-51	-17.619	263	17	0.725	124	-53	-1.221
Ymax, 190.000	14	344	-49	-17.219	134	22	0.942	9	-54	-1.242
Instrument Orientation, VDM (I)	15	174	-48	-16.611	-12	27	1.161	-130	-51	-1.173
Frequencies:,1000,8000, 15000,	16	-13	-49	-17.198	-196	28	1.213	-293	-47	-1.102
InPhase Zero Levels:,499,7027,-1,	17	-79	-52	-17.969	-274	29	1.254	-366	-43	-1.004
Quad Zero Levels:, N/A	18	-16	-56	-19.629	-233	24	1.031	-325	-47	-1.098
Number of Stacks:, 16	19	109	-57	-19.746	-121	20	0.863	-256	-53	-1.231
Data Smoothing:, ON	20	279	-58	-20.016	37	13	0.555	-124	-59	-1.363
Calibration Height, 0.25	21	352	-53	-18.593	120	14	0.58	-63	-56	-1.302
Power Line Frequency, 60	22	417	-51	-17.914	191	13	0.57	13	-54	-1.258
	23	374	-49	-17.229	156	16	0.67	-20	-48	-1.112
	24	320	-51	-17.842	97	17	0.707	-78	-38	-0.899
	25	315	-55	-19.039	79	15	0.643	-106	-30	-0.713
	26	371	-58	-20.209	132	13	0.557	-61	-35	-0.826
	27	505	-62	-21.36	261	8	0.333	49	-55	-1.273
	28	458	-60	-20.991	227	13	0.555	12	-62	-1.428
	29	388	-58	-20.317	149	18	0.779	-75	-60	-1.38
	30	181	-55	-19.16	-58	28	1.187	-272	-44	-1.031
Line 4										

GSSI Profiler Ver.#, 1 0 8 9	Record #	InPhase[1000]	Quad[1000]	Conductivity[1000]	InPhase[8000]	Quad[8000]	Conductivity[8000]	InPhase[15000]	Quad[15000]	Conductivity[15000]
GSSI Profiler Firmware Ver.#, 1060	1	644	-50	-17.335	208	23	0.977	-179	-32	-0.762
Project Name, rock_glacier	2	564	-50	-17.531	143	22	0.943	-251	-34	-0.786
Date, 08/18/2017 11:55:14.000	3	546	-50	-17.385	154	22	0.936	-250	-38	-0.889
Units, METRIC	4	509	-47	-16.361	168	22	0.952	-258	-35	-0.813
Gps Status, Disabled	5	594	-45	-15.71	289	23	1.001	-141	-34	-0.805
Collection Mode, Stationary	6	598	-45	-15.723	319	25	1.056	-107	-34	-0.803
Grid Type, xLTZ	7	544	-48	-16.799	255	25	1.084	-158	-42	-0.97
Line Spacing, 50.000	8	423	-51	-17.67	122	25	1.08	-284	-41	-0.951
Station Spacing, 5.000	9	368	-53	-18.532	55	23	0.997	-336	-43	-1.01
Mark Spacing, 25.000	10	353	-58	-20.094	26	21	0.91	-376	-39	-0.91
Xmin, 0.000	11	358	-59	-20.354	16	21	0.885	-399	-39	-0.906
Ymin, 140.000	12	322	-58	-20.005	-25	21	0.879	-470	-29	-0.679
Xmax, 150.000	13	291	-48	-16.868	-25	24	1.037	-448	-23	-0.549
Ymax, 140.000	14	271	-42	-14.552	-14	27	1.169	-417	-22	-0.517
Instrument Orientation, VDM (I)	15	279	-37	-13.02	3	32	1.375	-377	-30	-0.704
Frequencies:,1000,8000, 15000,	16	281	-41	-14.297	-27	31	1.322	-401	-37	-0.857
InPhase Zero Levels:,499,7027,-1,	17	262	-46	-16.088	-77	29	1.237	-440	-36	-0.838
Quad Zero Levels:, N/A	18	204	-50	-17.311	-138	26	1.117	-486	-31	-0.725
Number of Stacks:, 16	19	232	-63	-21.738	-137	15	0.66	-493	-40	-0.925
Data Smoothing:, ON	20	305	-75	-26.112	-90	6	0.243	-451	-50	-1.158
Calibration Height, 0.25	21	445	-90	-30.926	14	-5	-0.238	-363	-61	-1.413

Power Line Frequency, 60	22	435	-79	-27.212	54	4	0.186	-327	-54	-1.242
	23	367	-67	-23.172	30	13	0.552	-356	-51	-1.184
	24	244	-52	-18.221	-48	22	0.951	-430	-50	-1.155
	25	358	-51	-17.739	62	20	0.867	-312	-54	-1.258
	26	506	-48	-16.859	205	20	0.87	-174	-55	-1.28
	27	706	-50	-17.537	400	21	0.914	16	-51	-1.18
	28	634	-49	-17.154	320	22	0.947	-65	-49	-1.135
	29	573	-51	-17.707	260	22	0.932	-97	-44	-1.035
	30	498	-46	-16.154	183	20	0.863	-154	-48	-1.109
Line 5										
GSSI Profiler Ver.#, 1 0 8 9	Record #	InPhase[1000]	Quad[1000]	Conductivity[1000]	InPhase[8000]	Quad[8000]	Conductivity[8000]	InPhase[15000]	Quad[15000]	Conductivity[15000]
GSSI Profiler Firmware Ver.#, 1060	1	1074	-40	-13.88	739	-16	-0.712	316	-74	-1.701
Project Name, rock_glacier	2	1008	-41	-14.19	675	-17	-0.781	251	-82	-1.896
Date, 08/18/2017 11:11:45.000	3	982	-45	-15.843	647	-19	-0.87	217	-82	-1.883
Units, METRIC	4	878	-47	-16.433	545	-17	-0.788	105	-81	-1.865
Gps Status, Disabled	5	778	-47	-16.33	446	-11	-0.495	-9	-70	-1.616
Collection Mode, Stationary	6	666	-45	-15.839	348	-1	-0.065	-116	-75	-1.728
Grid Type, xLTZ	7	571	-51	-17.642	226	-4	-0.215	-251	-76	-1.757
Line Spacing, 50.000	8	530	-57	-19.738	160	-12	-0.563	-313	-77	-1.765
Station Spacing, 5.000	9	515	-60	-20.787	111	-22	-0.988	-349	-66	-1.522
Mark Spacing, 25.000	10	549	-49	-17.211	191	-11	-0.52	-235	-59	-1.365
Xmin, 0.000	11	611	-42	-14.584	295	-1	-0.094	-108	-63	-1.466
Ymin, 90.000	12	633	-37	-13.115	359	6	0.261	-32	-74	-1.708

Xmax, 150.000	13	608	-43	-15.03	333	2	0.106	-64	-83	-1.901
Ymax, 90.000	14	572	-45	-15.815	287	0	-0.015	-118	-82	-1.889
Instrument Orientation, VDM (I)	15	578	-46	-16.154	287	-1	-0.089	-123	-83	-1.923
Frequencies:,1000,8000, 15000,	16	638	-46	-16.044	339	-3	-0.172	-79	-87	-2.003
InPhase Zero Levels:,499,7027,-1,	17	571	-45	-15.815	280	0	-0.027	-139	-86	-1.979
Quad Zero Levels:, N/A	18	503	-47	-16.284	210	1	0.03	-216	-80	-1.84
Number of Stacks:, 16	19	271	-45	-15.723	-15	5	0.2	-447	-74	-1.705
Data Smoothing:, ON	20	1140	-137	-47.17	573	-81	-3.479	57	-162	-3.71
Calibration Height, 0.25	21	1153	-140	-48.064	578	-84	-3.643	61	-167	-3.814
Power Line Frequency, 60	22	949	-104	-35.702	480	-61	-2.666	-4	-146	-3.336
	23	878	-88	-30.363	446	-58	-2.517	-35	-142	-3.258
	24	828	-67	-23.25	449	-48	-2.103	-36	-127	-2.924
	25	916	-62	-21.373	558	-43	-1.875	70	-118	-2.712
	26	884	-52	-18.085	551	-31	-1.348	86	-96	-2.215
	27	742	-43	-14.875	442	-9	-0.427	33	-76	-1.745
	28	564	-40	-14.025	273	5	0.215	-91	-65	-1.512
	29	518	-39	-13.677	266	26	1.121	-64	-59	-1.374
	30	596	-44	-15.392	344	26	1.124	11	-65	-1.508
Line 6										
GSSI Profiler Ver.#, 1 0 8 9	Record #	InPhase[1000]	Quad[1000]	Conductivity[1000]	InPhase[8000]	Quad[8000]	Conductivity[8000]	InPhase[15000]	Quad[15000]	Conductivity[15000]
GSSI Profiler Firmware Ver.#, 1060	1	942	-76	-26.209	748	-2	-0.131	717	-70	-1.608
Project Name, rock_glacier	2	898	-59	-20.326	772	17	0.736	754	-51	-1.183
Date, 08/18/2017 10:27:03.000	3	808	-42	-14.618	744	35	1.512	729	-35	-0.808

Units, METRIC	4	713	-22	-7.959	719	52	2.226	703	-18	-0.425
Gps Status, Disabled	5	704	-30	-10.605	661	31	1.311	605	-37	-0.873
Collection Mode, Stationary	6	804	-43	-15.001	696	7	0.302	604	-61	-1.413
Grid Type, xLTZ	7	963	-58	-20.121	784	-12	-0.573	655	-82	-1.901
Line Spacing, 50.000	8	1094	-60	-20.959	902	-15	-0.667	768	-82	-1.882
Station Spacing, 5.000	9	1122	-59	-20.4	914	-20	-0.905	772	-84	-1.925
Mark Spacing, 25.000	10	1079	-57	-19.962	846	-29	-1.276	698	-81	-1.875
Xmin, 0.000	11	1021	-62	-21.423	748	-42	-1.819	578	-84	-1.939
Ymin, 40.000	12	1003	-64	-22.281	712	-47	-2.034	514	-86	-1.987
Xmax, 150.000	13	997	-57	-19.763	738	-38	-1.664	506	-88	-2.016
Ymax, 40.000	14	896	-40	-14.08	706	-14	-0.657	461	-86	-1.987
Instrument Orientation, VDM (I)	15	745	-24	-8.471	636	13	0.541	392	-78	-1.797
Frequencies:,1000,8000, 15000,	16	572	-21	-7.656	478	25	1.068	255	-78	-1.788
InPhase Zero Levels:,499,7027,-1,	17	565	-31	-10.847	433	14	0.587	210	-90	-2.067
Quad Zero Levels:, N/A	18	585	-44	-15.483	388	-3	-0.176	154	-104	-2.381
Number of Stacks:, 16	19	651	-54	-18.856	413	-21	-0.926	156	-123	-2.818
Data Smoothing:, ON	20	636	-58	-20.061	392	-23	-1.025	107	-129	-2.953
Calibration Height, 0.25	21	627	-58	-20.009	393	-25	-1.097	103	-132	-3.023
Power Line Frequency, 60	22	630	-53	-18.502	424	-16	-0.708	150	-117	-2.694
	23	582	-51	-17.632	401	-6	-0.315	181	-101	-2.315
	24	630	-50	-17.395	458	0	-0.019	261	-91	-2.087
	25	630	-54	-18.698	438	0	-0.025	243	-86	-1.989
	26	697	-54	-18.755	485	-1	-0.094	259	-88	-2.033
	27	653	-54	-18.782	423	0	-0.044	178	-84	-1.933

	28	635	-50	-17.389	398	2	0.088	143	-84	-1.929
	29	635	-50	-17.481	389	1	0.06	125	-78	-1.801
	30	632	-49	-16.92	385	1	0.054	126	-81	-1.878
Line 7										
GSSI Profiler Ver.#, 1 0 8 9	Record #	InPhase[1000]	Quad[1000]	Conductivity[1000]	InPhase[8000]	Quad[8000]	Conductivity[8000]	InPhase[15000]	Quad[15000]	Conductivity[15000]
GSSI Profiler Firmware Ver.#, 1060	1	450	-55	-19.019	261	14	0.607	219	-56	-1.305
Project Name, rock_glacier	2	451	-56	-19.38	268	13	0.539	218	-56	-1.288
Date, 08/18/2017 09:42:15.000	3	482	-55	-19.202	319	15	0.65	259	-53	-1.22
Units, METRIC	4	556	-55	-19.022	407	17	0.731	329	-46	-1.078
Gps Status, Disabled	5	658	-51	-17.634	531	24	1.014	444	-42	-0.988
Collection Mode, Stationary	6	726	-49	-17.005	592	22	0.957	493	-43	-0.999
Grid Type, xLTZ	7	704	-42	-14.671	586	27	1.135	475	-43	-1.01
Line Spacing, 50.000	8	607	-38	-13.354	467	24	1.004	331	-46	-1.074
Station Spacing, 5.000	9	525	-35	-12.199	376	25	1.053	212	-50	-1.165
Mark Spacing, 25.000	10	524	-40	-14.048	340	18	0.758	148	-62	-1.439
Xmin, 0.000	11	547	-47	-16.272	346	13	0.546	134	-68	-1.569
Ymin, 0.000	12	532	-51	-17.64	309	5	0.225	85	-75	-1.74
Xmax, 150.000	13	451	-52	-18.122	219	1	0.026	-2	-75	-1.73
Ymax, 0.000	14	415	-51	-17.886	184	0	0.016	-32	-78	-1.791
Instrument Orientation, VDM (I)	15	400	-51	-17.721	177	3	0.123	-30	-71	-1.639
Frequencies:,1000,8000, 15000,	16	389	-50	-17.363	172	6	0.254	-30	-69	-1.583
InPhase Zero Levels:,499,7027,-1,	17	362	-51	-17.867	152	5	0.221	-21	-67	-1.551
Quad Zero Levels:, N/A	18	316	-54	-18.838	135	10	0.41	22	-69	-1.595

Number of Stacks:, 16	19	385	-55	-19.15	258	15	0.651	236	-67	-1.543
Data Smoothing:, ON	20	461	-53	-18.57	389	24	1.038	451	-63	-1.447
Calibration Height, 0.25	21	635	-54	-18.755	579	23	0.968	678	-60	-1.38
Power Line Frequency, 60	22	645	-55	-19.175	582	21	0.895	678	-58	-1.342
	23	689	-56	-19.506	615	17	0.729	680	-51	-1.176
	24	684	-53	-18.512	615	18	0.775	668	-39	-0.915
	25	765	-50	-17.566	698	18	0.787	737	-29	-0.686
	26	756	-46	-15.98	697	25	1.053	743	-23	-0.545
	27	676	-44	-15.432	614	33	1.429	645	-21	-0.497
	28	570	-45	-15.835	499	43	1.834	522	-13	-0.312
	29	490	-53	-18.431	377	44	1.888	370	-7	-0.177
	30	463	-59	-20.617	322	43	1.83	300	-1	-0.041

APPENDIX D

PROFILER EMP-400 GRAPHS FOR ALL LINES

In-phase and Quad components in ppm, apparent conductivity in mS/m

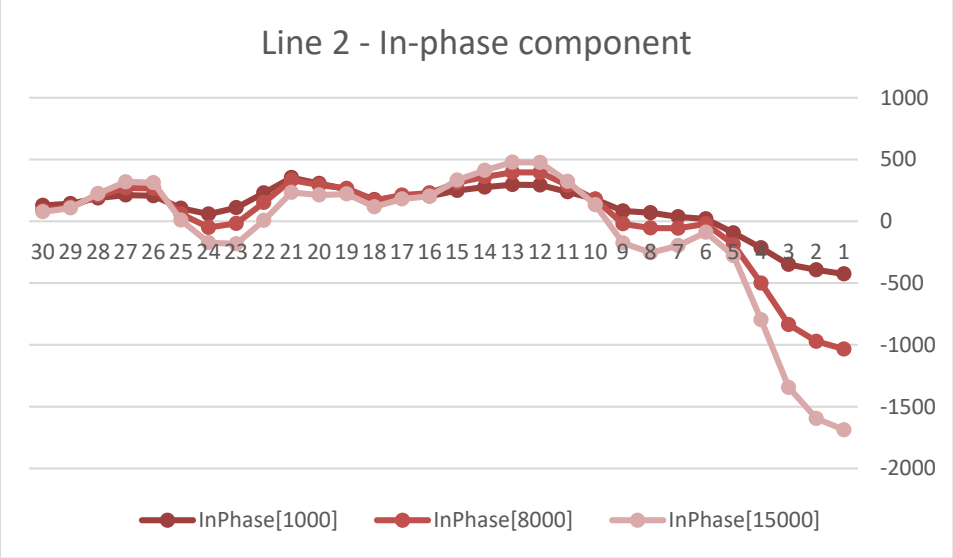

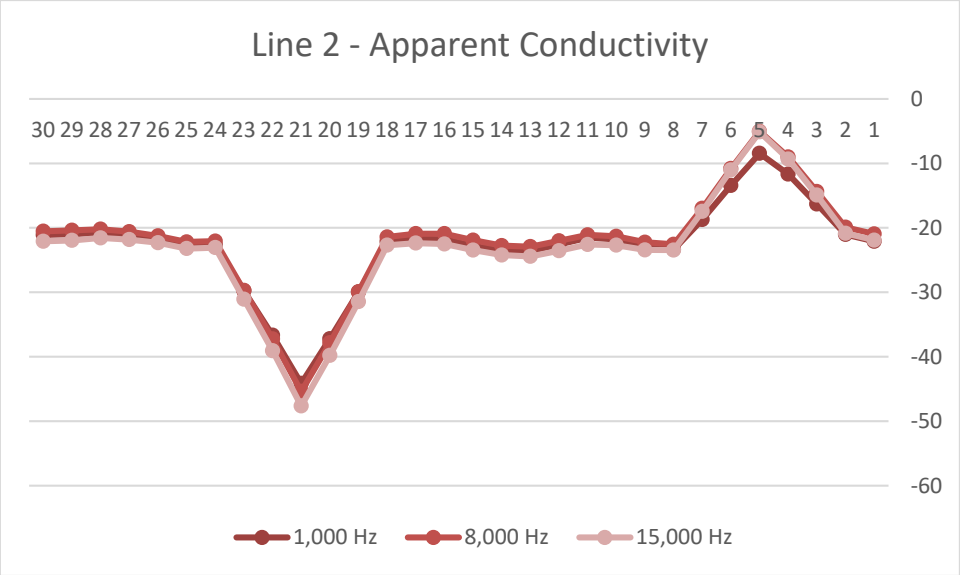
Line 2 - Apparent Conductivity
30 29 28 27 26 25 24 23 22 21 20 19 18 17 16 15 14 13 12 11 10 9 8 7 6 5 4 3 2 1
0
-10
-20
-30
-40
-50
-60
1,000 Hz
8,000 Hz
15,000 Hz

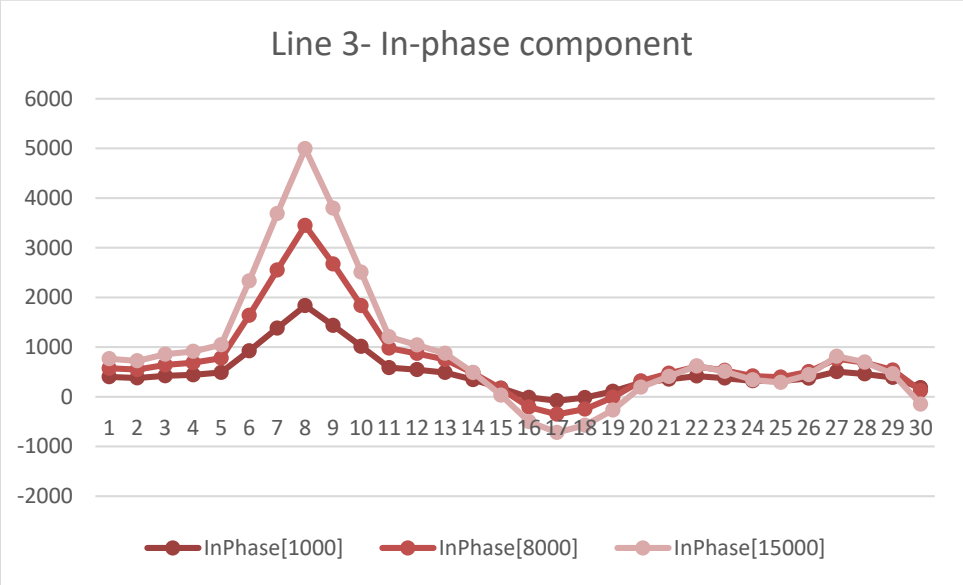
Line 3- In-phase component
6000
5000
4000
3000
2000
1000
0
-1000
-2000
1 2 3 4 5 6 7 8 9 10 11 12 13 14 15 16 17 18 19 20 21 22 23 24 25 26 27 28 29 30
InPhase[1000]
InPhase[8000]
InPhase[15000]

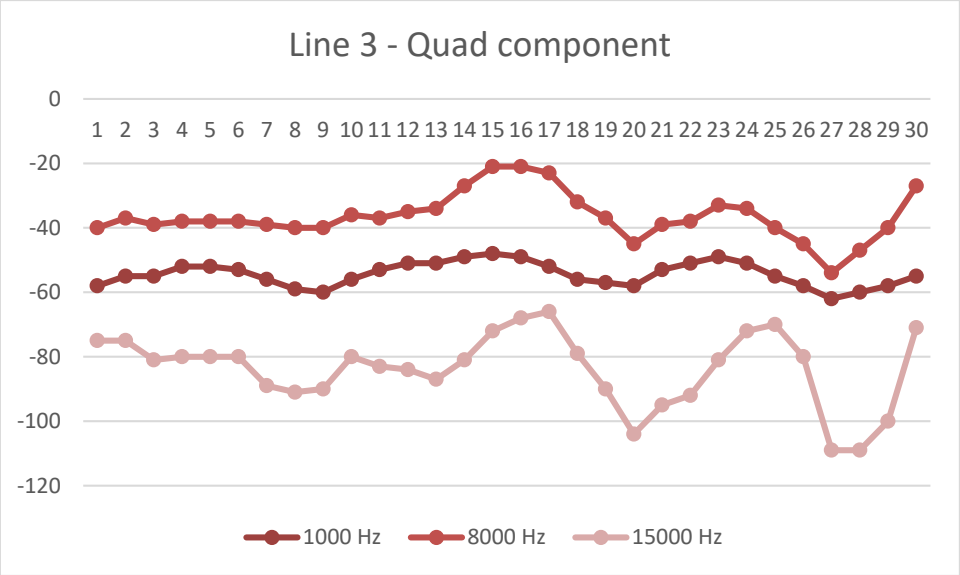
Line 3 - Quad component
0
-20
-40
-60
-80
-100
-120
1 2 3 4 5 6 7 8 9 10 11 12 13 14 15 16 17 18 19 20 21 22 23 24 25 26 27 28 29 30
1000 Hz
8000 Hz
15000 Hz

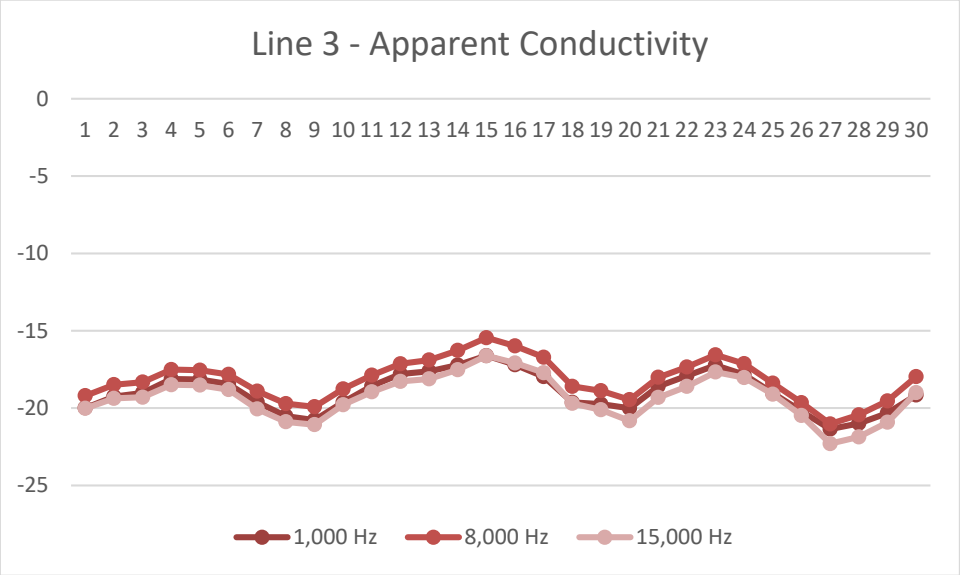
Line 3 - Apparent Conductivity
0
-5
-10
-15
-20
-25
1 2 3 4 5 6 7 8 9 10 11 12 13 14 15 16 17 18 19 20 21 22 23 24 25 26 27 28 29 30
1,000 Hz
8,000 Hz
15,000 Hz

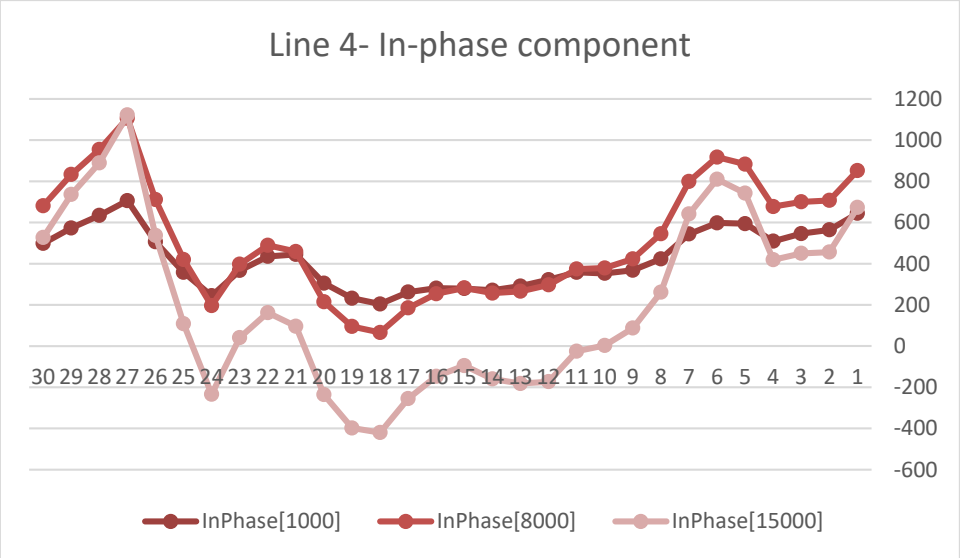
Line 4- In-phase component
1200
1000
800
600
400
200
0
-200
-400
-600
30 29 28 27 26 25 24 23 22 21 20 19 18 17 16 15 14 13 12 11 10 9 8 7 6 5 4 3 2 1
InPhase[1000]
InPhase[8000]
InPhase[15000]

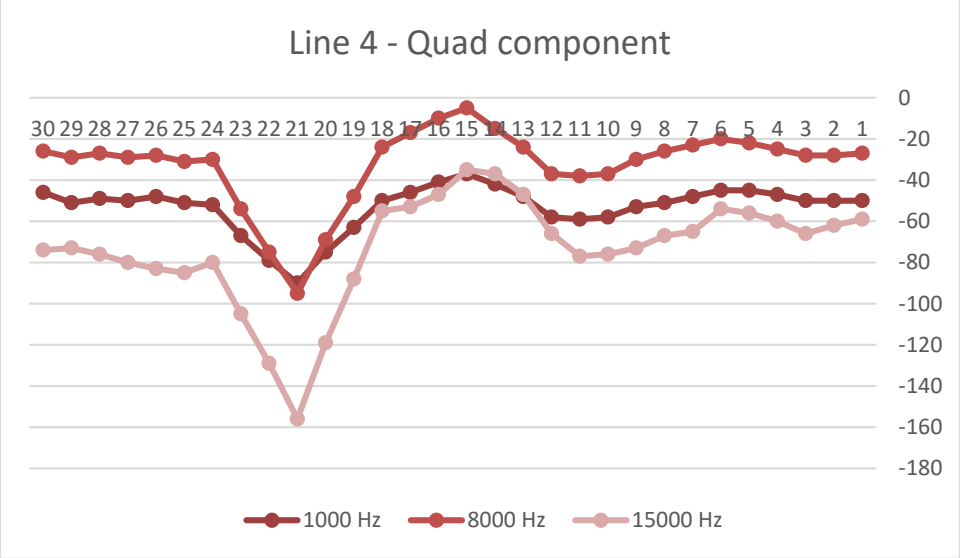
Line 4 - Quad component
0
-20
-40
-60
-80
-100
-120
-140
-160
-180
30 29 28 27 26 25 24 23 22 21 20 19 18 17 16 15 14 13 12 11 10 9 8 7 6 5 4 3 2 1
1000 Hz
8000 Hz
15000 Hz

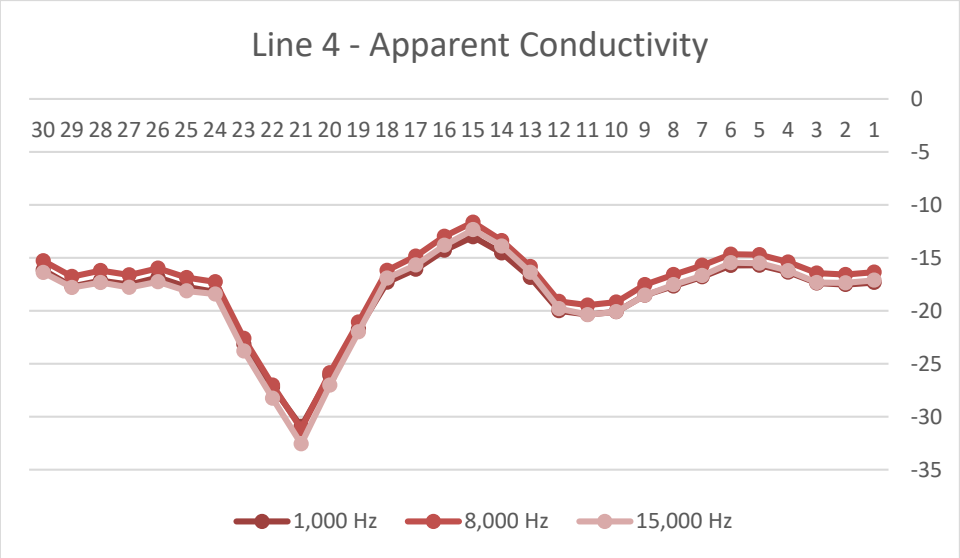
Line 4 - Apparent Conductivity
30 29 28 27 26 25 24 23 22 21 20 19 18 17 16 15 14 13 12 11 10 9 8 7 6 5 4 3 2 1
0
-5
-10
-15
-20
-25
-30
-35
1,000 Hz
8,000 Hz
15,000 Hz

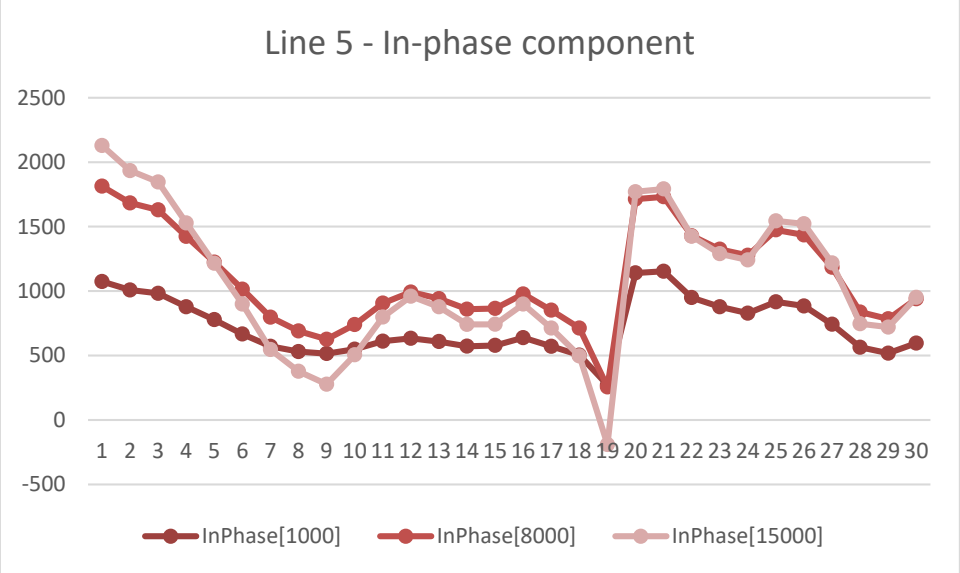
Line 5 - In-phase component
2500
2000
1500
1000
500
0
-500
1 2 3 4 5 6 7 8 9 10 11 12 13 14 15 16 17 18 19 20 21 22 23 24 25 26 27 28 29 30
InPhase[1000]
InPhase[8000]
InPhase[15000]

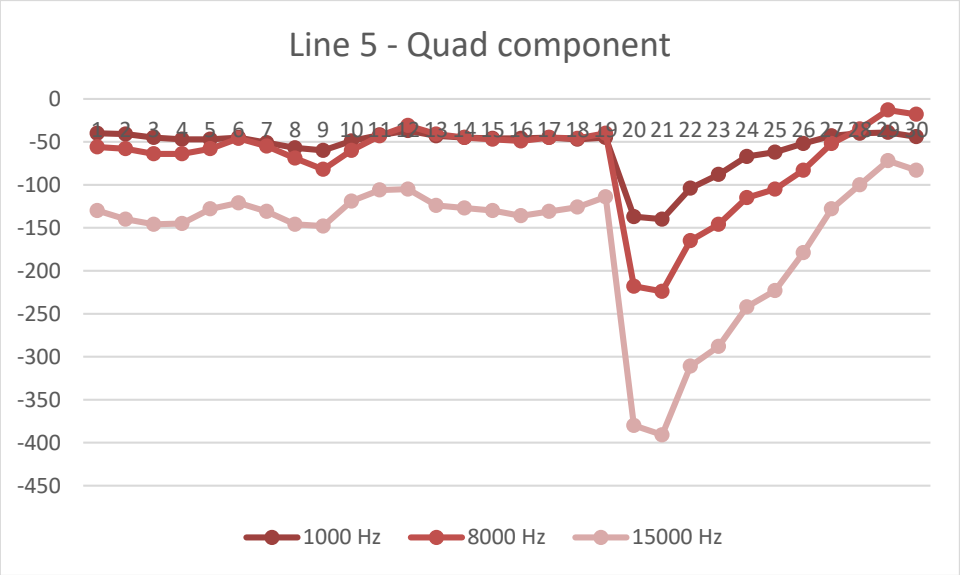
Line 5 - Quad component
0
-50
-100
-150
-200
-250
-300
-350
-400
-450
1 2 3 4 5 6 7 8 9 10 11 12 13 14 15 16 17 18 19 20 21 22 23 24 25 26 27 28 29 30
1000 Hz
8000 Hz
15000 Hz

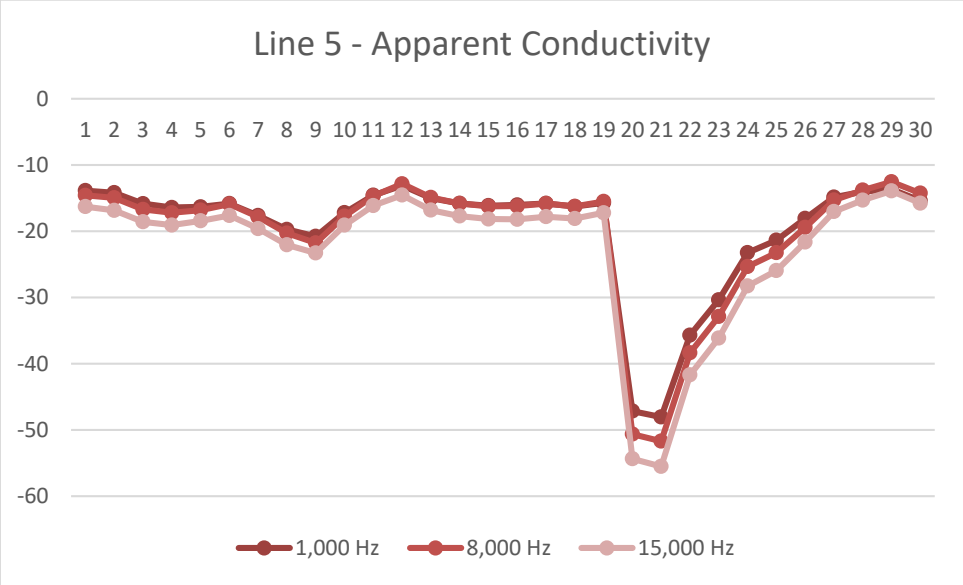
Line 5 - Apparent Conductivity
0
-10
-20
-30
-40
-50
-60
1 2 3 4 5 6 7 8 9 10 11 12 13 14 15 16 17 18 19 20 21 22 23 24 25 26 27 28 29 30
1,000 Hz
8,000 Hz
15,000 Hz

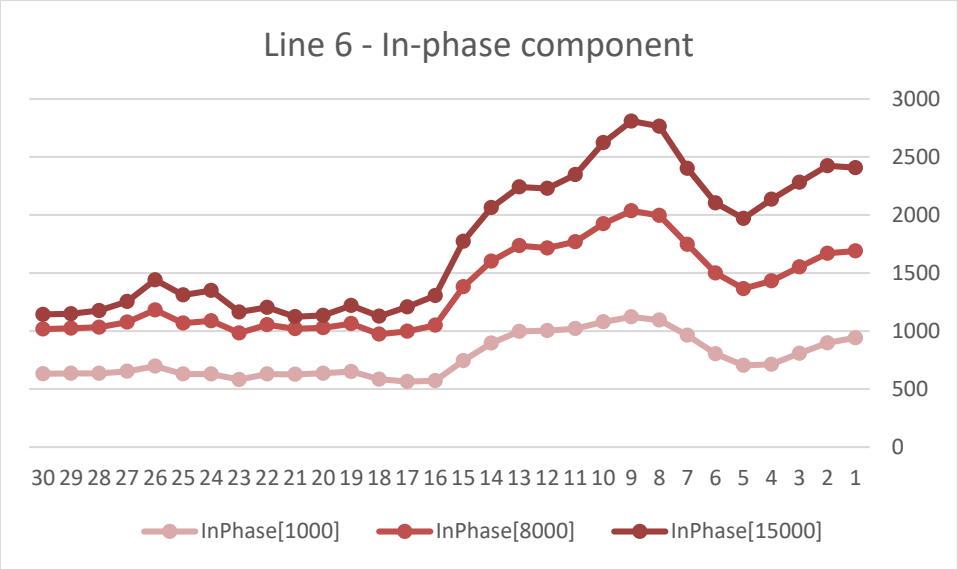
Line 6 - In-phase component
3000
2500
2000
1500
1000
500
0
30 29 28 27 26 25 24 23 22 21 20 19 18 17 16 15 14 13 12 11 10 9 8 7 6 5 4 3 2 1
InPhase[1000]
InPhase[8000]
InPhase[15000]

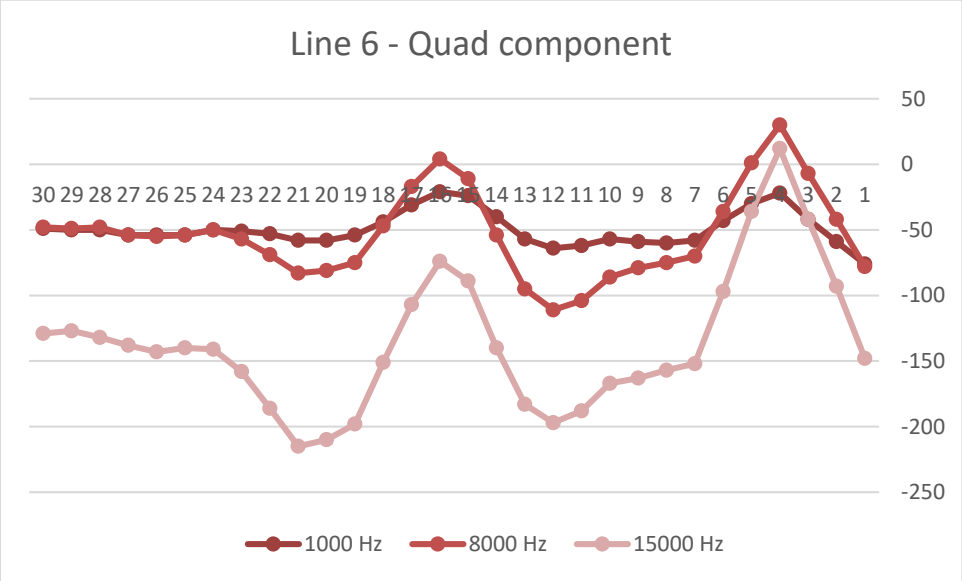
Line 6 - Quad component
50
0
-50
-100
-150
-200
-250
30 29 28 27 26 25 24 23 22 21 20 19 18 14 13 12 11 10 9 8 7 6 3 2 1
1000 Hz
8000 Hz
15000 Hz

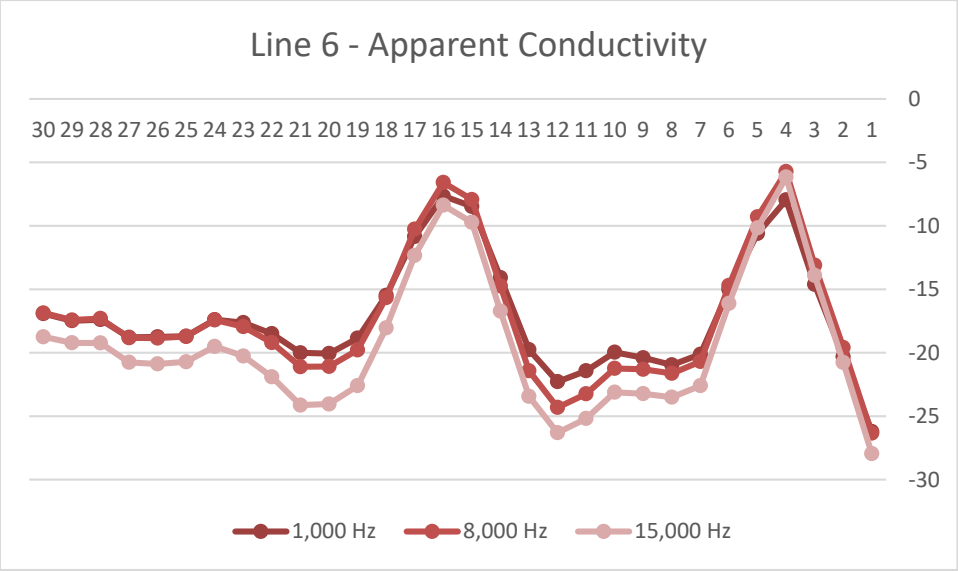
Line 6 - Apparent Conductivity
30 29 28 27 26 25 24 23 22 21 20 19 18 17 16 15 14 13 12 11 10 9 8 7 6 5 4 3 2 1
0
-5
-10
-15
-20
-25
-30
1,000 Hz
8,000 Hz
15,000 Hz

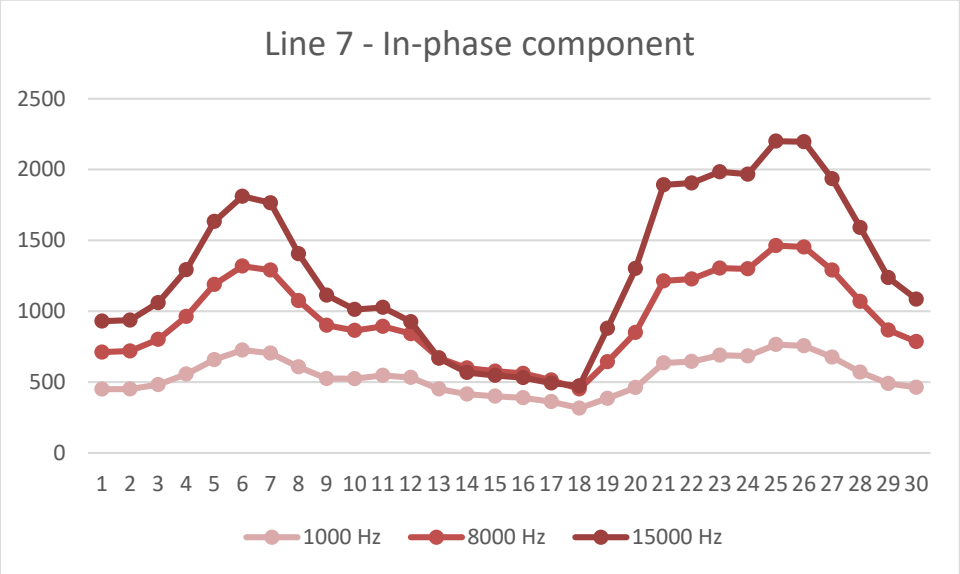
Line 7 - In-phase component
2500
2000
1500
1000
500
0
1 2 3 4 5 6 7 8 9 10 11 12 13 14 15 16 17 18 19 20 21 22 23 24 25 26 27 28 29 30
1000 Hz
8000 Hz
15000 Hz

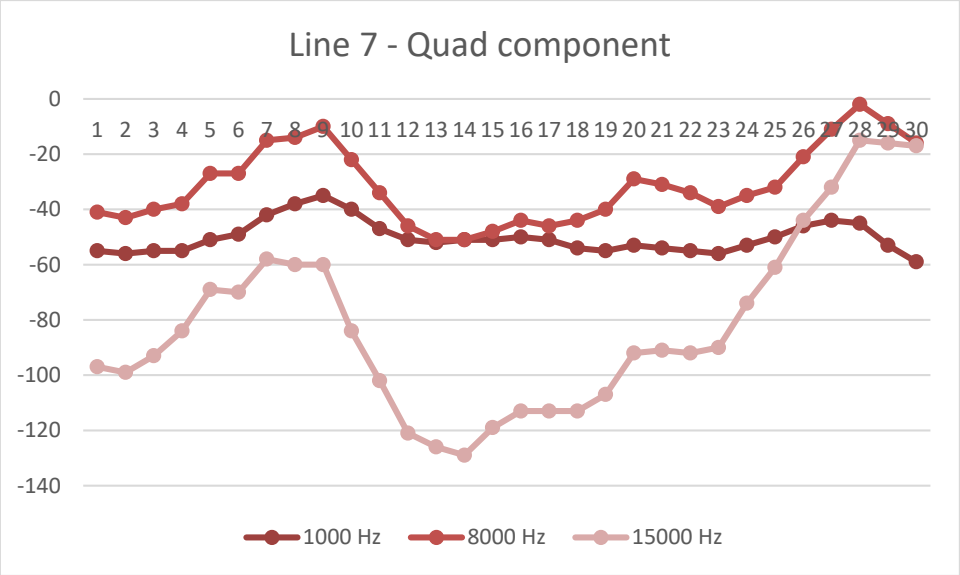
Line 7 - Quad component
0
-20
-40
-60
-80
-100
-120
-140
1 2 3 4 5 6 7 8 9 10 11 12 13 14 15 16 17 18 19 20 21 22 23 24 25 26 27 28 29 30
1000 Hz
8000 Hz
15000 Hz

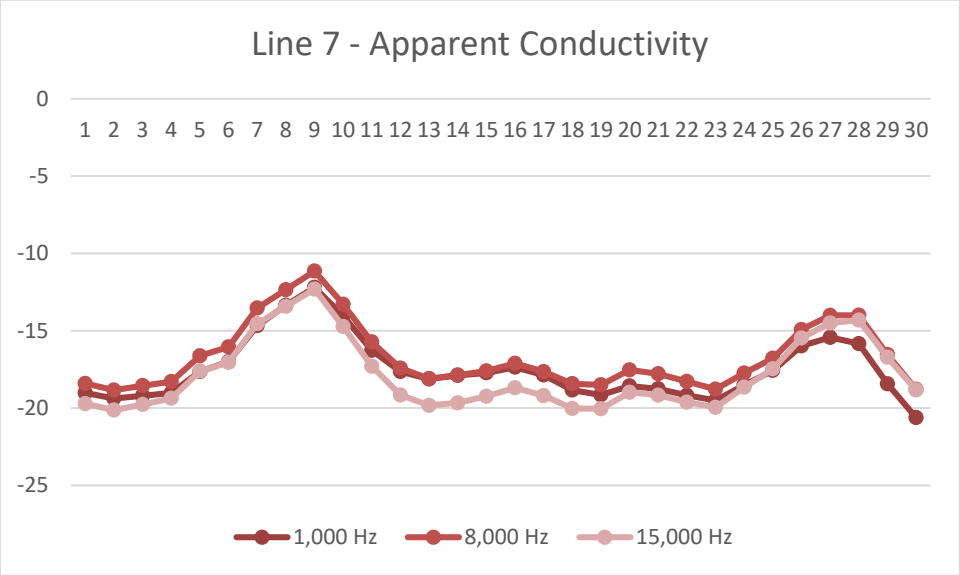
Line 7 - Apparent Conductivity
0
-5
-10
-15
-20
-25
1 2 3 4 5 6 7 8 9 10 11 12 13 14 15 16 17 18 19 20 21 22 23 24 25 26 27 28 29 30
1,000 Hz
8,000 Hz
15,000 Hz

APPENDIX E

FDEM profiler data with G-TEM stations